Optimization of the mechanical and environmental performance for the treated dredged marine sediments with eco-friendly binders

Hongwei Wang

N° d'ordre :

IMT NORD EUROPE **UNIVERSITÉ DE LILLE**

THÈSE

présentée en vue
d'obtenir le grade de

DOCTEUR

en

Discipline : Génie Civil

par

Hongwei WANG

DOCTORAT DE L'UNIVERSITÉ DE LILLE
DÉLIVRÉ PAR IMT NORD EUROPE

Titre de la thèse :

Optimisation des performances mécaniques et environnementales des sédiments marins dragués traités avec des éco-liants
(Optimization of the mechanical and environmental performance for the treated dredged marine sediments with eco-friendly binders)

Soutenue le **20/06/2022** devant le jury d'examen :

Présidente :	Mahdia HATTAB	Professeure, Université de Lorraine
Rapporteur :	Ouali AMIRI	Professeur, Université de Nantes
Rapportrice :	Naima BELAYACHI	Maîtresse de conférences, HDR, Université d'Orléans
Examinateur :	Nor-Edine ABRIAK	Professeur, Institut Mines-Télécom Nord Europe
Examinateur :	Damien RANGEARD	Maitre de conférences, HDR, INSA de Rennes
Examinateur :	Dongxing WANG	Professeur, Université de Wuhan
Directeur de thèse :	Rachid ZENTAR	Professeur, Institut Mines-Télécom Nord Europe

Laboratoires d'accueil : Laboratoire de Génie Civil et géo-Environnement (LGCgE)
CERI Matériaux & Procédés, IMT Nord Europe
École Doctorale ENGSYS 632 (Univ. Lille, Centrale Lille Institut, IMT Nord Europe, Univ. Gustave Eiffel)

Acknowledgements

First, I would like to express my deepest gratitude to my supervisor, Prof. Rachid ZENTAR, for his consistent support, guidance and encouragement during my doctoral dissertations. He helped me learn how to do scientific research and express the results in articles and thesis. He has taught me invaluable experiences and given me wonderful insights into my research and personal life. These will be a big fortune and benefit me all of my life.

Second, I want to express my deepest appreciation to Prof. Dongxing WANG at Wuhan University, who encouraged me to come to France for Ph.D. study and helped me apply for the scholarship from the China Scholarship Council (CSC). Thanks a lot for his encouragement, support, advice and concern.

I look forward to sincerely thanking Prof. Ouali AMIRI from Université de Nantes and Dr. Naima BELAYACHI from Université d'Orléans, for their willingness as reviewers to evaluate my dissertation work. Besides, I wish to acknowledge Prof. Nor-Edine ABRIAK from IMT Nord Europe, Prof. Mahdia HATTAB from Université de Lorraine and Dr. Damien RANGEARD from INSA de Rennes, for agreeing to be examiners and evaluate my work.

I'd also like to convey my gratitude to the technicians in our department, Guillaume POTIER, Damien BETRANCOURT, Johanna CABOCHE, Dominique DUBOIS and Michael D'HELFT. Although our communication was difficult due to language problem, they were always patient and willing to listen and help me. Their kind assistance greatly smoothed my experimental work. I would also like to give special thanks to Madame Carole DELCHAMBRE. Thanks for her patience in understanding my poor French and sign language, and for solving many administrative and life problems for me.

Besides, I would like to thank all the professors and researchers in our department for their help. They are: Nor-Edine ABRIAK, Mahfoud BENZERZOUR, Frédéric BECQUART, Walid MAHERZI, Vincent THIERY, Claire ALARY, Agnès ZAMBON, Joelle KLEIB…

I would also like to thank all my colleagues and friends for their help in my experimental work and daily life. They are Mokrane BALA, Ahmed ZERAOUI, Océane LY, Mathilde BETREMIEUX, Zeinab MKAHAL, Duc Chinh CHU, Fouad BELAYALI, Hamza EL MOUEDEN, Estelle HYNEK, Fatima OUENDI, Jana

DAHER, Bader BOUZAR, Marwa JEBBAWY, Maria TALEB, Reine KARAM, Salim KOURTAA, Mohammad ALMOKDAD…

In addition, I'd like to express my gratitude to my Chinese friends for their support: Jingzhou BAI, Xiao MA, Jinjian LI, Hua LIU, Junchao XU, Leming HE…I'll always treasure the amazing memories we shared. I am also grateful to my friends in China: Yang HE, Qile HUANG, Weihua JIANG, Jun LIU, Yao LAN, Di WU, Daoyuan SUN…They were always the first to offer help when I was in trouble. I'm especially grateful to Daorui XUE, who helped me a lot when I was in Shanghai before I came to France. He also helped me learn a lot about Chinese road construction.

I also wish to acknowledge the financial support from the China Scholarship Council (CSC) and École nationale supérieure Mines-Télécom Nord Europe. Thank you for the support of my motherland during my study.

Besides, I would like to express my love and gratitude to my parents. They were always supportive of my decision, regardless of how difficult it was for them. As a Chinese poet wrote, “Such kindness of warm sun, can't be repaid by grass.” I will do my best to repay my parents in the years to come. I would also like to thank my brother, my grandparents, aunts, uncles and other family members. I cannot insist on finishing my doctoral study without their endless love and unconditional support.

Finally, I would like to express my particular appreciation for the most important girl in my life. The distance of more than 10000 kilometers between China and France does not stop our love. We support each other and share our joys and sorrows together. In ancient China, there was a romantic story of the Cowherd and the Weaver Girl, who meet once a year on the seventh day of the seventh month of the lunar calendar. But we haven't seen each other in almost three years since the Covid-19 outbreak. Thank you for your constant companionship and love, Miss Yu Kong. Will you marry me? For the rest of my life, no matter where we are, no matter spring, summer, autumn or winter, I will always be the "ice cream" that protects you!

谢谢(Xiexie)!

Abstract

Global warming and climate change caused by Greenhouse Gases (GHG) have become the most pressing challenges worldwide. CO_2 is the main part of GHG. Thus, as the world's leading economic power, the European Union established the target of transitioning to a circular economy and achieving climate neutrality by 2050. Preventing waste generation and improving waste management play a vital role in the circular economy model. Dredged sediments are regarded as a typical waste. With the rapid growth of urbanization and industrialization, many construction and maintenance activities for riverways and ports are carried out each year, which produce a huge volume of dredged sediment waste. Besides, the Ordinary Portland Cement (OPC) is the most extensively used construction material. The manufacturing of OPC has significantly contributed to CO_2 emissions. Therefore, under the circular economy and climate-neutral concept, reusing solidified dredged sediments with low carbon and sustainable binder as road material is a promising green method.

In this context, this research first evaluated the basic physical, chemical and environmental characteristics of raw dredged sediments. The used green and low carbon binder-Calcium Sulfoaluminate (CSA) cement was chosen with the SWOT (Strengths, Weaknesses, Opportunities and Threats) analysis. Then, this research investigated the rheological behavior of dredged fine-grained sediment to improve the understanding of sediment, particularly the pipeline transport of dredged sediment. After that, this research focused on the engineering performance of treated sediments with the low carbon CSA and OPC-CSA binder, to verify the selected novel binder's effectiveness in treating dredged sediments in road construction. Besides, the simplified carbon footprint of the used low carbon binders was investigated. In the end, a database of treated sediments was first established. Then, the observed compacted behavior of treated dredged sediments was modeled by using the statistical approach. In order to correlate the compaction performance of solidified dredged sediments with the basic physical parameters of raw sediments and treatment binder types and quantities.

Key words: Marine sediments; valorization/recycling; calcium sulfoaluminate cement; mechanical strength; environmental performance; road material; modeling; rheology.

Résumé

Le réchauffement de la planète et le changement climatique causés par les gaz à effet de serre (GES) sont devenus les défis les plus urgents au niveau mondial. Le CO_2 est la principale composante des GES. Ainsi, en tant que première puissance économique mondiale, l'Union européenne s'est fixé pour objectif de passer à une économie circulaire. La prévention de la production de déchets et l'amélioration de leur gestion jouent un rôle essentiel dans le modèle d'économie circulaire. Les sédiments de dragage sont considérés comme un déchet typique. Avec la croissance rapide de l'urbanisation et de l'industrialisation, de nombreuses activités de construction et d'entretien des voies fluviales et des ports sont menées chaque année, ce qui produit un énorme volume de déchets de sédiments de dragage. Par ailleurs, le ciment Portland ordinaire (OPC) est le matériau de construction le plus utilisé. La fabrication du ciment Portland ordinaire a contribué de manière significative aux émissions de CO_2. Par conséquent, dans le cadre du concept d'économie circulaire, la réutilisation des sédiments de dragage solidifiés avec un liant à faible teneur en carbone et durable comme matériau routier est une méthode verte prometteuse.

Dans ce contexte, cette recherche a d'abord évalué les caractéristiques physiques, chimiques et environnementales de base des sédiments de dragage bruts. Le liant vert et à faible teneur en carbone utilisé, le ciment de sulfoaluminate de calcium (CSA), a été choisi en fonction de l'analyse SWOT (forces, faiblesses, opportunités et menaces). Ensuite, cette recherche a étudié le comportement rhéologique des sédiments à grain fin dragués afin d'améliorer la compréhension des sédiments, en particulier le transport par canalisation des sédiments dragués. Ensuite, cette recherche s'est concentrée sur les performances techniques des sédiments traités avec le liant à faible teneur en carbone CSA et OPC-CSA, afin de vérifier l'efficacité du nouveau liant sélectionné pour traiter les sédiments de dragage dans la construction routière. En outre, l'empreinte carbone simplifiée des liants à faible teneur en carbone utilisés a été étudiée. Enfin, une base de données des sédiments traités a d'abord été établie. Ensuite, le comportement compacté observé des sédiments de dragage traités a été modélisé en utilisant l'approche statistique. Afin de corréler la performance de compactage des sédiments de dragage solidifiés avec les paramètres physiques de base des sédiments bruts et les types et quantités de liants de traitement.

Mots clés : Sédiments marins ; valorisation/recyclage ; ciment de sulfoaluminate de calcium ; résistance mécanique ; performance environnementale ; matériau routier ; modélisation ; rhéologie.

Publications

Journal papers

- 1. **Hongwei WANG**, Rachid ZENTAR, Dongxing WANG. Rheological characterization of fine-grained sediments under steady and dynamic conditions. ***International Journal of Geomechanics, ASCE***. 2022, 22(1), 04021260. DOI: 10.1061/(ASCE)GM.1943-5622.0002243**.**
- 2. Rachid ZENTAR, **Hongwei WANG**, Dongxing WANG. Comparative study of Stabilization/Solidification of dredged sediments with Ordinary Portland cement and Calcium Sulfo-Aluminate cement in the framework of valorization in road construction material. ***Construction and Building Materials***, 2021, 279, 122447. DOI: 10.1016/j.conbuildmat. 2021.122447.
- 3. **Hongwei WANG**, Rachid ZENTAR, Dongxing WANG, et al. New applications of Ordinary Portland and Calcium Sulfoaluminate composite binder for recycling marine sediments as road materials. ***International Journal of Geomechanics, ASCE***. 2022, 22(6), 04022068. DOI: 10.1061/(ASCE)GM.1943-5622.0002373.
- 4. **Hongwei WANG**, Rachid ZENTAR, Dongxing WANG. Predicting the compaction parameters of solidified dredged sediments with statistical approach. ***Marine Georesources & Geotechnology*.** DOI: 10.1080/1064119X.2021.2023827.

Conference papers

- 1. **Hongwei WANG**, Rachid ZENTAR, Dongxing WANG. Rheological characterization of kaolinite clay: experimental study. 37èmes Rencontres Universitaires de Génie Civil, June 19–21, 2019, Sophia Antipolis, France.
- 2. **Hongwei WANG**, Rachid ZENTAR, Dongxing WANG. Oscillatory rheological properties of fine-grained material. 8th International Conference on Sustainable Solid Waste Management. June 23–26, 2021, Thessaloniki, Greece (online).
- 3. Rachid ZENTAR, **Hongwei WANG**, Dongxing WANG. Organic dredged sediments treated with Portland Cement: compaction characteristics. 38èmes Rencontres Universitaires de Génie Civil, September 23-24, 2020, Marrakech, Morroco (online).
- 4. **Hongwei WANG**, Rachid ZENTAR, Dongxing WANG. Apparent and complex viscosity versus the water content of clay. 38èmes Rencontres Universitaires de Génie Civil, September 23-24, 2020, Marrakech, Morroco (online).

- 5. **Hongwei WANG**, Rachid ZENTAR, Fatima Ouendi. Valorisation of marine sediments with novel eco-friendly OPC-CSA composite binder. 39èmes Rencontres Universitaires de Génie Civil, May 26-28, 2021, Nantes, France (online).
- 6. **Hongwei WANG**, Rachid ZENTAR, Dongxing WANG. Study of Proctor compaction and CBR property for dredged marine sediments solidified with Calcium Sulfoaluminate cement for road material valorisation. 7th International Symposium on Sediment Management. June 29–July 3, 2021, Lille, France (online).
- 7. Rachid ZENTAR, **Hongwei WANG**, Dongxing WANG. Mechanical behavior of treated sediment with Calcium Sulfoaluminate cement for road material valorisation. 7th International Symposium on Sediment Management. June 29–July 3, 2021, Lille, France (online).
- 8. **Hongwei WANG**, Rachid ZENTAR, Dongxing WANG. Stabilization/ solidification (S/S) dredged sediments as road materials. 1st Mediterranean Geosciences Union (MedGU). November 25–28, 2021, Istanbul, Turkey (online).
- 9. Rachid ZENTAR, **Hongwei WANG**, Dongxing WANG. Modeling of the maximum dry density of the treated dredged sediments. 40èmes Rencontres Universitaires de Génie Civil. (Revisions)
- 10. **Hongwei WANG**, Rachid ZENTAR, Dongxing WANG. Compaction and compression strength properties of the solidified dredged sediments with various binders. 40èmes Rencontres Universitaires de Génie Civil. (Revisions)

Content

List of Figures

List of Tables

General introduction

Context

Global warming and climate change caused by Greenhouse Gases (GHG) have become the most pressing challenges worldwide [1]. CO_2 is the main part of GHG. Thus, as the world's leading economic power, the European Union established the goal toward the circular economy. The goal is to eliminate the linear economy paradigm of "extract-create-consume-dispose" and reduce the environmental effect of economic activities [2]. The circular economy follows the 3R approach: reduce, reuse and recycle.

Preventing waste generation and improving waste management play a vital role in the circular economy model. Dredged sediments are regarded as a typical waste [3]. With the rapid growth of urbanization and industrialization, many riverways and ports construction and maintenance activities are carried out each year, which produce a huge volume of dredged sediments. Every year, the volume of the dredged sediments is about 160 million m^3 in China [4] and more than 50 million m^3 in France [5]. Therefore, faced with such a huge volume of sediments waste, the scientific and reasonable method of sediments management is mandatory to diminish the potential environmental risks. Under the circular economy concept, reusing dredged sediments as an effective material in civil engineering is a promising method.

The construction industry consumes large amounts of natural aggregate materials. There are more than 400 million tonnes of aggregate materials used for the construction industry in France every year [6]. The aggregate materials consumption in China is approximately 20 billion tonnes per year [7]. However, obtaining natural aggregates is more and more difficult to face such severe environmental problems. Thus, the stabilization/solidification (S/S) of the dredged sediments would be a helpful novel eco-friendly resource to replace the natural aggregates in construction engineering.

The construction industry is one of the important contributors to CO_2 emissions. In the European Union, construction activities consume nearly half of the total energy consumption and contribute above half of all CO_2 emissions released into the atmosphere [8]. In China, the construction sector consumes more than 25% of total

energy consumption [9] and produces exceeding 1/3rd of the total CO_2 emissions [10]. Ordinary Portland Cement (OPC) is widely regarded as the most extensively used construction material in the construction industry, owing to its multiple benefits, durability, property stability and low price. However, it's well-known that OPC manufacturing has significantly contributed to CO_2 emissions. The raw materials (such as limestone) and the fuel-burning at about 1450°C are the primary sources of CO_2 emissions in the OPC manufacturing process [11]. Cement industry-related CO_2 emissions are estimated to account for 5–7% of total CO_2 emissions worldwide [12]. The prediction of global cement demand from 2015 to 2050 by the International Energy Agency (IEA) [13] indicated that the global cement demand is gradually increasing by the year. Although, the proportion of China may decrease from above 50% now to roughly 30% by 2050. As a result, low carbon and sustainable cement are being researched and developed to solve this serious challenge worldwide.

Based on the above analysis, it would be interesting to reuse the low carbon and sustainable binder-treated dredged sediments in road construction.

Objective and organization of this manuscript

This study was focused on three original objectives:

(i) The first objective is to study the rheological behavior of the dredged fine-grained sediment, to improve the understanding of sediment, particularly the pipeline transport of dredged sediments.

(ii) The second objective is to solidify the dredged marine sediments with the selected low carbon and sustainable binder for road construction. The investigation of the engineering properties, microscopic mechanisms and environmental properties of the treated sediments is carried out, to verify the effectiveness of using the selected novel binder to treat the dredged sediments in road construction. The low carbon and sustainable binder is selected by SWOT analysis first.

(ii) The third objective is to develop simple statistical models in order to enhance and optimize the valorization of the dredged sediments. This model allows determining an approach to predict the compaction parameters of the treated dredged sediments using the properties of raw sediments and the type and dosages of binders.

The results of this research are presented in this manuscript. The manuscript is

organized into six chapters.

The first chapter presented a literature review on the basic concepts of the dredged sediments, the valorization way of the dredged sediments in civil engineering and the different binders. From this literature review, the main research objectives were defined.

In the second chapter, the basic physical, chemical and environmental characterizations of raw dredged sediments were first studied. After, the used green and low carbon binder in this study was chosen with the SWOT (Strengths, Weaknesses, Opportunities and Threats) analysis. In the end, the basic physical and chemical properties of the used binder were clarified.

Chapter three is devoted to the rheological characterization of fine-grained sediments. First, artificial fine-grained sediment (kaolinite with tap water) was used to avoid the effects of natural sediments' heterogeneity in such tests. The measured yield stress was defined and compared with the predicted yield stress by several rheological models. The influence of water to solid (W/S) ratios on yield stress and plastic viscosity was also discussed. In the end, the same protocol on natural dredged sediments from Dunkirk port was performed, the results were compared with the finding of artificial sediments.

Chapter four compared the performance of the treated dredged sediments with the OPC/CSA single binder, especially immediate California Bearing Ratio (I-CBR), unconfined compressive strength, splitting tensile strength and elastic modulus. Besides, the microscopic mechanism and environmental characterization of the OPC/CSA treated sediments were investigated. These parameters are important for evaluating the potential use of the treated sediments as road materials.

Chapter five focused on the properties of the treated dredged sediments with the OPC-CSA composite binder. The compaction, I-CBR, unconfined compressive strength, splitting tensile strength and elastic modulus tests were carried out on the OPC-CSA treated sediments. These results were compared with the OPC/CSA single binder treated materials. In addition, chemical and environmental tests were conducted to further understand the OPC-CSA treated sediments behavior. Another interesting work in this chapter is that the simplified carbon footprint for the used OPC/CSA single and OPC-CSA composite binders was calculated and compared.

In chapter six, a database about the compaction properties (Maximum Dry Density (MDD) and Optimum Moisture Content (OMC)) of the treated dredged sediments, was first established from literature. The second step was to analyze the database with a statistical approach. The third step was to develop models to predict the MDD and OMC of the treated dredged sediments with the basic physical parameters of raw sediments and treatment binder types and quantities. Furthermore, the variance and residual of the proposed models were analyzed. The proposed models were validated with new data and compared with previous models from the literature.

Last, general conclusions are made, along with some considerable perspectives.

Chapter 1 Literature review

1.1 Introduction

As the concept of sustainable development and the circular economy became more and more popular, people began to pay attention to the proper management of dredged sediments. The traditional solutions to manage dredged sediments, such as land disposal and ocean dumping, are gradually abandoned due to the environmental impacts. Stabilization/solidification (S/S) has been one of the most popular approaches to recycling sediments, due to the advantages of low cost, time efficiency, and high compatibility. However, the most frequently used binder, Ordinary Portland Cement (OPC), has significant environmental impacts, high energy consumption and high CO_2 emissions. Therefore, developing low-carbon and green binders to replace the OPC used for the S/S of dredged sediments is important to reduce CO_2 emissions.

This chapter can be divided into three parts. The first part presents the definition, origin and composition of the sediment. The dredging operation is also discussed. The pipeline transport of sediments after dredging has become an essential method during dredging and sediments management. The rheological property is an important factor affecting the resistance of pipeline transport. Meanwhile, it is an important parameter for engineering applications of pipeline transport technology. The dredged sediments' regulations and valorization of sediments in civil engineering could help us choose the best method to reuse and manage the dredged sediments. The second part of this chapter analyzes the properties of different types of binders, hoping to help find a more green and environmentally friendly novel binder with excellent performance, that could be used for the S/S of dredged sediments in road engineering. In the end, the third part introduces a few modeling works of the dredged sediment treatment and management. These modeling works could provide a better way to optimize the valorization of dredged sediments.

1.2 Basic concepts of dredged sediments

1.2.1 Definition

Sediment is mainly a natural mineral matrix formed by the weathering and erosion of

bedrocks under water, climatic and biotic factors. It is transported by wind, water or gravity force. It is deposited by sedimentation even at long distances from its origin [14]. Schneider et al. [15] stated that the sediment is a material derived from erosion, transported and deposited by watercourse. The formation of sediments is related to the process that the organic or mineral particles stop moving and settle during suspension and transit.

The particle size distribution of the sediments is very variable. It depends on origin, transport type, sedimentary environment and climate [16]. Typically, the sediments could be classified according to the particle size distribution. Table 1-1 lists the usually used particle size classification of sediments.

It can be concluded from Table 1-1, that the coarse fractions of sediments consist of sand (63 μm -2 mm), gravels and cobbles (2 mm - 20 mm), and pebbles (> 20 mm). The sandy sediments have low cohesion and insignificant contact surface. Due to the prevalence of clay minerals, the fine-grained fractions have larger cohesion, high surface area and negatively charged surface [17]. These characteristics of the fine size particles give them great adsorbing power for metallic contaminants. This explains the presence of the majority of pollutants and organic matter in this fine fraction [18].

Table 1-1 Particle size classification of material.

Particle size	Classification
> 20 mm	Pebbles
2 mm-20 mm	Gravels and cobbles
63μm-2 mm	Sand
2μm-63 μm	Silt
< 2 μm	Clay

1.2.2 Origin and types

Figure 1-1 shows the origin of sediment. Generally, it could be classified into two broad categories according to environments of deposition: land sediment and marine sediment. Land sediment is usually from the river, lake, canal, etc., while marine sediment is generally from the deep sea, delta, beach, etc.

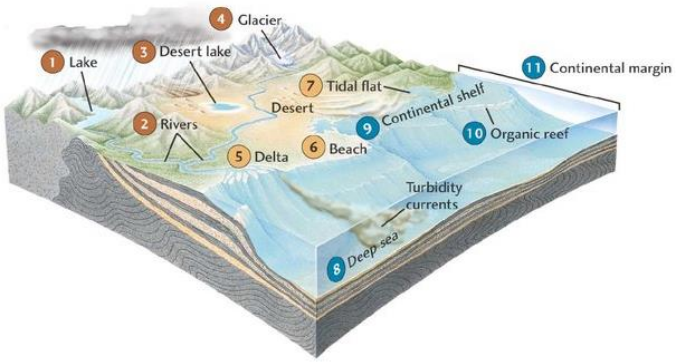

Figure 1-1 Depositional environments: the number (1,2,3,4), (5,6,7) and (8,9,10) indicate respectively the origin of sediments, the different types of transported and where the sediments are deposited in the sea [19].

1.2.3 Dredging

Dredging removes sediments and debris from the bottom of lakes, rivers, harbors and other water bodies [20]. It can effectively maintain the navigability of waterways or harbors, ensure the safe passage of boats and ships, improve the environmental quality of the water body. There are many regular dredging activities worldwide every year. These dredging activities (Figure 1-2) produce many dredged materials. Every year, the volume of dredged sediments is about 160 million m^3 in China [4] and more than 50 million m^3 in France [5].

Figure 1-2 Dredging activity [21].

1.2.4 Composition of dredged sediments

The composition of the sediments is complex. As shown in Figure 1-3, the composition of the sediments includes the mineral phase, organic phase, liquid phase and pollution phase [22-24].

- Mineral phase (silicates, carbonates).
- Organic phase.
- Liquid phase (generally is water).
- Pollution (nutrients, organic and heavy metals).

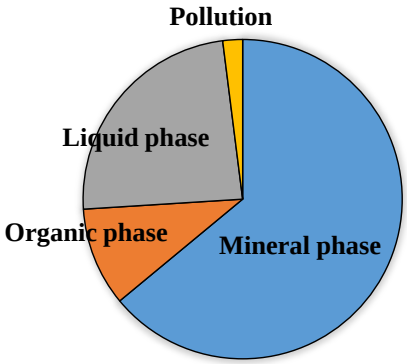

Figure 1-3 Composition of the sediments [25].

1.2.4.1 Mineral phase

The mineral phase consists mainly of minerals from the earth's crust and shellfish debris. It primarily consists of carbonates and silicates. The carbonates present mainly in the sediments are Calcite ($CaCO_3$), Magnesite ($MgCO_3$), Dolomite ($CaMg(CO_3)_2$), Sodium carbonate ($Na_2CO_3.10H_2O$) and Siderite ($FeCO_3$) [26]. The quartz (SiO_2) and clay minerals are the typical silicates in sediments. The latter is, in fact, responsible for multiple physicochemical phenomena of the sediments. The clays are composed of silicate molecules of hydrated calcium with phyllite morphology (in layers: kaolinite, illite, smectite, chlorite) or fibrous (sepiolite, attapulgite, palygorskite). The structure in layers results in fixing water or microparticles [27].

1.2.4.2 Organic phase

Organic matter is another important sediment component, that occupies from nearly zero to more than ten weight percent of the sediment. The organic matter in sediment results from the activities of living organisms. In general, the organic phase of the dredged marine sediments is from marine and terrestrial sources (Figure 1-4), most are from the marine environment (more than 50%) [28] [29].

- The marine organic compounds are from the remains of organisms, such as plants, animals and aquatic microorganisms (plankton, meiofauna and bacteria) rich in nitrogen. The chemical components are predominantly proteins (amino acids),

carbohydrates (sugars) and lipids.

- The terrestrial organic matter is largely brought by rainfall to the river or marine environment, either dissolved or particulate. The terrestrial organic matter consists of living biomass, plant litter and soil organic matter. The latter is largely composed of this living terrestrial biomass's highly altered and degraded remains, such as plant debris, micro-organisms, humic, fulvic and humic acids.

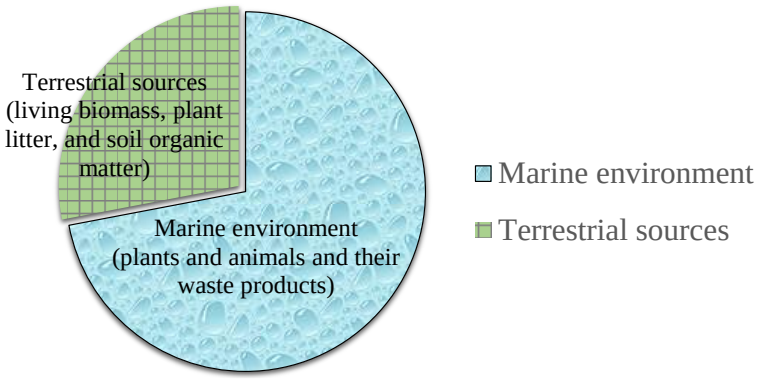

Figure 1-4 Organic matter of the dredged marine sediments [28] [29].

1.2.4.3 Liquid phase

The liquid phase is a very important component of the sediment. However, it is usually a very variable component fraction of the sediments, depending on several factors, such as the dredging conditions and the position of the deposits.

Usually, the water of the sediments has different types:

- Free water: is the water filling the macro-porosities of the sediments. It is free to circulate and percolate under the action of gravity.
- Capillary water: is held in pores that are small enough to hold water against gravity.
- Bound water: is attached to the surface of the sediment grains by intermolecular forces.
- Constitution water: water present in a molecule that cannot be removed without disrupting the molecule.

1.2.4.4 Pollution

The major contaminants of the sediments are heavy metals and organic pollutants [30]. Furthermore, the nutrient (phosphorus and nitrogen) is regarded as contaminants, if

the nutrient values of the sediments are over the environmental standard value [31]. Sediments have the property of absorbing contaminants from water. They are considered contaminated when the concentration of the chemical substances (toxic or hazardous) is sufficiently available to affect human or environmental health [22]. Contaminants are introduced into the aquatic system due to anthropogenic and natural activities. The chemical contamination of the marine sediments is mainly anthropogenic. It can enter the sea through various routes, such as sewage discharge, industrial effluents (pesticides, paints, leather, textile, fertilizers and pharmaceutical), agricultural and urban runoff, deposition of airborne pollutants, dumping of waste and port activities [27, 32].

1.2.4.4.1 Heavy metals

Heavy metals pollution is a ubiquitous, persistent and complex environmental issue. Generally, heavy metals are present at a low level as natural constituents of the marine and freshwater environments [33]. Sediments are known to accumulate metals up to several orders of magnitude higher than in the water [34]. The levels of these heavy metals increased due to human activities (mine drainage, offshore oil and gas exploration, industrial and domestic effluents, agricultural runoff and acid rain) in water systems and eventually incorporated into aquatic sediments [35]. At trace levels, elements such as Fe, Mn, Ti, V, Cr, Co, Ni, Cu, Zn, As, Mo, Sn and Sb are essential for living organisms but toxic in high doses. Other elements (Pd, Ag, Cd, Pt, Au, Hg and Pb) are harmful to living organisms even at low concentrations.

1.2.4.4.2 Persistent organic pollutants (POPs)

The main persistent organic pollutants (POPs) encountered in the sediments are: polycyclic aromatic hydrocarbons (PAHs) (e.g., naphthalene and phenanthrene), phenolic compounds (e.g., phenol) and chlorinated derivatives (polychlorinated biphenyls (PCBs)). The PCBs were used before the end of the 1970s as additives in paints, insulators for electrical equipment. The PAHs present in the environment can be due to biosynthesis, pyrolysis of organic matter, oil spills, or the use of fuels fossils. The tributyltin (TBT) is an active ingredient of antifouling paints to protect ship hulls. Other compounds are also found in the sediments, such as dioxins, organochlorine pesticides, organophosphorus pesticides and endocrine disruptors [36, 37].

1.2.4.4.3 Nutrients

The nutrients are elements or compounds that are necessary for organisms' growth and survival. Most living cells in water need many nutrients, such as phosphorus, carbon,

calcium and potassium. The most important nutrients are phosphorus (P) and nitrogen (N) compounds. These nutrients are stored in the sediments for short or long terms during the natural cycle. The environmental standard values of the P and N are 600 mg/kg and 550 mg/kg [31]. If the nutrient values of the sediments are over these limits, suggesting that the sediments are polluted by phosphorus and nitrogen. The high nutrient levels from the sediment could provide necessary nutrition for phytoplankton, thus accelerating eutrophication and generating deleterious consequences in the aquatic ecosystem [31]. The nutrients at the origin of the eutrophication of environments come from municipal and rural waste and water, agriculture, industrial waste and aquaculture [38] [39].

1.2.5 Pipeline transport and rheological properties of the dredged sediments

1.2.5.1 Pipeline transport of the sediments after dredging

As shown in Figure 1-5, the three important steps of dredging activities are excavation, transport and disposal of sediment [40]. Each step requires particular technologies. Ocean dumping and land disposal are the most widely used disposal method of sediments. Usually, pipelines are used to transport the dredged sediments onto land for land disposal. This process includes loading the sediments into the hopper, then pumping them to land through the pipeline. Besides, reclaiming land from the sea is also an effective way to dispose of dredged sediments. The pipeline transport of the dredged sediments is also a common method for this reclaiming land. Therefore, the pipeline transport of the dredged sediments has become an important method during the dredging and the reclaiming land.

The resistance along the pipeline during pipeline transport is affected by many factors. Among them, the rheological property of the sediments is an important factor affecting the resistance of pipeline transport. Thus, investigating the rheological properties of the sediment can provide a more comprehensive and detailed understanding of the inherent characteristics of the sediments. Besides, it could provide scientific support for the pipeline transport of the sediments.

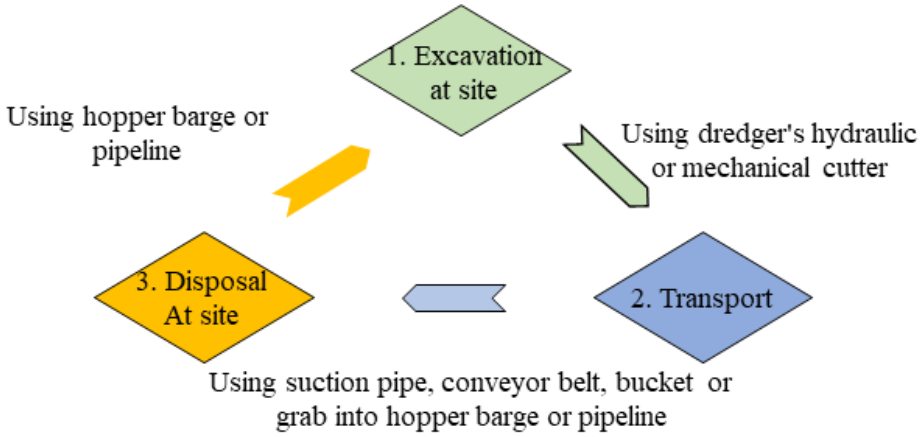

Figure 1-5 Stages of dredging [40].

1.2.5.2 Rheological properties of the sediments

The basic rheological properties of the fine sediments can be expressed by some parameters, such as the shear stress, shear rate, thixotropy, viscosity and yield stress.

The flow properties of the fine sediments are usually expressed by rheological curves in which shear stress and shear rate are variables. The viscosity of the fine sediments represents the resistance factor of the fine sediments in response to deformation. The viscosity of the fine sediments is not constant, but a function of the shear rate. The apparent viscosity is the ratio of the shear stress to the shear rate. Generally, the fine sediments exhibit shear-thinning behavior. That is, its viscosity decreases with the increase of the shear rate.

Yield stress is defined as the minimum shear stress that must be applied to the material to initiate flow. Specifically, there are two kinds of yield stress: static and dynamic [41] [42]. The steady-state flow curve is frequently used to calculate the dynamic yield stress. The dynamic yield stress is regarded as the shear stress when the shear rate is zero [41]. When the applied shear stress is lower than this value, the material shows a solid-like behavior (no flow, no permanent deformation). Thus, this minimum stress to sustain or terminate the flow of the material, is commonly called dynamic yield stress. The dynamic yield stress is widely used because the steady-state flow curve is a convenient measurement method.

Meanwhile, the critical value of shear stress corresponds to a state before the structure is broken down. Once the shear stress is larger than the critical value, the material appears the flow [43]. This is defined as the static yield stress. The static yield stress measurement involves incrementally increasing stress or strain until it exceeds the

critical value, the material begins to flow. Usually, the static yield test is performed by shearing the sample at a very low and constant shear rate. The peak value of stress is obtained before the flow of material [42], this peak value is defined as the static yield stress.

Little research about the rheological analysis of cohesive sediments has been reported. Van Kessel and Blom [44] compared the rheological properties of natural and artificial muds, they concluded that both materials showed yield stress and strong shear-thinning behavior. Faas and Wartel [45] reported the rheological behavior of the dense near-bottom suspensions from the Eckernforde in Germany and Kieler Forde bays of the Baltic Sea. They found that the differences in dense suspensions' yield stress and flow behavior result primarily from the grain size distributions. Soltanpour and Samsami [46] investigate the rheological behavior of the kaolinite and Hendijan mud, the comparisons of the behavior of the natural Hendijan mud with commercial kaolinite show rheological similarities. Yang et al. [47] present the findings that the rheological properties of the sediments depended not only on the magnitude of the shear load but also on its duration. Yang et al. [48] also investigated the rheological characteristics of three different cohesive sediments from the Yangtze River, the shoal of the Hangzhou Bay and Yangcheng Lake of China. The results revealed the three different deformation regions in the flow curves obtained from the shear rate sweep tests. Xu and Huhe [49] studied the rheology of mudflows at Lianyungang in China. They found that the sediments' volume concentration affects both the steady and dynamic rheological properties. Shakeel et al. [50] investigated changes in the rheological properties of the mud from along the river in the Port of Hamburg, Germany. They confirm that the fluid mud layer exhibited relatively small yield stress values and weak thixotropic behavior in all the locations where it was observed.

The above research reported the rheological analysis of the sediments from different parts of the world. Including the sediments from the Caland channel in Netherland [44]; the Eckernforde [45] and the Port of Hamburg in Germany [50]; Kieler Forde bays in the Baltic Sea [45]; the northwest of the Persian Gulf [46]; the beach in Singapore [47]; the Yangtze River [48], the shoal of the Hangzhou Bay [48], Yangcheng Lake [48] and Lianyungang of China [49]. Besides, other literature reported the rheological analysis of the sediments from the Port of Santos, the Port of Itajaí, the Port of Rio Grande and the Amazon south navigation channel in Brazil [51] and the Chorfa dam in Algeria [52]. However, there has been no detailed investigation of the rheological analysis of the sediments from the Port of Dunkirk in France,

although this Port is very important in France.

Although various studies have been reported about the rheological properties of the sediments, most of the research is based on steady measurement. Only a few authors studied the rheological properties of the sediments by combining both steady and dynamic measurements. In fact, the dynamic measurement is a useful analysis method to determine the viscoelasticity properties of the sediments, as it is supplementary to a better understanding of the sediments rheology in the static condition. It can provide meaningful insight into the technical matters in the sediment treatment process, such as mixing and pumping. In addition, based on the literature reviewed, it is shown that the yield stress of the sediment is mainly obtained by fitting experimental data with various rheological models. Whether the yield stress obtained is correct is completely dependent on the model's applicability and the rheological data's reliability. Therefore, a more direct and accurate method is needed to determine the yield stress of the sediment.

Hence, it’s necessary to evaluate the change in the static and dynamic shear rheological properties of the fine-grained sediments, especially for the sediments from Dunkirk Port.

1.2.6 Regulations of dredged sediments

In the context of sustainable development, the dredging operations and management of the dredged sediments are subject to increasingly strict regulations. As shown in Figure 1-6, several regulations involve dredging operations and the management of the dredged sediments at international and national levels.

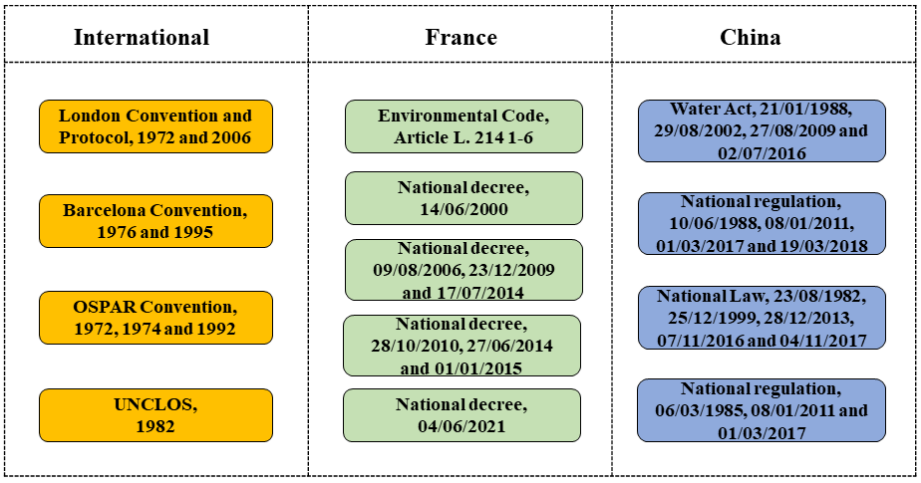

Figure 1-6 Main regulations of dredged sediments management.

1.2.6.1 International regulations

At the international level, the four important international regulations involving dredging operations and dredged sediment management should be noticed, including:

- **London Convention and Protocol:** The "Convention on the Prevention of Marine Pollution by Dumping of Wastes and Other Matter 1972" (often known as the "London Convention"), which has been in force since 1975, is one of the first global conventions to protect the marine environment from human activities. This Convention had 89 members until September 2016. On 17 November 1996, a special meeting of the Contracting Parties adopted the "1996 Protocol to the Convention on the Prevention of Marine Pollution by Dumping of Wastes and Other Matter, 1972," which is to replace the 1972 Convention, subject to ratification. The 1996 protocol has effectively moved the scope of the original London convention landwards, relating it to the policy and management issues of land and sea waste disposal.
- **Barcelona Convention:** The " Convention for the Protection of the Marine Environment and the Coastal Region of the Mediterranean," originally the "Convention for the Protection of the Mediterranean Sea against Pollution," is a regional convention adopted in 1976 to prevent and abate pollution in the Mediterranean Sea from ships, aircraft and land-based sources. It is also known as the "Barcelona Convention." It includes but is not limited to dumping, run-off and discharges. Signers agreed to cooperate and assist in dealing with pollution emergencies, monitoring and scientific research. The convention was adopted on 16 February 1976 and amended on 10 June 1995.
- **OSPAR Convention:** The "Convention for the Protection of the Marine Environment of the North-East Atlantic" or "OSPAR Convention" is the current legislative instrument regulating international cooperation on environmental protection in the North-East Atlantic. The "OSPAR Convention" was concluded in Paris on 22 September 1992. It combines and updates the "1972 Oslo Convention" on dumping waste at sea and the "1974 Paris Convention" on land-based sources of marine pollution.
- **UNCLOS**: The “United Nations Convention on the Law of the Sea (1982)” is an international agreement that establishes a legal framework for all marine and maritime activities. Until June 2016, there were 167 countries and the European Union are members of this Convention. Article 210 is about pollution by dumping.

It shall adopt laws and regulations to prevent, reduce and control pollution of the marine environment by dumping.

1.2.6.2 French regulations

In France, all the activities that involve dredging operations and dredged sediment management are subject to various national decrees and laws. The typical French regulations are:

- **Environmental code:** Dredging operations are subject to declaration or authorization from the prefect (Articles L. 214 1-6).
- **National decree of June 14, 2000:** This regulation relates to the conditions and standards of using marine or estuarine sediments in the natural or port environment.
- **National decree of August 09, 2006:** "The levels to be taken into account during an analysis of discharges into surface water or marine sediments, estuaries or extracts from watercourses or canals," defines the reference thresholds N1 and N2 for eight heavy metals and seven congeners of PCBs and tributyltin. After, the Ministerial Decree of 23/12/2009 set TBT thresholds, the Ministerial Decree of 17/07/2014 set the thresholds for 16 types of PAH.
- **National decree of October 28, 2010:** "Inert waste storage facilities," defines the thresholds to be respected for the physical parameters (pH, temperature, etc.), in total content (TOC, BTEX, etc.) and on leachate (metals, chlorides, phenol indices, etc.). Some articles of this decree were subsequently repealed or consolidated by the Decrees of 27/06/2014 and 01/01/2015.
- **National decree of June 4, 2021:** setting the criteria for exiting waste status for excavated soil and sediments prepared for use in civil engineering.

1.2.6.3 Chinese regulations

Currently, China promulgated laws and regulations involving the dredging operations and the dredged sediment management at the national level. Below is some information about these national regulations.

- **Water Act January 21, 1988:** The "Water Law of the People's Republic of China," revised on August 29, 2002, August 27, 2009 and July 2, 2016. River dredging belongs to river channel improvement and river sand mining. Article 39 of the "Water Act" expressly stipulates that the state implements the sand mining

permit system in rivers, the State Council of China formulates the implementation methods.

- **National regulation of June 10, 1988:** The "Regulations of River Management the People's Republic of China" was revised on January 8, 2011, March 1, 2017 and March 19, 2018. Article 25 states: the following activities within the scope of river management must be reported to the river competent authority for approval: sand mining, soil extraction, gold panning, disposal of sand and gravel or sediment.
- **Law of August 23, 1982:** The "Marine Environment Protection Law of the People's Republic of China," revised on December 25, 1999, December 28, 2013, November 07, 2016 and November 4, 2017. Article 38 states that units that need to dump wastes must apply with the state administrative department of marine affairs. The dumping may be carried out only after the department has permission.
- **Regulation of March 06, 1985:** The "Regulations of the People's Republic of China on control over dumping of wastes in the sea waters," revised on January 8, 2011 and March 1, 2017. Article 11 states: Dumping of dredged sediment requires a permit.

1.2.7 Valorization of sediments in civil engineering

1.2.7.1 Various valorization methods

Because of the main composition of sand, silt and clay in the dredged sediments, the valorization of sediments in civil engineering field has significant economic and environmental benefits. As shown in Figure 1-7, several recent studies have successfully reused the dredged sediments in several civil engineering sub-fields, such as: road [53], concrete/ mortar [54-59], block [60] and brick [61], aggregates [62], clinker and Supplementary Cementitious Materials (SCM) [63].

For the valorization of dredged sediments in concrete/mortar, the dredged sediments are transported from the dredging site to the treatment factory first. Then, the pre-treatment process, such as grind, high temperature [54] [64] or chemical reagent [65], is carried out to remove or reduce organic matter and activate clay minerals. This process increases the cost of the sediments transport and treatment, costs large extra energy and causes extra environmental problems [66] [67]. Besides, the sediments normally only could replace 0-25% cement in concrete/mortar [64] [65].

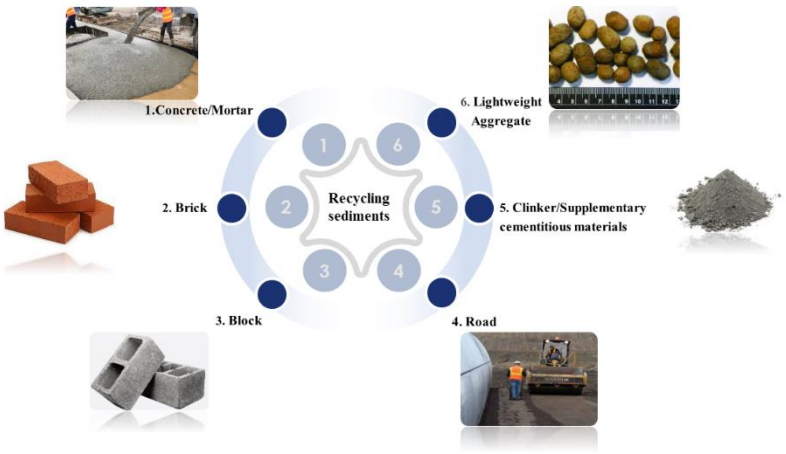

Figure 1-7 Valorization of dredged sediments in civil engineering.

Table 1-2 gives a simple comparison of various potential valorization methods, based on the technical, economic and environmental impact.

For the valorization of dredged sediments in brick, the dredged sediments still need to be transported from the dredging site to the treatment factory first. This step increases the cost of sediment transport. Besides, producing bricks must be fired at high temperatures [61] [68]. From the view of sediment treatment, this process also costs large extra energy and causes extra environmental problems. Although the dredged sediments could replace 0-100% natural clay soil in brick [68] [69], due to the limited outputs of brick products in the factory, it could only reuse a limited volume of dredged sediments.

For the valorization of dredged sediments in the block, the sediments don't need pre-treated with high temperature or chemical reagent before being reused, although they need be transported to the treatment factory first. These studies only use dredged sediments to replace the fine fraction of the raw materials to produce the block. Due to the outputs of the products or technical limitations, this method could reuse a limited volume of dredged sediments.

It's possible to make lightweight aggregates by sintering dredged material. However, this valorization method needs first to transport the dredged sediments to the factory, then pellet making and sintering with high temperatures [70] [71]. This process costs extra energy and causes extra environmental problems.

For the valorization of dredged sediments in the conventional manufacture of the Ordinary Portland Cement (OPC) clinker, the dredged sediments still need to be transported from the dredging site to the treatment factory first. After, it needs to be

ground and sieved, then calcined with limestone at 1450°C in the kiln to produce clinkers. This process increases the cost of the sediments transport and grinding, costs extra energy and causes extra environmental problems. The sediments could be used to replace only 1-15% of raw material to produce clinkers [5] [72].

Some research uses the dredged sediments as Supplementary Cementitious Materials (SCM) by the flash calcination method. Before calcination, the dredged sediments must be transported to the treatment factory and dried until a constant mass. After, the dried sediments must be ground and sieved, then calcined in the flash calciner. This process increases the cost of sediments treatment, costs extra energy and causes extra environmental problems. However, this flash calcination process usually is carried out with a temperature of 600-1100℃ and a few tenths of a second time [63] [73].

In comparison, the valorization of dredged sediments in road construction could achieve in-site treatment without transport. The sediments could be reused as road materials, after being treated only with a small amount of binder. This process doesn't need extra pre-treatment for the sediments. It could reuse a large volume of dredged sediments in road engineering. Thus, the application in road construction is one of the most effective ways to recycle dredged sediments to the greatest extent.

Table 1-2 Comparison of various valorization methods.

Valorization methods	Potential valorization volume	Valorization cost	Environmental impact
Concrete/Mortar	Low	High	High
Brick	Medium	High	High
Block	Medium	Medium	Medium
Lightweight aggregate	Medium	High	High
Clinker (kiln)	Low	High	High
SCM (flash calcination)	Low	Medium	Medium
Road	High	Low	Low

1.2.7.2 Valorization of sediments in road engineering

Several studies have proved the feasibility for the valorization of marine or fluvial sediments in road engineering [74-76]. Studying sediments' physical, geotechnical, mechanical and environmental characterization is essential for their recycling in road engineering. Laboratory study shows the feasibility of the cement- and lime-treated dredged sediments for beneficial use as road material [74]. Yoobanpot et al. [77] have

a multiscale laboratory investigation for the mechanical and microstructural properties of the dredged dam sediments stabilized with cement and fly ash. The results indicate that the combination of cement and fly ash is more effective for stabilizing sediments than only cement or fly ash. Li et al. [78] use the incinerated sewage sludge ash (ISSA) to replace the Ordinary Portland Cement (OPC) and lime to improve the properties of the marine sediments as fill material. The solidified sediments complied with the acceptance criteria for the engineering fill applications. The lime–ISSA binder performs better than the OPC–ISSA binder.

At Dunkirk harbour of France, a full-scale test road was built in 2005 with dredged marine sediments [76]. This test road is 50 m long and 6 m large. The test road is parallel to the main road used mainly by trucks to transport goods and sand. The construction of the test road has proved the feasibility for the reusing of the treated sediments as road materials. In 2012, a re-constructed road was developed with the fine dredged material (mainly silty material). This road is over 550 m in length and is situated in the east harbor of Dunkirk (Figure 1-8) [53]. This road is the first road built based on marine sediments in France. However, the studies are very limited at the industrial level. No real application has been made to more than one kilometer to a significant extent.

Figure 1-8 Build Freycinet 12 experimental road with solidified sediments at Dunkirk, France [53].

In China, the first large-scale engineering application of solidified dredged sediments was to produce fill materials in 2006 (Figure 1-9) [79]. This project treated approximately 1.8×10^6 m^3 of dredged sediments from Taihu Lake with OPC. The compressive strength measured after a 28-day in-situ curing time was 137.8 kPa. This value was completely satisfied with this engineering-designed request (75 kPa). After two years (after project completion), the mean compressive strength achieved 236.6 kPa. The Wuxi Taihu City Science and Technology Industrial Park has been established on top of the solidified dredged sediments storage yard.

Figure 1-9 Using solidified dredged sediments as fill materials at Wuxi, China: (a) dredged sediments before treatment; (b) used machine for solidification; (c) the large-scale working field for treatment of sediments; (d) backfilling with treated sediments; (e) construction activities on the backfilled treated sediments; (f) the project is completed and put into use [79].

Based on the above analysis, the valorization of dredged sediments in road engineering is feasible. Thus, we chose this method to recycle the dredged sediments in this study. However, we can easily find that the most used binder for treating the sediments is the OPC and lime. The manufacturing of these traditional binders usually causes serious environmental problems. With the requirements of sustainable development, more and more green and low-carbon binders are developed in construction engineering. In the next part, we will summarize the properties of the different types of binders, hoping to find a more green and environmentally friendly binder with excellent performance. It could be used for the S/S of dredged sediments in road engineering.

1.3 Basic concepts of different binders

The stabilization/solidification (S/S) of dredged sediments usually uses the Ordinary Portland Cement (OPC) and lime (L). However, some other binders could be used for the S/S, such as the Reactive Magnesium oxide Cement (RMC), Geopolymer (G), Alkali-Activated Materials (AAM) and Calcium Sulfo-Aluminate cement (CSA). In view of these aforementioned different binders, this part summarizes their basic properties, which may be used for the S/S of sediments/soils.

1.3.1 Ordinary Portland cement (OPC)

OPC is the most widely used basic material for civil engineering construction. It's the basic ingredient of concrete and mortar. The OPC is one of the lowest-cost construction materials and is still widely used. The materials (limestone and shales) used for OPC manufacturing are cheap and widely available. The OPC sets and becomes adhesive due to the chemical reaction between the dry ingredients and water. The chemical reaction results in mineral hydrates that are not very water-soluble, so it is quite durable in water and safe from chemical attacks. Thus, the OPC is a cheap and robust binder for treating sediments. The justification has been proved by the efficiency shown over time, low cost, availability and reliability. Wang et al. [74] [80] and Yoobanpot et al. [77] studied the mechanical properties of the stabilized dredged sediments with OPC/OPC-fly ash. Their results indicated that the OPC/OPC-fly ash could effectively stabilize the dredged sediment. Huang et al. [81] compared the mechanical behavior of the intact and the remolded solidified dredged material. They found that the strength difference between the two materials decreases as consolidation pressure increases. Kang et al. [82] evaluated the strength development of the cement-treated dredged sediments under different stages of curing time. They developed two formulas to estimate the strength during the early and later curing stages. Chiu et al. [83] studied the cement-treated dredged materials' yielding and shear behavior.

However, the OPC is caustic. It can cause chemical burns. The powder can irritate, even cause lung cancer with severe exposure. It may contain hazardous components, such as crystalline silica and hexavalent chromium. The production of OPC is usually associated with significant environmental impacts. Such as high CO_2 emissions (0.95 t CO_2/t OPC), high energy consumption (5000 MJ/t OPC) and high non-renewable resources consumption (1.5 t limestone and clay/t OPC) [84]. OPC manufacturing

acts as a significant contributor to anthropogenic CO_2 emissions (5-7%) [12]. Due to the increasing demand for construction, the share of CO_2 emissions attributed to cement production is predicted to increase from 16% to 24% by 2050, demonstrating the urgent need to improve its sustainability [85].

The main components of the OPC include tricalcium silicate (C_3S), silicate dicalcium (C_2S), tricalcium aluminate (C_3A) and calcium aluminate ferrite (C_4AF). The C_3A and the C_3S phases are the most reactive phases, the C_2S reacts more slowly than the other compounds. When the OPC is mixed with water, the hydration of the different components at early times can be written as below.

$$C_3S + H_2O \rightarrow CSH + CH \quad (1\text{-}1)$$

$$C_2S + H_2O \rightarrow CSH + CH \quad (1\text{-}2)$$

$$C_3A + H_2O \rightarrow CAH \quad (1\text{-}3)$$

$$C_3A + C\bar{S}H_2 + H_2O \rightarrow CA\bar{S}H \quad (1\text{-}4)$$

$$C_4AF + C\bar{S}H_2 + H_2O \rightarrow CA\bar{S}H + CH + FH_3 \quad (1\text{-}5)$$

The calcium silicate hydrate (C-S-H), portlandite (CH) and ettringite (AFt) are the main products of the hydration of the OPC and are primarily responsible for the strength of the OPC.

1.3.2 Lime (L)

Lime is a calcium-containing inorganic mineral composed primarily of oxides and hydroxide, usually calcium oxide and/or calcium hydroxide. There are two main types of lime produced, quicklime and hydrated lime. Quicklime is the most frequently used binder. Quicklime is calcium oxide (CaO), produced from limestone calcination ($CaCO_3$) [86]. Global anthropogenic CO_2 emissions from the lime industry are estimated to be around 1% [87]. In fact, the production of 1 t lime involves about 4000 MJ energy consumption and around 0.8 t CO_2 emission. [88] [89]. The temperature of the calcination of limestone is around 850-1200℃. Lime as a building material can be dated back throughout the last 10000 years [90]. However, the introduction of cement in the middle of the 19th century decreased its importance. The revival of lime occurred in the 1970s when developments on the harmful effect of cement on historical buildings emerged [86]. The reactivity of the lime product determines the intended end use of the lime product. Lime products with higher granulometry and reactivity are used in the S/S of sediments/soils, because they are the most cost-effective in most instances.

The hydration of quicklime in contact with water is shown as Equation (1-6). The quicklime reaction product-calcium hydroxide CH with the silica and alumina from clay minerals may cause the pozzolanic reaction, forming C-S-H and C-A-H gels. These gels could bond particles to increase strength.

$$CaO + H_2O \rightarrow CH \quad (1\text{-}6)$$

$$CH + SiO_2 + H_2O \rightarrow CSH \quad (1\text{-}7)$$

$$CH + Al_2O_3 + H_2O \rightarrow CAH \quad (1\text{-}8)$$

Currently, lime is one of the most extensive applications in stabilization/solidification technologies. Wang et al. [91] investigated the geotechnical properties of the lime-treated sediments with a series of laboratory tests, including the unconfined compressive strength tests, standard oedometer tests, direct shear tests and triaxial tests. Todaro et al. [92] found that the high organic matter and fine-grained particles can negatively affect the effectiveness of the lime/OPC-treated dredged sediments in terms of metal immobilization. Federico et al. [93] compared the physical properties of the natural sediments and the cement/lime treated sediments after being cured for four years. Wang et al. [94] proved that the increases of cement/lime content and curing period could reduce the shrinkage and increase the strength of the treated dredged sediments.

1.3.3 Reactive Magnesium oxide Cement (RMC)

RMC is an eco-friendly substitute for traditional OPC [95-97]. Magnesium oxide (MgO) is a white hygroscopic solid mineral that occurs naturally as periclase and is a source of magnesium. The raw materials for MgO production are natural magnesium carbonate and brucite or magnesium chloride from seawater and brines. MgO is produced by the calcination of magnesium carbonate or magnesium hydroxide. Calcining at different temperatures produces MgO of varying reactivity. High temperatures 1500-2000°C diminish the available surface area and produce dead-burned (often called dead burnt) magnesia, an unreactive form used as a refractory. The calcining temperatures of 1000-1500°C make hard-burned magnesia with limited reactivity. Reactive MgO is generally calcinated from magnesite ($MgCO_3$) at a lower temperature (~ 700-800°C) than dead burned MgO [98].

Compared to OPC, less energy is required for the manufacturing reactive MgO (~2400 MJ/t MgO) [98], due to its lower calcination temperature and renewable energy sources can be used. However, despite reactive MgO needing lower production temperatures, the decomposition of $MgCO_3$ releases a higher amount of

CO_2 than limestone [99]. Manufacturing 1 t reactive MgO consumes 2.08 t $MgCO_3$ and induces ~1.4 t CO_2 emissions, higher than OPC [98] [100]. However, when the carbonation capability of MgO is considered, the CO_2 emissions are lower than OPC [99]. The fundamental characteristics of MgO provide its unique performance upon production, hydration, carbonation and other reactions. It has wide-ranging potential applications in waste treatment and cementitious composites [101].

In the hydration process, Mg^{2+} required for $Mg(OH)_2$ precipitation is released from the dissolution of MgO. When the concentration of Mg^{2+} and OH^- in the solution reaches a certain degree of saturation, they begin to nucleate, resulting in close coupling between the precipitation and dissolution reactions [102]. The precipitation reaction of magnesium hydroxide is as Equation (1-9).

$$MgO+H_2O \rightarrow Mg(OH)_2 \quad (1\text{-}9)$$

Some studies have been carried out to treat dredged sediments with MgO. Wang et al. [95] [97] investigate the strength, compressibility and durability behavior of the MgO solidified dredged sediments. Wang et al. [103] use Si-rich minerals and reactive MgO for the stabilization/solidification of contaminated sediment as fill materials. Besides, they [104] also recycled the contaminated sediment into the eco-friendly paving blocks by OPC-MgO binder and carbon dioxide curing.

1.3.4 Geopolymer (G)

Geopolymer is now receiving more attention as an alternative building material. Geopolymer is made from aluminosilicate source materials activated with high alkali solutions [105]. Inorganic, typically ceramic, materials form long-range, covalently bonded, non-crystalline (amorphous) networks. Raw materials used in the synthesis of silicon-based polymers are mainly rock-forming minerals of geological origin, hence the name: geopolymer. Joseph Davidovits coined the term in 1978 and created the non-profit French scientific institution Geopolymer Institute [106]. Geopolymers have excellent potential to reduce the climate change impacts on cement production. However, the CO_2 emissions of geopolymer have been associated with the use of alkali activators. There is significant potential for variability, depending on the production process and the source of raw materials [107]. It's reported that 40-60% less energy is needed to manufacture geopolymer than OPC production [108] [109]. McLellan et al. [110] think an estimated 44-64% improvement in CO_2 emissions over OPC for the geopolymer product.

Geopolymers are framework structures produced by condensation of tetrahedral aluminosilicate units, with alkali metal ions balancing the charge associated with tetrahedral Al. Conventionally, geopolymers are synthesized from a two-part mix, consisting of an alkaline solution and solid aluminosilicate materials. Geopolymerization occurs at ambient or slightly elevated temperatures. The leaching of the solid aluminosilicate raw materials in alkaline solutions leads to the transfer of leached species from solid surfaces into a growing gel phase, followed by nucleation and condensation of the gel phase to form a solid binder [111].

Geopolymers are an element of the push for the sustainable concrete industry, with a much smaller CO_2 footprint than the traditional OPC. The possible advantages of these materials can be a high early and/or final strength, high resistance against chemical attack, the excellent passivation of reinforcement, a very dense microstructure and heat resistance [111]. However, the activators' prices and energy intensiveness (with associated CO_2 emissions) limit the use of geopolymer binders and their potential to replace OPC. For example, NaOH is one of the most used activators, the energy for NaOH production is 20500 MJ/t [112]. Additionally, it is widely known that the widespread uptake of geopolymer technology is hindered by many factors, in particular issues to do with a lack of long-term (20+ years) durability data in this relatively young research field. There are also difficulties in compliance with some regulatory standards in Europe and North America, specifically those defining minimum clinker content levels or chemical compositions in cement [113]. At an ambient temperature of around 25°C, the fly ash geopolymer gains strength slowly. The fly ash-based geopolymer usually requires curing at 40-75°C to obtain reasonable strength. This requirement is difficult for the construction practice in real construction [114]. Some laboratory studies try to use geopolymer to treat dredged sediments. Jaditager and Sivakugan [115] [116] investigated the sedimentation and consolidation behavior of the fly ash-based geopolymer-stabilized dredged sediments. They found that the geopolymer stabilization reduced the duration of the dredged sediments and improved their compressibility, permeability and consolidation characteristics.

1.3.5 Alkali-Activated Materials (AAM)

During the past decades, the development and use of AAM as an alternative to OPC has advanced extremely rapidly. The first use of alkalis as a component of cementitious materials dates back to 1930, when Kuhl studied the setting behavior of

mixtures of slag ground to a powder and a KOH solution. Since then, many studies have been conducted on the alkalis' role in potential cementitious systems. One early milestone was reached in 1940, when Purdon conducted the first extensive laboratory study on the clinker-less cement consisting of slag and NaOH [117, 118]. Since then, much research has been undertaken in this area. They have been commercially produced worldwide for the infrastructure, general construction and paving, nuclear waste immobilization and other applications.

Alkali-activated cement usually consists of two components, i.e., cementing components and alkaline activators. Usually, the caustic alkalis or alkaline salts are the alkaline activators of alkali-activated cement and concrete. In 1980, Glukhovsky et al. [119] classified them into six groups, according to their chemical compositions: Caustic alkalies; Non-silicate weak acid salts; Silicates; Aluminates; Aluminosilicates and Non-silicate strong acid salts. NaOH, Na_2CO_3, $Na_2O{\cdot}nSiO_2$ and Na_2SO_4 are the most widely available and inexpensive alkaline activators. Some potassium compounds have been used in laboratory studies. However, their potential applications could be restricted due to their availability and costs. Various industrial by-products and wastes have been used as the cementing components in the alkali-activated cement and concrete, including granulated blast furnace slag, granulated phosphorus slag, steel slag, coal fly ash, volcanic glasses, zeolite, metakaolin, silica fume and non-ferrous slags [120]. Based on the composition of the cementing component, the alkali-activated cement can be classified into five categories: alkali-activated slag-based cement; alkali-activated Portland blended cement; alkali-activated pozzolan cement; alkali-activated lime-pozzolan/slag cement and alkali-activated calcium aluminate blended cement [121]. The energy consumption and the CO_2 emissions of AAM depend on the raw materials and alkaline activators. It's reported that the AAM offers 30-80% reductions in CO_2 emissions compared to OPC-based concrete [85] [122]. The AAM could save 50-70% energy consumption than OPC [122].

Figure 1-10 depicts the general distinctions between the alkali-activated materials and geopolymers, in terms of the raw material characteristics, activating solutions and reaction mechanisms.

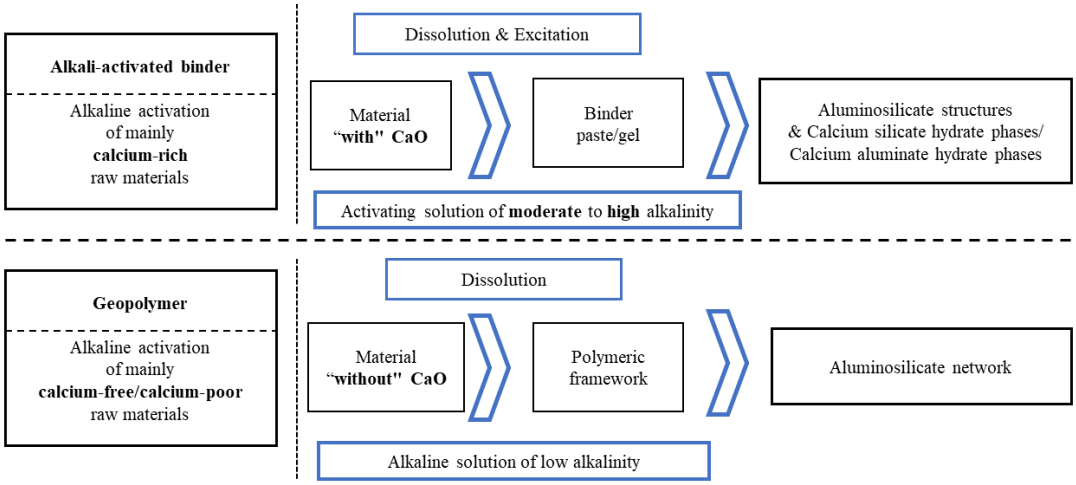

Figure 1-10 Difference between alkali-activated materials and geopolymer [123].

The raw materials related to the manufacturing of OPC, such as limestone and clay, are non-renewable resources. The precursors of the AAM are mainly industrial by-products or wastes. Some of them can be used directly, some may need grinding and some may require calcination or thermal activation at 700-900°C. Thus, it has been identified that the AAMs should have advantages in the sustainable development over the conventional OPC, even when the emissions associated with the production of the activator are taken into consideration. Many studies have used the AAM to solidify sediments. Gu et al. [124] used the alkali-activated cementitious materials to solidify the high organic matter content dredged material. The solidified dredged material can reach the requirement of the roadbed material. Cho et al. [125] measured the mechanical strength, heavy metal leachability and microstructural characterization of the treated dredged sediment with alkali-activated slag. Obana et al. [126] examined the durability properties of the treated marine sediments with pozzolan and alkali-activated binders.

1.3.6 Calcium Sulfo-Aluminate cement (CSA)

The continuous push toward developing sustainable cementitious binders has increased research on CSA cement in the last few decades. The CSA cement was developed in China in the 1970s [127, 128]. The CSA cement is mainly based on yeelimite (C_4A_3S), belite, C_4AF and gypsum in varying ratios. It is a very interesting hydraulic binder for achieving both sustainability and durability.

The production of the CSA cement has lower CO_2 emissions than that of the OPC. In fact, industrial production requires essentially gypsum, bauxite and limestone as raw materials, which are burnt at ~1250°C in a conventional rotary kiln. The kiln

temperature required is 200°C lower than the temperature used for OPC clinker [129]. These starting materials lead to a final clinker based on the quinary system CaO–SiO_2–Al_2O_3–Fe_2O_3–SO_3 and formed by three main minerals: tetracalcium trialuminate sulphate or yeelimite C_4A_3S; dicalcium silicate or belite (C_2S) and calcium sulphate or anhydrite (CS). The minor phases, such as tricalcium aluminate (C_3A), tetracalcium aluminoferrate or brownmillerite (C_4AF), dodecalcium heptaaluminate or mayenite ($C_{12}A_7$) and dicalcium aluminum silicate or gehlenite (C_2AS), can be present. Due to the lower temperatures, the specific CO_2 emissions of the CSA cement are lower than those of OPC, assuming other production conditions are the same [130]. The energy consumption associated with the CSA clinker manufacture accounts for about 2700 MJ/t [131].

Moreover, the lower limestone demand (35-40%) for the manufacture of CSA cement reduces its carbon footprint. The CO_2 emissions derived from electricity consumption for grinding in OPC clinker production are not negligible. The energy savings also occur in the grinding of the CSA clinker compared to the OPC, since the lower firing temperatures lead to the clinker being easier to grind. Altogether, 1 t of OPC clinker production releases 0.95 t of CO_2. The CO_2 emissions of CSA clinker depend on its composition, the value is approximately 0.60 t/t for a typical CSA clinker, which consists of predominantly ye'elimite, belite and smaller amounts of aluminoferrite [132].

Ye'elimite (C_4A_3) is the main constituent of the CSA cement. The hydration products of ye'elimite depend on sulfate quantities. Ye'elimite reacts with gypsum/anhydrite in water according to reaction (1-10) to form ettringite, as the main hydrate phase. When the amount of sulfate is insufficient, ye'elimite hydration forms monosulfoaluminate ($C_4A\overline{S}_3H_{12}$) and gibbsite (AH_3) in the absence of sulfate, according to reaction (1-11) [105, 133]. Belite can hydrate to form strätlingite (C_2ASH_8) at the aluminum-rich environment, according to reaction (1-12). If gibbsite (AH_3) was depleted, according to reaction (1-13), it could take place to form C-S-H gel and portlandite (CH) [134].

$$C_4A_3\overline{S} + 2C\overline{S} + 38H \rightarrow C_6A\overline{S}_3H_{32} + 2AH_3 \quad (1\text{-}10)$$

$$C_4A_3\overline{S} + 18H \rightarrow C_4A\overline{S}_3H_{12} + 2AH_3 \quad (1\text{-}11)$$

$$C_2S + A\mathit{H}_3 + 5H \rightarrow C_2ASH_8 \quad (1\text{-}12)$$

$$C_2S + 2.6H \rightarrow C_{1.1}SH_{1.7} + 0.9CH \quad (1\text{-}13)$$

The commercial CSA cement contains 50-80 wt% C_4A_3S and 30-10 wt% C_2S [127]. It exhibits many interesting properties, such as short setting time, high early strength,

impermeability, sulfate, chloride corrosion resistance and low alkalinity [135-138]. Hence, the CSA cement is mainly used when rapid setting, early strength or shrinkage compensation is required [127]. It has also demonstrated considerable potential in the S/S of hazardous materials, such as low-level radioactive or heavy metal waste, sewage sludge, bottom ash and galvanic sludge [139-141]. Further, some studies found that the OPC-CSA composite cement seems to have more outstanding mechanical properties, due to combining each OPC and CSA cement advantage [11, 139, 142, 143]. However, only a few studies use CSA cement in geotechnical applications, especially ground improvement. For example, it has been proved that the CSA-treated sand has significantly high initial strength, which powerfully indicates that the use of CSA in the geotechnical applications may lead to reduce the construction period and the carbon footprint [144-146]. It's still worthwhile considering treating sediments with CSA-based binder (CSA and OPC-CSA) in road construction.

1.4 Modeling the mechanical behavior of treated sediments

The management of the dredged sediments is a significant challenge for the international ports and the dredging industry. Many scientists are committed to managing these dredged materials with environmentally friendly methods. As shown in Figure 1-7, some potential applications for dredged materials have been suggested in civil engineering. It is to note that, the recycling of dredged sediments as road materials, with the stabilization/solidification (S/S) technology, has become one of the most popular ways. However, these researches and practices for treating the dredged sediments are often based on experience. Indeed, if feasible, using some model tool to assess the beneficial use and behavior of the treated dredged sediment first, could provide potentially valuable information for the optimum management of the dredged sediments. Therefore, it's necessary to develop some models to optimize the valorization of dredged sediments.

Moghrabi et al. [147] developed a model tool to predict the unconfined compressive strength of the treated sediments at 28 d, using the multiple linear regression method. Besides, another model in terms of unconfined compressive strength development of the treated sediments versus time was also developed, based on a least square method. When comparing the measured and predicted values, both models exhibited acceptable accuracies.

Harrington et al. [148] created a financial model tool to evaluate the financial aspect

of the various dredged marine sediment management options for different countries. Figure 1-11 depicts the overview of the developed financial modeling approach for the analysis of dredged marine sediments. The financial model was used in a preliminary analysis for a specific case of the beneficial use of dredged silt in Ireland, which involved wetland construction. This model can be used as a decision support tool by stakeholders in the sector, including ports, engineering consultancies and regulators.

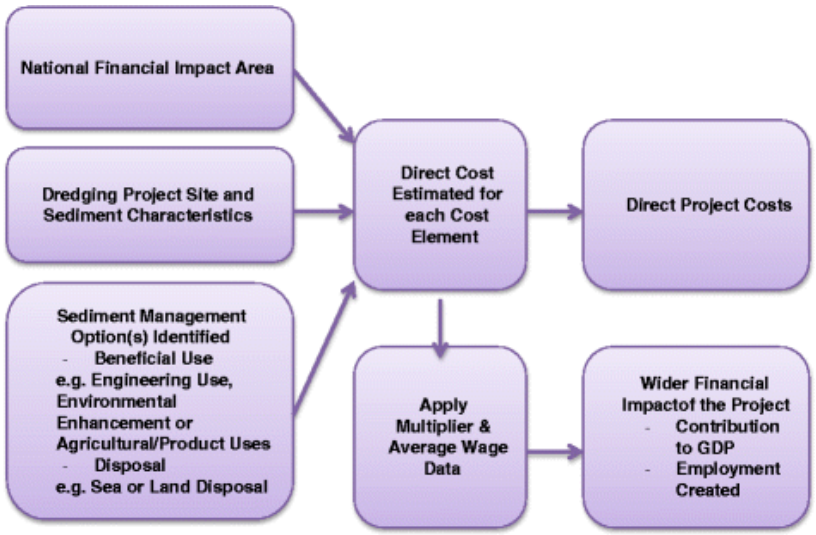

Figure 1-11 Financial modeling approach [148].

In most situations, the design of road pavements requires knowledge of the geotechnical properties of soils, especially the compaction parameters [149]. The compaction parameters are intimately linked to other soil characteristics, such as compressibility, permeability, strength and bearing capacity. The optimal degree of compaction could reduce the potential settlement, increase the bearing capacity and reduce the negative consequences of volumetric changes [150]. Fine-grained soils are generally compacted on-site with tampers and various rollers [151]. However, before the on-site construction, the Proctor compaction test is usually carried out in the laboratory to determine compaction parameters. Figure 1-12 is an obtained typical compaction curve of the raw sediments from the Proctor compaction test. From this compaction curve, it's easy to obtain the two compaction parameters (Maximum Dry Density (MDD) and Optimum Moisture Content (OMC)) at the optimum compaction point. Thus, to reuse the sediments in road construction field, the compaction characteristics of the sediments, such as MDD and OMC, must be obtained from the Proctor compaction test in the laboratory. However, the laboratory compaction test often needs a lot of time, which could cause project delays and cost overruns.

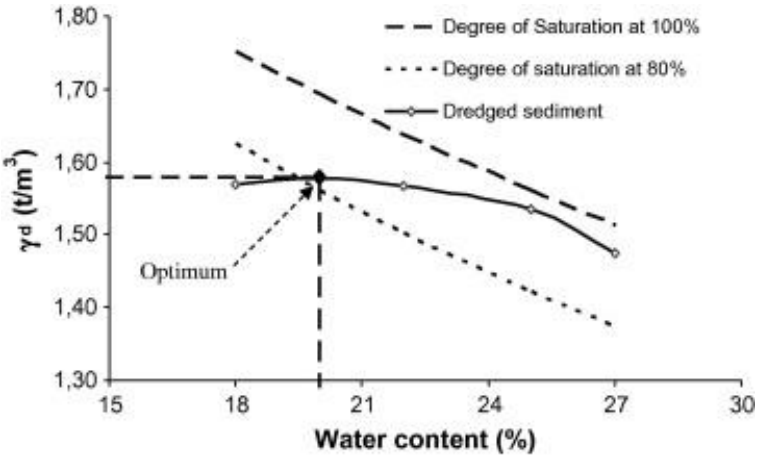

Figure 1-12 Compaction curve of raw sediments [152].

The previous studies indicated that many physical parameters could affect the compaction characteristics of the fine-grained soil, such as the compaction energy, the soil grain size, the Atterberg limits, the addition of binders and so on [153, 154]. Some research has focused on predicting the compaction parameters for fine-grained soil with their physical parameters [155, 156]. Table 1-3 lists these models from the literature for predicting the OMC and MDD. However, the influencing factors for the compaction parameters were not completely integrated into these models. The liquid limit (LL), plastic limit (PL) or plasticity index (PI) were considered for these previous models, while only some models included the compaction energy (E). The particle size distribution (the percentages of sand, silt and clay), the methylene blue value (MBV) and the organic matter content (OM) were not considered.

However, these previous models from the literature are about the compaction parameters of soil. It's still worth developing a model for the compaction parameters of dredged sediments. Try to integrate more of the important influencing factors for the compaction parameters into the proposed model. Such a model allows correlating the compaction parameters with the simple physical properties of sediments and the treatment binder types and quantities, to preliminary assess the suitability of recycling of the sediments in road engineering.

Table 1-3 Prediction models for OMC and MDD of soil in the literature.

Reference	Models	
	OMC	MDD
Blotz et al. [157]	OMC=(12.39−12.21×logLL) ×(3+logE)+0.67×LL+9.21	MDD=(2.27×logLL-0.94) ×(3+logE)-0.16×LL+17.02
Sridharan and Nagaraj [158]	OMC=0.92×PL	MDD=0.23×(93.3−PL)
Saikia et al. [159]	OMC=0.35×LL+0.163×PL+6.26	MDD=21.07-0.119×LL+0.02×PL
Nagaraj et al. [160]	OMC=0.76×PL	MDD=20.82−0.17×PL
Farooq et al. [161]	OMC=0.133×LL+0.02×PI −5.99×(3+logE)+28.60	MDD=−0.055×LL+0.014×PI+ 2.21×(3+logE)+12.84

Note: these models have been modified to keep the same symbols and units. Where OMC is optimum moisture content (%), MDD is maximum dry density (KN/m^3), LL is liquid limit (%), PL is plastic limit (%), PI is plasticity index (%) and E is compaction energy (MJ/m^3).

In addition, it is worth mentioning the statistical approach, especially the Multiple Linear Regression (MLR) techniques. The MLR could estimate the compaction parameters of the treated dredged sediments, by considering the basic physical parameters of raw sediments and the treatment binder types and quantities. The MLR method has been widely used to predict the geotechnical parameters of soils [162-165]. However, there is still lacking relevant research work about the prediction of the compaction parameters for the treated dredged sediments with the MLR approach.

Therefore, it's important to develop models by MLR approach in this study, to predict the compaction parameters (MDD and OMC) of the treated dredged sediments.

1.5 Conclusion

The literature review has shown that the valorization of dredged sediments has become an effective solution to manage the dredged sediments, especially in road construction. Recycling the dredged sediments as road materials could solve the problems related to sediment management and provide a new source of construction materials.

Pipeline transport of dredged sediments has become an important method during the dredging and the reclaiming land. Pipeline transport involves the rheological properties of the dredged sediments. In fact, the rheological property of the dredged sediments is an important factor affecting the resistance of pipeline transport. However, various studies have been reported about the rheological properties of the sediments, from different parts of the world. There has been no detailed investigation of the rheological analysis of the sediments from the Port of Dunkirk in France, in spite of the importance of this Port.

The yield stress of the sediment is mainly obtained by fitting experimental data with various rheological models. Whether the obtained yield stress is correct depends on the model's applicability and the rheological data's reliability. Therefore, research on the change in the fine-grained sediments' static and dynamic shear rheological properties needs to be strengthened. A more direct and accurate method is required to determine the yield stress of the sediment.

Many studies currently focus on the valorization of dredged sediments in road engineering by the stabilization/solidification (S/S) method. However, the most frequently used binders for treating sediments are OPC and lime. The manufacturing of these traditional binders usually causes serious environmental problems. With the requirements of sustainable development, it's urgent to find an alternative binder with low energy consumption and excellent performance, to use for the treatment of dredged sediments. This chapter has summarized the advantages and disadvantages of the different types of binders. In the next stage, we will compare and choose the used green and low carbon binder with SWOT (Strengths, Weaknesses, Opportunities and Threats) analysis. Then, we will characterize the used materials (raw sediments and binders). After that, the mechanical characteristics of the treated sediments with the chosen green and low carbon binder will be investigated, to see if the selected binder is effective.

In most situations of road engineering practice, the design of road pavements and subgrade requires the knowledge of the geotechnical properties of soils, especially the compaction parameters. To reuse the sediments in road construction, the compaction characteristics of the sediments, such as MDD and OMC, must be obtained from the Proctor compaction test in the laboratory. However, the laboratory compaction test often needs much time, which could cause project delays and cost overruns. Therefore, it's necessary to develop a model that correlates the compaction properties with the simple physical properties of sediments and the treatment binder types and quantities,

to be preliminary assess the suitability of recycling the sediments in road engineering.

Hence, this research was focused on three original objectives:

(i) The first objective is to study the rheological behavior of the dredged fine-grained sediment, to improve the understanding of the sediment, particularly the pipeline transport of the dredged sediments.

(ii) The second objective is to solidify the dredged marine sediments with the selected low carbon and sustainable binder for road construction. The investigation of the engineering properties, microscopic mechanisms and environmental properties of the treated sediments is carried out, to verify the effectiveness of using the selected novel binder to treat the dredged sediments in road construction. The low carbon and sustainable binder are selected by SWOT analysis first.

(ii) The third objective is to develop simple statistical models in order to enhance and optimize the valorization of dredged sediments. This allows determining an approach to predict the compaction parameters of the treated dredged sediments using the properties of raw sediments and the type and dosages of binders.

Chapter 2 Materials and methods

2.1 Introduction

For the valorization of dredged sediments in road construction, the first essential step is to characterize the basic properties of raw materials. Therefore, the first part of this chapter introduces the test methods for the required physical and chemical parameters of raw materials. The second part of this chapter summarizes and analyzes the basic physical, chemical and environmental properties of the used Dunkirk dredged sediments, following the test methods of the first part. The third part of this chapter compares and chooses the used green and low carbon binder in this study, with the SWOT (Strengths, Weaknesses, Opportunities and Threats) analysis. The fourth part characterizes the basic physical and chemical properties of the used binders in this study.

2.2 Test methods

This part summarizes the test methods and standards for the raw sediments and binders.

2.2.1 Test methods for the sediments

Table 2-1 lists the physical parameters of the raw sediments that need to be measured and their corresponding testing standards. Usually, the sediments have high initial water content after dredging. This value is more than 100%. Thus, dredged sediments need dewatering before reusing, especially as road materials. In this study, the initial water content of the dredged sediments was determined according to the standard NF EN ISO 17892-1 [166], with drying in the oven at 105°C. In the road industry in France, particle size is a decisive parameter for the classification of materials according to the GTR guide [167]. In this study, the particle size distribution analysis of the sediments is carried out using the laser diffraction method (Beckman-Coulter LS230 particle size analyzer), which is according to the standard ISO 13320 [168]. The Atterberg limits are indicators of soil/sediment plasticity. There are three important parameters to be measured according to the standard EN ISO 17892-12 [169]: plastic limit, liquid limit and plasticity index. The solid density, also called

absolute density, is a physical quantity that characterizes the mass of a material per unit volume. The solid density of the studied sediment is determined according to the standard NF EN ISO 17892-3 (2015) [170] using a helium pycnometer (Micromeritics Accupyc 1330). The methylene blue value (MBV) is a parameter of the identification and classification of sediments. It represents the adsorption methylene blue capacity of the sediments. The test is carried out according to the standard NF P94-068 [171]. The organic matter content of raw sediment is measured according to the standard XP P94-047 [172] at 450°C and NF EN 15169 [173] at 550°C.

The modified Proctor compaction tests are especially important to define the application of the subgrade material in road construction. Thus, the modified Proctor compaction test is necessary to be carried out according to NF EN 13286-2 [174], to determine the feasibility of the raw sediments as a subgrade material in the road. The immediate California Bearing Ratio (I-CBR) test is carried out according to the standard NF EN 13286-47 [175] to determine the bearing capacity of the raw sediments.

Table 2-1 Physical parameters of the sediments and their corresponding testing standards.

Parameters	Symbol	Test standards
Initial water content (%)	ω	NF EN ISO 17892-1 [166]
Particle size distribution		ISO 13320 [168]
Liquid limit (%)	LL	EN ISO 17892-12 [169]
Plastic limit (%)	PL	EN ISO 17892-12 [169]
Plasticity index (%)	PI	EN ISO 17892-12 [169]
Solid Density (g/cm^3)	ρ_S	NF EN ISO 17892-3 [170]
Methylene Blue Value (g/100g)	MBV	NF P94 068 [171]
Organic content (%) [450°C]	OM [450°C]	XP P94-047 [172]
Organic content (%) [550°C]	OM [550°C]	NF EN 15169 [173]
Maximum dry density (g/cm^3)	MDD	NF EN 13286-2 [174]
Optimum moisture content (%)	OMC	NF EN 13286-2 [174]
I-CBR index (%)	I-CBR	NF EN 13286-47 [175]

Table 2-2 lists the chemical parameters of the raw sediments that need to be measured and their corresponding testing standards. Soil pH represents soil acidity or alkalinity. According to the standard NF EN15933 [176], the pH of raw sediments is tested using

a pH meter. Soil electrical conductivity (EC) could be used principally to measure soil salinity. According to the standard XP CEN/TS 15937 [177], the EC of the sediment can be measured with a conductivity meter. Identifying the chemical and mineral compositions of dredged sediments is essential, to better know the raw sediments material and anticipate the influence of certain chemical matter. The X-ray fluorescence spectrometry (XRF) determines the amount of chemical constituents in the studied sediment. The mineral composition of the raw sediment is revealed by the X-ray diffraction (XRD) test, using the Bruker D2 Advance diffractometer. The scan with a Cu Kα radiation in the range from 8° to 70° 2θ, at 0.02° 2θ increments with 1-s scanning time per step range. The DiffracPlus EVA software was used to identify mineral species. The mineral quantification of the studied sediments was made by Rietveld analysis with the Diffracplus Topas software (Bruker-AXS). The mineral crystal structure data was taken from the ICDD PDF and Bruker Structure Database. The thermal characterization can provide information on the composition of the studied material. In this context, the thermogravimetric analysis and derivative thermogravimetry (TGA-DTG) were used to analyze the raw sediments sample. The test condition is: under an inert atmosphere (Ar) with a heating rate of 10°C/min from 20°C to 1000°C.

Table 2-2 Chemical parameters of the sediments and their corresponding testing standards/methods.

Parameters	Test methods/standards
pH	NF EN15933 [176]
Electrical Conductivity (mS/cm)	XP CEN / TS 15937 [177]
Chemical composition (%)	XRF
Mineral composition (%)	XRD
Thermal analysis	TG-DTG

To comprehensively evaluate the potential of raw sediments as road material, according to the European standard NF EN 12457-2 [145], the leaching test is carried out on the raw sediments to determine the environmental characteristics. Firstly, the rotary oscillator was used to shake the sieved specimens (through the 4 mm sieve) and deionized water for 24 hours at 25℃. The liquid/solid (L/S) ratio remains unchanged at 10:1. Then, the leachates were passed through the 0.45 μm filters before analysis. The inductively coupled plasma-atomic emission spectrometer (ICP-AES) analyzed the solution recovered from the sediment to identify metallic trace elements. Chlorides, fluorides and sulfates were identified by Dionex® Ionic Chromatography

(IC).

2.2.2 Test methods for the binders

Table 2-3 lists the physical and chemical parameters of the binders that need to be measured and their corresponding testing standards/methods. The particle size is an important parameter, it affects the hydration reaction of binders. In this study, the particle size distribution of the binders is determined according to the standard ISO 13320 [168], with the Beckman-Coulter LS230 particle size analyzer. The solid density is an important physical property of building materials, controlling material quality from the raw powders to the formed final product. In this study, the solid density of the binder is determined using a helium pycnometer (Micromeritics Accupyc 1330), according to the standard NF P 15-435 [178]. The loss on ignition is a test used in inorganic analytical chemistry, particularly in the analysis of minerals. The test for the loss on ignition of binders is performed following NF EN 196-2 [179]. The chemical composition of the binder is analyzed by X-ray fluorescence (XRF). Moreover, the mineral composition of the binder is revealed by X-ray diffraction (XRD).

Table 2-3 Basic parameters of the binders and their corresponding testing standards/methods.

Parameters		Test standards
Physical characterization	Particle size distribution	ISO 13320 [168]
	Solid Density (g/cm^3)	NF P15-435 [178]
	Loss on ignition (%)	NF EN 196-2 [179]
Chemical characterization	Chemical composition (%)	XRF
	Mineral composition (%)	XRD

2.3 The studied sediments

The sediments used in this study were dredged from the Grand Port Maritime of Dunkirk. The location of the Grand Port Maritime of Dunkirk is shown in Figure 2-1. It is located in the North of France (GPS coordinates of port: 51°02′24.8″N 2°22′26.0″E). This Port is only 10 kilometers from the Belgian border and 40 kilometers from Dover of the United Kingdom. It is one of the busiest harbors in France. The Port Maritime of Dunkirk consists of east port and west port. It stretches over 17 kilometers from the seafront to the seabed with approximately 7000 hectares.

Figure 2-1 Location of Dunkirk port (from Google Maps).

2.3.1 Physical characterization of the studied sediments

The following content summarizes the results of the physical tests for the studied sediment. The used methods and testing standards have been given in the first part of this chapter. Therefore, here, we only provide the results and analysis.

2.3.1.1 Water content

As shown in Table 2-4, the measurements of water content were repeated three times with similar results. The average water content of studied sediments is 5.20%, after drying at 105°C.

Table 2-4 Water content of the studied sediments.

Sample No.	1	2	3	Average
Water content (%)	5.21	5.24	5.15	5.20

For comparison, Table 2-5 lists the water contents measured on the sediments of the Port of Dunkirk from earlier studies. The water content value is low for the studied sediment due to the in-situ treatment after a few months of natural drying. After, the sediments were stored in the hermetic plastic drums, then used for this study. In fact, it should be noted that the water content of freshly dredged sediments is generally very high, they are of the order of 100% to 300% at the port of Dunkirk. The used sediments in the studies of Miraoui [180], Wang [39] and Dia [181], were immediately stored in hermetic plastic drums after being dredged, to keep them in fresh states. Therefore, the initial water contents are more than 100% (see Table 2-5). However, the sediments used in the study of Hamouche [15] were taken from the settlement lagoons, which means the sediments were naturally drying. Thus, the initial water content is only 20.19%.

Table 2-5 Water content of sediments in Dunkirk ports (France).

Researches	Water content (%)
Miraoui (2010) [180]	222.49, 105.22
Wang (2011) [39]	131.50
Dia (2013) [181]	135.10
Hamouche (2018) [25]	20.19

2.3.1.2 Particle size distribution

Figure 2-2 illustrates the particle size curves of the dredged marine sediment. The results were obtained from an average of three measurements. The particle size curves were obtained by laser diffraction and used two kinds of sample preparation methods: (a) dry sediments with laser diffraction method and (b) wet sediments with laser diffraction and ultrasound.

The results obtained by two different sample preparation methods show a divergence in particle size distribution. The results by laser diffraction and ultrasound method show that the sediments are finer than the results with only the laser diffraction method. This can be confirmed in Figure 2-2 (b). Both results show that the main particle size ranges are 2-60 μm and 60-400 μm. However, for the volume frequency of the 60-400 μm fraction, the value of the laser diffraction method is higher than that of laser diffraction with ultrasound. Such a difference is related to the initial big particle aggregate may be decomposed into small particles, under the impact of water wetting and ultrasonic dispersion.

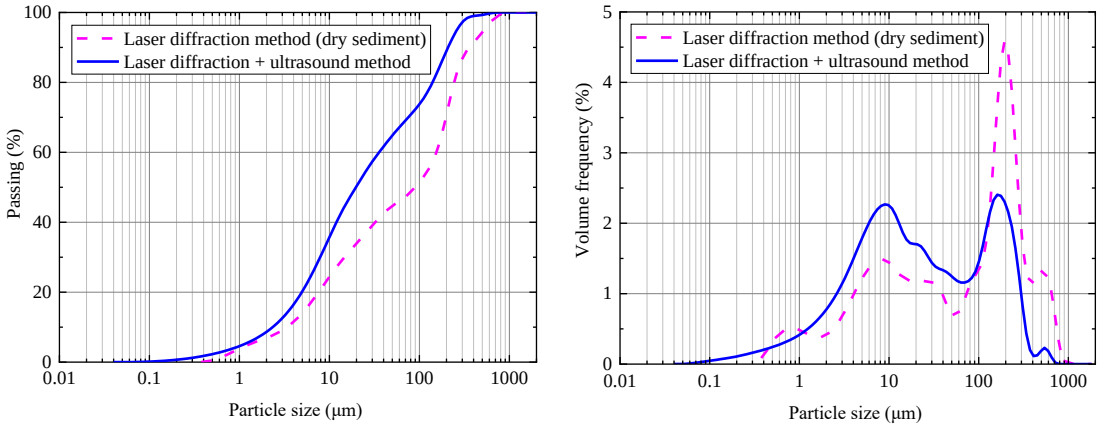

(a) (b)

Figure 2-2 Particle size distribution of the studied sediments: (a) cumulative and (b) frequency curve.

Table 2-6 lists the measured results of the different particle size fractions on the Port of Dunkirk sediments from this study and earlier studies. The result obtained by the laser diffraction method indicates that the marine sediment is composed of 6.97% clay, 39.48% silt and 53.55% sand. While the result of the laser diffraction and ultrasound method, indicated that the sediment has 8.70% clay, 59.19% silt and 32.11% sand. The results obtained by laser diffraction underestimate the number of small particles (clay and silt), compared to the results obtained by the laser diffraction and ultrasound method. A similar conclusion could be found from the previous studies in Table 2-6.

Uniformity coefficient (Cu) and coefficient of curvature (Cc) are the grading characteristics of the soil. However, according to the European standard EN ISO 14688-2 [150] and American standard ASTM D2487-17 [151], these parameters are only used to classify coarse-grained soil. The studied raw sediment belongs to fine-grained soil. Thus, Cu and Cc are not very important parameters to analyze.

Table 2-6 Summary of the particle size distribution of sediments in Dunkirk ports (France).

Researches	Method	Location	Particle sizes					
			% < 2μm	2-63 μm	63μm < %	d_{50} (μm)	C_U	C_C
Classification	GTR	/	Clay	Silty	Sand	/	/	/
This study	Laser	West port	6.97	39.48	53.55	90.00	48.45	0.46
	Laser + U	West port	8.70	59.19	32.11	20.00	14.98	0.76
Hamouche (2018)	Laser	West port	20.00	56.00	24.00	7.10	12.03	0.62
Dia (2013)	Laser	East port	1.60	25.30	73.10	202.00	18.55	2.81
	Laser + U	East port	5.90	34.00	60.10	102.00	60.45	0.62
Wang (2011)	Laser	East port	11.40	66.60	22.00	10.10	11.75	0.82
	Laser + U	East port	16.40	74.20	9.40	6.00	8.47	1.00
Miraoui (2010) S1	Laser + U	East port	8.52	90.24	0.15	11.81	5.99	1.49
Miraoui (2010) S2	Laser + U	East port	7.65	90.20	2.10	10.44	5.07	1.19

Based on the particle size analysis, the dredged sediments can be classified according to the triangular classification system of fine soils (Figure 2-3). In this study, the dredged marine sediments can be classified as sandy loam based on the result of the laser diffraction method. In comparison, the studied sediment is classified as silt loam with laser diffraction and ultrasound method. The classification is similar to other results. The main composition of Dunkirk ports sediments is silt or sand. The clay is

the smallest amount of fraction.

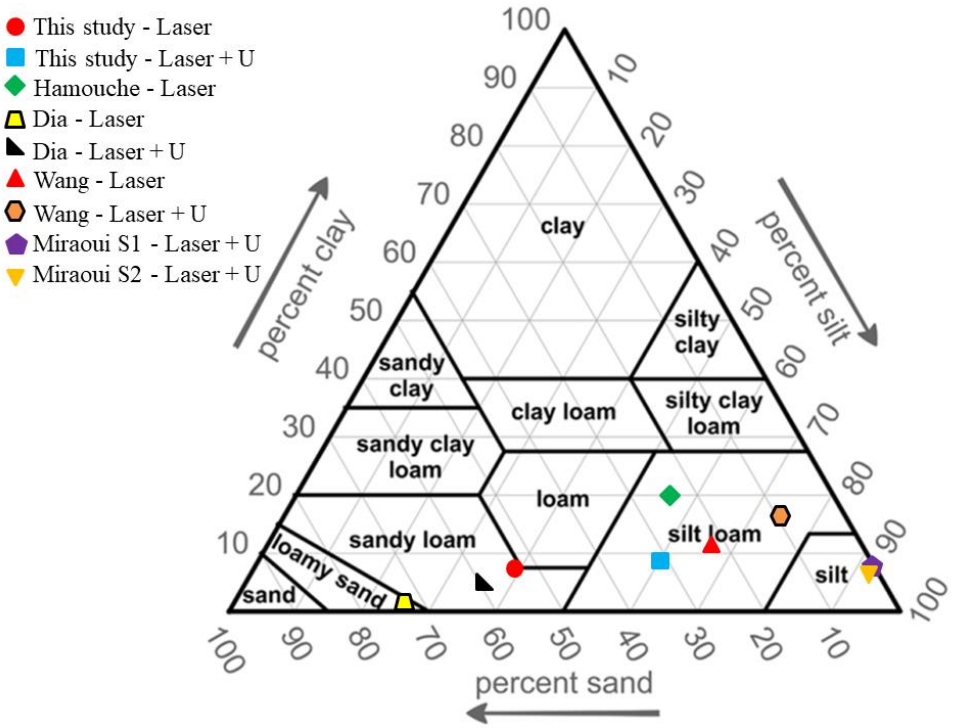

Figure 2-3 Classification of marine sediments in the triangular classification of fine soils.

2.3.1.3 Atterberg limits

Figure 2-4 illustrates the results of the liquid limit test for the studied sediments. All the results of the Atterberg limits are summarized in Table 2-7. The average liquid limit (LL) value is 40.20%, which means the transition from the plastic-state to the liquid-state, corresponds to 40.20% water content. The studied sediments' average plastic limit (PL) value is 28.00%. This is to say the transition of the studied sediment from the plastic-state to the solid-state, corresponds to 28.00% water content.

The plasticity index (PI) is considered one of the key parameters required for classifying soil and similar materials. Indeed, PI presents the water content range in which the soil and similar materials remain plastic. The PI value of the studied sediment is 12.20%.

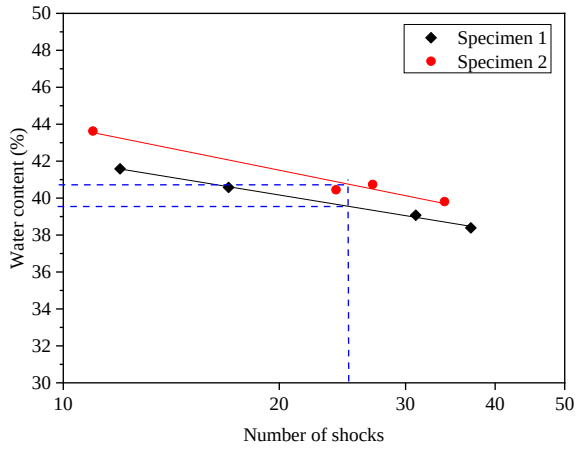

Figure 2-4 Liquid limit of the studied sediments.

Table 2-7 Atterberg limits of the studied sediments.

Parameters	Values		
Sample No.	1	2	average
LL (%)	39.60	40.70	40.20
PL (%)	28.10	27.90	28.00
PI (%)	11.50	12.80	12.20

We can classify the sediments according to the liquid limit and the plasticity index with the Casagrande diagram. In Figure 2-5, it is observed that the sediment in this study is associated in the Casagrande diagram with the class of medium plastic silt. Based on the results obtained by Miraoui [180], Wang [39], Dia [181] and Hamouche [25], we found that all the studied Dunkirk sediments tend to cluster around line A: PI=0.73×(LL-20). This result makes it possible to appreciate that the Dunkirk sediments remain in the same range and have similar characteristics.

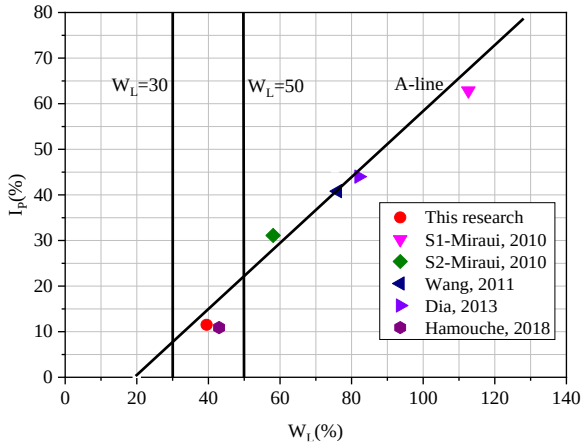

Figure 2-5 Classification of marine sediments according to the Casagrande diagram.

2.3.1.4 Solid density

Figure 2-6 describes the measurement results of the solid density for the studied sediments. Table 2-8 compares the result with the previous studies for Dunkirk sediments. It could be found that the average solid density of the studied sediments is 2.58 g/cm^3. This value is lower than that of quartz (2.65 g/cm^3) and carbonates (2.60 to 2.80 g/cm^3). This difference could be explained by organic matter in the dredged sediments, which are lighter than mineral particles. Besides, this value is close to the others' results, in comparison with the studies of Miraoui [180], Wang [39], Dia [181] and Hamouche [25].

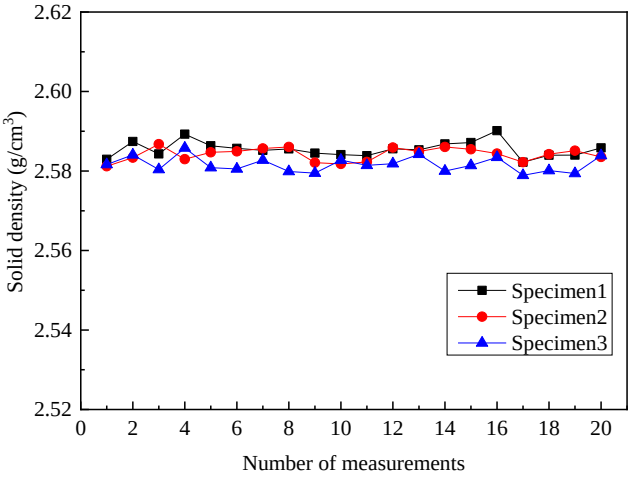

Figure 2-6 Solid density of the studied sediments.

Table 2-8 Solid density of sediments in Dunkirk ports (France).

	This study			Miraoui (2010)	Miraoui (2010)	Wang (2011)	Dia (2013)	Hamouche (2018)
Sample No.	1	2	3	S1	S2	/	/	/
ρ_s (g/cm^3)	2.59	2.58	2.58	/	/	/	/	/
Average (g/cm^3)		2.58		2.52	2.54	2.53	2.54	2.55

2.3.1.5 Methylene Blue Value (MBV)

The MBV results of the dredged sediments are reported in Table 2-9. The results of Miraoui [180], Hamouche [25], Wang [39] and Dia [181] are also presented in Table 2-9. The MBV for the used sediment in this study is 1.33 g/100g. This measured value is lower than those measured results of Miraoui [180], Wang [39] and Dia [181], but close to the result of Hamouche [25].

Table 2-9 Methylene blue value of the studied sediments.

	This study			Miraoui (2010) S1	Miraoui (2010) S2	Wang (2011)	Dia (2013)	Hamouche (2018)
MBV (g/100g)	1.35	1.39	1.25	4.08	3.25	3.10	3.20	1.09
Average (g/100g)		1.33						

The MBV of soil is an important parameter for classifying fine soils according to the GTR Guide [167]. Figure 2-7 illustrates the soil classification thresholds based on MBV. Therefore, the studied sediments could be classified in the group of loamy soils.

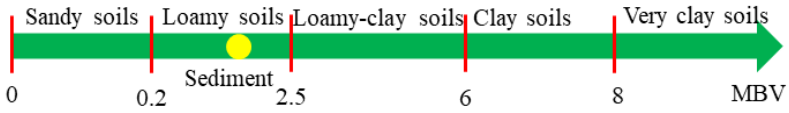

Figure 2-7 Soil classification according to MBV [167].

2.3.1.6 Organic matter (OM) content

The organic matter content of the dredged sediments is reported in Table 2-10. This result shows that the used sediments have 7.62% mass loss (attributed to the decomposition of OM) after calcination at 450°C. This value increases to 10.22% with the calcination temperature increase to 550°C. The phenomenon that the different measurement results at the two temperatures have been discovered in previous studies [25] [39] [180] [181], as shown in Table 2-10. The difference may be attributed to the incomplete combustion of organic matter at 450°C. The combustion of organic materials for dredged sediments occurs in four distinct temperature ranges, according to some research [182] [183].

- 120°C-300°C: the light carbohydrate molecules and the small organic compounds are not volatilized before decomposition;
- 300°C–450°C: the decomposition might be associated with the aromatic carbon and lignin;
- 450°C–600°C: corresponding to the poly-condensed forms of lipids and aromatic carbons, so-called black carbon-like materials;
- 600°C–900°C: residual refractory organic matter (not residual carbonate).

Table 2-10 Organic matter content of the studied sediments.

OM (%)	This study			Miraoui (2010)	Miraoui (2010)	Wang (2011)	Dia (2013)	Hamouche (2018)
Sample No.	1	2	3	S1	S2	/	/	/
OM [450°C]	7.84	7.89	7.28	/	/	/	/	/
Average		7.67		10.02	5.39	6.27	/	8.02
OM [550°C]	10.29	10.02	10.36	/	/	/	/	/
Average		10.22		16.36	10.12	9.93	11.1	10.55

2.3.1.7 Compaction characterization

In this part, the Maximum Dry Density (MDD), Optimum Moisture Content (OMC) and Immediate California Bearing Ratio (I-CBR) of the raw sediments, were determined to explore the potential for using raw sediments in road engineering. Figure 2-8 illustrates the modified Proctor compaction curve and I-CBR curve of raw sediments. It can be found that the MDD is 1.641 g/cm^3 and the corresponding OMC is 21.1% for raw sediment. The I-CBR index of raw sediments is 15% at the OMC. This value is lower than the requirement (I-CBR ≥ 25%) of subgrade material, according to the specifications in French standards [139]. Table 2-11 compares the compaction results of this work with those of Miraoui [180], Hamouche [25], Wang [39] and Dia [181]. It seems the MDDs and OMCs of the sediments in Dunkirk ports change in a small range in these studies. The MDDs are in the range of 1.570-1.700 g/cm^3, while the OMCs are 18.0-22.4%. All the I-CBR values are small and belong to the 14-25% range.

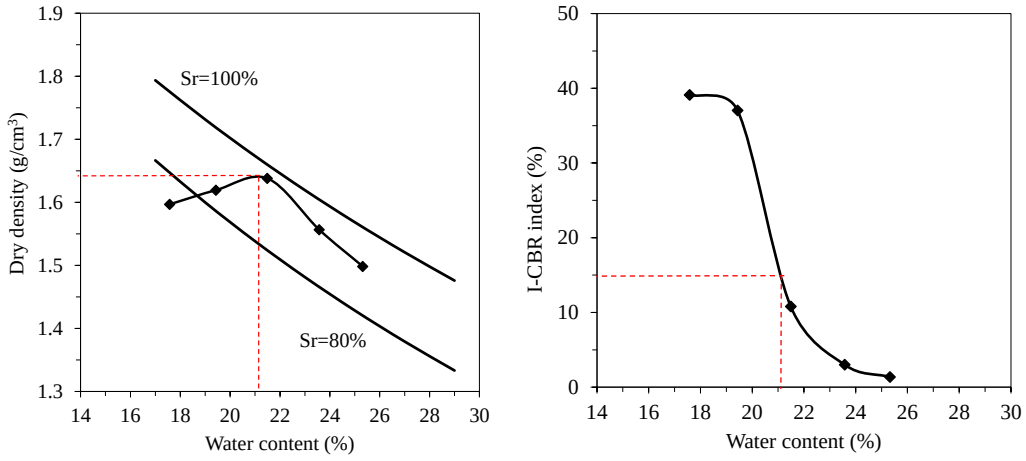

(a) (b)

Figure 2-8 (a) Modified Proctor compaction curve and (b) I-CBR curve of the studied sediments.

Table 2-11 Compaction characterization of sediments in Dunkirk ports (France).

Parameters	This study	Miraoui (S1) (2010)	Wang (2011)	Dia (2013)	Hamouche (2018)
MDD (g/cm^3)	1.641	1.580	1.612	1.570	1.700
OMC (%)	21.1	20.0	21.6	22.4	18.0
I-CBR (%)	15	14	25	25	23

2.3.2 Chemical characterization of the studied sediments

2.3.2.1 pH and electrical conductivity

The pH and electrical conductivity (EC) results of raw sediment are shown in Table 2-12. The results of Hamouche [25] and Dia [181] are also presented in Table 2-12. The average pH value of the studied sediment is 7.76, which corresponds to a slightly alkaline material. This measured pH value is lower than the results of Hamouche [25] and Dia [181]. The average EC value of the studied sediment is 4.30 mS/cm. It could be classified as slightly saline soil, according to the USDA-NRCS soil survey handbook [184]. This measured EC value is less than the result of Hamouche [25]. This difference may attribute to the different saline of the used sediments.

Table 2-12 The pH and electrical conductivity of the studied sediments.

Parameters	This study			Dia (2013)	Hamouche (2018)
Sample No.	1	2	3	/	/
pH	7.78	7.76	7.75	/	/
Average		7.76		8.10	8.10
EC (mS/cm)	4.33	4.32	4.26	/	/
Average		4.30		/	8.20

The lower pH and EC values in this study could be attributable to the natural weathering of the dredged sediment materials. Before beginning this study, the used dredged sediment materials were stored outdoors for nearly one year without any special protection. Mamindy-Pajany et al. [185] and Couvidat et al. [186] [187] also observed similar phenomena, the storage in the open air under natural weather conditions could reduce the pH and EC values of the dredged sediment. The weather of wind, sun and rain cycle cause the natural leaching (washing) of base cations such as Na^+, K^+, Ca^{2+} and Mg^{2+} of the sediments particles. These leached base cations are then replaced by protons (H^+) originating from H_2O or organic acids to balance the

charges of sediments particles [188]. These changes could cause a decrease in the pH of the storage sediments. The reduction in the EC of the sediments is probably due to the natural leaching (washing) of the soluble salts by rainwater under open-air storage [186] [187].

2.3.2.2 Thermal analysis (TGA-DTG)

The thermal analysis (TGA/DTG) result of raw sediments is reported in Figure 2-9. The results were obtained from an average of three measurements. The weight loss increases with increasing the temperature. The existence of three distinct peaks for the DTG curve is attributed to:

- Dehydration phase (20-200°C): associated with dehydration of free water and the removal of adsorbed water in pores [189] [190].
- Dehydroxylation phase (400-600°C): the mass loss of this phase may be due to the elimination of organic fractions and the reactions relating to the various pollutants (PAHs, PCBs, TBT, etc.) [190]. According to some studies [191], at 550°C, kaolinite can transform into metakaolin. However, the kaolinite mineral is only 0.33% (see XRD analysis) in the studied sediment. As a result, the influence of kaolinite could be ignored in this study.
- Decarbonization phase (600-900°C): the loss of mass (the average value is 10.30%) of this phase corresponds mainly to the decomposition of carbonates phase, producing CO_2 [192]. Besides, some studies point out that muscovite undergoes dehydroxylation at around 770-950 °C [193] [194]. The used raw sediment has 17.32% muscovite (see XRD analysis). Thus, the dehydroxylation of muscovite may also cause mass loss.

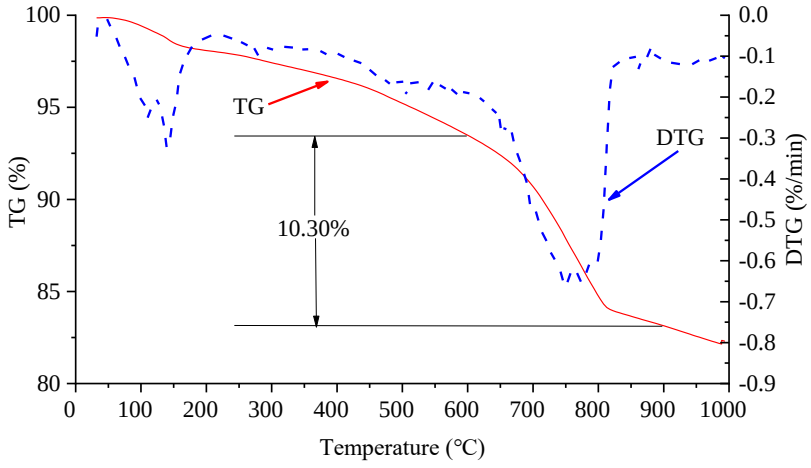

Figure 2-9 Thermogravimetric analysis (TGA) of the studied sediments.

The organic matter content of the dredged sediments is calculated with the mass loss at 450°C or 550°C. Therefore,

Table 2-13 shows the comparison of the mass loss results (at 450°C and 550°C) of this work with those of Miraoui [180], Hamouche [25], Wang [39] and Dia [181]. The results of this study are closest to the results of Hamouche [25].

Mass loss (%)	This study				Miraoui (S1) (2010)	Wang (2011)	Dia (2013)	Hamouche (2018)
	1	2	3	Average	/	/	/	/
450°C	4.07	4.31	3.59	3.99	10.75	7.00	5.00	3.65
550°C	5.93	6.07	4.93	5.64	13.98	12.50	7.90	5.80

Table 2-13 Mass loss of the studied sediment with ATG method.

Mass loss (%)	This study				Miraoui (S1) (2010)	Wang (2011)	Dia (2013)	Hamouche (2018)
	1	2	3	Average	/	/	/	/
450°C	4.07	4.31	3.59	3.99	10.75	7.00	5.00	3.65
550°C	5.93	6.07	4.93	5.64	13.98	12.50	7.90	5.80

Table 2-14 compares the mass loss of the studied sediment with the different methods. The mass loss measured by ATG is less than that by calcination. On the one hand, this is attributed to the complete decomposition of organic matter by calcination for three hours at 450/550°C [195]. On the other hand, calcination is under an air atmosphere, while ATG is under an inert atmosphere (argon, Ar). The air atmosphere could provide enough O_2 to ensure the complete combustion of all organic matter [195] [196].

Table 2-14 Comparison of the mass loss of the studied sediment with the different methods.

Temperature (°C)	Mass loss (%)	
	Calcination	ATG
450	7.67	4.07
550	10.22	5.93

The total carbon content (C_{Total}) includes organic carbon content ($C_{Organic}$) and mineral carbon content ($C_{Mineral}$).

According to NF ISO 10694 [197], the relationship between organic matter content (OM) and organic carbon content ($C_{Organic}$) for soil, could be expressed by Equation

(2-1).

$$OM = 1.724 \times C_{Organic} \quad (2\text{-}1)$$

Thus, the organic carbon content ($C_{Organic}$) of the studied sediments is:

$$C_{Organic} = \frac{OM}{1.724} = \frac{7.67\%}{1.724} = 4.45\% \quad (2\text{-}2)$$

The mineral carbon content ($C_{Mineral}$) could be calculated according to the loss of mass of ATG (600-900℃), as shown:

$$CaCO_3 \xrightarrow{600-900℃} CaO + CO_2 \uparrow \quad (2\text{-}3)$$

$$C_{Mineral} = \frac{M_C}{M_{CO_2}} \times \text{loss of mass } (600 - 900℃) \quad (2\text{-}4)$$

In which, $\frac{M_C}{M_{CO_2}}$ is the mass percentage of carbon in carbon dioxide. Based on the molar masses of oxygen (16 g/mol) and carbon (12 g/mol), the molar mass of carbon dioxide is 12+2(16)=44 g/mol. Therefore, the mass percentage of carbon in carbon dioxide ($\frac{M_C}{M_{CO_2}}$) is 12/44=27.27%.

So, the mineral carbon content ($C_{Mineral}$) of the studied sediments is:

$$C_{Mineral} = \frac{M_C}{M_{CO_2}} \times \text{loss of mass } (600 - 900℃) = 27.27\% \times 10.30\% = 2.81\% \quad (2\text{-}5)$$

Therefore, the total carbon content (C_{Total}) of the studied sediments is:

$$C_{Total} = C_{Organic} + C_{Mineral} = 4.45\% + 2.81\% = 7.26\% \quad (2\text{-}6)$$

2.3.2.3 Chemical composition (XRF)

The XRF analysis results of the dredged sediments are summarized in Table 2-15. It should be noted that the result of carbon is from the ATG test (C_{Total}). The major chemical elements of the Dunkirk sediments include 49.60% oxygen, 19.70% silicon, 10.30% calcium, 4.00% aluminum and 3.50% iron. These values were similar to previous studies [58] [54]. The XRF result identifies the chemical elements of the sediments. It could provide helpful information for X-ray diffraction to better identify the major mineral phases.

Table 2-15 X-ray fluorescence analysis results of the studied sediments.

Element	Values (%)	Element	Values (%)
C	7.26	K	1.10
O	49.60	Ca	10.30
Na	0.90	Ti	0.20
Mg	1.40	Mn	0.10
Al	4.00	Fe	3.50
Si	19.70	Cu	< 0.10
P	0.10	Zn	< 0.10
S	1.10	Ba	< 0.10
Cl	0.60	Pb	< 0.10

2.3.2.4 Mineral composition (XRD)

The XRD analysis result of the studied sediments (Figure 2-10) shows that silicates and carbonates are major compositions. This result is consistent with the elements identified by XRF and the main constituent elements are oxygen, silicon and calcium. Besides, the XRD result indicated minor phases, such as kaolinite, aragonite, microcline, albite, etc. This result agrees well with the research for the sediments in Dunkirk ports from Miraoui [180], Hamouche [25], Wang [39] and Dia [181].

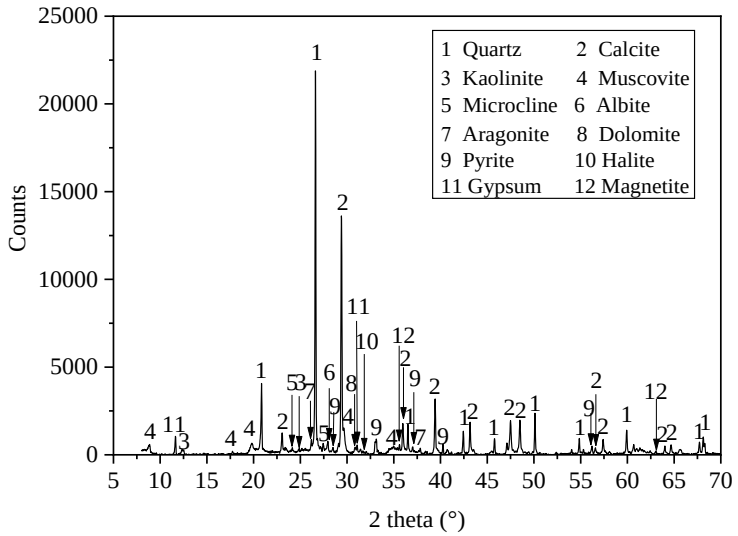

Figure 2-10 X-ray diffractograms of the studied sediments (Cu Kα).

Table 2-16 reports the mineralogical composition of the studied sediments, which was determined by XRD using the Rietveld method [198]. The 10 wt% Corundum (Al_2O_3) was added to the samples as an internal standard to determine the content of the mineral phase.

Table 2-16 The mineralogical analyses of the studied sediments.

Mineral		Chemical formula	Composition (wt.%)			
			No. 1	No. 2	No. 3	Average
Silicates	Quartz	SiO_2	33.25	26.75	28.19	29.40
	Muscovite	$KAl_2(Si_3Al)O_{10}(OH, F)_2$	15.96	18.03	17.97	17.32
	Microcline	$KAlSi_3O_8$	2.09	6.63	4.54	4.42
	Kaolinite	$Al_2Si_2O_5(OH)_4$	0.32	0.33	0.34	0.33
	Albite	$NaAlSi_3O_8$	2.43	5.49	5.19	4.37
Carbonates	Aragonite	$CaCO_3$	5.11	5.14	5.58	5.28
	Dolomite	$CaMg(CO_3)_2$	0.53	0.16	0.16	0.28
	Calcite	$CaCO_3$	35.04	31.71	32.86	33.20
Sulfides	Pyrite	FeS_2	1.62	1.57	1.61	1.60
Other minerals	Halite	NaCl	0.09	0.08	0.03	0.07
	Gypsum	$CaSO_4 \cdot 2H_2O$	2.58	2.74	2.40	2.57
	Magnetite	Fe_3O_4	0.97	1.36	1.12	1.15
Sum	/	/	100.00	100.00	100.00	100.00

The powder sample with 10 wt% Corundum was analyzed using a Bruker D2 Advance diffractometer system with Cu-Kα radiation. The scans were run from $2\theta = 8°$ to 70°, with a step interval of $2\theta = 0.02°$ and a time acquisition of 1 s per step. Once the diffraction data were collected, the mineral species of the studied sediments were identified using Bruker DiffracPlus EVA software and the ICDD (the International Centre for Diffraction Data) Powder Diffraction File (PDF) 2015 database. After, the quantification of all identified mineral species for the studied sediments was made by Rietveld analysis with the Diffracplus Topas software (Bruker-AXS). The Rietveld analysis with Diffracplus Topas software is highly programmed and automated. The Rietveld method consists of minimizing the difference between an experimental diffractogram and a diffractogram calculated for a given starting model. The minimization is done by simultaneously adjusting instrumental and sample parameters by a non-linear multivariable least square procedure. The mineral crystal structure data was taken from the ICDD PDF and Bruker Structure Database [199]. The Rietveld refined parameters used in this study are the same as described in Trincal et al. [200].

It's worth noting that the absolute content of various identified mineral phases was calculated by removing the internal standard's content and normalizing the sum of all phase contents to 100 wt.%. The results were the average value of the three samples.

The results indicated that the most important minerals of raw sediments are 29.40% quartz, 33.20% calcite and 17.32% muscovite. Sulfur was present as sulfides with 1.60% pyrite and 2.57% gypsum (sulfates form) in the sediment.

2.3.3 Environmental characterization of the studied sediments

Table 2-17 shows the average values of the leaching test results. The natural pH of the raw sediment determined in demineralized water is 7.42.

According to the prescribed limits criteria and procedure for accepting waste at landfills in European directive 2003/33/CE [201], all the heavy elements were within Class III's limit (inert waste) for the raw sediments. The chlorides content, sulfates content and soluble fraction conform to the specifications for Class II (non-hazardous waste), while fluorides content was within the limit of Class III (inert waste). Thus, the studied sediment materials can be classified as non-hazardous waste. The origin of the studied sediments could explain the high values of chlorides and sulfates contents. The sediments were dredged from Dunkirk harbor in France. There is a high value of sulfates elements in the environment of marine harbors. Some chlorides and sulfates come from agricultural activities, accumulate in sediments together with chlorides and sulfates from the ocean. Thus, high chlorides and sulfates contents in the studied sediments could not be a problem. The sediment is slightly polluted for the marine environment, but reusing it as an alternative material in road construction could be a suitable alternative to discharging the ocean.

In comparison with the considered elements of the French SETRA guide [202], the values of chlorides, sulfates and soluble fraction were over the thresholds of level 1, but less than the leaching thresholds. This means the studied sediments could still be alternative materials in road engineering. It should be noted that the surface layer of this road must be impermeable, made by asphalt, bituminous mixes, surface wear coatings, concrete, cement or jointed pavers, having a minimum slope of 1% [202].

Table 2-17 Comparison of the leaching results for raw sediment with the limits of different regulations.

Element	Raw sediment (mg/kg)	European directive 2003/33/CE [201]			SETRA road guide (mg/kg) [202]			
		Class III	Class II	Class I	Level 1			Limit values
					At least 80 %	At least 95 %	At least 100 %	
As	< 0.10	0.5	2	25	0.5	1	1.5	2
Ba	0.06	20	100	300	20	40	60	100
Cd	< 0.009	0.04	1	5	0.04	0.08	0.12	1
Cr	< 0.004	0.5	10	70	0.5	1	1.5	10
Cu	0.16	2	50	100	2	4	6	50
Hg	< 0.06	0.01	0.2	2	0.01	0.02	0.03	0.2
Mo	0.38	0.5	10	30	0.5	1	1.5	10
Ni	< 0.05	0.4	10	40	0.4	0.8	1.2	10
Pb	< 0.06	0.5	10	50	0.5	1	1.5	10
Sb	0.06	0.06	0.7	5	0.06	0.12	0.18	0.7
Se	< 0.08	0.1	0.5	7	0.1	0.2	0.3	0.5
Zn	< 0.05	4	50	200	4	8	12	50
Chlorides	**4220**	800	15000	25000	800	1600	2400	15000
Fluorides	6.10	10	150	500	10	20	30	150
Sulfates	**9250**	1 000	20000	50000	1000	2000	3000	20000
Soluble fraction	**15774**	4000	60000	100000	4000	8000	12000	60000

(Note: Class I is hazardous waste, Class II is non-hazardous waste, Class III is inert waste.)

2.3.4 Classification of the studied sediments

The purpose of the classification systems is to classify soil materials with similar geotechnical characteristics. The engineers could predict soils' engineering properties and behaviors based on this classification. As shown in Figure 2-11, there are several classification systems of soil materials in different countries. Table 2-18 summarizes the basic physical and chemical characteristics of raw sediments. These results allow us to classify the studied sediments according to different classification systems.

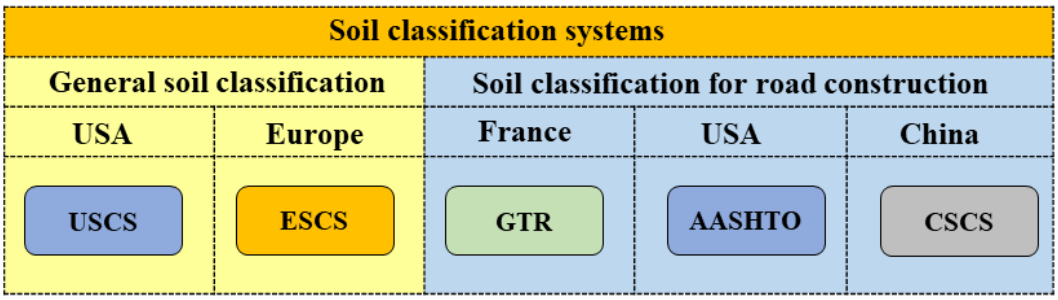

Figure 2-11 Different soil classification systems.

Table 2-18 Basic physical and chemical characteristics of the studied sediments.

Parameters	Symbol	Value
Initial water content (%)	ω	5.20
Solid density (g/cm^3)	ρs	2.58
Organic content (%) [450°C]	OM [450°C]	7.67
Organic content (%) [550°C]	OM [550°C]	10.22
Liquid limit (%)	LL	40.20
Plastic limit (%)	PL	28.00
Plasticity index (%)	PI	12.20
Clay fraction (% < 2 µm)		8.70
Silt fraction (2 µm < % < 63 µm)		59.19
Sand fraction (% > 63 µm)		32.11
Uniformity coefficient	C_U	48.45
Curvature coefficient	C_C	0.46
Methylene blue value (g/100g)	MBV	1.33
pH	pH	7.76
Electrical conductivity (mS/cm)	EC	4.30
Maximum dry density (g/cm^3)	MDD	1.641
Optimum moisture content (%)	OMC	21.1
I-CBR index (%)	I-CBR	15

2.3.4.1 American soil classification system (USCS)

The most common engineering classification system for soil in America is the Unified Soil Classification System (USCS), determined by the standard ASTM D2487-17 [203]. The USCS is based on the particle-size characteristics and the Atterberg limits (Figure 2-12). It has three major classification groups: coarse-grained soils, fine-grained soils and highly organic soils.

- Coarse-grained soils are broken up into gravels (more than 50% of coarse fraction

retained on No. 4 sieve (4.75 mm)) and sands (50% or more of coarse fraction passes No. 4 sieve (4.75 mm)).

- Fine-grained soils are defined broadly by the characteristic of having 50% or more pass the No. 200 sieve (0.75 mm). These soils are further placed into the following groups: (a) silt and clay with liquid limit < 50%; (b) silt and clay with liquid limit ≥ 50%. After, according to the plasticity chart (Figure 2-12), the silt and clay could be continue classified based on the liquid limit, plasticity index and organic matter.
- Highly organic soils are primarily organic matter, dark in color and have an organic smell. The only group classification for highly organic soils is peat (PT).

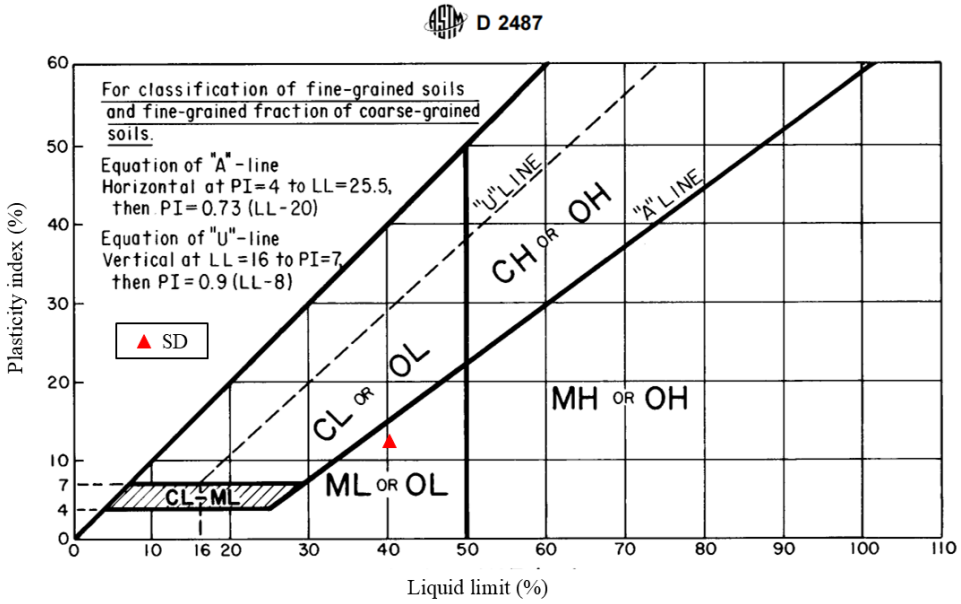

OL:	Organic soil with low plasticity	CH:	Clay of high plasticity, fat clay
ML:	Silt of low plasticity	CL:	Clay of low plasticity, lean clay
OH	Organic soil with high plasticity	MH:	Silt of high plasticity, elastic silt

Figure 2-12 Plasticity chart of USCS [203].

According to the USCS, the studied sediment is fine-grained soils, due to the particle size of less than 0.75 mm is 71%. As shown in Figure 2-12, the liquid limit (LL) is 40.2% and the plasticity index (PI) is 12.2%. The studied sediment is classified as OL (Organic soil with low plasticity).

2.3.4.2 European soil classification system (ESCS)

The European Soil Classification System (ESCS) is for engineering purposes. It uses soil description and symbols, according to the European standard EN ISO 14688-2

[204]. It generally complies with guidelines defined by the USCS soil classification system following the standard ASTM D 2487-17 [203]. According to the ESCS in Figure 2-13, the studied sediment is classified as SiM (Silt of medium plasticity).

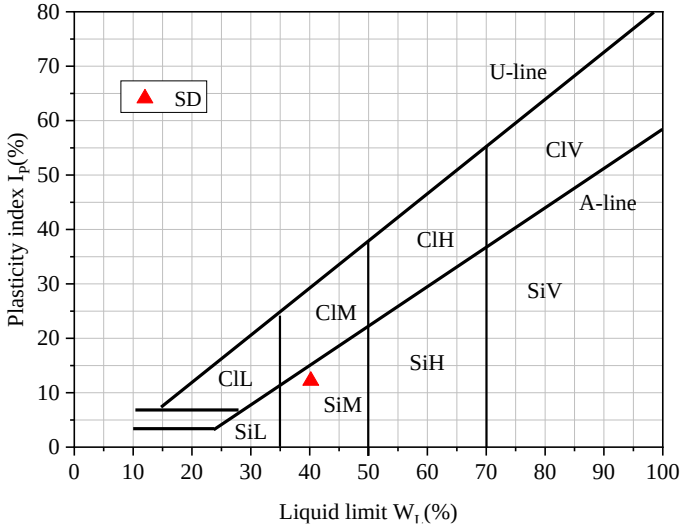

ClL:	Clay of low plasticity	SiL:	Silt of low plasticity
ClM:	Clay of medium plasticity	SiM:	Silt of medium plasticity
ClH:	Clay of high plasticity	SiH:	Silt of high plasticity
ClV:	Clay of very high plasticity	SiV:	Silt of very high plasticity

Figure 2-13 Plasticity chart of ESCS [204].

2.3.4.3 French soil classification system for road construction (GTR)

The GTR soil classification system is used in France according to French GTR Guide [167]. The GTR systems propose prescriptions and conditions to use the studied soils as road materials, with these basic parameters: particle size distribution, Atterberg limits, MBV and I-CBR. Figure 2-14 shows this soil classification. The detailed process can be found in the GTR Guide [167].

According to the GTR guide, the studied sediment is subclass F11, because the organic matter content is between 3% and 10%. The particle size distribution shows that the D_{max} of the studied sediments is less than 50 mm. The fraction passing through the 0.08-mm sieve is 71%. Therefore, the studied sediments belong to type A. Considering the MBV is 1.33 g/100g and the I-CBR value is 15%, the studied sediment is classified as F11A1m soil.

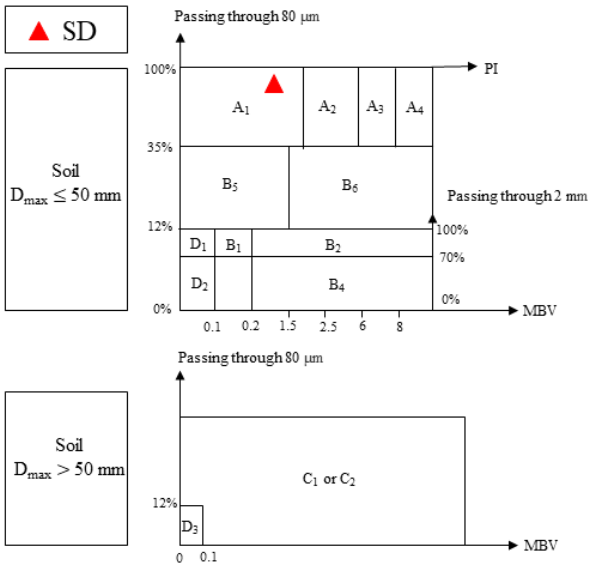

Figure 2-14 Soil classification system of GTR [167].

2.3.4.4 American soil classification system for road construction (AASHTO)

The AASHTO soil classification system is determined by the standard ASTM D3282-15 [205]. It was developed by the American Association of State Highway and Transportation Officials (AASHTO). It is used to classify soils and soil-aggregate mixtures for highway construction purposes. This classification considers the particle-size characteristics and the Atterberg limits. It has seven major groups: A1, A2, A3, A4, A5, A6 and A7. The detailed information could be found in the standard ASTM D3282-15 [205]. According to the AASHTO (Figure 2-15), the studied sediment is classified as the A-7-6 subgroup (clayey soils).

For qualitative evaluation of the studied soil, the Group Index (GI) has been developed, as determined by Equation (2-7) [205]. The quality of performance of soil as a subgrade material is inversely proportional to GI. When GI equals zero, the soil is a good subgrade material. While GI is 20 or more, the soil is a very poor subgrade material. In this study, GI is 8 for the sediment. Thus, the studied sediment has a medium ability as road materials.

$$\mathrm{GI} = (F_{200} - 35)[0.2 + 0.005(\mathrm{LL} - 40)] + 0.01(F_{200} - 15)(\mathrm{PI} - 10) \quad (2\text{-}7)$$

Where, F_{200} is the percentage passing through the No. 200 sieve (0.75 mm), LL is the liquid limit, PL is the plasticity index.

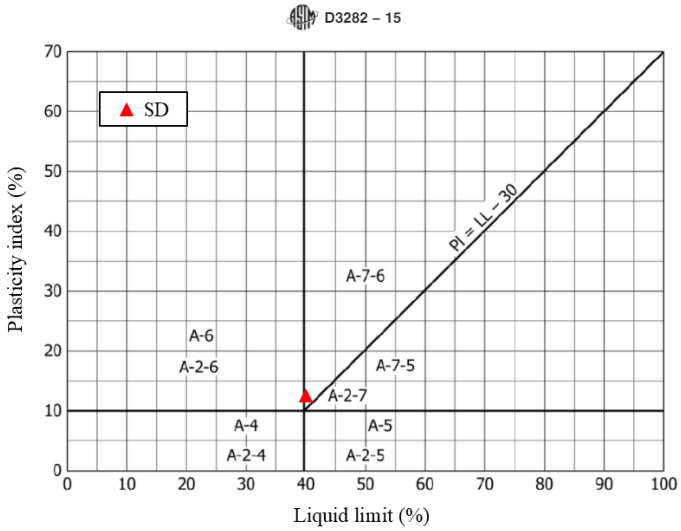

Figure 2-15 Classification of AASHTO [205].

2.3.4.5 Chinese soil classification system for road construction (CSCS)

In China, the soil classification system is determined by the standard JTG 3430-2020 [206] for highway engineering. This classification is the same as USCS. It is based on the particle-size characteristics and the Atterberg limits. As shown in Figure 2-16, fine-grained soils (having 50% or more pass the No. 200 sieve (0.75 mm)) could be classified with the liquid limit and the plasticity index. Based on the CSCS, the studied sediment is classified as MLO (low liquid limit silt containing organic).

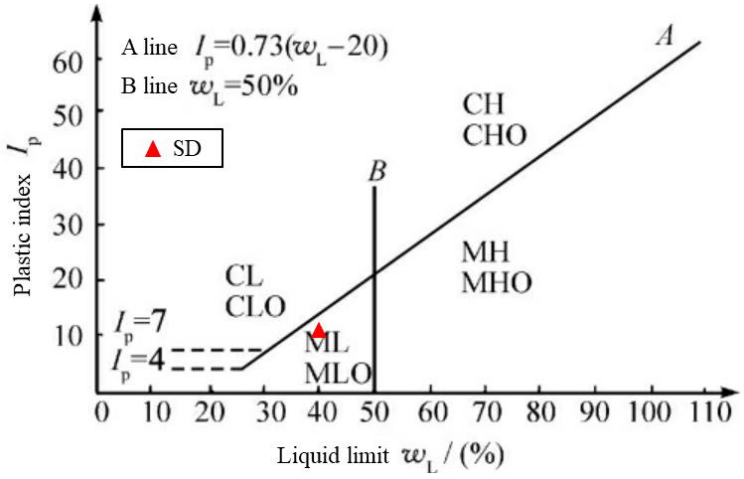

CH:	High liquid limit clay	CHO:	High liquid limit clay containing organic
MH:	High liquid limit silt	MHO:	High liquid limit silt containing organic
CL:	Low liquid limit clay	CLO:	Low liquid limit clay containing organic
ML:	Low liquid limit silt	MLO:	Low liquid limit silt containing organic

Figure 2-16 Plasticity chart of CSCS [206].

Table 2-19 lists the classification of the studied sediment according to different

classification systems. By comparing these classification results of different classification systems (GTR, USCS, ESCS and CSCS), it could be found that although the group symbols are different, the characteristic of the classification remains the same for the studied sediments. The studied sediment belongs to organic and low plastic (LL＜50% and PI<26%) soil (silt).

For the applications of the studied sediments in road construction, according to the GTR guide [32], the studied sediment can be used in embankments without treatment, while used in subgrade with hydraulic binder treatment. The studied sediment has a medium ability as road materials, according to the AASHTO [205]. The CSCS has no suggestions for the applications of materials in road construction, but the Chinese standard JTG D30-2015 [207] points out that dredged sediments can't be used in embankments. It could be reused in embankments after being treated with lime and/or other binders.

Table 2-19 Classification of the studied sediments according to different classification systems.

Classification system	USCS	ESCS	GTR	AASHTO	CSCS
Group symbol	OL	SiM	F11A1m	A-7-6	MLO
Classification	Organic soil with low plasticity	Silt of medium plasticity	Weakly organic and low plastic silt	Clayey soils	Low liquid limit silt containing organic
Applications	/	/	Used in embankment (without treatment) and subgrade (with the treatment of hydraulic binder)	Has a medium ability as road materials	Used in embankment with the treatment of lime and/or other binders

2.4 SWOT analysis of different binders

A SWOT analysis of the various binders was performed to compare and choose a binder used to treat the dredged sediments in road construction. The results are shown in Table 2-20 and Table 2-21. It should be noted that OPC represents the Ordinary Portland Cement; L represents the lime; RMC represents the Reactive Magnesium Oxide cement; G represents the Geopolymer; AAM represents the Alkali-Activated Materials; CSA represents the Calcium Sulfo-Aluminate cement. Besides, Figure 2-17 compares the different binders' CO_2 emissions, price and energy consumption. The prices of the different binders are from the regional e-commerce platform (www.alibaba.com). Owing to the cost of G and AAM associated with the use of alkali activators, only using the price of typical alkali activator-NaOH represents the cost of G and AAM in Figure 2-17 (b).

It's evident that the CSA has significant potential for improving the environmental impact of the OPC. However, the price of the CSA is higher than the OPC, which is because of the excessive need for aluminum in raw materials to manufacture the CSA clinker [208]. In France, the price of CSA cement is approximately 2.3 times more than the CEM I 52.5 R Portland cement [209]. The CSA cement is chosen as the binder used to treat sediments in this study. The CSA cement has a few disadvantages: the risk of expansion, cracking and the high price. But it has many advantages: lower calcination temperature (1250°C), lower CO_2 emission, lower limestone demand (35-40%), energy-saving for better grind-ability properties, high early and final strength, impermeability, sulfate, chloride corrosion resistance and low alkalinity [135-138]. At the same time, we also use the standard binder OPC for comparisons.

Table 2-20 SWOT analysis of different binders (I).

	OPC	**L**	**RMC**
Strength	Low-cost materials; availability; reliability; durable in water and chemical attacks.	Highly porous and has high permeability; cost-effective.	Lower calcination temperature (~700-800°C); less energy consumption (2400 MJ/t MgO); hydrates more rapid; renewable energy sources can be used; low pH (8-10); superior buffering capacity, cost-effectiveness and ease/safety of handling.
Weakness	Caustic; significant environmental impacts; high CO_2 emissions (0.95 t CO_2/t OPC); high energy consumption (5000 MJ/t OPC); high non-renewable resources (1.5 t limestone and clay/t OPC); slow early strength development.	Limestone mining and calcination cause a series of environmental problems; high CO_2 emissions (0.80 t CO_2/t L); high energy consumption (4000 MJ/t L); causes severe irritation for the skin or eyes; the quicklime is not stable and easy to carbonize in the air.	High CO_2 emissions (1.4 t CO_2/ t MgO); high non-renewable resources (2.08 t $MgCO_3$/ t MgO); low strength; poor water resistance.
Opportunities	Mature technology; the product is easy to produce and obtain; stable performance and easy to be accepted by engineers; the use guidebook/standard is more comprehensive.	Historical and easy to be accepted; easy to obtain.	Special environmental applications; for S/S of hazardous materials.
Threats	Replaced by other environmentally friendly and low-carbon binders; in order to reduce carbon emissions, the government may require cement plants to reduce production or even close.	Replaced by other environmentally friendly and low-carbon binders.	Shorter development time; the actual application is immature; relatively high cost.

Table 2-21 SWOT analysis of different binders (II).

	G	AAM	CSA
Strength	Lower CO_2 footprint; high early and/or final strength, high resistance against chemical attack, the good passivation of reinforcement, a very dense microstructure and heat resistance; excellent thermal (e.g. fire); high permeability.	The precursors of AAM are mainly industrial by products or wastes; sustainability; high strength; low environmental impact.	Lower calcination temperature (1250°C); lower CO_2 emission; the lower limestone demand (35%-40%); improving energy saving for easily grindable; a wide range of industrial wastes and by-products be used in manufacturing CSA; high early and final strength.
Weakness	The prices of the activators, their energy intensiveness and the availability of the raw materials limit the use of geopolymer binders; lack of long-term (20+ years) durability data.	Activators are expensive and environmental footprint; durability.	The risk of expansion induced cracking; local expansion or cracking.
Opportunities	Replace OPC and lime for less environmental impact; reuse industrial waste as raw materials.	Have been commercially produced; replace OPC and lime for less environmental impact; reuse industrial waste as raw materials.	Sustainability; durability; Used for rapid setting, early strength and S/S of hazardous materials.
Threats	Need high temperature curing for higher strength; regulatory standards limit.	Uncertainty risk: raw materials and activators significantly affect strength.	Relatively small quantity product; not easy to get in some areas.

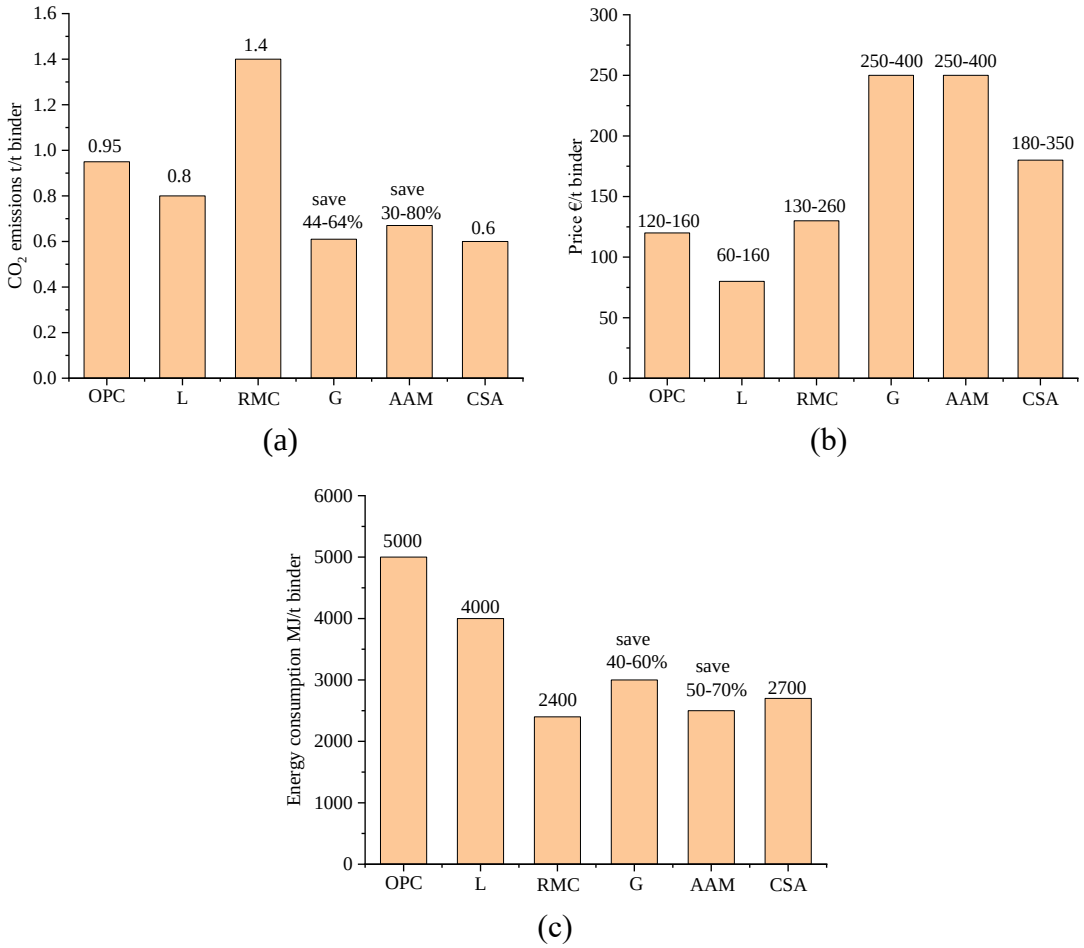

Figure 2-17 (a) CO_2 emissions, (b) price and (c) energy consumption of the different binders (Source: Data from the publications [84] [85] [88] [89] [98] [100] [108] [109] [110] [122] [131] [132] and the regional e-commerce platform (www.alibaba.com)).

2.5 The studied binders

The Ordinary Portland Cement (OPC) used throughout this study was from LafargeHolcim Saint-Pierre-La-Cour Company, which was white and CEM I 52.5 R type. In terms of the second binder, the used Calcium Sulfo-Aluminate (CSA) cement Alpenat R² was from the Vicat company, composed of sulfoaluminate clinker and gypsum.

2.5.1 Physical characterization of the studied binders

2.5.1.1 Particle size distribution

According to the result obtained by the laser diffraction technique, the particle size distributions of the used OPC and CSA binders are shown in Figure 2-18. The results

were obtained from an average of three measurements. It is noted that the particle size ranges of the OPC and CSA binder are the same, between 0.38 µm and 78 µm. This means both binders are finer than the studied sediments.

The 10th, 50th and 90th percentile particle sizes of the OPC, d_{10}, d_{50} and d_{90}, are 2.20, 9.98, 26.51 µm. This result conforms to several studies undertaken on the same type of cement from the same company [210] [211]. For the CSA, particles smaller than 1.81 µm is around 10% by volume (d_{10}), the amount of particles smaller than 8.99 µm is around 50% (d_{50}) and the amount of particles smaller than 43.65 µm is around 90% (d_{90}).

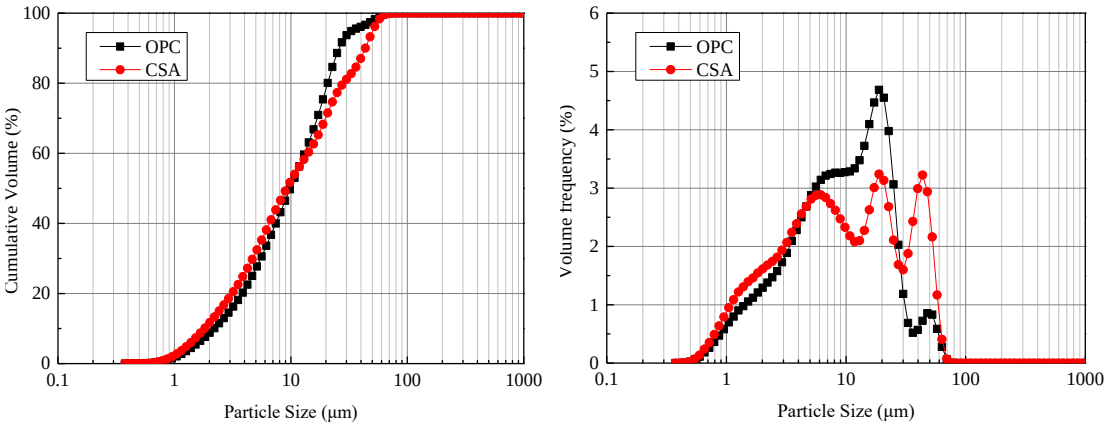

(a) (b)

Figure 2-18 Particle size distribution of the studied binders: (a) cumulative and (b) frequency curve.

2.5.1.2 Solid density

Figure 2-19 and Table 2-22 show the results of the solid density, with the three measurements performed on the OPC and CSA. It could be found that the average solid density values of the OPC and CSA binders are 3.20 g/cm^3 and 3.02 g/cm^3, respectively. These values are close to previous studies' results with the same type of cement from the same company (Table 2-22). Both binders have higher solid densities than raw sediments (2.58 g/cm^3).

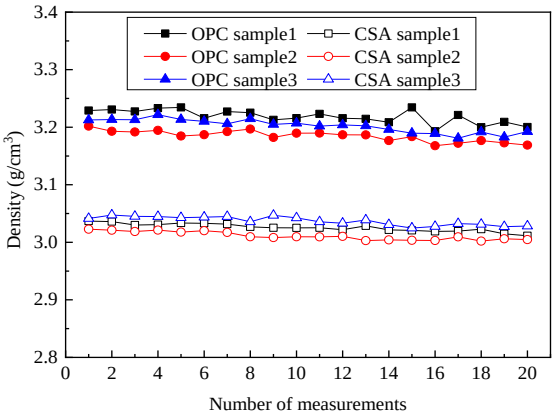

Figure 2-19 Solid density of the studied binders.

Table 2-22 Solid density of the studied binders.

		ρ_s (g/cm^3)			
	Sample No.	1	2	3	Average
This study	OPC	3.22	3.18	3.20	3.20
	CSA	3.03	3.01	3.04	3.02
Other studies	OPC [210]	/	/	/	3.14
	OPC [212]	/	/	/	3.11
	CSA [209]	/	/	/	2.97

2.5.1.3 Loss on ignition (LOI)

Table 2-23 shows the LOI values of the used OPC and CSA binders. This test was performed at 950°C for two hours, according to the European standard EN 196-2 [179]. It can be concluded that the LOI values of the OPC and CSA binders are 1.90% and 3.38%, respectively. These values agree well with other studies in Table 2-23, which indicates that the used OPC and CSA are qualified. Besides, these LOI values are less than the limit of 5.0%, as specified by the European standard EN 197-1 [213]. The LOI could be attributed to the decomposition of carbonate. The cement is in contact with CO_2 in the air during transportation and storage, forming $CaCO_3$ from free lime (CaO) or $Ca(OH)_2$ [214].

Table 2-23 Loss on ignition of the studied binders.

		LOI (%)			
	Sample No.	1	2	3	Average
This study	OPC	1.95	2.01	1.75	1.90
	CSA	3.29	3.67	3.19	3.38
Other studies	OPC [212]	/	/	/	1.45
	CSA [209]	/	/	/	3.80

2.5.2 Chemical characterization of the studied binders

2.5.2.1 Chemical composition (XRF)

The X-ray fluorescence (XRF) analysis was carried out for the used OPC and CSA binders. For comparison with other studies' results, the results were calculated and expressed in the form of oxides, as reported in Table 2-24. The OPC binder's principal components include 64.10% CaO, 19.90% SiO_2, 4.80% Al_2O_3, 3.30% SO_3, 2.60% Fe_2O_3 and 1.00% MgO. The composition of the CSA binder includes 40.50% CaO, 17.40% Al_2O_3, 13.70% SO_3, 8.50% SiO_2, 7.30% Fe_2O_3, 1.10% MgO and other trace components. These values are close to previous studies' results with the same type of cement from the same company (Table 2-24).

Table 2-24 Chemical composition of the studied binders. (wt %)

Components	Percentage (%)				
	This study		Other studies		
	OPC	CSA	OPC [210]	OPC [212]	CSA [209]
MgO	1.00	1.10	0.95	/	/
Al_2O_3	4.80	17.40	4.86	4.93	18.22
SiO_2	19.90	8.50	20.07	20.06	8.16
SO_3	3.30	13.70	3.55	3.67	15.24
K_2O	1.00	0.30	1.00	/	/
CaO	64.10	40.50	64.25	63.94	43.60
Fe_2O_3	2.60	7.30	3.07	2.86	7.64

2.5.2.2 Mineral composition (XRD)

Figure 2-20 shows the XRD patterns of the studied OPC and CSA binders. Table 2-25 reports the mineralogical composition of the OPC and CSA binder determined by XRD using the Rietveld method [198]. The 20 wt% Corundum (Al_2O_3) was added to

the samples as an internal standard to determine the content of the mineral phase. The mineral quantification of the binders was made by Rietveld analysis with the Diffracplus Topas software (Bruker-AXS). The mineral crystal structure data was taken from the ICDD PDF and Bruker Structure Database [199].

The mineralogical composition of the used OPC binder includes the major phase of 63.74% C_3S and 18.04% C_2S, the minor phase of 9.82% C_4AF, 7.25% C_3A and 1.14% $C\bar{S}H_2$. The used CSA binder in this study contains 45.45% $C_4A_3\bar{S}$, 26.11% C_2S, 15.53% Anhydrite, 6.13% Calcite and other minor phases. These compositions agree well with the same type of cement from the same company (Table 2-25).

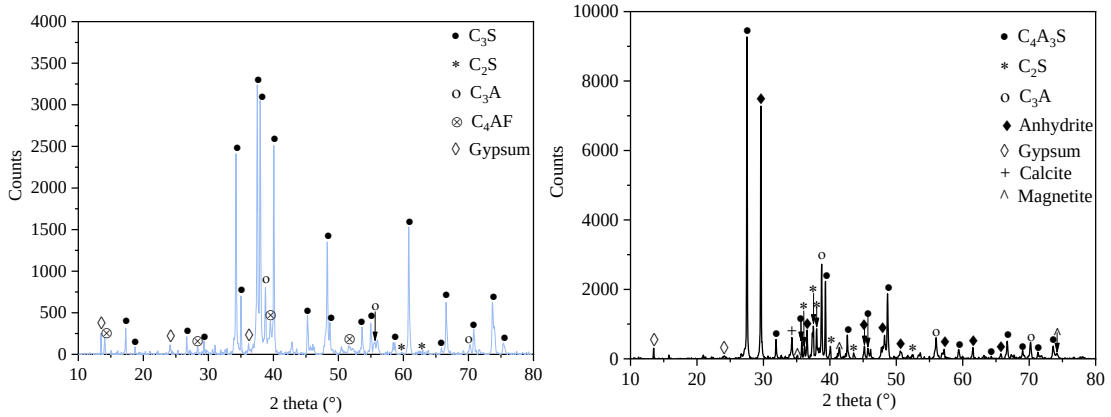

(a) (b)

Figure 2-20 X-ray diffractions patterns of the studied binders (Co Kα): (a) OPC and (b) CSA.

Table 2-25 Mineralogical compositions of the used binders in this study. (wt %)

Mineral	Symbol	Percentage (%)				
		This study		Other studies		
		OPC	CSA	OPC [210]	OPC [212]	CSA [209]
Alite	C_3S	63.74	/	61.00	59.90	/
Ferrite	C_4AF	9.82	1.20	10.00	9.40	/
Aluminate	C_3A	7.25	0.82	8.00	7.40	/
Gypsum	$C\bar{S}H_2$	1.14	1.90	/	0.30	0.31
Belite	C_2S	18.04	26.11	15.00	17.60	22.41
Ye'elimite	$C_4A_3\bar{S}$	/	45.45	/	/	41.81
Anhydrite	$C\bar{S}$	/	15.53	/	/	18.00
Calcite	Cal	/	6.13	/	/	5.00
Magnetite	Mag	/	2.87	/	/	/

2.5.3 Basic physical and chemical characteristics of different binders

The basic physical and chemical characteristics of the OPC and CSA are summarized in Table 2-26. The solid density values, measured by a helium pycnometer, are about 3.20 g/cm^3 and 3.02 g/cm^3 for the OPC and CSA, respectively. The losses on ignition of the OPC and CSA are 1.90% and 3.38%, respectively. The main chemical composition of OPC is 64.10% CaO, 19.90% SiO_2 and 4.80% Al_2O_3. However, the CSA has lower CaO content and higher Al_2O_3 content, with the main chemical composition of 40.50% CaO, 13.10% SiO_2 and 17.40% Al_2O_3. The two major mineralogical elements of the OPC were 63.74% C_3S and 18.04% C_2S. Meanwhile, the CSA contained 45.45% $C_4A_3\bar{S}$ and 26.11% C_2S.

Table 2-26 Basic physical and chemical characteristics of the used OPC and CSA binders.

Parameters		Symbol	OPC	CSA
Physical characterization	Solid Density (g/cm^3)	ρ_S	3.20	3.02
	Loss on ignition (%)	LOI	1.90	3.38
	Particle size distribution			
	d_{10} (μm)		2.20	1.81
	d_{50} (μm)		9.98	8.99
	d_{90} (μm)		26.51	43.65
Main chemical composition (%)	MgO		1.00	1.10
	Al_2O_3		4.80	17.40
	SiO_2		19.90	8.50
	SO_3		3.30	13.70
	K_2O		1.00	0.30
	CaO		64.10	40.50
	Fe_2O_3		2.60	7.30
Mineralogical composition (%)	Alite	C_3S	63.74	/
	Ferrite	C_4AF	9.82	1.20
	Aluminate	C_3A	7.25	0.82
	Gypsum	$C\bar{S}H_2$	1.14	1.90
	Belite	C_2S	18.04	26.11
	Ye'elimite	$C_4A_3\bar{S}$	/	45.45
	Anhydrite	$C\bar{S}$	/	15.53
	Calcite	Cal	/	6.13
	Magnetite	Mag	/	2.87

2.6 Conclusion

Before the valorization of dredged sediments, this chapter investigates the physical, chemical, and environmental characteristics of raw sediments. For this proposal, a series of tests were carried out following the French/European standards in this chapter, including the water content, particle size distribution, Atterberg limited, solid density, specific surface, methylene blue value, organic matter content, compaction, chemical composition, thermal analysis and environmental properties. Based on these results, the studied sediments can be classified in class F11A1m, which indicates weakly organic and low plastic silt, according to the French GTR guide.

The SWOT analysis showed that the low carbon and sustainable binder-Calcium Sulfo-Aluminate cement (CSA) was the best for sediment treatment. The Ordinary Portland Cement (OPC) was chosen as a standard binder for comparisons. In addition, the basic characteristics of the OPC and CSA binders were investigated to better understand their properties and apply them to solidify dredged sediments.

Therefore, the CSA cement is innovatively introduced in the stabilization/solidification (S/S) of dredged marine sediments in this research. A series of experiments are conducted to explore the possibility of the valorization of dredged sediments in road construction with the CSA-based binders (CSA and OPC-CSA).

Before starting the treatment of sediments, we first study the sediment's rheological properties (Chapter 3) to provide a more comprehensive and detailed understanding of the inherent characteristics of sediment, especially, to provide scientific support for the pipeline transport of sediments. Such as, for the design of engineering applications involving the pumping of sediments, the rheological properties of dredged sediments are required. The fluids require a minimum pressure or head to overcome the yield stress and start to flow in the pipe [215]. The minimum head (H_{st}) could be calculated with the yield stress. Besides, the pressure drop could be calculated with apparent viscosity and yield stress [215] [216].

Chapter 3 Rheological characterization of fine-grained sediments

3.1 Introduction

This chapter evaluates the change in the static and dynamic shear rheological properties of fine-grained sediments. In the first step of this work, the artificial fine-grained sediment (kaolinite with tap water) is used to avoid the effects induced by the heterogeneity of natural sediments in such tests. Kaolinite with tap water is widely used as bed sediments in the laboratory experiments, because its similar rheological behavior with the natural sediment [217] [218], also because its reproducible properties as well as easy handling [46]. The measured yield stress is defined and compared with the predicted yield stress by several rheological models. Among the studied parameters, the influence of the water to solid (W/S) ratios on the yield stress and the plastic viscosity is discussed. In addition, the influence of the W/S ratios on the shear modulus, complex viscosity and loss factor of this material is discussed. In the second step of this work, the same protocol on the natural dredged sediments from Dunkirk port will be performed. The results will be compared with the finding of artificial sediments.

3.2 Experimental materials and methods

3.2.1 Materials

The physical characteristics of the kaolinite (in the form of manufactured powder) and the dredged sediments used in this study are presented in Table 3-1 and Figure 3-1. It should be noted that in this chapter, the big particle fraction of the dredged sediments were removed by sieving the dry sediment with the 100 μm sieve, following the previous study [44] [219]. Because the big particles may damage the rheometer geometry. It's evident that the particle size of the natural sediments is bigger than the kaolinite. There are 95.05% particles of kaolinite less than 20.00 μm, while this value is only 68.52% for sediments.

Table 3-1 Basic physical characteristics of the used materials.

Parameter	Kaolinite	Sediments	Test standard
Initial water content (%)	0.74	5.20	EN ISO 17892-1 [166]
Solid density (g/cm^3)	2.72	2.58	EN ISO 17892-3 [170]
Atterberg limit tests			EN ISO 17892-12 [169]
Liquid limit (%)	49.00	40.20	
Plastic limit (%)	30.30	28.00	
Plasticity index (%)	18.70	12.20	
Grain size distribution			ISO 13320 [168]
d_{50} (μm)	5.72	10.78	
d_{max} (μm)	39.80	100.00	
＜20.00 μm (%)	95.05	68.52	
＜30.00 μm (%)	99.60	77.65	
＜39.80 μm (%)	100	83.30	

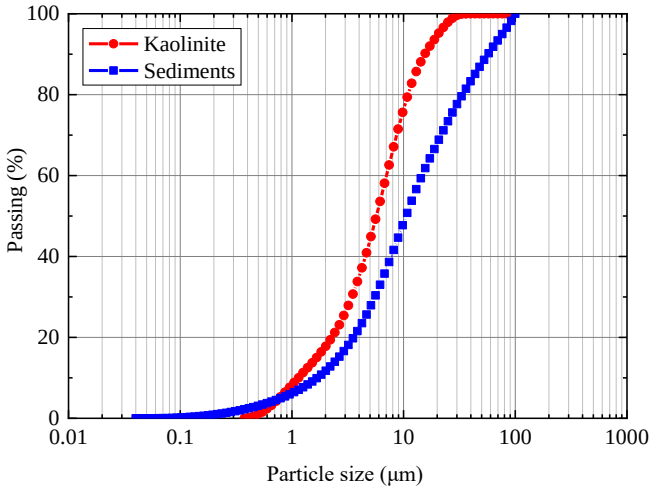

Figure 3-1 Particle size distribution curves of the used materials.

3.2.2 Rheological measurements

The rheological characterization was performed using the Anton Paar MCR102 rheometer, equipped with a parallel plate geometry (Φ=25 mm) and a Peltier system for temperature control (±0.1°C). The rheometer is characterized by high precision and accuracy. All the tests were carried out at a controlled temperature of 20±0.1°C. The gap value is 2 mm.

In this study, the preparation of samples was conducted by mixing the fine materials (kaolinite powder or natural sediment) with water for 5 minutes using a handheld mixer. The mixtures were made with the different ratios in mass (W/S) of 0.90, 1.00,

1.10, 1.20, 1.30 and 1.40. The rheological test started at 7 min after the contact of the fine materials (kaolinite powder or natural sediment) and water.

The static shear test to measure the rheological properties of the sample is the controlled shear rate (CSR) test. The main objective of such tests is to obtain the so-called flow curve by drawing the measured shear stress (τ) versus the applied shear strain rate ($\dot{\gamma}$). The apparent viscosity (η) was also obtained for analysis, which is defined as the ratio of the shear stress to the corresponding shear strain rate (Equation (3-1)).

$$\eta = \frac{\tau}{\dot{\gamma}} \tag{3-1}$$

The whole test procedure includes two stages: the first stage consists of pre-shearing the sample with a high shear strain rate (100 s^{-1} for 100 s) to homogenize the sample and remove any build-up structure of kaolinite. In the second stage, the shear rate was decreased in steps from 100 to 0.01 s^{-1}, to draw the flow curve of the material. The same protocol was followed for all the presented flow curve tests.

Furthermore, in the oscillatory mode of shearing, the strain sweep tests at a constant frequency of 1 Hz were performed prior to the following measurement of oscillatory frequency, to determine the linear viscoelastic domain (LVED) for each sample.

Next, the frequency sweep oscillatory tests were carried out at the different W/S ratios samples. First, the samples underwent a pre-shearing for 100 s at the high shear rate of 100 s^{-1}, then the frequency (ω) was increased in steps from 0.07 to 100 rad/s and subsequently decreased from 100 to 0.07 rad/s in order to check for the presence of hysteresis. This allowed monitoring the evolution of all the complex viscosity (η^*), the elastic modulus (G'), the loss modulus (G") and the loss factor (tan δ) in a non-destructive regime.

Figure 3-2 is a vector diagram illustrating the relationship among the complex shear modulus G^*, the storage modulus G', the loss modulus G" and the phase-shift angle δ. The storage modulus G' (Pa) represents the elastic portion of the viscoelastic behavior, which quasi describes the solid-state behavior of the sample. The definition of G' for oscillatory shear tests is

$$G' = G^* \cos\delta \tag{3-2}.$$

The loss modulus G" (Pa) characterizes the viscous portion of the viscoelastic behavior, which can be seen as the liquid-state behavior of the sample. It represents the deformation energy lost (dissipated) through internal friction when flowing. The definition of G" for oscillatory shear tests is

$$G'' = G^* \sin\delta \quad (3\text{-}3).$$

The definition of complex viscosity for oscillatory shear tests is

$$\eta^* = \frac{G^*}{\omega} \quad (3\text{-}4).$$

The definition of loss factor tan δ for oscillatory shear tests is

$$\tan\delta = G''/G' \quad (3\text{-}5).$$

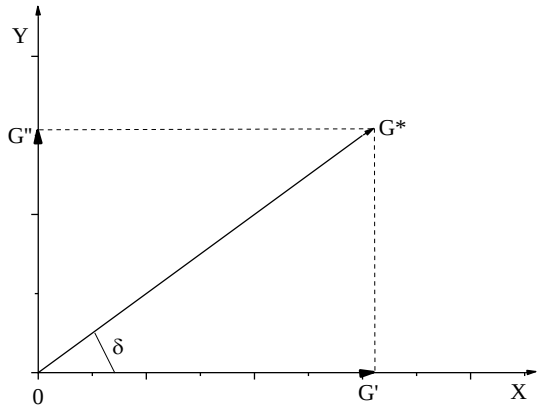

Figure 3-2 Relationship among the complex shear modulus G*, the storage modulus G', the loss modulus G" and the phase-shift angle δ.

3.3 Results and discussions

3.3.1 Steady rheological characterization of artificial fine-grained sediments

3.3.1.1 Rheological properties of artificial fine-grained sediments

Figure 3-3 presents the evolution of the shear stress (τ) versus the shear strain rate ($\dot{\gamma}$), for different W/S ratios samples. The analyses of these curves clearly demonstrate that the test samples exhibit yield stress. Moreover, the relation between the shear stress and the shear strain rate is nonlinear in the linear scale axis. Finally, the W/S ratios affect the absolute value of the shear stress and the curvature of the flow curves over the range of shear strain rates explored. With increasing W/S ratios, the curvature of the flow curves increases, while the shear stress values decrease for a given shear rate. The shear stress of the W/S ratio=0.9 is much higher than other W/S ratio cases, due to the less water causing higher particle density and poor liquidity of the materials, thereby increasing the measured shear stress.

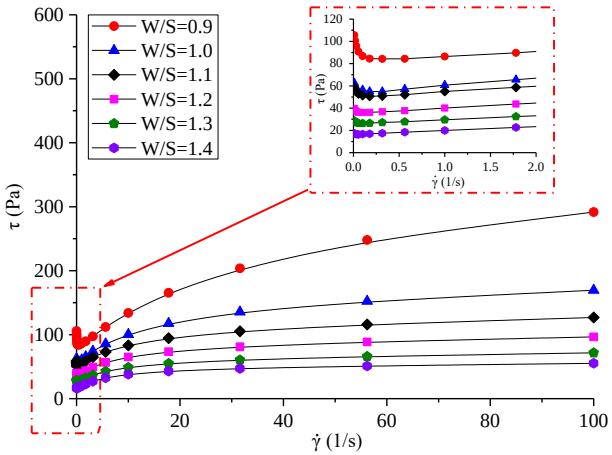

Figure 3-3 Shear stress-shear strain rate curves of artificial fine-grained sediments.

In Figure 3-4, the apparent viscosity, defined as the ratio of the shear stress to the corresponding shear strain rate, versus the shear strain rate is reported. The results in Figure 3-4, are deduced from the flow curves of Figure 3-3 in the stage where the shearing is undertaken by decreasing the shear strain rate. From Figure 3-4, it can be seen that the apparent viscosity values increase nearly linearly with the shear rate decreases, on a log-log scale within the measured interval. Moreover, for a given shear strain rate, the apparent viscosity decreases with the increase of the W/S ratios. These results indicate that the artificial fine-grained sediments samples with lower water content are deformed more slowly than samples with higher water content, under the same shear strain rate. Furthermore, the samples showed a strong shear-thinning rheological behavior.

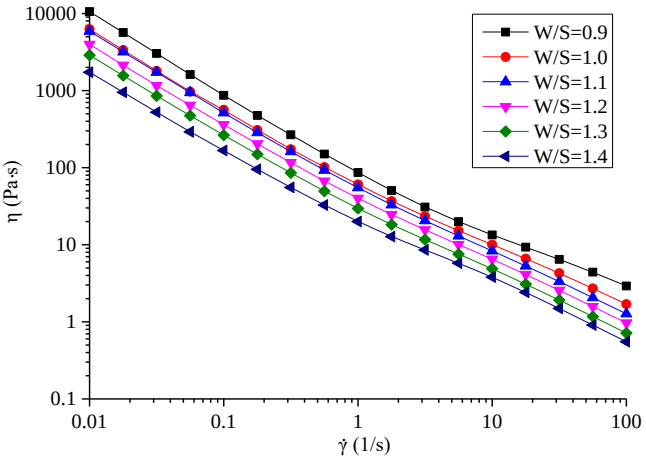

Figure 3-4 Apparent viscosity-shear strain rate curves of artificial fine-grained sediments.

The measured yield stress is defined as the minimum value of shear stress from flow curves in the semi-log scale, as presented in Figure 3-5. This value corresponds to the

critical stress that allows the fluid to maintain stable flow [220] [221] [211]. At very low shear rates, the shear stress increases further, indicating flow instability [222] [223]. With the decrease of shear rates, at very low shear rates, the buildup speed of the particles is higher than the speed of breakdown by the shear gradient, causing particles settling, increasing local particle density and thereby increasing the measured shear stress. The measured yield stresses of the different samples are presented in Figure 3-6. From Figure 3-6, we can address the effects of the W/S ratios on the measured yield stress of the artificial fine-grained sediments samples. This means that the measured yield stresses decrease with the increase of W/S ratios.

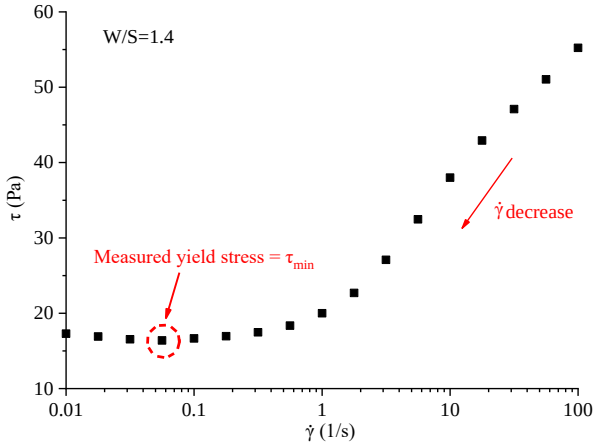

Figure 3-5 The definition of measured yield stress from flow curves in semi-log scale [211].

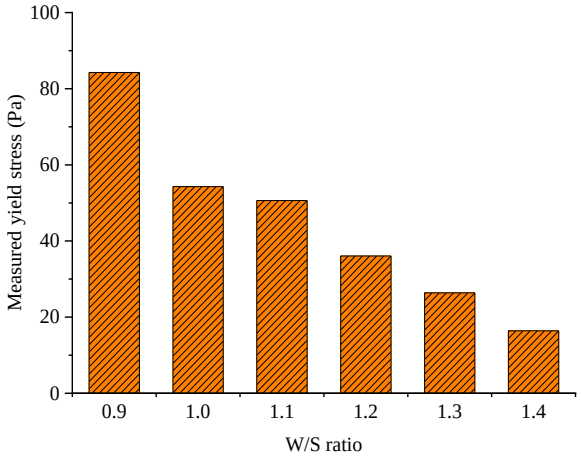

Figure 3-6 The measured yield stress of artificial fine-grained sediments with different W/S ratios.

3.3.1.2 Rheological models of artificial fine-grained sediments

In terms of modeling, the following three models that could take into account the observed behaviors (yield stress and nonlinear relationship between shear stress and shear strain rate) were used: modified Bingham, Herschel-Bulkley and Casson models. The performance of these models is reported in many past works [211] [224] [225]. As listed in Table 3-2, in these models, τ = shear stress (Pa); $\dot{\gamma}$ = shear rate (1/s); τ_0 = yield stress (Pa); η_p = plastic viscosity (Pa•s); c = constant; K = consistency index (Pa•s^n); n = flow behavior index; and η_∞ = infinite viscosity (Pa•s). For comparison, the Bingham model is also used in this study.

Table 3-2 The conventional rheological models.

Models	Equations	References
Bingham model	$\tau=\tau_0 + \eta_p\dot{\gamma}$	[211] [225]
Modified Bingham model	$\tau=\tau_0 + \eta_p\dot{\gamma} + c\dot{\gamma}^2$	[211] [225]
Herschel-Bulkley model	$\tau=\tau_0 + K\dot{\gamma}^n$	[211] [225]
Casson model	$\tau^{1/2}=\tau_0^{1/2} + (\eta_\infty\dot{\gamma})^{1/2}$	[225]

It is seen from Table 3-2 that the Bingham and modified Bingham models, respectively, employ linear and second-degree responses with the yield stress to derive mathematical approximations of the samples. The Herschel-Bulkley model describes the nonlinearity of the flow curve as a function of power index n. It exhibits the nonlinearity behaviors of pseudoplastic (shear-thinning) when $n < 1$. While it expresses the dilatant behaviors (shear-thickening) when $n > 1$. It could also be reduced to the Bingham model when $n = 1$. The Casson model is a non-Newtonian fluid model with yield stress. It has been widely used for the plastic fluid that exhibits shear thinning.

The comparisons of the different rheological models with the experimental data of flow curves, for the different W/S ratios samples, have been reported in Figure 3-7.

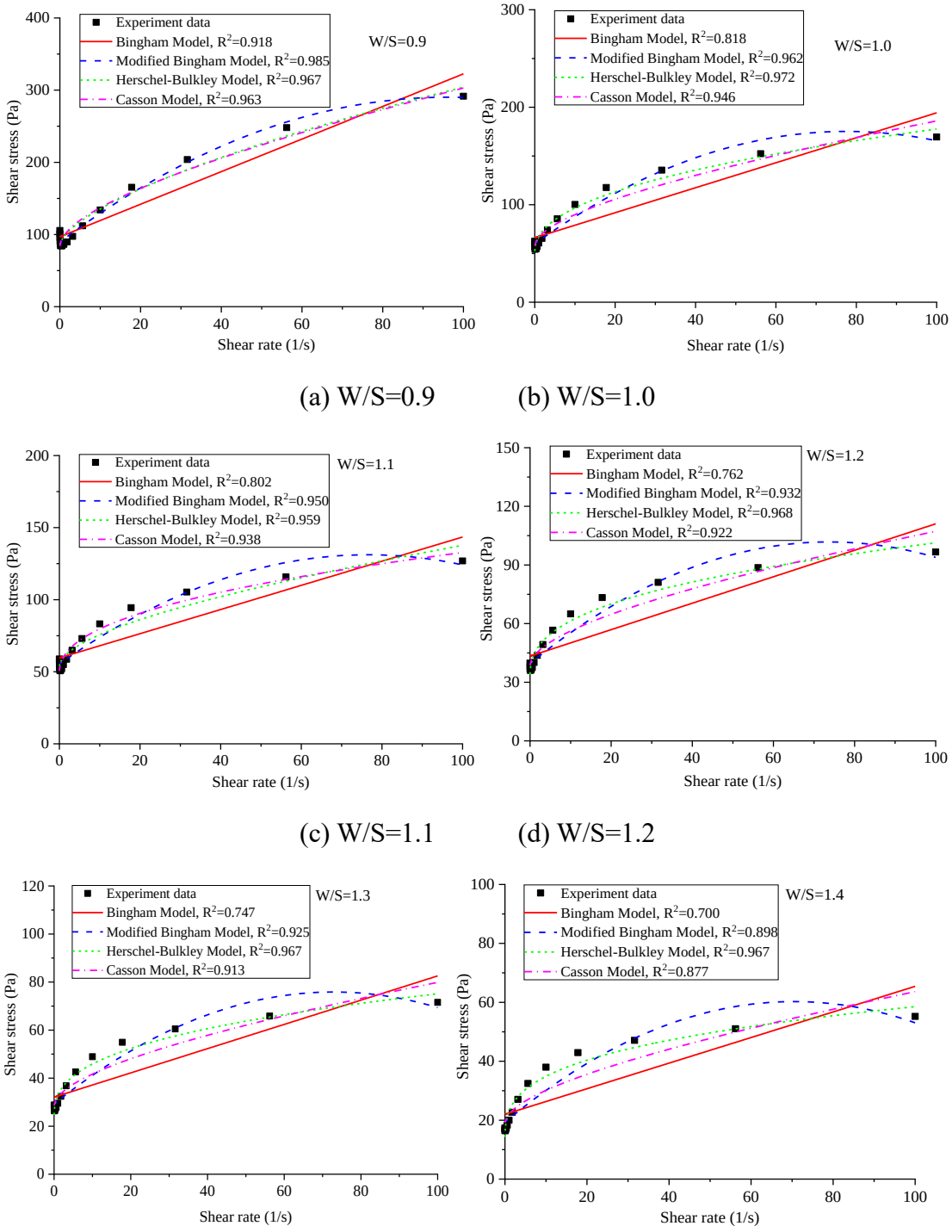

(a) W/S=0.9 (b) W/S=1.0

(c) W/S=1.1 (d) W/S=1.2

(e) W/S=1.3 (f) W/S=1.4

Figure 3-7 Comparison of the expression of different rheological models of the flow curves for artificial fine-grained sediments.

In order to identify the models' parameters, an optimization procedure based on the least square method is used. In Figure 3-8, the yield stress calculated by the different models is shown and compared with the measured values as discussed previously. According to Figure 3-8, the effects of the W/S ratios on the yield stress identified

from all four models are confirmed. All the yield stress values predicted by the four models decrease, with the W/S ratios increasing from 0.9 to 1.4. However, the comparisons of the absolute values show very high discrepancies. The yield stress value predicted by the Bingham model is the largest, the Herschel-Bulkley model predicts the lowest yield stress, the modified Bingham model and the Casson model predict values that are close to the measured values. This shows that the proposed measured yield stress method is successful and can assess the yield stress of the artificial fine-grained sediments.

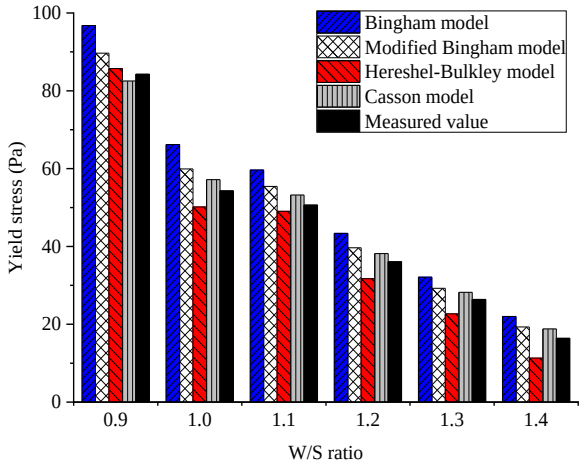

Figure 3-8 Comparison between the measured yield stress and the predicted values of the different models for artificial fine-grained sediments.

The obtained results in terms of the model parameters identification are summarized in Table 3-3. It can be seen from Table 3-3 that:

-For the modified Bingham model, both parameters η_p and c are affected by the change in the W/S ratio. The η_p decreases with the increase of the W/S ratio, whereas c increases with the increase of the W/S ratio.

-For the Bingham model, the calculated plastic viscosity η_p values are about 37%-54% of those predicted by the modified Bingham model. The same trend in terms of variation with the change in W/S ratio is observed (n_p decrease with W/S increase).

-For the Hershel-Bulkley model, it can be observed that the consistency index K change with the W/S ratio, all of the n values are less than 1, which means that all of the artificial fine-grained sediments samples exhibit shear-thinning behavior. Especially the lower n value indicates a higher intensity of shear-thinning, when $n < 1$ [226]. The flow behavior index n decrease when the W/S ratios increase.

-For the Casson model, the infinite viscosity predicted by the model seems to decrease with the increase of the W/S ratio. This result is in accordance with the expected results.

Table 3-3 Plastic viscosity(η_p), consistency index(K), infinite viscosity(η_∞), constant c and flow behavior index (n) values of the different models.

Models	Parameters	W/S ratios					
		0.90	1.00	1.10	1.20	1.30	1.40
Bingham	η_p/(Pa•s)	2.258	1.281	0.838	0.677	0.505	0.434
Modified Bingham	η_p/(Pa•s)	4.185	2.971	1.977	1.685	1.280	1.163
	c	-0.022	-0.019	-0.013	-0.011	-0.009	-0.008
Herschel-Bulkley	K/(Pa•s^n)	11.270	17.015	11.233	12.644	10.272	11.773
	n	0.644	0.437	0.436	0.370	0.354	0.302
Casson	η_∞/(Pa•s)	0.692	0.369	0.197	0.174	0.131	0.132

The correlation coefficient R^2 for all the models is reported in Figure 3-9. Considering the values of R^2, the Bingham model exhibits the lowest fit and the largest errors, R^2 varies from 0.70 to 0.92. The Herschel-Bulkley model has the highest R^2 (all R^2 > 0.96), regardless of the W/S ratios (except for 0.9 W/S ratios), which indicates that the Herschel-Bulkley model gives the best correlation with the experimental data. The Modified Bingham model and the Casson model exhibit comparable values of R^2.

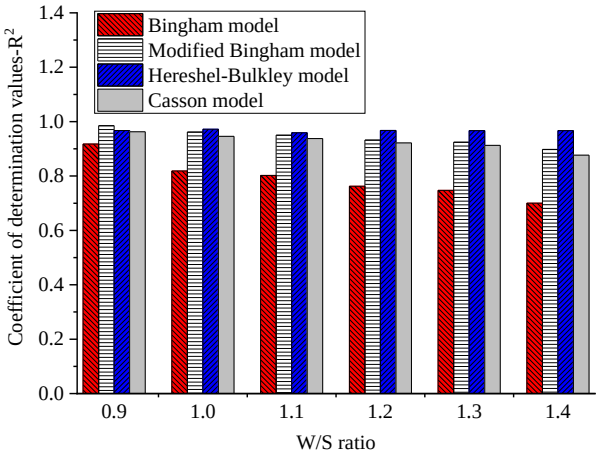

Figure 3-9 Correlation coefficients (R^2) for the models investigated.

In Figure 3-10, the predicted yield stresses obtained by the different rheological models are compared with those measured yield stress. At the same time, the mean absolute percentage error (MAPE) values are calculated as Equation (3-6).

$$\text{MAPE} = \frac{1}{n}\sum_{i=1}^{n}\left|\frac{\tau_{pre} - \tau_{mea}}{\tau_{mea}}\right| \times 100\% \quad (3\text{-}7)$$

Where, τ_{mea} = measured shear stress; τ_{pre} = predicted shear stress by the rheological models.

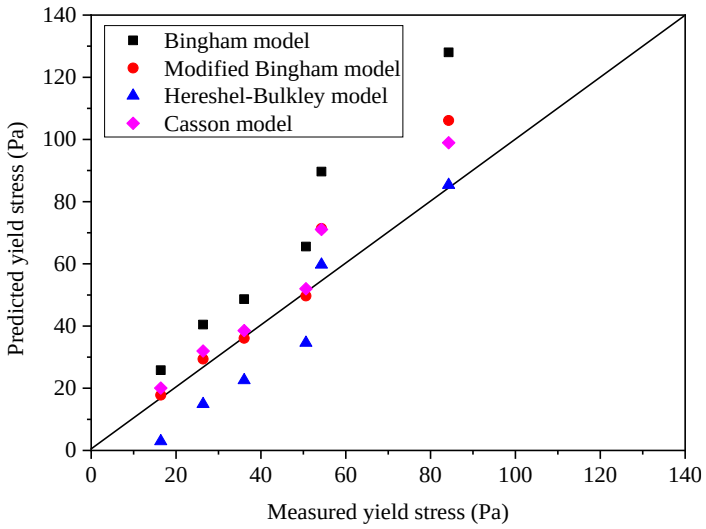

Figure 3-10 Comparison of the measured and predicted yield stress.

For the Casson model, the value of MAPE is just 6.67 %, which indicates the outstanding ability of this model to predict the measured yield stress. The Bingham model shows the worst ability, the value of MAPE reaches 21.77 %. This is because the fitting of the Bingham model is more suitable for the linear part of the flow curve observed in the range of low shear rates [211]. However, the non-linear models of Herschel-Bulkley and modified Bingham show moderate differences with the experiments, where the value of MAPE is 11.60% and 10.79%, respectively. The values of predicted yield stresses confirm that the Herschel-Bulkley model predicts smaller values and the modified Bingham model superior values, which agrees with Bala et al. [211] and Vance et al. [220].

Although all three models (the Modified Bingham model, Herschel-Bulkley model and Casson model) have high R^2 values. Considering the Carson model has the lowest MAPE. In this study, we consider that the Carson model is the best model for predicting the rheological properties of artificial fine-grained sediments.

3.3.2 Dynamic rheological characterization of artificial fine-grained sediments

3.3.2.1 Dynamic strain sweep tests for artificial fine-grained sediments

In the oscillatory measurement conditions, a shear strain sweep at a constant frequency (f = 1 Hz) is performed prior to the oscillatory frequency in order to ensure that the selected shear strain is in the linear viscoelastic region. Figure 3-11 shows the variations of the elastic modulus (G') and the loss modulus (G") with the shear strain at a constant frequency of 1 Hz for all samples. It can be observed that below a critical strain of 0.03 %, all the samples exhibited a LVED characterized by constant elastic (G′) and loss (G″) modulus. The suspension can recover elastically at shear strain values lower than the critical strain and act as a solid structure [227]. The results agree with the results of the similar system studied by Xu and Huhe [49]. All samples exhibit G′ greater than G″ in the linear region, where the system's structure is not disturbed. When the strain increases, both G′ and G″ decrease significantly and a crossover is observed, indicating the transition to a prevalent liquid-like behavior. Thus, based on these results, a shear strain of 0.02% (lower than 0.03%) was selected to perform the frequency sweep oscillatory shear measurements in the following study.

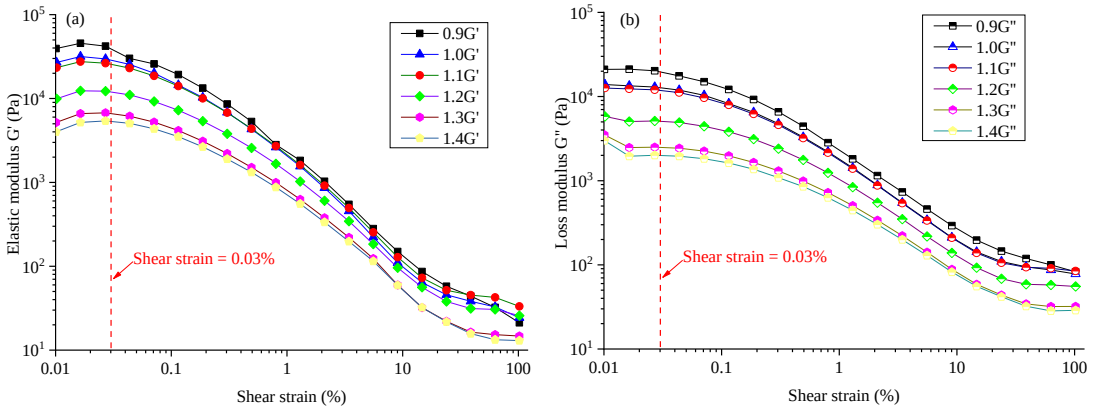

(a) Elastic modulus G' (b) Loss modulus G"

Figure 3-11 An amplitude sweep at a fixed frequency of 1 Hz: variation of the G' and G" with the shear strain.

3.3.2.2 Dynamic frequency sweep tests for artificial fine-grained sediments

Figure 3-12 shows the variations of the complex viscosity (η^*), the elastic modulus (G') and the loss modulus (G") with the frequency for all the samples. From Figure 3-12(a), it can be concluded that for the sample with the W/S ratio equal to 0.9, no hysteresis is observed in the considered frequency range. It can be seen that both G'

and G" have a nearly parallel linear trend in a log-log scale, with G" smaller than G'. This indicates that the elastic behavior is more dominant than the viscous behavior of these samples. The similar behavior was observed for all the samples, but these parameters were lower with a higher W/S ratio. Especially in terms of loss modulus, it measures the energy dissipated as heat, when the specimen turns viscous. Once the W/S ratio increases, the higher W/S ratio means the sample has higher water content

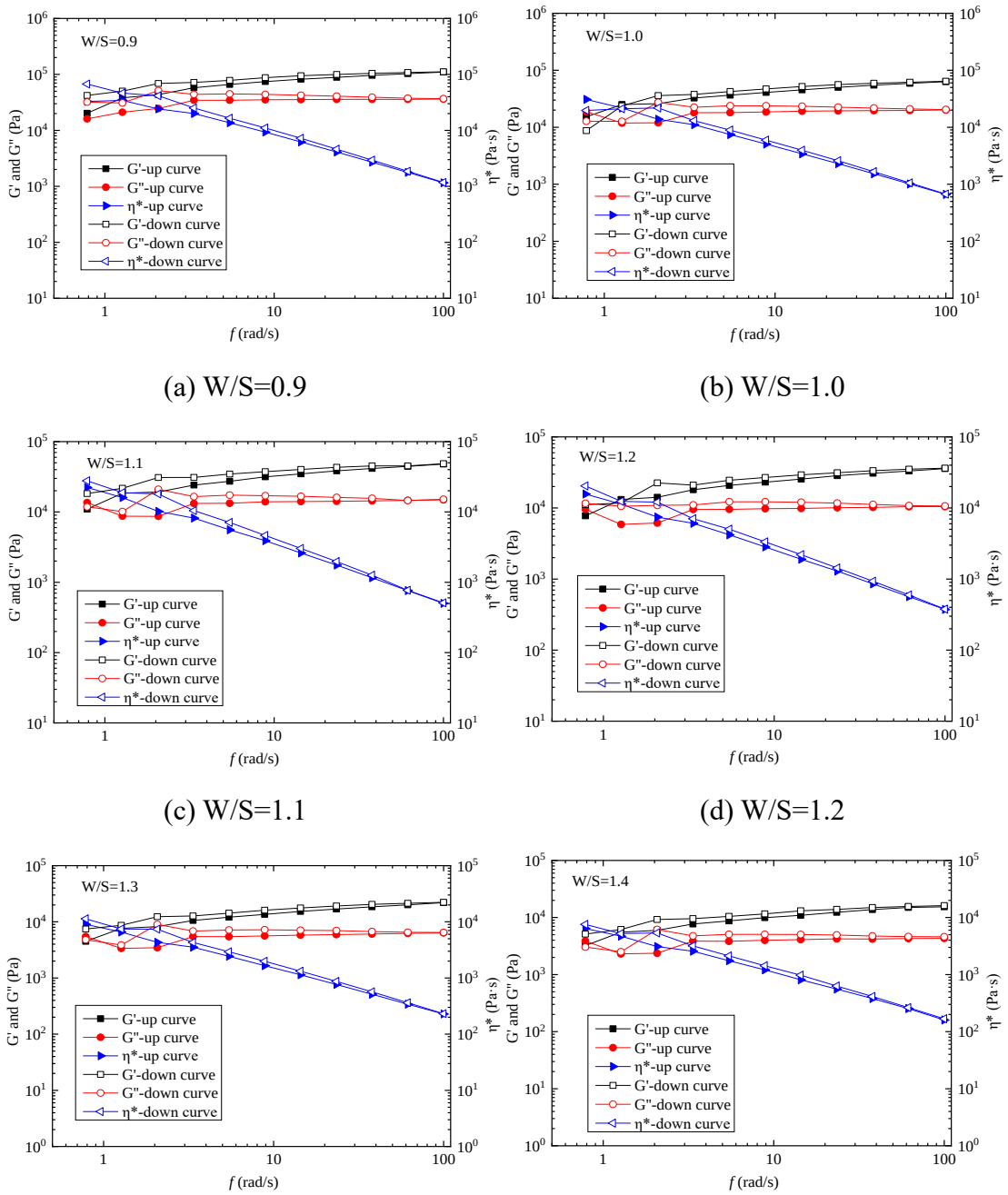

(a) W/S=0.9 (b) W/S=1.0

(c) W/S=1.1 (d) W/S=1.2

(e) W/S=1.3 (f) W/S=1.4

Figure 3-12 Variations of the complex viscosity, the elastic modulus and the loss modulus as a function of the frequency.

and fewer viscous responses, thus the loss modulus value decreases. Moreover, Figure 3-12 demonstrates that the complex viscosity sharply decreases with the increase of frequency. The frequency dependence of the loss modulus and the elastic modulus is rather weak over the studied frequency range (0.7-100 rad/s).

To better highlight the observed trends, Figure 3-13 shows the variations of the elastic modulus, the loss modulus and the complex viscosity with the W/S ratios at the frequency of 5.46 and 100 rad/s. It can be seen that the elastic modulus, the loss modulus and the complex viscosity significantly decrease with the increase of the W/S ratios. The regression equations obtained by the curve fitting method are given in Table 3-4. A high correlation between the data and fitting curves is obtained for the complex viscosity, the elastic modulus and the loss modulus, respectively. All the regression correlation coefficients (R^2) are larger than 0.994.

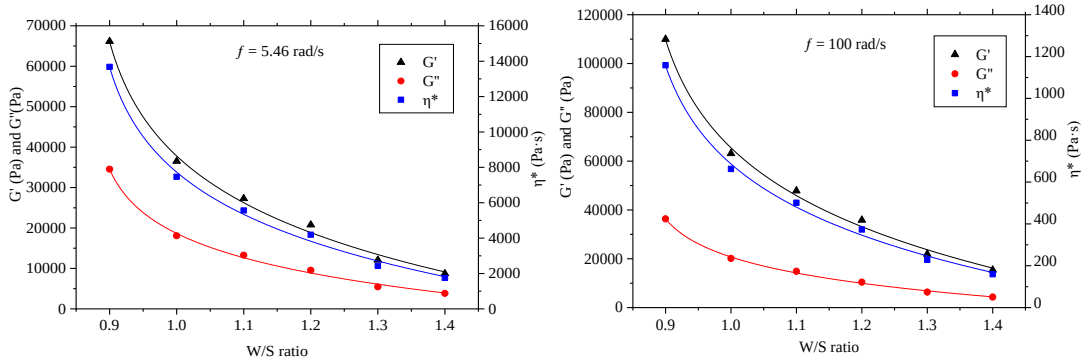

(a) f = 5.46 rad/s (b) f = 100 rad/s

Figure 3-13 Variations of the complex viscosity, the elastic modulus and the loss modulus with the W/S ratios.

Table 3-4 Fitting equations of Figure 3-13.

Frequency	Parameters	Equations	R^2
f = 5.46 rad/s	G'	G' = −3887.4−20789.2×ln(W/S−0.9)	0.994
	G"	G" = −2710.2−10385.7×ln(W/S−0.9)	0.996
	η*	η* = −854.7−4253.4×ln(W/S−0.9)	0.994
f = 100 rad/s	G'	G' = −6344.1–36936.7×ln(W/S−0.9)	0.994
	G"	G" = −3033.9–11981.3×ln(W/S−0.9)	0.997
	η*	η* = −69.4–388.0×ln(W/S−0.9)	0.995

Figure 3-14 displays the scatter diagram of the relationship between the loss factor and the W/S ratios at the frequency of 5.46 and 100 rad/s. The loss factors decreased almost linear with the increase of W/S ratios. The curve fitting method obtains the regression Equations (3-8) and (3-9). The loss factor describes the ratio of the two

portions (viscous flow behavior and elastic deformation behavior) of the viscoelastic behavior. All loss factors are between 0 and 1, which means that the elastic behavior is dominant for all the samples.

For the frequency of 5.46 rad/s,

$$\tan \delta = 0.66 - 0.16\,(W/S) \tag{3-8}$$

For the frequency of 100 rad/s,

$$\tan \delta = 0.42 - 0.10\,(W/S) \tag{3-9}$$

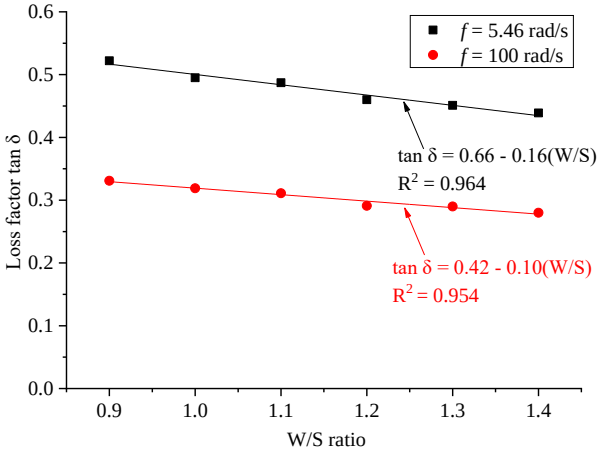

Figure 3-14 Variations of the loss factor with the W/S at the frequency of 5.46 and 100 rad/s.

This analysis is based on dynamic measurement. It could provide a better understanding for the dynamic behavior of the artificial fine-grained sediments. It is a useful analysis method to determine the elastic and viscosity properties of the artificial fine-grained sediments, which can provide meaningful insight for technical matters, such as mixing, pumping and improving the sediment treatment process efficiency. For example, it can be found that the viscosity under the action of high-frequency vibration is lower. The viscosity reduction is obvious for the concentrate slurry (low W/S ratio) at high-frequency (Figure 3-12). Thus, it may use high-frequency mechanical vibration to reduce viscosity. The low viscosity helps the flow of sediments in the pipeline, reducing the resistance loss and energy consumption.

3.3.3 Comparison of the rheological properties for natural and artificial fine-grained sediment

Figure 3-15 (a)-(b) shows the shear stress-shear strain rate curves and the apparent viscosity-shear strain rate curves, for natural sediment samples. The properties of the used natural sediment have been given in chapter 2. It should be noted that the big

particle fraction was removed by sieving the dry sediment with the 100 μm sieve, following the previous study [44]. Because the big particles may damage the rheometer geometry. Besides, the gap value must be at least ten times larger than the maximum particle of the sample. Similar trends could be observed for the natural sediment compared with the flow behavior of the artificial fine-grained sediments.

However, the change of the apparent viscosity with shear strain rate is different between the artificial and natural fine-grained sediments. For artificial fine-grained sediments, the apparent viscosity values increase nearly linearly with the shear rate decreases in Figure 3-4. While the increase of the apparent viscosity is not large in the high shear strain rate range (around 1-100 1/s), for the natural fine-grained sediments in Figure 3-15 (b).

After pre-shearing, the different waiting times (0s, 10s, 100s and 1000s) were performed on the identical W/S ratio sample (W/S=1.0) to see if settlement may influence the rheological properties of natural fine-grained sediments. Figure 3-16 shows the flow curves for various waiting times. Because the results of these flow curves are so similar, it's plausible to assume that the differences in the rheological properties between the artificial and natural fine-grained sediments aren't due to settlement.

The yield stress is mainly determined by the electrostatic double-layer forces between particles [45] [228] for very fine sediments particle or clay particle. At rest, the fine particles group into small clusters and flocculated aggregates, with the power of electrostatic forces [45]. Under the high shear rate, the flocculated aggregates are reduced to smaller flocs and individual particles, decreasing particle interaction and resulting in low apparent viscosity. With the shear rate dropped from 100 to 0.01 1/s for the artificial fine-grained sediments, the effect of flocculation between fine particles is enhanced, the apparent viscosity is significantly increased.

The natural fine-grained sediments have larger particle sizes than the artificial fine-grained sediments (d_{50} is 5.72 μm for kaolinite and 10.78 μm for sediments), with more silt-sized particles and fine sand-sized particles [45] [228]. It is more likely to be influenced by hydrostatic rather than electrostatic forces. The particles would tend to form framework structures through direct physical interactions. Under the high shear rate, the framework of silt-sized particles was disrupted. The fine clay particles become dispersed among the larger silt particles and serve as a lubricant between them, resulting in the low apparent viscosity. With the shear rate dropped from 100 to

1 1/s for the natural fine-grained sediments, the rate of structure breakdown is faster than the rate of framework structure buildup, the apparent viscosity does not increase much.

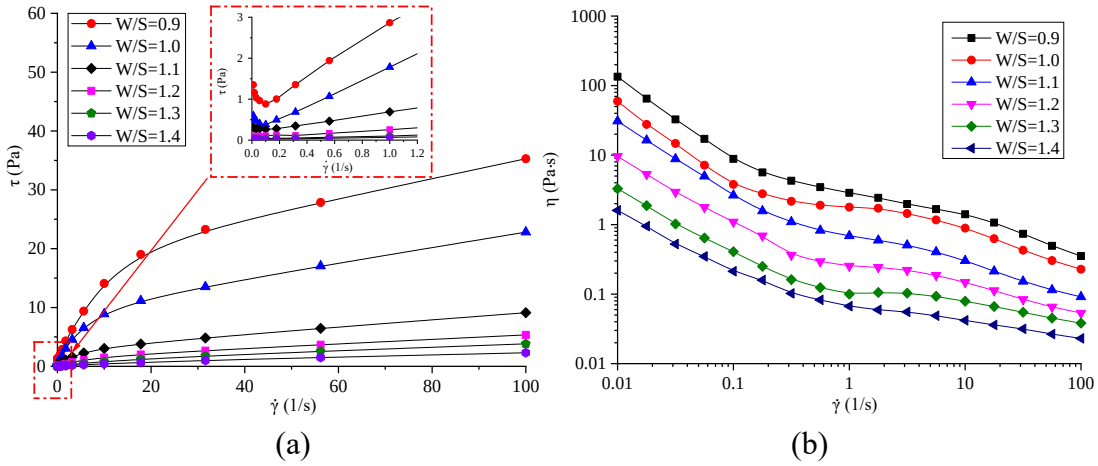

Figure 3-15 (a) Shear stress-shear strain rate curves and (b) apparent viscosity-shear strain rate curves of natural sediment samples.

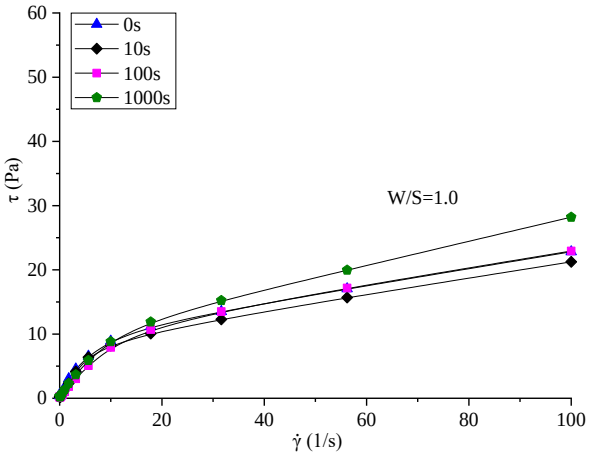

Figure 3-16 Effect of different waiting time after pre-shearing (W/S=1.0).

Figure 3-17 displays the measured yield stresses of the natural sediments samples. The effects of the W/S ratios on the measured yield stresses are similar to those of artificial sediments. This means that the measured yield stress values of the natural fine-grained sediments decrease with the increase of the W/S ratios. However, the higher measured yield stresses for the artificial sediments, may be attributed to the strong flocculation between fine particles [45]. It's important to note the minimum torque rotation of the MCR 102 rheometer is 5 nNm, the radius of the parallel plate geometry is 12.5 mm. Thus, the minimum shear stress for the used rheometer is 1.22×10^{-3} Pa, based on Equations (3-10) and (3-11). Therefore, these measured

yield stress values are acceptable in Figure 3-17.

$$\mathrm{M} = \int_0^R 2\pi r^2 \tau dr = \frac{2}{3}\pi R^3 \tau \tag{3-10}$$

$$\tau = \frac{3M}{2\pi R^3} \tag{3-11}$$

Where, M is the torque (Nm), R is the radius of the parallel plate geometry (m), τ is the shear stress (Pa), r is the distance from the rotation axis ($0 \leq \mathrm{r} \leq \mathrm{R}, \mathrm{m}$).

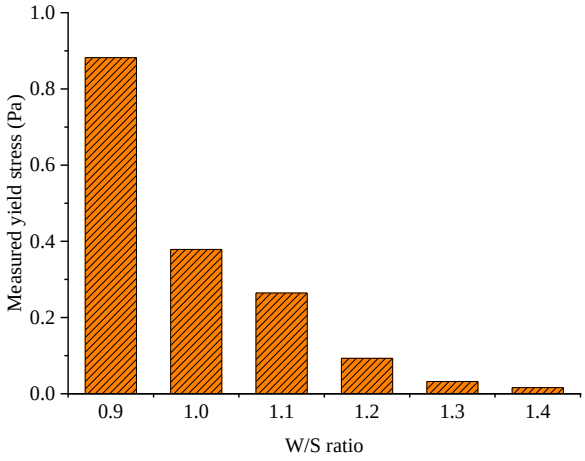

Figure 3-17 Measured yield stress of natural fine-grained sediments with different W/S ratios.

Figure 3-18 compares the yield stress calculated by the different models for the natural fine-grained sediments. The corresponding R^2 values are presented in Figure 3-19. It is apparent that the yield stress value predicted by the Bingham model is the largest, the Herschel-Bulkley model predicts the lowest yield stress, the modified Bingham model and the Casson model predict comparable values of yield stress. Considering the values of R^2, the Bingham model has the lowest R^2 values (0.84-0.98). The Herschel-Bulkley model has the highest R^2 values (0.99-1). The Modified Bingham model (0.94-1) and the Casson model (0.92-0.99) exhibit comparable values of R^2. These results are similar to the artificial sediment. However, the yield stress predicted using the Herschel–Bulkley model, for the samples with the W/S ratios of 0.9, 1.0 and 1.3, was negative (-0.852 Pa for 0.9 W/S ratio, -0.615 Pa for 1.0 W/S ratio and -0.003 Pa for 1.3 W/S ratio), which is physically impossible. Messaoudi et al. [52] also obtained the same results for the predicted yield stress of the Chorfa dam sediments, by using the Herschel–Bulkley model. Therefore, the Herschel–Bulkley model is not suitable for the part of the W/S ratios of nature sediments.

In addition, all the yield stress values predicted by models are significantly different

from the measured values for the natural fine-grained sediments. The values of MAPE can confirm this. The MAPE values corresponding to the Bingham model, the Modified Bingham model, the Herschel-Bulkley model and the Casson model are 3.43, 1.57, 1.34 and 1.85, respectively. This means none of them can be claimed to be a superior model to predict the yield stress for natural fine-grained sediments. It's worth finding and comparing other more advanced models to predict the yield stress of the natural sediments.

Previous studies have proved that the rheological behavior of the sediments or the kaolinite slurries, can be complex. It is influenced by the temperature [229], soil type [230], pH [231], salinity [232], particle size distributions [45], organic matter [45], mineralogy [228], the type of rheometer used and the test procedures followed [228]. Shakeel et al. [50] found the yield stress of the sediments from Hamburg Port, was dependent on the depths and locations in the harbor. The yield stress of the sediments samples increased by going deeper into the sediments bed. Therefore, the study of the rheological parameters for sediment is complex and highly site-specific. The different values of the rheological parameters for natural and artificial sediment in this study, highlight the necessity of the direct rheological tests on the natural sediment to obtain accurate rheological parameters [46]. Easy handling of conducting laboratory experiments with tap water and kaolinite should not prevent the direct measurements on natural sediment. Moreover, the non-uniformity of the natural sediments results in difficulties in conducting laboratory experiments on the natural sediments compared to kaolinite. It should also be noted that extracting proper rheological parameters of the natural sediments is somehow challenging in picking a small homogeneous natural sediments sample and changing the natural water content ratio [46].

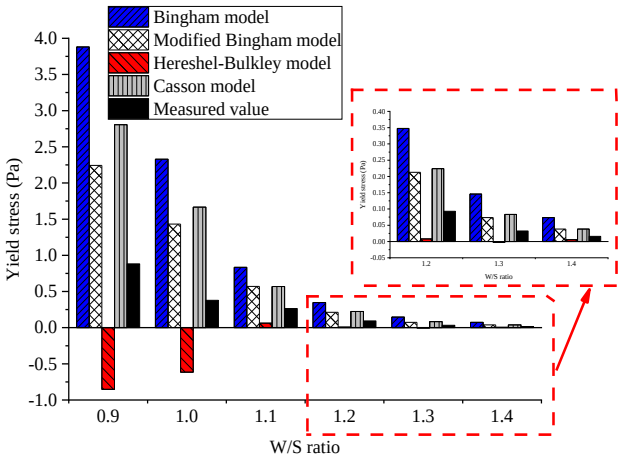

Figure 3-18 Comparison of the measured yield stress and the predicted values of the different models for natural fine-grained sediments.

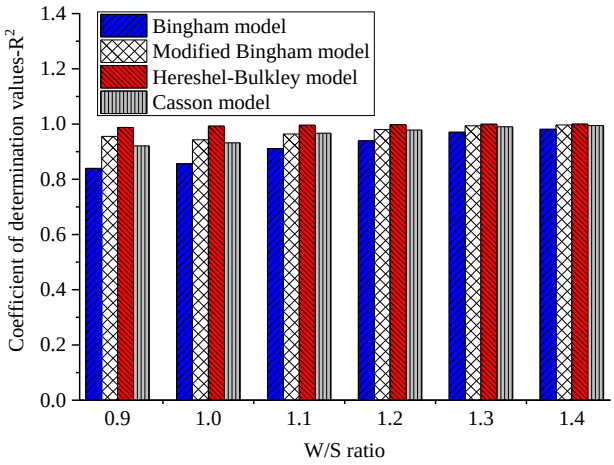

Figure 3-19 Correlation coefficients (R^2) of the different models for natural fine-grained sediments.

3.4 Engineering application

This study described the flow behavior of the fine-grained sediments, which can provide the scientific support for understanding and solving all kinds of natural and manmade activities involving fine-grained sediments, such as:

(i) Dredged sediments handling and transport by pipelines. For the design of engineering applications involving the pumping of sediments, the rheological properties of the dredged sediments are required, such as shear stress, viscosity, yield stress and water content. As reported by Mehrabani and Goharkhah [215], Slatter [233] and Sellgren et al. [234], these design parameters such as pipe diameter, flow velocity and line pressure can be predicted from the rheological parameters. However, these applications are complex and beyond the scope of this study, the detailed information can be found in these research articles. Here, we only list some examples.

The plastic Bingham fluids require a minimum pressure or head to overcome the yield stress and start to flow in the pipe [215]. The minimum head (H_{st}) is related to the yield stress, as Equation (3-12) [215] [235]. For large industrial-sized pipes conveying non-Newtonian slurries, the estimation of the laminar/turbulent transition velocity (V_c) could use Equation (3-13) [233]. Besides, the pressure drop could be calculated with apparent viscosity and yield stress [215] [216]. Sellgren et al. [234] point out that concentrated viscous sediments characterized by yield stresses in the range of about 100 to 200 Pa can be pumped effectively with the centrifugal pumps. With the yield stresses up to 200 Pa, the pressure required to overcome pipe friction may be 8 and 2 kPa/m, for the pipeline diameters of 0.1 and 0.4 m, respectively.

$$H_{st} = \frac{4\tau_0 L}{\rho g D} \quad (3\text{-}12)$$

$$V_c = 26\sqrt{\frac{\tau_0}{\rho}} \quad (3\text{-}13)$$

Where, H_{st} = minimum head, V_c = transition velocity, τ_0 = yield stress, ρ = slurry density, g = the gravitation acceleration, L = the length of the design pipe, D = the pipe diameter.

Besides, it can be found that the viscosity under the action of high-frequency vibration is lower. The viscosity reduction is obvious for the concentrate slurry (low W/S ratio) at high-frequency (Figure 3-12). Thus, it may use high-frequency mechanical vibration to reduce viscosity, the low viscosity helps the flow of the sediments in the pipeline, reducing the resistance loss and energy consumption.

(ii) Geological hazards, like the landslide caused by rainfall or earthquake, the generation and movement of mudflow. Landslide and mudflow are considered serious geological hazards. Indeed, the rheological properties play a role in the initiation and evolution of a landslide or mudflow, yield stress may be in terms of the triggering conditions of a landslide or mudflow, while the flow curve with its subsequent evolution.

(iii) Ocean energy development includes laying and maintaining submarine cables and pipelines; deep-sea mining engineering. Due to submarine waves and mudflows, submarine sediments routinely evolve into fluidized sediments flows, establishing flow mobility and impact energy, during long-distance migration. This may seriously endanger marine engineering facilities, such as submarine cables and pipelines, deep-sea mining equipment. Thus, studying the rheological properties of the sediments will be helpful in ocean energy development.

3.5 Conclusion

This study set out to better understand fine-grained sediments' steady and dynamic rheological properties. The artificial and natural fine-grained sediments were used for comparison. Based on the analysis of the results, the following conclusions can be obtained:

(1) In the steady flow curve measurements, similar flow curves and different rheological parameters could be observed for artificial and natural sediments. It can be conducted that, no matter the artificial or natural samples, the fine-grained

sediments are non-Newtonian viscous fluids. The presence of yield stress of fine-grained sediments is evident, the W/S ratios influence it. The apparent viscosity decreases with the increase of the W/S ratio for a given shear strain rate.

(2) The results obtained for the artificial fine-grained sediments demonstrated the efficiency of the proposed method, for determining measured yield stress. It can be considered as a method of determining the yield stress, which is more direct and accurate. The Casson model was the best one to predict the yield stress of the artificial fine-grained sediments, because of its high R^2 and the lowest MAPE, also close to the measured yield stress value. However, all the models have very high MAPE values for the natural fine-grained sediments. This means none of them can be claimed to be a superior model to predict the yield stress for natural fine-grained sediments. It's worth finding and comparing other more advanced models to predict the yield stress of the natural sediments.

(3) For the artificial fine-grained sediments, in the dynamic oscillatory shear measurement with the considered shear strain of 0.02 %, the loss modulus (G'') is markedly smaller than the elastic modulus (G'), indicating that elastic behavior is more dominant than viscous behavior of these samples. The complex viscosity (η^*) sharply decreases with the increase of frequency. But the frequency dependence of the loss modulus and the elastic modulus is rather weak over the range of the studied frequency (0.7-100 rad/s), both loss and elastic modulus have not changed much.

(4) For the artificial fine-grained sediments, the elastic modulus, the loss modulus, the complex viscosity and the loss factor significantly reduced with the increase of W/S ratios. The dynamic rheological properties of the artificial fine-grained sediments can be expressed as appropriate functions of the W/S ratios.

(5) The study of the rheological parameters for sediment is complex and highly site-specific. The different values of rheological parameters for natural and artificial sediment in this study, highlight the necessity of the direct rheological tests on the natural sediment to obtain accurate rheological parameters. The difference in rheological parameters between the artificial and natural fine-grained sediments may be attributed to the differences in particle size (d_{50} is 5.72 μm for kaolinite and 10.78 μm for sediments). The strong flocculation between fine particles for kaolinite, enhanced the yield stress and the apparent viscosity. It should also be noted that extracting proper rheological parameters of natural sediments is somehow challenging.

Chapter 4 Characterization of the solidified sediments with single binder: OPC/CSA

4.1 Introduction

In chapter 2, the low carbon and sustainable binder-CSA has been chosen to treat the dredged sediments. OPC was selected as a standard binder for comparisons. Therefore, this chapter evaluates the effectiveness of the treatment for dredged marine sediment with OPC/CSA single binder in road construction.

In this context, the main works of this chapter are: (i) assess the Proctor compaction properties and immediate California Bearing Ratio (I-CBR) index of the treated sediments with the OPC/CSA single binder; (ii) compare and validate the efficacy of the OPC/CSA single binder in enhancing the mechanical properties (e.g., unconfined compressive strength, splitting tensile strength and elastic modulus) of the treated sediment; (iii) investigate the environmental characterization and microscopic mechanism of the treated sediments with the OPC/CSA single binder.

4.2 Experimental materials and methods

4.2.1 Raw Materials

The characterizations of dredged sediments, OPC and CSA used in this chapter have been given in chapter 2.

4.2.2 Methods

In the current study, the mix proportions of different samples are shown in Table 4-1, which was designed regarding our previous research [95] [236] [237]. The abbreviation SD represents untreated sediments. While SDxOPC represents the treated sediments using x% OPC, SDyCSA represents the treated sediments using y% CSA. It should be mentioned that the mass ratio of the binder and dry sediments was used to establish the percentage content of OPC and CSA. The mixing water was tap water. The mass ratio of water and solid (dry sediments plus dry binders) was used to calculate the percentage water content for treated sediments.

Table 4-1 Mix proportions of different samples.

Samples	OPC (%)	CSA (%)	OPC+CSA (%)
SD	0	0	0
SD2OPC	2	0	2
SD4OPC	4	0	4
SD6OPC	6	0	6
SD2CSA	0	2	2
SD4CSA	0	4	4
SD6CSA	0	6	6

The prepared dry sediments powder and a certain amount of water were mixed for five minutes with a Hobart mixer for modified Proctor compaction and I-CBR tests. After curing in the plastic bags for 24 h, the wet sediments were mixed with the design amount binder for five minutes. Then the modified Proctor and I-CBR tests were carried out directly with the obtained homogeneous mixture, in accordance with the standards NF EN 13286-2 [174] and NF EN 13286-47 [175]. The test carries out in a Proctor mould with a diameter of 150 mm and a height of 120 mm. The sediment was filled up in five equal layers and 25 strokes were applied to each layer with a 4.5 kg hammer by performing falls from a height of 457 mm. Finally, the maximum dry density (MDD), optimum moisture content (OMC) and I-CBR index values of the solidified sediments were determined.

The workability period (Wp) of the hydraulically bound mixture is determined by the European standard NF EN 13286-45 [238]. The Wp presents the time that the hydraulically bound mixture can be placed, before the binder setting prevents compaction. The Wp is the value of time that corresponds to a reduction of 2% of dry bulk density.

To assess the mechanical performance of the OPC/CSA solidified dredged marine sediments, the cylindrical specimens (D=5 cm, H=10 cm) were prepared with the static compaction method, in accordance with the standard NF EN 13286-53 [239]. Firstly, the dry sediments and binder were mixed in an electric mixer for five minutes. Then, the tap water was added, mixing was performed for another five minutes. Afterward, the mixtures were transferred into the cylindrical mould with a diameter of 50 mm and a length of 100 mm. The mixture was compacted to reach the desired height by using axial compression. These cylindrical specimens were hermetically sealed in the plastic boxes and cured at 20±2°C for 3, 7 and 28 d. Three specimens

were prepared to obtain the average values for each design mixture.

The unconfined compressive strength was measured using the INSTRON testing machine according to NF EN 13286-41 [240], as shown in Figure 4-1(a). The unconfined compressive strength is given by Equation (4-1).

The elastic modulus is determined in an unconfined compression test according to NF EN 13286-43 [221], which uses the secant slope at 30% of peak compressive strength. Firstly, the maximum compression strength of the specimen is measured (for a given mix). Then the elastic modulus is measured on another sample. As shown in Figure 4-1(b), to measure the elastic modulus, three local small strain sensors were mounted on the middle height of the specimens to get the actual local small strain of the specimen. The maximum compressive effort applied corresponds to 30% of the maximum compression strength during the elastic modulus measurement. The elastic modulus is determined according to Equation (4-2).

The indirect tensile strength test was chosen to obtain the splitting tensile strength, which was determined according to NF EN 13286-42 [241]. The specimen was placed horizontally between the two-plywood bands. The compressive force was applied perpendicularly to the axis of symmetry of the cylinder specimen, as shown in Figure 4-1(c)-(d). The splitting tensile strength is calculated by Equation (4-3).

$$q_c = \frac{4F_c}{\pi D^2} \tag{4-1}$$

$$\mathrm{E} = \frac{1.2F_c}{\varepsilon_E \pi D^2} \tag{4-2}$$

$$q_{it} = \frac{2F_{it}}{\pi HD} \tag{4-3}$$

Where, q_c is the unconfined compressive strength; q_{it} is the splitting tensile strength; F_c is the maximum force of the compressive test; F_{it} is the maximum force of the tensile test; H and D are the height and diameter of the specimens; ε_E is the longitudinal strain of the specimen, when F = 0.3 F_c.

The XRD analysis was determined on the OPC/CSA paste samples (W/S=0.5, 28d), by the BRUCKER AXS D2 ADVANCE X-ray diffractometer with a Cu Kα radiation source. The scanning electron microscopy (SEM) and mercury intrusion porosimetry (MIP) analysis were investigated on the typically treated samples. The small samples were taken from the broken samples after compressive strength tests, and dried at 40°C for at least seven days. For SEM investigations, the dried samples were coated with carbon and observed by a Hitachi S-4300SE/N electron microscope. The MIP measurements were conducted with a Micromeritics Autopore V 9600 porosimeter.

The leachability of the treated sediments was measured by standard leaching tests, following the standard NF EN 12457-2 [242]. The specimens used for leaching tests were collected after the unconfined compressive strength test, then comminuted and passed through the four mm sieve. The rotary oscillator was used to shake the sieved specimens and deionized water for 24 hours at 25℃. The liquid/solid (L/S) ratio remains unchanged at 10:1. After that, the leachates were passed through the 0.45 μm filters. The heavy metal elements of the filtrates were analyzed by the inductively coupled plasma-atomic emission spectrometer (ICP-AES) and the SPS4® autosampler. Free anions (F^-, Cl^- and SO_4^{2-}) were measured by Dionex® Ionic Chromatography (IC).

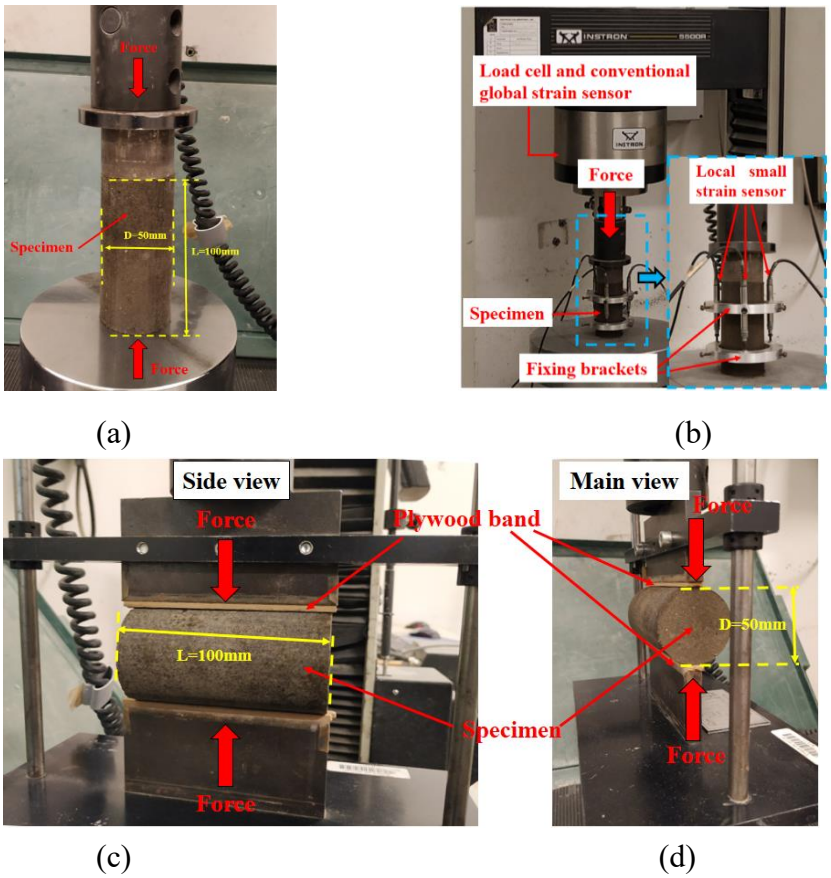

Figure 4-1 The view of the equipment: (a) unconfined compressive strength; (b) elastic modulus; (c) and (d) indirect tensile strength.

4.3 Results and discussion

4.3.1 Compaction properties and I-CBR Index

The effects of CSA and OPC binders on the compaction curves under the modified

Proctor compaction test are shown in Figure 4-2. The saturation degree curves for Sr = 80% and Sr = 100% are also presented in Figure 4-2. According to European standard NF EN 13286-2 [174], we can easily get the values of maximum dry density (MDD) and optimum moisture content (OMC) from the Proctor curve, which corresponds to the coordinate of maximum position on the Proctor curve.

It can be seen from Figure 4-2 that for the untreated sediments, the MDD is 1.641 g/cm^3 and the corresponding OMC is 21.1%. For OPC-treated sediments, the MDD is highly reduced with the addition of 2% OPC, whereas for 4% and 6% addition, the changes of MDD are less important (decrease from 1.578 g/cm^3 to 1.558 g/cm^3 and 1.574 g/cm^3). At the same time, with the decrease in MDD, the OMC increases in the same way. For CSA-treated sediments, as for OPC addition, the MDD is highly reduced and the OMC increases with the addition of 2% CSA. However, with the addition of 4% and 6% CSA, the MDD seems to increase again and the OMC decreases (an increase of MDD from 1.575 g/cm^3 to 1.615 g/cm^3 and a decrease of OMC from 23.5% to 20.2%). These results are well highlighted in Figure 4-4(a)-(b). Pourakbar et al. [243] also reported a similar phenomenon, higher binder (OPC and ultrafine palm oil fuel ash) dosage results in the increase of the MDD and the decrease of the OMC for the solidified soil. The change of MDD is attributed to the particle size and solid density of the binder and sediment [243] [244]. The binder has a low specific area and fineness [236], with the hydration and cementitious sediment particles, causing particle aggregation, forming larger macro-pores within the mixes. Thus, MDD appears to decrease compared with untreated sediments [245]. With the binder dosage increase, the fine and heavy binder compensate for the pore spaces, increasing the MDD. Additionally, the OMC increase is because part of water consumption from binder hydration, also may be due to the addition of binders leading to an increase in the specific surface area of the mixture [244] [246].

Figure 4-3 shows the I-CBR index curves of the untreated and OPC/CSA-treated sediments. The measured I-CBR index values at the OMC for all the mixtures are shown in Figure 4-4 (c). The I-CBR index value of untreated sediments is about 15% at the OMC. This value is lower than that for a subgrade material (I-CBR $\geq$ 25%) according to the specifications of the French standard [247]. The addition of CSA to dredged sediments leads to an increase linearly of the I-CBR index with the increase in the CSA content. After adding 2% CSA, the I-CBR index value reaches 20% at the OMC, then increases to 30% and 40% as the CSA content increases to 4% and 6%. This finding suggests that treating sediments with 3% CSA may be sufficient to reach

an I-CBR index value of 25%, which is the required value for subgrade material (I-CBR 25%). To be used in the pavement layer (I-CBR ≥ 35%), treatment with 5% CSA could be a reasonable value according to the specifications in French standard [247]. The I-CBR index values of OPC-treated sediments increase from 30% to 45% as the OPC content increases from 2% to 6%. This finding suggests that the I-CBR index value of treated sediments with 1.5% OPC may be sufficient to reach 25%, which is the required value for subgrade material (I-CBR 25%). To be used in the pavement layer (I-CBR ≥ 35%), treatment with 4% OPC could be a reasonable content.

The addition of binders increases the I-CBR values of treated sediments significantly. This is beneficial for road construction. Further, higher binder dosage results in higher I-CBR values. This is due to the fact that a larger binder dosage causes a stronger hydration reaction, resulting in more hydration products that connect the sediment particles and fill the pores, improving the bearing capacity of treated sediments [246].

These results show that some of the treated sediment specimens (including SD2OPC, SD4OPC, SD6OPC, SD4CSA and SD6CSA) present adequate properties for reuse as road material. However, the results of modified Proctor and I-CBR index tests reflect the behavior of solidified sediment in a short time (curing for less than 1 hour). To further examine the mechanical behavior of the treated sediment in the long term (curing for several days or even longer periods), we need to measure the mechanical characteristics in terms of compressive strength, splitting tensile strength and elastic modulus.

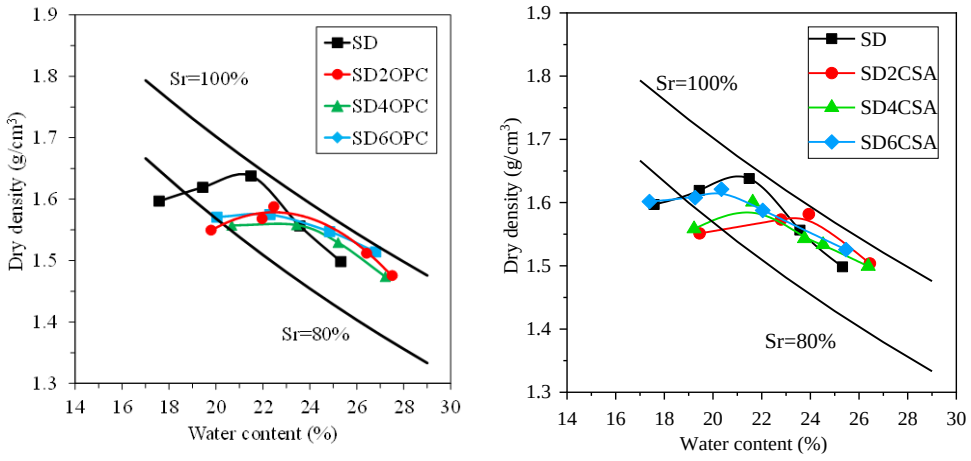

Figure 4-2 Compaction curves of the treated sediments with (a) OPC and (b) CSA.

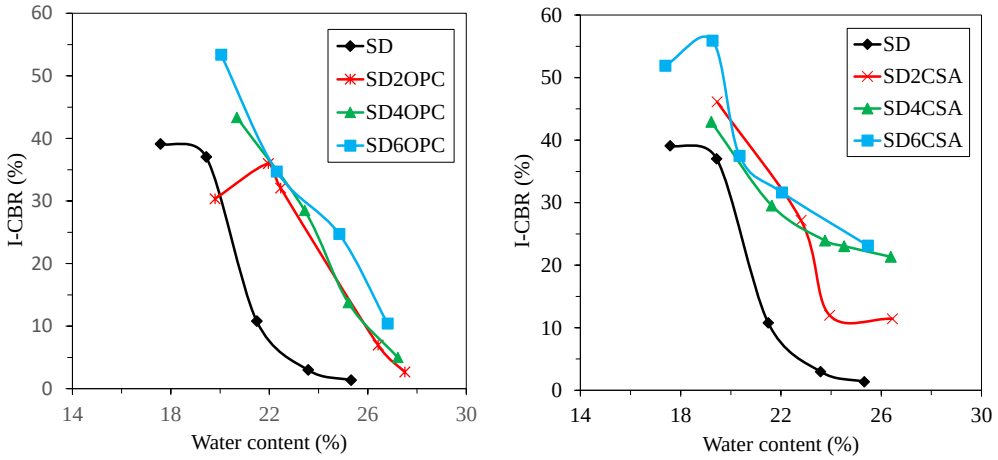

Figure 4-3 I-CBR index curves of the treated sediments with (a) OPC and (b) CSA.

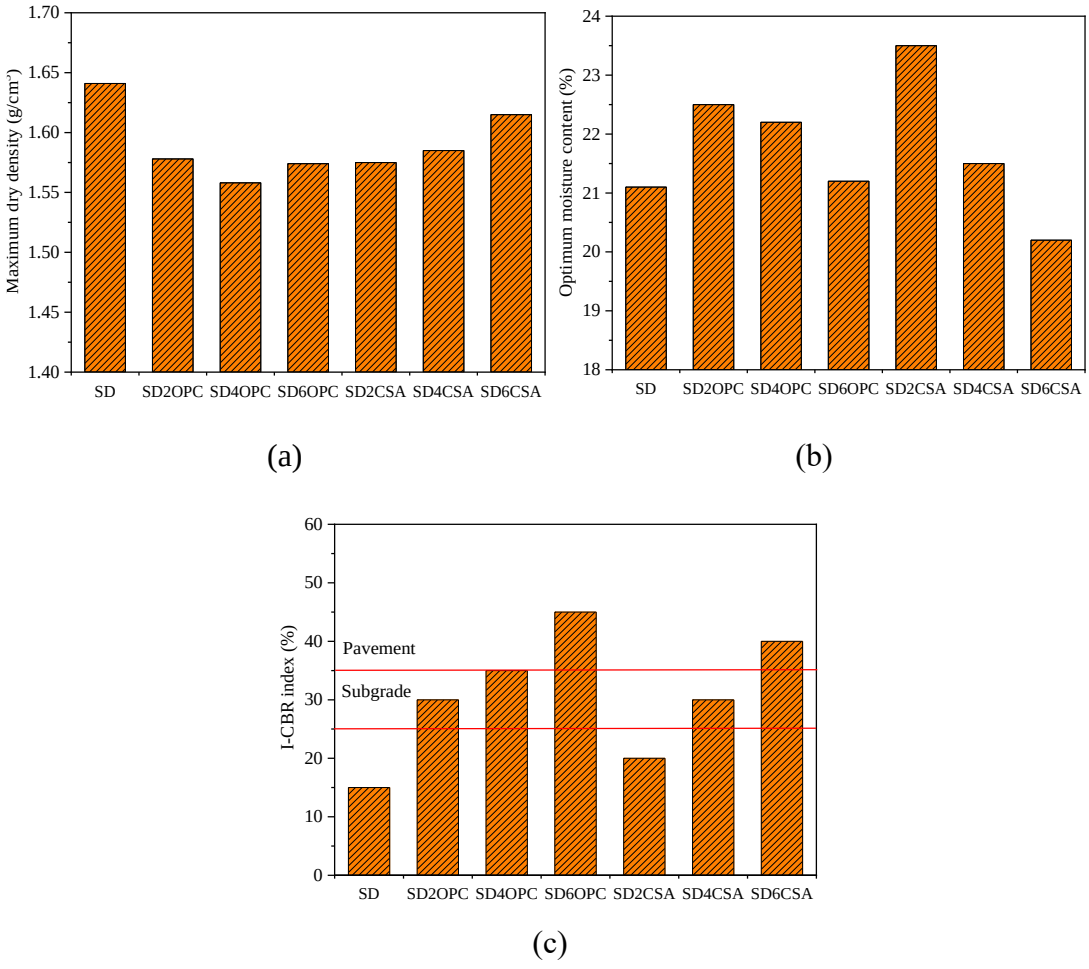

Figure 4-4 (a) Maximum dry density; (b) Optimal moisture content; (c) I-CBR index of different samples.

4.3.2 Workability period

Table 4-2 summarizes the workability period (WP) results of the OPC/CSA treated sediments. The WP achieved for SD6OPC is 205 minutes and for SD6CSA is 176 minutes. As expected, the value of WP for CSA-treated sediments is less than OPC-treated sediments. With the development of the hydration reactions for binder, the sediments particles were connected by the hydration product and formed aggregated particles. More hydration products are provided over time, resulting in the formation of coarser particle aggregation. Thereby, the formation of greater voids in the sediments matrix, resulting in a further drop in the MDD. The rate of hydration reactions for CSA is higher than OPC. Thus, the WP of the CSA treated sediments is less than OPC treated sediments.

Table 4-2 The workability period of the OPC/CSA treated sediments.

Specimens	SD6OPC	SD6CSA
Workability period (min)	205	176

4.3.3 Unconfined compressive strength

Figure 4-5 and Figure 4-6 show the variation of unconfined compressive strength (q_c) and unconfined compressive strength ratio (η_c, defined as Equation (4-4)) for OPC/CSA-treated sediments, with the different amount of OPC/CSA and curing time.

$$\eta_c = \frac{q_{cn}}{q_{c0}} \tag{4-4}$$

Where η_c is the unconfined compressive strength ratio; q_{cn} is the ratio of unconfined compressive strength of treated sediments; q_{c0} is the unconfined compressive strength of untreated sediments.

For instance, under the condition of 28 d curing, the untreated sediment (SD) displays the lowest q_c value (0.50 MPa). The q_c of treated sediments with 2%, 4% and 6% OPC inclusion increases to 0.76 MPa (SD2OPC), 1.40 MPa (SD4OPC) and 1.91 MPa (SD6OPC). Meanwhile, the η_c correspondingly increases to 1.52 (SD2OPC), 2.80 (SD4OPC) and 3.82 (SD6OPC) as compared with that of SD (1.00). In addition, under the 4% OPC content condition, the q_c of treated sediments (SD4OPC) is 1.05 MPa, 1.14 MPa and 1.40 MPa at 3 d, 7 d and 28 d, while the corresponding η_c change from 2.10 to 2.28 and 2.80. This experimental result is consistent with the previous study performed [74] [237].

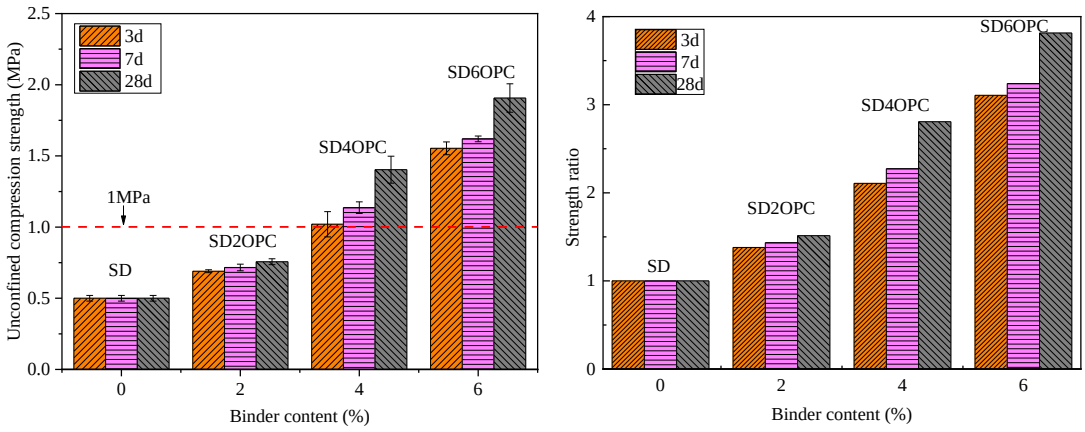

(a) (b)

Figure 4-5 (a) Unconfined compressive strength and (b) strength ratio of the treated sediments with OPC.

For CSA-treated sediments specimens, the q_c and η_c are reported in Figure 4-6. It is similar to OPC-treated sediments specimens, both CSA content and curing time lead to possibly changing trend of the q_c and η_c. After the same curing time of 28 d, the q_c of CSA-treated sediments specimens increases from 0.50 MPa (SD) to 0.59 MPa (SD2CSA), 1.20 MPa (SD4CSA) and 1.71 MPa (SD6CSA) with the increase of CSA content from 0% to 6%. The η_c correspondingly increases from 1.00 (SD) to 1.18 (SD2OPC), 2.40 (SD4OPC) and 3.42 (SD6OPC). Under the condition of 4% CSA inclusion, the q_c of SD4CSA specimens is 1.04 MPa (3 d), 1.08 MPa (7 d) and 1.20 MPa (28 d) with the curing time changes from 3 d to 28 d, while the corresponding η_c is 2.07 (3 d), 2.17 (7 d) and 2.40 (28 d), respectively.

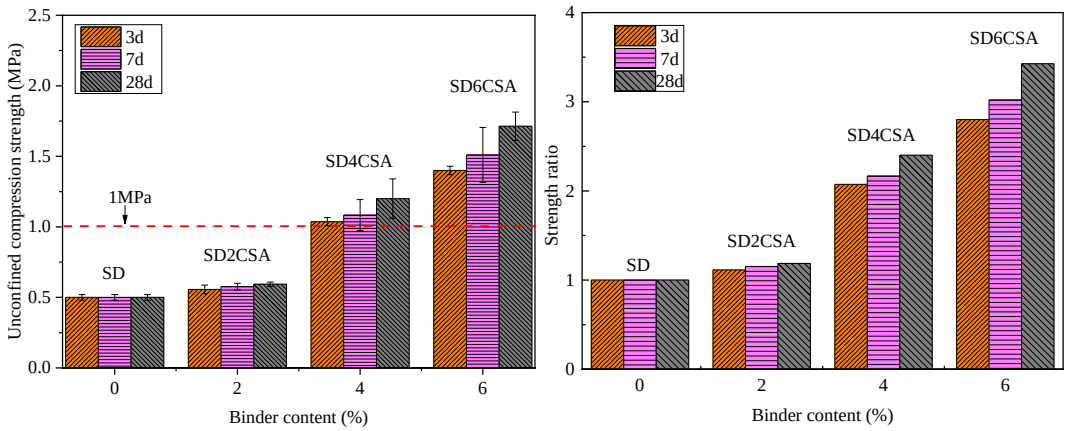

(a) (b)

Figure 4-6 (a) Unconfined compressive strength and (b) strength ratio of the treated sediments with CSA.

Besides, both 4% and 6% OPC/CSA treated sediments meet the minimum strength requirement (1 MPa) of subgrade [167]. However, if considering the effects of OPC and CSA on the treatment of dredged sediments, the CSA lead lower engineering performance than OPC under the same conditions (binder content and curing time). To find the reason to explain this, we compared the compressive strength of the standard mortar by the used CSA and OPC, according to European standard NF EN 196-1 [248]. The results are shown in Figure 4-7(a). Figure 4-7(b) illustrates the compressive strength of standard mortar for different kinds of cement from the Vicat company [249]. It could conclude that the compressive strength of standard mortar with used CSA is less than OPC (CEM I 52.5 R) at 3, 7 and 28d. For the compressive strength of standard mortar at 1d, although the average value of CSA is still less than OPC, considering the standard error in Figure 4-7(a), we can think they have a similar compressive strength at 1d. Our results are the same as the results from Vicat company (Figure 4-7(b)). The compressive strength of the used CSA is less than OPC (CEM I 52.5 R) after curing 3d. This could explain the CSA did not show its high early strength property for the treatment of sediments in this study, even at 3d. Indeed, the compressive strength of solidified sediments with CSA still can be reached to 78.41-98.42% that of using OPC in this study. Therefore, considering the main advantages of CSA: green, low carbon, environmentally friendly and energy-saving, we still consider CSA as an effective alternative for the treatment of sediments to replace traditional binder OPC.

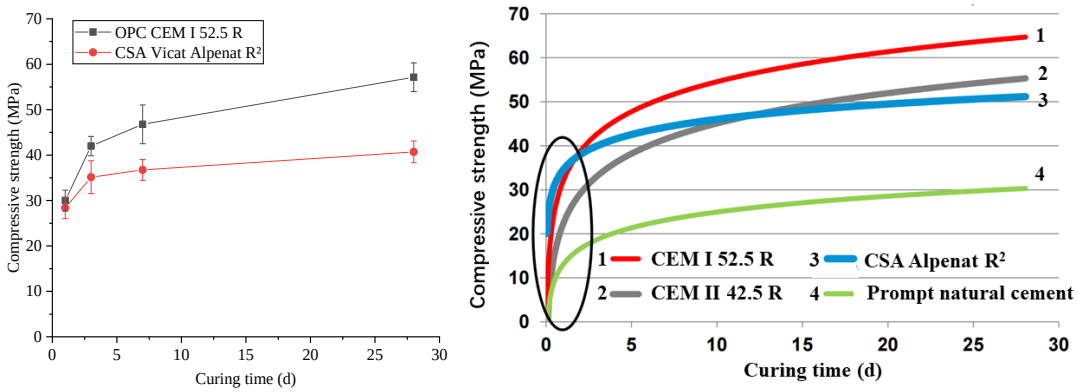

(a) (b)

Figure 4-7 (a) Compressive strength of standard mortar by the OPC and CSA of this study; (b) Compressive strength of standard mortar for different kinds of cement from the Vicat company [249].

4.3.4 Elastic modulus

Elastic modulus is an important characteristic to evaluate the ability of solidified sediments to resist deformation. However, as shown in Figure 4-1(b), the conventional strain measurement technique determines the axial strain of samples using the relative displacement of the top and bottom loading platens from the press machine. Therefore, the axial strain of samples may include some common errors, such as seating errors, alignment errors, bedding errors and system compliance errors, particularly when the axial strain is less than 0.1% (small strain) [250, 251]. These errors result in the measured E value is significantly less than the actual E value of the samples under the field condition [252] [251]. Currently, most of the research measures the elastic modulus of soil by the conventional strain measurement method [97, 237, 253-255], only a few are focused on using small strain measuring devices [251, 252]. In this study, three local small strain sensors (Figure 4-1(b)) were used to measure the axial strain of the treated sediments specimen.

Figure 4-8 shows a typical stress-strain curve that can be used to calculate E value. Elastic modulus E is defined as the ratio of stress/strain corresponding to 30% of peak stress[256]. The strain value for calculating E is from the local small strain sensor in this study. Furthermore, the measured axial strain of the treated sediments specimen by the local small strain sensors was substantially less than that of the conventional method, which agrees well with the results of previous research [251, 252].

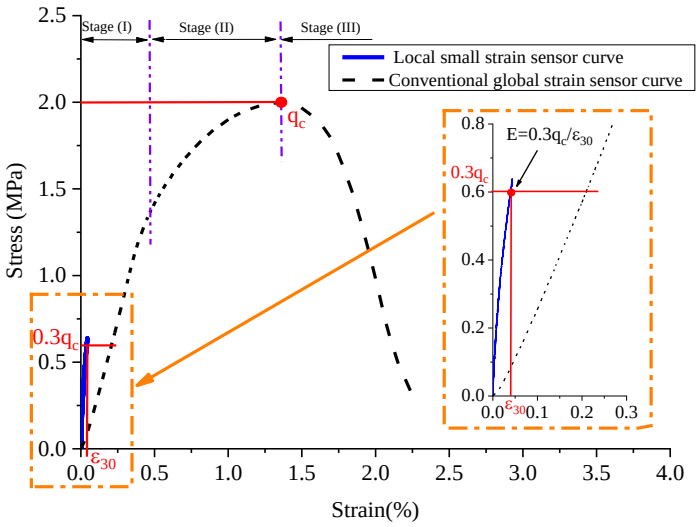

Figure 4-8 Example of elastic modulus in a typical stress-strain curve.

For the typical stress-strain curve from the conventional strain measurement method, it is evident that this curve can be divided into three stages: (I): initial elastic

deformation stage; (II): plastic deformation stage; (III): post-failure stage.

The variations of elastic modulus E of solidified sediments with different binder contents and curing time are plotted in Figure 4-9. The results indicated that the variation in the elastic modulus has an upward trend as the increase of binder content and the curing time. After 28 d of curing, the E values of OPC-treated sediments increases by 2.33 times (0.50 GPa), 7.87 times (1.33 GPa) and 8.53 times (1.43 GPa) as compared with untreated sediment (0.15 GPa), with increasing OPC content from 2% to 6%. Additionally, the SD4OPC specimen has higher E values after 7 d and 28 d curing than that at 3 d curing time, E changed from 0.76 GPa (3 d) to 1.18 GPa (7 d) and 1.33 GPa (28 d). A similar conclusion can be observed for CSA-treated sediment specimens. Both CSA content and curing time had a great influence on the elastic modulus. Higher CSA content and longer curing time benefit the development of elastic modulus. Such the specimens cured 28 d, achieved the higher E values of 0.41 GPa (SD2CSA), 0.86 GPa (SD4CSA) and 1.07 GPa (SD6CSA), when the CSA contents were 2%, 4% and 6%, respectively. At the same time, the E value was only 0.15 GPa for SD. Besides, with the curing time increase from 3 d to 28 d, the E values of CSA-solidified sediment samples were increased significantly, the E values of SD4CSA still as high as 0.64 GPa (3 d), 0.77 GPa (7 d) and 0.86 GPa (28 d). Achour et al. [53] also reported similar conclusions, elastic modulus increases with the increase of binder content and curing time.

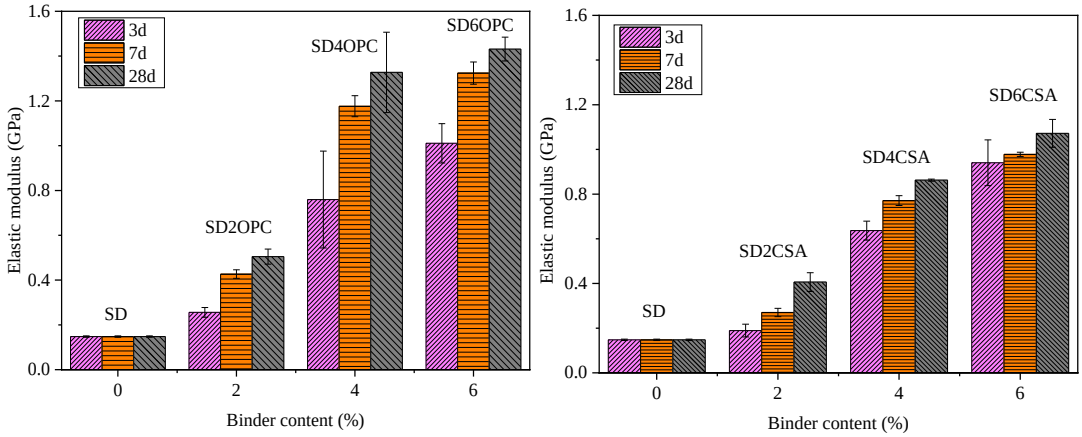

(a) (b)

Figure 4-9 Elastic modulus of the treated sediments with (a) OPC and (b) CSA.

4.3.5 Splitting tensile strength

Figure 4-10 and Figure 4-11 show the variation of the splitting tensile strength (q_{it}) and the tensile strength ratio (η_{it}, defined as Equation (4-5)) for OPC/CSA-treated

sediments, with the amount of OPC/CSA and curing time.

$$\eta_{it} = \frac{q_{itn}}{q_{it0}} \tag{4-5}$$

Where, η_{it} is the tensile strength ratio; q_{itn} is the splitting tensile strength of treated sediments; q_{it0} is the splitting tensile strength of untreated sediment.

It can be observed that the OPC inclusion contributes to the enhancement of the splitting tensile strength of treated sediments. In the same curing time of 28 d, the splitting tensile strength q_{it} increases from 0.050 MPa (SD) to 0.077 MPa (SD2OPC), 0.162 MPa (SD4OPC) and 0.192 MPa (SD6OPC) with the increase of OPC content from 0% to 6%, the η_{it} correspondingly increases to 1.54 (SD2OPC), 3.24 (SD4OPC) and 3.84 (SD6OPC) as compared with that of SD (1.00). Moreover, increasing curing time can effectively improve the q_{it} and η_{it} of the treated sediments with OPC. The splitting tensile strength of the SD4OPC specimen increases to 0.109 MPa (7 d) and 0.162 MPa (28 d) as compared with that at 3 d (0.104 MPa), meanwhile, the corresponding η_{it} changes to 2.18 and 3.24 as compared with that of SD4OPC specimen at 3 d (2.08).

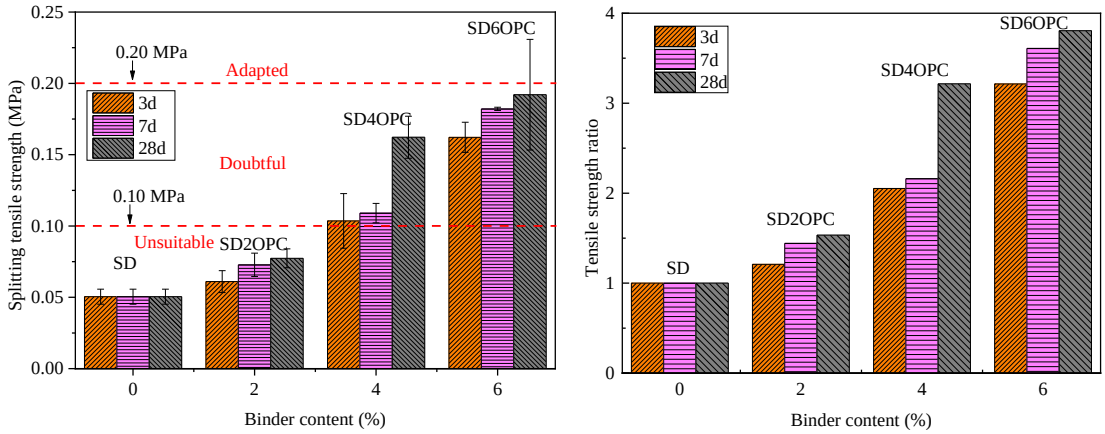

Figure 4-10 (a) Splitting tensile strength and (b) tensile strength ratio of the treated sediments with OPC.

Figure 4-11 shows the q_{it} and η_{it} values of CSA-treated sediments specimens cured for 3 d, 7 d and 28 d. As expected, the CSA has an obviously positive effect on the splitting tensile strength during all times. The CSA contact with water produced many hydration products that formed filled pores to give a higher strength for treated sediments.

Especially for the specimens with 2%, 4% and 6 % CSA at 28 d, had a higher splitting tensile strength of 0.057 MPa, 0.114 MPa and 0.119 MPa than that of SD (0.050 MPa).

The η_{it} correspondingly is 1.14 (SD2CSA), 2.28 (SD4CSA), 2.38 (SD6CSA) and 1.00 (SD). This indicated that the addition of CSA could significantly improve the splitting tensile strength of the treated sediments. As the reaction proceeds, there was an increase in splitting tensile strength for SD4CSA specimens after curing. The splitting tensile strength achieved 0.082 MPa, 0.100 MPa and 0.114 MPa at 3 d, 7 d and 28 d, respectively. While the η_{it} correspondingly is 1.64 (3 d), 2.00 (7 d) and 2.28 (28 d). According to the research of Zhang et al. [134], ettringite is the main hydration product. It plays a significant role in improving the strength of CSA-treated specimens. The ettringite continues to increase with curing time and CSA content. This is why the splitting tensile strength of CSA-treated sediments specimens increases with the increasing curing time and CSA content.

Besides, both 4% and 6% OPC/CSA treated sediments are doubtful (0.1 MPa < q_{it} < 0.2 MPa) [257], this means the decision on applied treatment depends on the anticipated site conditions, it might be beneficial to increase the percentage of used binders.

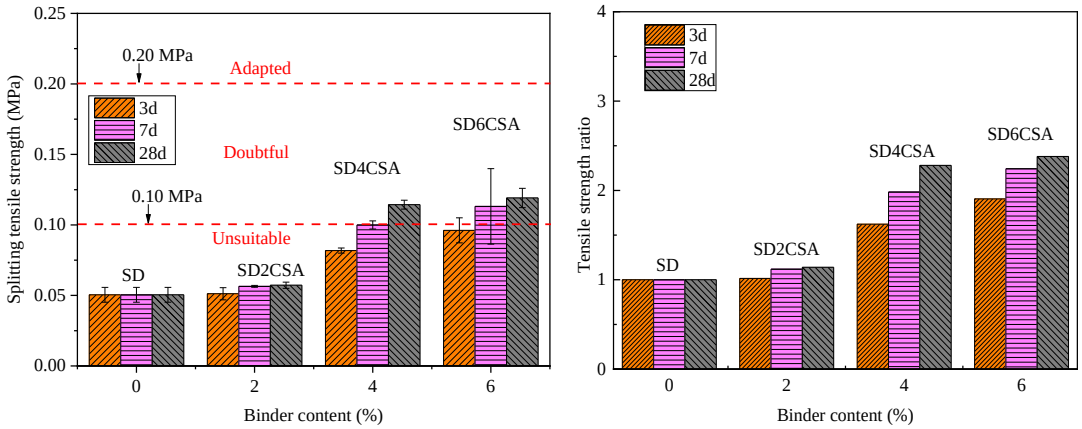

Figure 4-11 (a) Splitting tensile strength and (b) tensile strength ratio of the treated sediments with CSA.

4.3.6 Relationship of q_c, q_{it} and E

This study performed a regression analysis on the relationship between q_c and q_{it} values. From many other investigators [252, 253, 258, 259], one of the most commonly used models for explaining the relationship between q_c and q_{it} of treated soil is the simple linear model. As shown in Figure 4-12(a), simple linear models have been used for describing the relationship between the q_c and q_{it} of treated sediments.

Equations (4-6) and (4-7) have been derived for describing the relationship between q_c and q_{it} of OPC-treated sediments and CSA-treated sediments in this study.

$$q_c(MPa) = 9.50 q_{it}(MPa) \quad (4\text{-}6)$$

$$q_c(MPa) = 12.20 q_{it}(MPa) \quad (4\text{-}7)$$

These equations are plotted in Figure 4-12(a) with the experimental data. It can be seen that the regression lines from Equations (4-6) and (4-7) showed a relatively good relationship between q_c and q_{it}. The coefficient of determination (R^2) indicates how much of the variation in the dependent variable can be accounted for by the regression equation. The obtained R^2 are 0.995 and 0.997 for Equations (4-6) and (4-7) in this study, respectively. In particular, it is found that a unified Equation (4-8) with R^2=0.974 can satisfactorily describe the correlation between q_c and q_{it} on all solidified sediment specimens. This relationship is consistent with the results of Yoobanpot et [77] ($q_c(MPa) = 9.09 q_{it}(MPa)$) and Wang et al. [253] ($q_c(MPa) = 9.90 q_{it}(MPa)$) for treated sediments. Therefore, the derived linear equations may successfully be used to represent the relationship between the compressive and splitting strength of OPC/CSA-treated sediments.

$$q_c(MPa) = 10.43 q_{it}(MPa) \quad (4\text{-}8)$$

Figure 4-12(b)-(c) show the variation of compressive strength q_c versus elastic modulus E and splitting tensile strength q_{it} versus elastic modulus E, respectively. According to the obtained test data points, it is observed that both q_c and q_{it} have a trend towards increasing with the increasing E. Previous research has demonstrated that elastic modulus and compressive strength have a strong linear relationship [251] [253] [260].

In this study, the simple linear model was used for describing the relationship between the strength and elastic modulus. The relationship between q_c and E of OPC-treated sediments is reflected in Equations (4-9) with the R^2=0.948. Equation (4-10) with the R^2=0.972 represents the relationship between q_c and E of CSA-treated sediments. The unified Equation (4-11) with R^2=0.950 can explain how elastic modulus is related to the compressive strength of OPC/CSA-treated sediment specimens. It was comparable with the result of Ho et al. [251] ($E(GPa) = 0.77 q_c(MPa)$) and Tan et al. [260] ($E(GPa) = 0.35$ to $0.80 q_c(MPa)$) for OPC-treated marine clay. Both of them measure the elastic modulus using similar local strain measurement methods. Additionally, the data points entirely fell into the range from $0.35q_c$ to $1.08q_c$, similar to those reported by Ho et al. [251] (the range from $0.50q_c$ to $1.08q_c$) and Tan et al.

[260] (the range from $0.35q_c$ to $1.08q_c$).

$$E(GPa) = 0.75q_c(MPa) \quad (4\text{-}9)$$

$$E(GPa) = 0.63q_c(MPa) \quad (4\text{-}10)$$

$$E(GPa) = 0.69q_c(MPa) \quad (4\text{-}11)$$

Equation (4-12) with R^2=0.957 is derived from the regression analysis to express the correlation of q_{it} and E of OPC-treated sediments. Equation (4-13) with R^2=0.937 expresses the q_{it} and E correlation of CSA-treated sediments. A unified equation can be expressed by Equation (4-14) with R^2=0.950, which can be acceptable to describe approximately the changing trend of splitting strength with elastic modulus on the designed materials.

$$E(GPa) = 7.20q_{it}(MPa) \quad (4\text{-}12)$$

$$E(GPa) = 7.60q_{it}(MPa) \quad (4\text{-}13)$$

$$E(GPa) = 7.34q_{it}(MPa) \quad (4\text{-}14)$$

In general, Equations (4-8), (4-11) and (4-14) demonstrate the relationships among the compressive strength, splitting tensile strength and elastic modulus. This is to say, these equations provide an alternative approach to predicting the approximate value of the other two parameters, if one parameter is given. For example, this leads to help to predict the splitting tensile strength and the elastic modulus from the compression strength. This test is simpler, cheaper, and faster than splitting tensile strength and elastic modulus measurements. Moreover, in designing a new formulation, this procedure could save time, reduce the number of samples and save the materials. Even if the ratio of 10 between the compressive strength over the splitting tensile strength is commonly encountered for OPC treated materials, the relation between the splitting tensile strength or the compressive strength with the elastic modulus has to be specific to a given material (in our case to treated sediments).

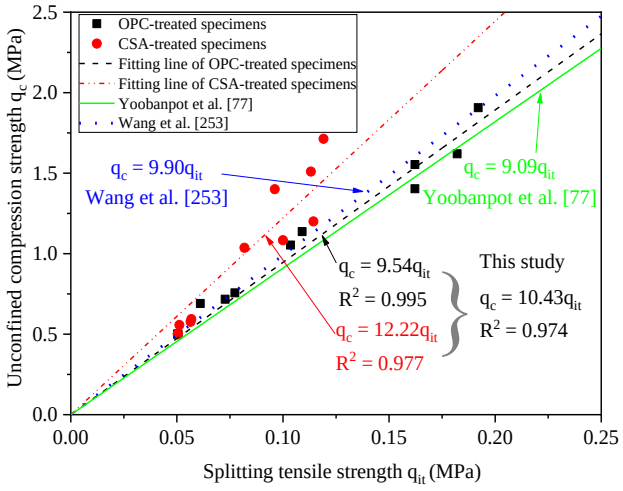

(a)

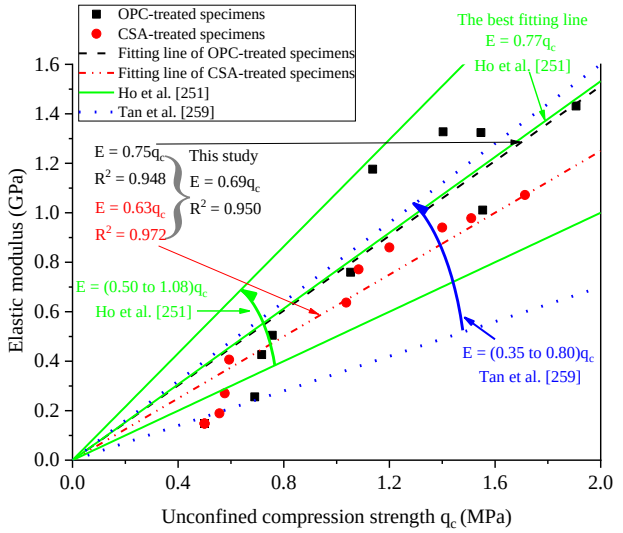

(b)

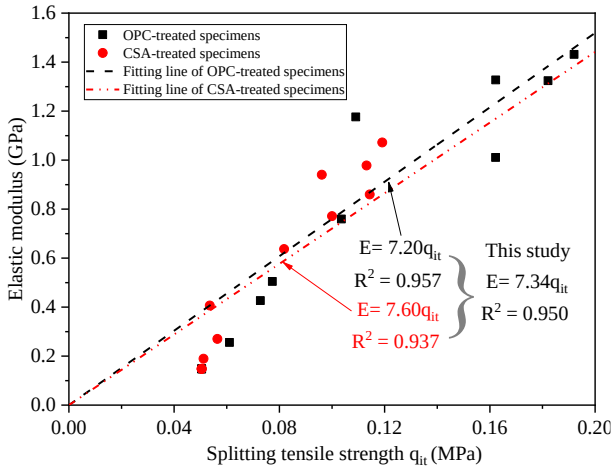

(c)

Figure 4-12 Relationship of (a) q_c versus q_{it}; (b) q_c versus E and (c) q_{it} versus E for the OPC/CSA treated sediments.

4.3.7 Evaluation of solidified sediments as road materials

Figure 4-13 assesses the suitability of solidified dredged sediments as road materials, according to the French GTS road guide [261]. The mechanical characteristics (direct tensile strength (q_t) and elastic modulus (E)) of treated materials are used after curing for 90 days or 180 days, according to the GTS road guide [261]. In this study, we prepared the 180d-curing time samples for this classification. It is noted that the direct tensile strength q_t shall be derived from q_{it} using the Equations (4-15) [261]. It should note that CSA cement is a relatively new cement, but it is still a kind of hydraulic binder. Thus, we think applying this equation to CSA-treated sediments is possible.

$$q_t = 0.8 q_{it} \tag{4-15}$$

However, a great improvement in material classification can be observed for treated sediments, compared with untreated sediments. This proves the beneficial effects of OPC and CSA treatment to increase the mechanical properties of dredged sediments. It should be noted that the minimum class required for potential use as subgrade material is class 5 (Zone 5). Hence, this means that the samples of SD4OPC and SD6OPC, which belong to class 5, might be possibly reused as subgrade materials for the road. This conclusion is consistent with the previous study [236]. Other treated materials (SD2OPC, SD2CSA, SD4CSA and SD6CSA) may be could be used as filling materials. Suppose the need arises to enhance the classification of CSA-treated material to class 5. The effective way may be to increase the amount of binder and/or explore the combined effect of OPC and CSA. This work will be carried out in the next stage.

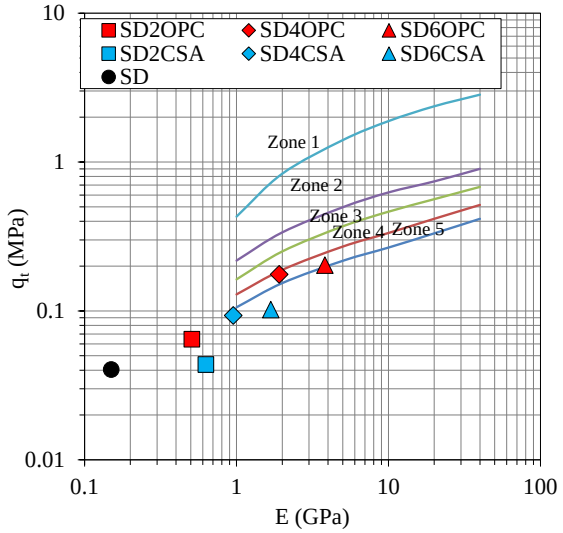

Figure 4-13 Classification of the treated sediments with OPC and CSA.

In China, the solidified fine soil can't be used for the base layer of pavement with heavy and medium traffic, according to the standard CJJ 169-2011 [262]. At the same time, the compressive strength threshold at 7d is 1.5 MPa, if the solidified soil is used for the sub-base layer of pavement. Thus, the samples of SD6OPC and SD6CSA could be used as the sub-base layer materials for roads of low traffic intensity.

Table 4-3 The 7d-compressive strength of solidified soil for different traffic levels according to the Chinese standard [262].

Road layer	Special heavy traffic (MPa)	Heavy and medium traffic (MPa)	Light traffic (MPa)
Base	/	/	2.5-3.5
Sub-base	≥2.5	≥2.0	≥1.5

4.3.8 X-ray diffraction analysis

The XRD analysis was performed to elucidate the difference of hydration products for OPC and CSA binders. It is noteworthy that potential mineralogical changes of various binders are challenging to detect, in solidified sediments specimens with low binder content (less than 10%). Hence, these mineralogical variations will be discussed based on OPC and CSA pastes specimens.

Figure 4-14 illustrates the XRD results of OPC and CSA pastes, with the water-to-binder ratio of 0.5 and 28 d curing time. The main hydration products observed in OPC are portlandite (CH), calcium silicate hydrate (C-S-H) and ettringite ($C_6A\bar{S}_3H_{32}$). Besides, minor hydration product-calcium aluminate monosulfate (AFm) phases could be found, such as monosulfate (Ms) and hemicarbonate (Hc). This is because some ettringite converts into AFm phases when lacking gypsums [263]. Ettringite is the only hydration product observed for CSA. No other hydration products are detected, apart from the residual unreacted mineral phase. This indicates that CSA hydration formed ettringite and gibbsite (AH_3), according to reaction (1-10). However, not observed gibbsite in the XRD pattern can be attributable to its amorphousness. The high peak density of residual belite indicated that the hydration of belite is generally slow [134]. The results agree well with the previous studies about the hydration products of OPC and CSA paste [134] [264].

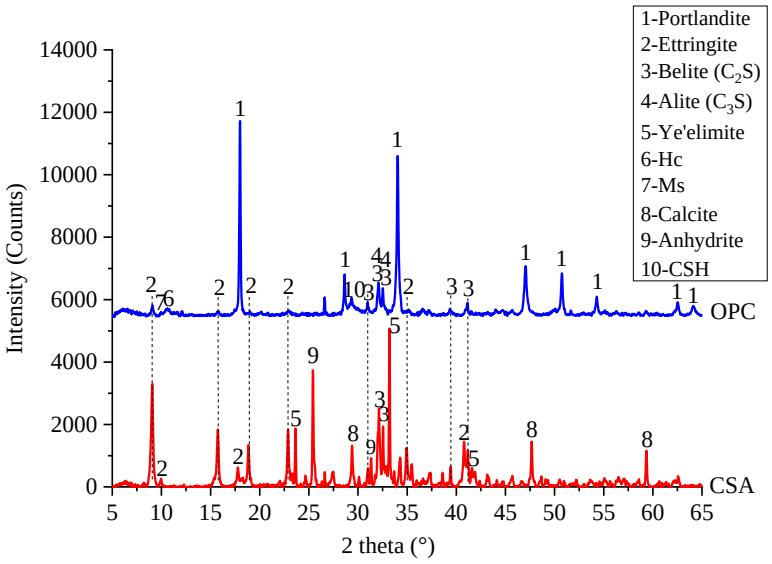

Figure 4-14 XRD traces of OPC and CSA paste (Cu Kα).

4.3.9 Scanning electron microscopy analysis

To better understand the macroscopic behavior of the OPC/CSA-treated sediments, scanning electron microscopy (SEM) was conducted to observe the surface morphology of typical specimens at 28 d.

Figure 4-15 (a) gives the SEM image of the untreated sediments (SD) after being subjected to compressive strength tests. Figure 4-15 (b) is the local marked magnified area of Figure 4-15 (a). It is easier to find the porous and loose microstructure. The interconnection between particles is quite weak, with distinct edges and boundaries.

Figure 4-15 (c) shows the SEM image of the typical treated sediments specimen with 6% OPC. Figure 4-15 (d) shows the local marked magnified area of Figure 4-15 (c). It is clear that the number of pores decreases significantly for OPC-treated sediments specimen. Hydration product-fine fibrillar C-S-H gels can be observed, they might grow gradually into the reticulate or honeycomb-like network as the reaction proceeds [265]. Besides, other hydration products could be observed, portlandite (CH) with hexagonal plate forms precipitated as well as rod-like ettringite (AFt) [266]. These hydration products fill in the pore spaces, interconnecting the particles together. The gel-covered aggregates are prevalently dispersed in the specimen. These cause a denser structure and higher strength of OPC-treated sediments.

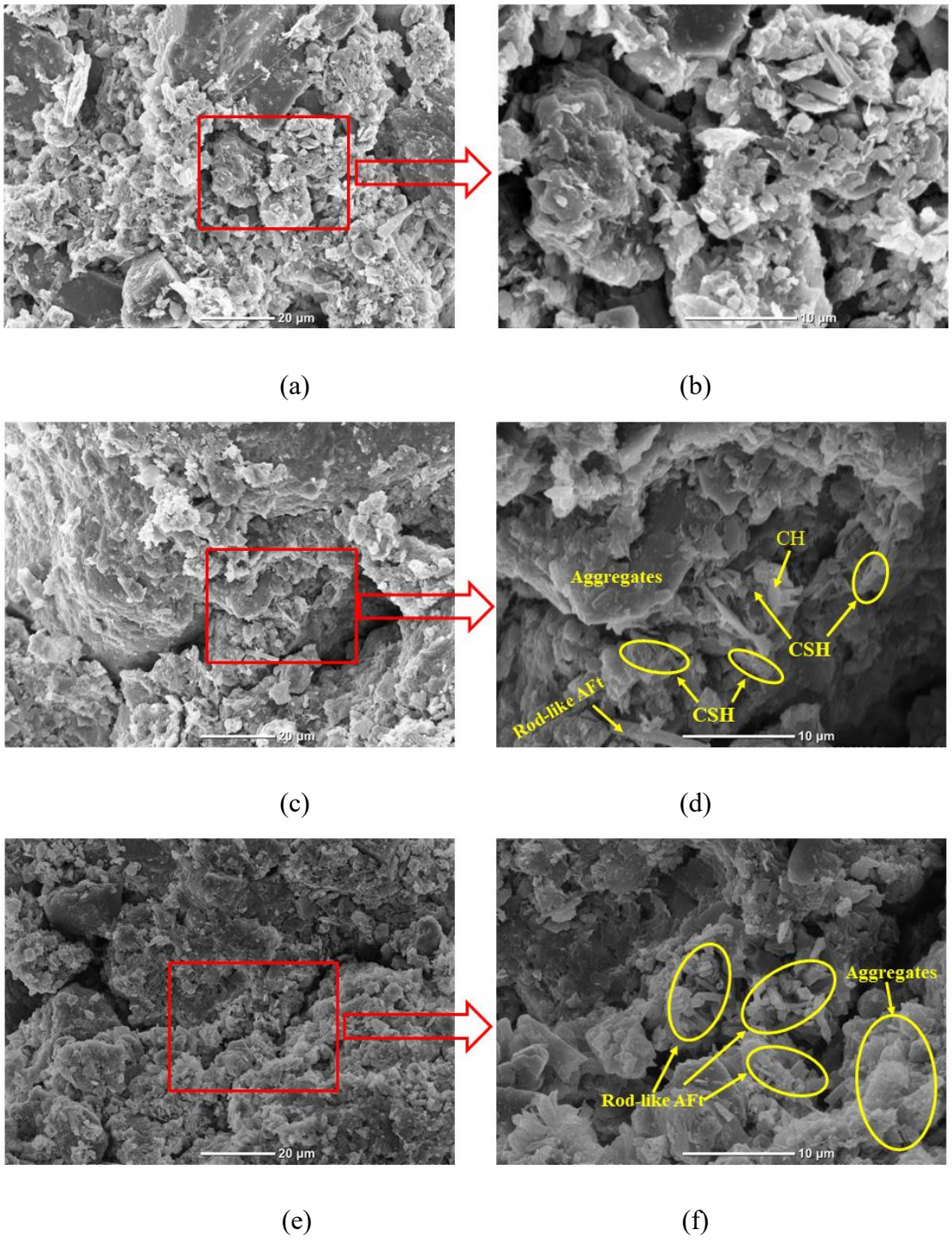

Figure 4-15 SEM images of typical specimens. (a) SD (×1000); (b) local marked magnified area of SD (×3000); (c) SD6OPC (×1000); (d) local marked magnified area of SD6OPC (×3000); (e) SD6CSA (×1000); (f) local marked magnified area of SD6CSA (×3000).

In terms of the treated sediments specimen with 6% CSA, Figure 4-15 (e) shows the typical SEM images. Figure 4-15 (f) shows the local marked magnified area of Figure 4-15 (e). A large amount of short rod-like ettringite (AFt) can be observed [134]. The hydration product AFt fills the pores among the sediment's particles, causing densification of treated sediments' microstructural. Besides, the gel-covered aggregates could be observed, which may be caused by hydration product-amorphous gibbsite (AH_3). These make the CSA-solidified sediments further denser and have higher strength than untreated sediments.

4.3.10 Micropore structure analysis

The micropore structure of the untreated and OPC/CSA-treated sediments was investigated. The results are shown in Figure 4-16 and Table 4-4. It's easily observed that the six typical samples showed approximately the same pattern with apparent diameters of pores in the range of 0.006-400 μm. All the pore size distribution models are bimodal. Indeed, the main pores of all the samples were distributed in the ranges of 0.01-1.00 μm and 1.00-40.00 μm.

According to previous research [255], the pore structure can be divided into four major ranges: < 0.01 μm, 0.01-1.00 μm, 1.00-40.00 μm and > 40.00 μm, as presented in Table 4-4. The untreated specimen has higher larger pores (1.00-40.00 μm and > 40.00 μm) percentages and fewer smaller pores (< 0.01 μm and 0.01-1.00 μm) percentages. The treatment of sediments makes the larger pores transform into smaller pores. Especially, the pores volume percentages of larger pores in the range of 1.00-40.00 μm and > 40.00 μm exhibit a decreasing trend, as the curing period increases from 3 days to 7 days and 28 days. While the pores volume percentages of the smaller pores in the range of < 0.01 μm and 0.01-1.00 μm show an increasing trend. This is due probably to the progress of hydration of binders causes the larger pores (1.00-40.00 μm and > 40.00 μm) to transform into smaller pores (< 0.01 μm and 0.01-1.00 μm), which induces the pores of the treated sediments to become finer and denser. Therefore, the strength of the treated sediments could be improved.

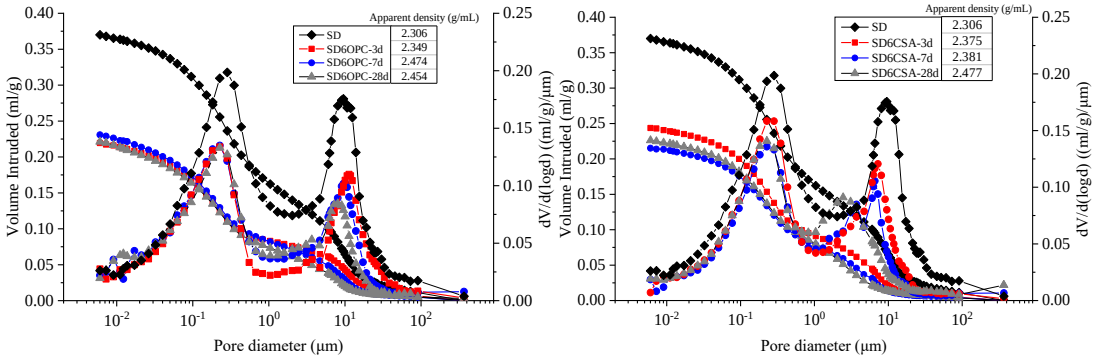

(a) (b)

Figure 4-16 Micropore structure analysis of the (a) OPC-treated sediments and (b) CSA-treated sediments.

Table 4-4 Pore size distribution of the treated sediments.

Pore size (μm)	Pore size distribution (%)						
	SD	SD6OPC -3d	SD6OPC -7d	SD6OPC -28d	SD6CSA -3d	SD6CSA -7d	SD6CSA -28d
>40.00	5.01	4.72	3.18	3.21	2.80	2.72	2.83
1.00-40.00	38.84	33.12	32.30	29.92	34.51	33.88	32.45
0.01-1.00	54.47	59.53	61.06	63.29	60.78	61.82	62.56
<0.01	1.68	2.63	3.45	3.58	1.91	1.57	2.16
Total	100.00	100.00	100.00	100.00	100.00	100.00	100.00

4.3.11 Environmental assessment

This part evaluates the environmental characterization of typical untreated and OPC/CSA-treated sediments, according to standard NF EN 12457-2 [145]. All the leaching tests were carried out with the same L/S (liquid/solid) ratio of 10:1. Table 4-5 shows the leaching test results. The results are the average value of two samples.

These results show that OPC/CSA-treated sediments could be classified as Class II: non-hazardous waste, according to European directive 2003/33/CE [201]. Besides, all leaching values are below the thresholds of the French SETRA road guide [202], indicating that all these specimens are allowed for reuse in road construction.

It can be seen that all the pH values of the treated sediments are higher than that of untreated sediments (7.42). These higher pH values indicated the leaching solution of treated sediments with strong alkalinity. While the pH values of the OPC-treated sediments are higher than that of CSA-treated specimens under the same condition.

In addition, the relation between pH and leaching values of some typical elements (Ba, Cr, Cu, Ni and fluorides) could be observed. The leaching values of these elements were observed to be higher at high pH. On the whole, the heavy metals elements have an amphoteric behavior. Their maximum release occurs when the pH is very low (acidic) or high (alkaline) [69]. Indeed, these observed leaching values are still below the limit of non-hazardous waste and the SETRA road guide [202], so these treated sediments could be reused as alternative materials in road construction.

Besides, the leaching values of As, Cd, Hg, Pb and Zn seem to be unrelated to pH. The chlorides levels in the treated sediments are lower than SD. The reaction of chlorides with OPC/CSA, which forms monochloroaluminates of calcium: Friedel's salt ($3CaO{\cdot}Al_2O_3{\cdot}CaCl_2{\cdot}10H_2O$) [267] [268], may be responsible for the reduction of chlorides in treated sediments. Furthermore, some investigations [269] [270] have discovered that the presence of sulfate inhibits the development of Friedel's salt and causes it to transform into ettringite. In any case, OPC/CSA could stabilize chlorides.

It's worth noting that the OPC treatment reduces sulfate leaching levels, whereas the CSA treatment increases levels. Karamalidis and Voudrias [271] reported comparable results: sulfate leaching values for OPC-solidified oily sludge were reduced in a highly alkaline environment. This is because sulfate ion could react with OPC to form ettringite [272]. Ettringite is a stable mineral when the pH is above 10.7 [273]. The pH of OPC-treated sediments was found to be higher than 10.7. As a result, sulfate leaching values in OPC-treated sediments are reduced. It is well known that the main hydration product of CSA cement is ettringite, which is a kind of hydrated sulfate. The measured pH values of CSA treated sediments are less than 10.7. Thus, a part of ettringite may dissolves in the leachate and may increase the leaching values of sulfates [274] for CSA-treated sediments. This result is consistent with the findings of Piekkari et al. [275], the leaching value of sulfate was enhanced, after the treatment of CSA for an industrial filter sludge with high sulfate content.

Table 4-5 Leaching results of the treated sediments with OPC/CSA single binder.

Elements	Values (mg/kg)						European directive 2003/33/CE [201]			SETRA road guide [202]
	SD6OPC -3d	SD6OPC -7d	SD6OPC -28d	SD6CSA -3d	SD6CSA -7d	SD6CSA -28d	Class III	Class II	Class I	Limit values
pH	11.48	11.46	11.39	9.25	9.92	9.34	/	/	/	/
As	< 0.1	< 0.1	< 0.1	< 0.1	< 0.1	< 0.1	0.5	2	25	2
Ba	0.17	0.17	0.15	0.10	0.05	0.07	20	100	300	100
Cd	< 0.009	< 0.009	< 0.009	< 0.009	< 0.009	< 0.009	0.04	1	5	1
Cr	0.69	0.74	0.35	0.69	0.34	0.35	0.5	10	70	10
Cu	2.62	2.64	2.66	0.30	0.45	0.56	2	50	100	50
Hg	< 0.06	< 0.06	< 0.06	< 0.06	< 0.06	< 0.06	0.01	0.02	0.03	0.2
Mo	0.55	0.56	0.56	0.63	0.58	0.65	0.5	10	30	10
Ni	0.33	0.33	0.32	< 0.05	< 0.05	< 0.05	0.4	10	40	10
Pb	< 0.06	< 0.06	< 0.06	< 0.06	< 0.06	< 0.06	0.5	10	50	10
Sb	< 0.06	< 0.06	< 0.06	< 0.06	< 0.06	< 0.06	0.06	0.7	5	0.7
Se	< 0.08	< 0.08	< 0.08	0.11	0.10	0.08	0.1	0.5	7	0.5
Zn	< 0.05	< 0.05	< 0.05	< 0.05	< 0.05	< 0.05	4	50	200	50
Chlorides	2250	2335	2855	3895	3685	2605	800	15000	25000	15000
Fluorides	19.00	18.00	23.30	9.30	6.75	9.30	10	150	500	150
Sulfates	7200	6935	6025	13885	11595	13970	1 000	20000	50000	20000
Soluble fraction	19709	18725	19273	29018	28696	30319	4000	60000	100000	60000

(Note: Class I is hazardous waste, Class II is non-hazardous waste, Class III is inert waste.)

4.4 Conclusion

This study performed a series of experiments to clarify the feasibility of recycling dredged marine sediments as road construction materials using novel eco-binder CSA cement. The results are compared with OPC-treated sediments. Based on the obtained results, the following conclusions can be drawn:

(1) Compared with the untreated sediments, the compaction performance of the OPC/CSA-treated sediments is significantly improved. The increase in the I-CBR index value is almost linear with the increase of the binder content (at least in the range of binder content studied in this work). In terms of the MDD and OMC of

OPC/CSA-treated sediments:

a. For OPC treatment, the MDD is decreased accompanied by increasing OMC.
b. For CSA treatment, after the first decrease of the treatment with 2% CSA, an increase in MDD is observed for higher CSA content. In the same way, after an increase in OMC of the treatment with 2% CSA, a decrease is observed for higher CSA content.

(2) The addition of OPC/CSA binder improves the mechanical behavior of treated dredged sediments, including compressive strength, splitting tensile strength and elastic modulus. These mechanical parameters increase with the increase of binder content and curing time.

(3) The effectiveness of treatment with OPC and CSA has been evaluated. It has been revealed that only SD4OPC and SD6OPC could be as subgrade material, the treated materials with 2-6% CSA didn't meet the thresholds of subgrade material. It could increase the amount of binder and/or explore the combined effect of OPC and CSA next stage, to enhance the classification of CSA-treated material to the class of subgrade material.

(4) The simple model can satisfactorily describe the relationships among the compressive strength, splitting tensile strength and elastic modulus. These equations provide an alternative approach to predicting the approximate value of two parameters if one parameter is given, which reduces the number and time of the experiments. It is to note that the relation between the strength and the elastic modulus is material-dependent.

(5) The XRD and SEM tests proved that the main hydration products observed in OPC are portlandite, calcium silicate hydrate, and ettringite. The ettringite is the only hydration product observed for CSA in this study. The microstructure induced by OPC treatment and CSA treatment seems comparable. The bimodal pore size distributions could be observed for OPC/CSA-treated sediments.

(6) The leaching values of OPC/CSA-treated sediments are below the limit of non-hazardous waste and the SETRA road guide. Therefore, the OPC/CSA-treated sediments could be reused as alternative materials in road construction.

Chapter 5 Characterization of the solidified sediments with composite binder: OPC-CSA

5.1 Introduction

The effectiveness of the treated marine sediment with OPC/CSA single binder as road materials was studied and validated in Chapter 4. The results have indicated that the materials treated with 2-6% CSA didn't meet the thresholds of subgrade material. Further, some studies found that the OPC-CSA composite binder seems to have more outstanding mechanical properties, due to combining each OPC and CSA advantage [11, 139, 142, 143]. Therefore, this chapter is dedicated to assessing the performance of the treated dredged marine sediments with the OPC-CSA composite binder. A set of mechanical tests were carried out, including modified Proctor compaction tests, immediate California Bearing Ratio (I-CBR) index tests, unconfined compressive strength tests, splitting tensile strength tests and measurements of elastic modulus. In addition, to better understand the microscopic mechanisms of the OPC-CSA composite binder treatment for dredged sediments, X-ray diffraction, scanning electron microscopy and mercury intrusion porosimetry tests were conducted. In the end, the standard leaching test and a simplified calculation of the carbon footprints were undertaken, to investigate the beneficial impact of the composite binder (OPC-CSA) on the environment.

5.2 Experimental materials and methods

5.2.1 Materials

The characterizations of dredged sediments, OPC and CSA used in this chapter have been given in chapter 2.

5.2.2 Mix proportions

Table 5-1 gives the detailed mix proportions of OPC-CSA composite binder treated sediments. The abbreviation SD represents untreated sediments, while SDxPyC represents the treated sediments using x% OPC (P) and y% CSA (C) binder. The OPC

and CSA binder were incorporated at dosages of percentage by weight of dry sediments. For example, the mix SD2P2C is treated sediments with 2% of OPC and 2% of CSA binder. Both the mass of OPC and CSA binder are calculated regarding the dry weight of sediments. The mixing water was tap water. The mass ratio of water and solid (dry sediments plus dry binders) was used to calculate the percentage water content for treated sediments. This experimental program is designed based on the work in chapter 4. For comparison, the properties of 6% OPC/CSA single binder treated dredged sediments (SD6P and SD6C) are listed.

Table 5-1 Mix proportions of OPC-CSA treated sediments.

Number	Mix	OPC: CSA	OPC (%)	CSA (%)	OPC+CSA (%)
1	SD	/	0	0	0
2	SD2P2C	1: 1	2	2	4
3	SD4P2C	2: 1	4	2	6
4	SD2P4C	1: 2	2	4	6
5	SD6P2C	3: 1	6	2	8
6	SD2P6C	1: 3	2	6	8
7	SD4P4C	1: 1	4	4	8

5.2.3 Testing procedures

For compaction and I-CBR tests, the prepared dry sediments powder and a certain amount of water were mixed with a Hobart mixer for five minutes. After curing in the plastic bags for 24h, the prepared wet sediments were mixed with the design amount binder for five minutes. Then, the modified Proctor and I-CBR test were carried out directly with the obtained homogeneous mixture, in accordance with the standard NF EN 13286-2 [174] and NF EN 13286-47 [175].

To assess the mechanical performance of OPC-CSA treated dredged marine sediments, the cylindrical specimens (D=5 cm, H=10 cm) were prepared with the static compaction method, in accordance with the standard NF EN 13286-53 [239]. Afterward, these cylindrical specimens were hermetically sealed in the plastic boxes and cured at 20±2°C for 3, 7 and 28 d. Three specimens were prepared to obtain the average values for each design mixture. Unconfined compressive strength (q_c) and indirect tensile tests (q_{it}) were performed using an INSTRON test machine, conforming to standards NF EN 13286-41 [240] and NF EN 13286-42 [241]. The elastic modulus is the scant slope at 30% of peak stress in the stress-strain curve from q_c test according to NF EN 13286-43 [256].

The XRD analysis was determined on the OPC-CSA paste samples (W/S=0.5, 28d), by the BRUCKER AXS D2 ADVANCE X-ray diffractometer with a Cu Kα radiation source. The SEM and MIP analysis were investigated on the typically OPC-CSA treated samples. The small samples were taken from the broken samples after compressive strength tests, and dried at 40°C for at least seven days. For SEM investigations, the dried samples were coated with carbon and observed by a Hitachi S-4300SE/N electron microscope. The MIP measurements were conducted with a Micromeritics Autopore V 9600 porosimeter.

The leachability of the untreated and treated sediments was measured by standard leaching tests, following the standard NF EN 12457-2 [242]. The specimens used for leaching tests were collected after the unconfined compressive strength test, then comminuted and passed through the 4 mm-sieve. The rotary oscillator was used to shake the sieved specimens and deionized water for 24 hours at 25℃. The liquid/solid (L/S) ratio remains unchanged at 10:1. After that, the leachates were passed through the 0.45 μm filters. The heavy metal elements of the filtrates were analyzed by the inductively coupled plasma-atomic emission spectrometer (ICP-AES) and the SPS4® autosampler. Free anions (F^-, Cl^- and SO_4^{2-}) were measured by Dionex® Ionic Chromatography (IC).

5.3 Results analysis

5.3.1 Proctor compaction test

To explore the suitability of the OPC-CSA composite binder treated sediments as subgrade materials, modified Proctor tests were examined in this part, to determine the Maximum Dry Density (MDD) and corresponding Optimum Moisture Content (OMC) of the treated dredged sediments. The compaction test results with the 80% and 100% saturation degree curves were plotted in Figure 5-1. These curves represent the correlation between moisture content and dry density of treated sediments with various OPC-CSA composite binder dosages. The OMC and MDD of treated sediments correspond to the coordinates of the maximum position on the Proctor curve.

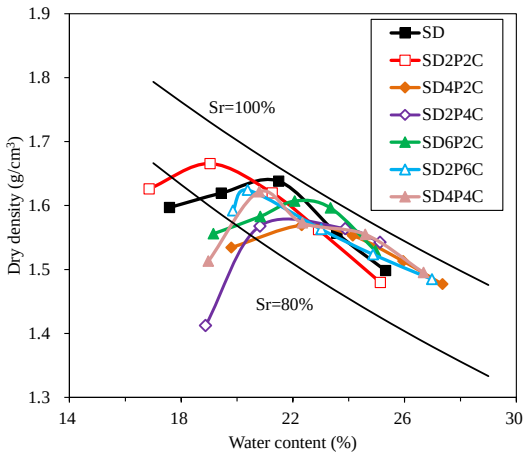

Figure 5-1 Compaction curves of the untreated and treated dredged marine sediments.

The MDD and corresponding OMC of these different mixes were presented in Figure 5-2 (a) and (b), respectively. Compared with untreated sediments SD (MDD=1.641 g/cm^3), the MDD of 4% OPC-CSA treated sediments (SD2P2C) improved to 1.666 g/cm^3, then decreases to 1.570 g/cm^3 (SD4P2C) and 1.573 g/cm^3 (SD2P4C) for 6% OPC-CSA treated sediments. After, it improved again to 1.607 g/cm^3 (SD6P2C), 1.636 g/cm^3 (SD2P6C) and 1.621 g/cm^3 (SD4P4C) for 8% OPC-CSA treated sediments. As for the OMC, it could be observed an increase with the decrease of the corresponding MDD and vice versa. Many studies [245] [276] also reported a similar phenomenon: the OMC increase and the corresponding MDD decrease with the binder content increases. This may be caused by particle aggregation with cement hydration, forming larger macro-pores within the mixes. Thus, MDD appears to decrease [245]. The OMC increase is because part of water consumption from cement hydration, also may be due to the surface area of the mixture changing that cement increased the mixture's total particle surface [246].

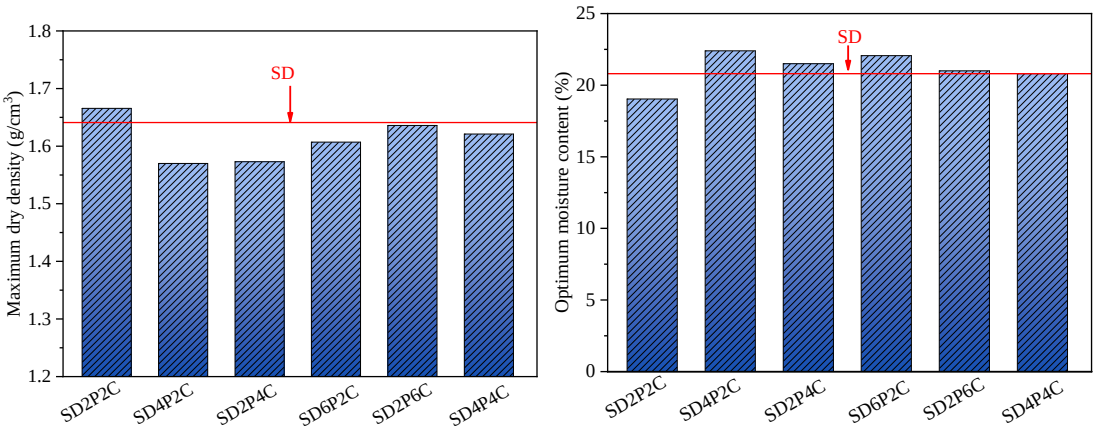

Figure 5-2 (a) MDD and (b) OMC of the untreated and treated dredged marine sediments.

5.3.2 Immediately California Bearing Ratio (I-CBR) test

I-CBR index value is a parameter that can analyze the bearing capacity of materials after compaction. I-CBR index curves of OPC-CSA treated sediments are shown in Figure 5-3. Figure 5-4 summarizes the I-CBR index at the OMC of treated sediments with various OPC-CSA contents. It's evident that I-CBR values of treated sediments increase more significantly than untreated sediments SD, due to the addition of the OPC-CSA composite binder. I-CBR values increase as the OPC-CSA binder content increase from 4% to 8%. This may be attributed to binder hydration reaction, a large quantity of hydration product formation, cementitious the sediments particles effectively, leading the I-CBR value of treated sediment to enhance [246].

Another interesting phenomenon in Figure 5-4 is the I-CBR values for treated sediments were more than 35%, which means all of these mixes meet the requirement of the sub-base layer [247]. Especially, the I-CBR values for some mixes (SD2P4C, SD2P6C and SD4P4C) were more than 50% and met the requirement of the base layer [247].

Besides, in terms of the impact of OPC and CSA binder on I-CBR index values, these results indicate that CSA binder addition has a greater effect than OPC addition. For instance, for the 8% of binder treated sediments, the OPC/CSA ratio decreased from 3:1 (SD6P2C) to 1:1 (SD4P4C) and 1:3 (SD2P6C), the I-CBR values of treated sediments increase from 40% to 50% and 60%. The results of the 6% of binder treated sediments are consistent with the 8% of binder treated, the I-CBR value of treated sediments increases from 40% to 55%, with the OPC/CSA ratio decrease from 2:1 (SD4P2C) to 1:2 (SD2P4C).

This perhaps is due to the OPC hydration being affected significantly by the addition of CSA in the OPC-CSA composite binder [134]. The fast hydration of CSA cement concentrated in the early stage, the large quantity of water consumed by ettringite formation could postpone the hydration of OPC (C_3S and C_2S) [11] [142]. Meanwhile, OPC also contributes to the ye'elimite hydration rate [134] [277]. The I-CBR index correlates the properties of OPC-CSA treated sediment during the initial one-hour period. The fast hydration of CSA cement is the main reason for increasing the I-CBR index. This is why the low OPC/CSA ratio binder treated dredged sediments have better I-CBR performance.

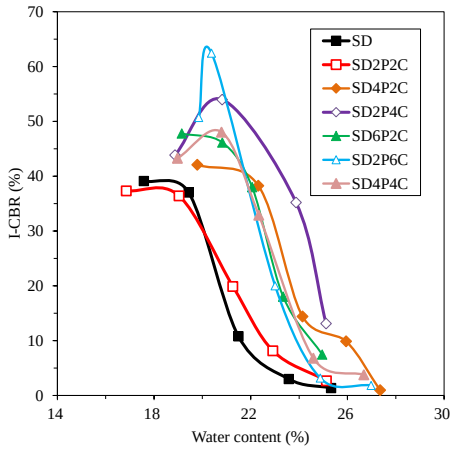

Figure 5-3 I-CBR index curves of the treated dredged marine sediments.

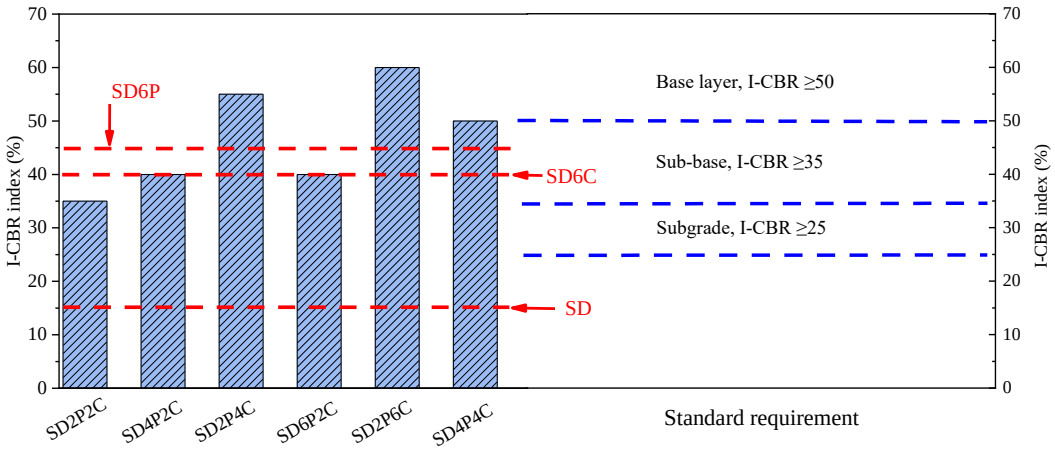

Figure 5-4 I-CBR index at the OMC of the treated dredged marine sediments.

5.3.3 Unconfined compressive strength

Figure 5-5 shows the q_c development of the treated dredged sediments with different amounts of OPC-CSA binder, the OPC/CSA ratio and curing time. The q_c of untreated sediments SD (0.50 MPa) is obviously lower than that of treated dredged sediments. This has been widely reported in previous research [53] [74] [237]. Even upon adding 4% OPC-CSA composite binder (SD2P2C), the 3d-q_c is increased by 158% (1.29 MPa) compared to SD. The development of q_c can be attributed to the hydration of OPC and CSA binder, which produces the cementitious substance and binding sediment particles [263]. Furthermore, the q_c of these mixes increased as the OPC-CSA binder amount and curing time increased. This is due to the development of hydration products, which contribute to the strength development of treated sediments [134] [263]. Besides, all of these OPC-CSA treated sediments meet the minimum strength requirement (1 MPa) of the subgrade [167].

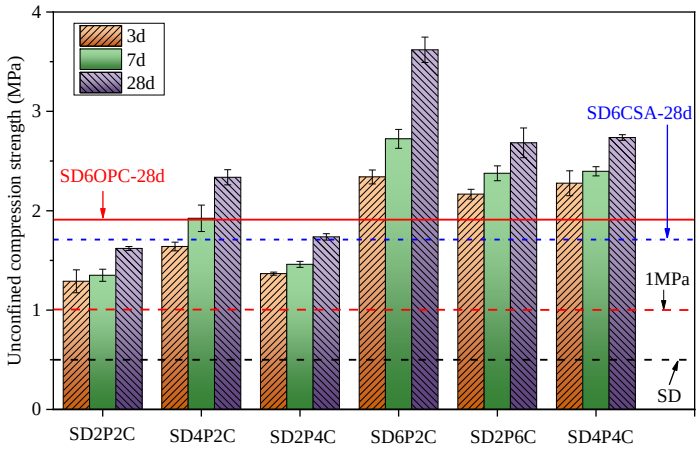

Figure 5-5 Unconfined compressive strength of the treated dredged marine sediments.

It's easy to find that compared to the reference specimens SD6P and SD6C at 28 d, 4% OPC-CSA binder treated sediments (SD2P2C) at 28 d achieved 95% (1.62 MPa) of the SD6C specimen strength (1.71 MPa). While 6% OPC-CSA binder treated sediments (SD4P2C) at 7 d (1.92 MPa) presented similar strength with SD6P at 28 d (1.91 MPa). The other authors [134] found the compressive strength of the OPC-CSA mortar is higher than CSA cement. This is due to the interaction of OPC and CSA cement at early age hydration, increasing reaction product ettringite. These results verified that the OPC-CSA composite binder outperforms the OPC/CSA single binder to improve the q_c of treated sediments.

It should be noted that under the condition of the 8% binder dosage, the SD6P2C specimen (2.34-3.62 MPa) is regarded as the best performance of the compressive strength specimen. Whereas the SD2P6C specimen (2.17-2.68 MPa) is the worst performance specimen, the performance of the SD4P4C specimen (2.28-2.74 MPa) is between them. This is to say, with the OPC/CSA ratio decreasing from 3:1 (SD6P2C) to 1:1 (SD4P4C) and 1:3 (SD2P6C), q_c of the OPC-CSA composite binder treated sediments correspondingly decreases. This indicates that the specimens with a high OPC/CSA ratio show better mechanical properties. In reality, the specimens with a high OPC/CSA ratio contain relatively more OPC, which could prompt the reaction of the CSA binder. Besides, C_3A from OPC can react with anhydrite and gypsum to form ettringite rapidly, increasing ettringite content. What's more, the pH value of the CSA binder is lower than 10.5 generally. However, the ettringite is easily decomposed at pH below 10.7. The addition of OPC enhances the pH value, which is positive for the stability of ettringite [273, 278, 279].

The concept of compressive strength ratio η_c is introduced, to quantify the increase in

q_c of treated sediments with the addition of OPC-CSA binder and curing time. The strength ratio η_c in Figure 5-6, is determined by the ratio of q_{cn} of OPC-CSA treated specimens to the q_{c0} of untreated specimen SD, as in Equation (5-1).

$$\eta_c = \frac{q_{cn}}{q_{c0}} \tag{5-1}$$

It is evident that there is an increasing tendency of η_c with curing time for each mixture. The η_c increases correspondingly from 2.58 to 4.68 at 3 d, from 2.70 to 5.45 at 7 d and from 3.24 to 7.24 at 28 d. This revealed the strength growth ratio of treated sediments at varying curing times due to the OPC-CSA binder's addition. Besides, at the same binder content and curing time condition, the high OPC/CSA ratio specimens (SD4P2C and SD6P2C) have a higher strength growth ratio than the low OPC/CSA ratio specimens (SD2P4C, SD2P6C and SD4P4C).

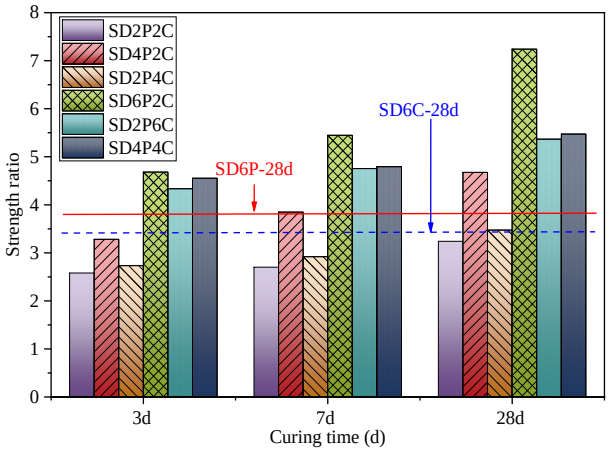

Figure 5-6 Development in compressive strength ratio of the OPC-CSA treated sediment.

This is to say, the high OPC/CSA ratio, high OPC-CSA binder content and extended curing time offered excellent q_c contributions for OPC-CSA treated sediments. However, the combined effect of OPC and CSA within sediment's matrix is not the simple summation of their individual chemical reaction contribution, but is a complex coupled effect on the strength improvement. Moreover, the quick hydration of lots of ye'elimite from CSA cement mostly contributes to the early strength growth of treated sediments [134]. The hydration of OPC mainly occurs after several days, which plays a key part in developing final strength [139].

5.3.4 Elastic modulus

In general, elastic modulus (E) is a key geotechnical parameter used for assessing the

property of deformation under load. The calculation of E is involved in the measurement of the stress-strain curve.

Figure 5-7 exhibits the E development of the treated dredged sediments with different amounts of OPC-CSA binder, the OPC/CSA ratio and curing time. A similar phenomenon with q_c can be discovered, for the changing trend of elastic modulus. All the treated sediments have a higher elastic modulus than untreated specimen SD. Besides, it could be found from Figure 5-7 that the OPC-CSA composite binder treated sediments have higher E values than the OPC/CSA single binder treated sediments. E values increase with the increase of OPC-CSA binder amount, OPC/CSA ratio and curing time. Higher binder dosage and OPC/CSA ratio benefit the development of elastic modulus.

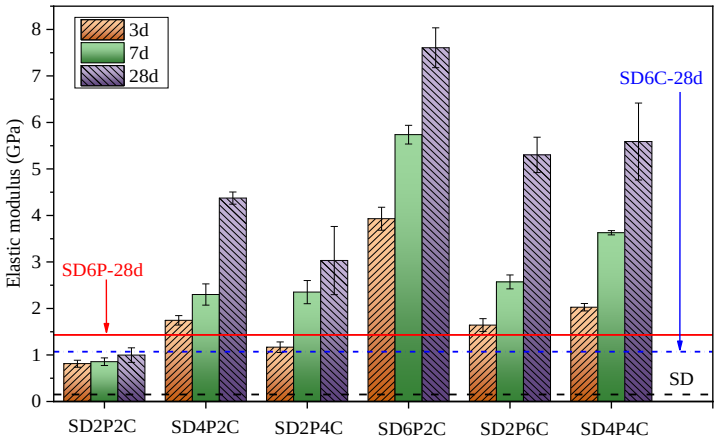

Figure 5-7 Elastic modulus of the treated dredged marine sediments.

5.3.5 Splitting tensile strength

Figure 5-8 plots the q_{it} development for OPC-CSA binder treated sediments. In fact, we can easily observe a similar q_{it} performance with q_c. As expected, the OPC-CSA composite binder effectively improved the q_{it} of treated dredged marine sediments. The q_{it} of the untreated specimen SD (0.050 MPa) was less than all the OPC-CSA binder treated dredged marine sediments specimens. The q_{it} increases are attributed to the incorporation of the OPC-CSA binder that causes a strong hydration reaction with water. Besides, both SD2P2C and SD2P4C are doubtful (0.1 MPa < q_{it} < 0.2 MPa) [257], which means the decision on applied treatment depends on the anticipated site conditions. While, SD4P2C, SD6P2C, SD2P6C and SD4P4C are suitable (q_{it} > 0.2 MPa) [257], these treated sediments are suitable for earthwork usage.

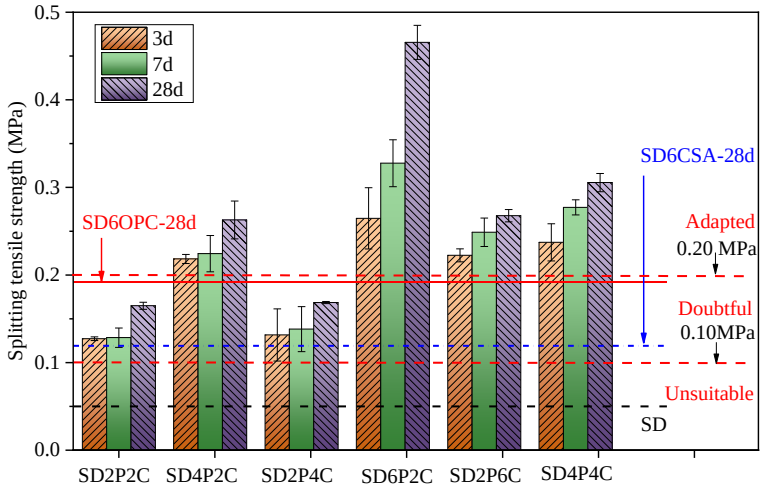

Figure 5-8 Splitting tensile strength of the treated dredged marine sediments.

Furthermore, it can be clearly seen a similar trend as q_c and E from Figure 5-8, that the OPC-CSA binder dosage, OPC/CSA ratio and curing time have a profound effect on the q_{it} of these treated specimens. To evaluate these effects quantitatively on q_{it} of treated dredged marine sediments, the concept of splitting tensile strength ratio η_{it} is introduced. The strength ratio η_{it} in Figure 5-9, is determined by the ratio of q_{itn} of OPC-CSA binder treated specimen to the q_{it0} of untreated specimen SD, as in Equation (5-2).

$$\eta_{it} = \frac{q_{itn}}{q_{it0}} \tag{5-2}$$

With the OPC-CSA binder dosage increase, the hydration reaction is more intensified. The reaction products C-S-H, CH and AFt continue to grow [134], fill the mixture's pores and cementitious sediment particles. This could result in q_{it} increase of OPC-CSA binder treated specimens. For instance, the q_{it} of SD2P2C specimen (4% binder) at 3 d is 0.127 MPa. By comparison, the q_{it} of SD4P4C specimens (8% binder) is 0.237 MPa at 3 d. While the corresponding η_{it} changed from 2.55 (SD2P2C) to 4.75 (SD4P4C). For the treated specimens with the same binder dosage (8%), the performance of splitting tensile strength was outstanding in the following order: SD6P2C > SD4P4C > SD2P6C. After curing 28 d, q_{it} is significantly enhanced from 0.268 MPa (SD2P6C) to 0.305 MPa (SD4P4C) and 0.466 MPa (SD6P2C) with an increase in the ratio of OPC/CSA. While the corresponding η_{it} increases from 5.35 (SD2P6C) to 6.11 (SD4P4C) and 9.31 (SD6P2C). This powerful proves high OPC/CSA ratio binder treated specimen has higher q_{it} than the low OPC/CSA ratio

binder treated specimen. Furthermore, the q_{it} of the SD2P6C specimen increases from 0.222 MPa to 0.249 MPa and 0.268 MPa, with an increase in curing time of 3 d to 7 d and 28 d.

Meanwhile, it should be noted that the OPC-CSA composite binder treated specimens have higher q_{it}, compared with the OPC/CSA single binder treated specimens. This is because the addition of OPC to CSA can significantly increase the ettringite content and early strength, followed by the decrease of porosity and the increase of compactness, resulting in the late high strength [134].

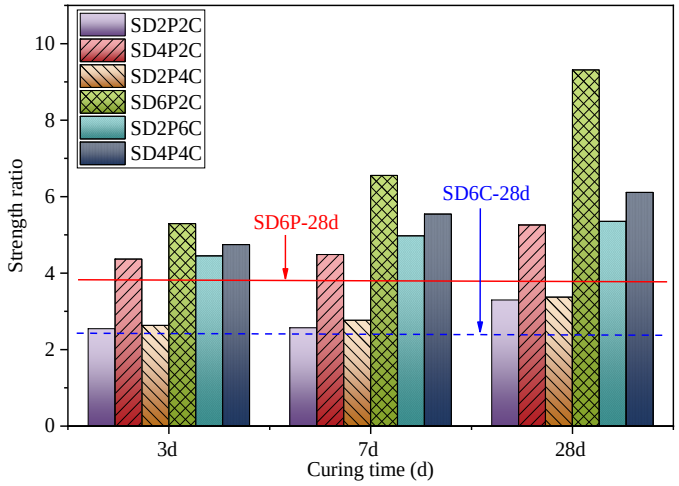

Figure 5-9 Development in tensile strength ratio of the treated dredged marine sediments.

5.3.6 Relationship of q_c, q_{it} and E

This section estimates the relationship between the q_c and q_{it} with E for the OPC-CSA composite binder treated sediments by the regression analysis method. From many other investigators [252, 253, 258, 259], one of the most commonly used models for explaining the relationship between q_c and q_{it} of treated soil is the simple linear model. As shown in Figure 5-10(a), based on the measured data, the new Equation (5-3) has been used to model the relationship between q_c and q_{it} for the OPC-CSA composite binder treated sediments in this study. This result is closed to the results of the OPC-fly ash treated sediments from Yoobanpot et al. [77] ($q_c(MPa) = 9.09q_{it}(MPa)$) and Wang et al. [253] ($q_c(MPa) = 9.90q_{it}(MPa)$) research. Besides, this equation is also closed to the results for OPC/CSA single binder treated sediments. In addition, it can be observed in Figure 5-10(a) that the fit curve of Equation (5-3) indicated that q_c and q_{it} had a good relationship. The coefficient of determination (R^2)

of Equations (5-3) in this study is 0.991.

$$q_c(MPa) = 8.83 q_{it}(MPa) \quad (5\text{-}3)$$

The measured data points of q_c versus E and q_{it} versus E, are gathered and presented in Figure 5-10(b)-(c), respectively. The mentioned figures show that both q_c and q_{it} followed similar trends with E. Owing to the similar present trends, the simple power model is suggested to be used to fit the relationship of q_c versus E and q_{it} versus E. By doing this, the analysis led to the equations presented in the same figure. The Equation (5-4) with R^2=0.843 could describe well the relationship of q_c and E for the OPC-CSA composite binder treated sediments specimens.

However, this model is different from the results of the OPC/CSA single binder treated sediments (Chapter 4) and the OPC-fly ash treated sediments (Ho et al. [251] and Tan et al. [260]). It should be noted that the data points are over the range of (0.35-1.08)q_c for OPC/CSA single binder solidified sediments and OPC-fly ash solidified sediments ((0.50-1.08)q_c of Ho et al. [251] and (0.35-0.80)q_c of Tan et al. [260]). This could be because the unconfined compressive strength of the OPC-CSA composite binder treated sediments is higher, while the failure strain is smaller, than those in the OPC-fly ash treated sediments of other studies and OPC/CSA single binder treated sediments, resulting in a higher elastic modulus [280].

$$E(GPa) = 0.69 {q_c}^{1.93}(MPa) \quad (5\text{-}4)$$

Similarly, by conducting regression analysis, we obtained a model that can be expressed by Equation (5-5) with R^2=0.818. Which could be used to estimate the relationship of q_{it} and E for the OPC-CSA composite binder treated sediments. The difference with the OPC/CSA single binder treated sediments, is also because of the higher elastic modulus for the OPC-CSA composite binder treated sediments.

$$E(GPa) = 26.18 {q_{it}}^{1.49}(MPa) \quad (5\text{-}5)$$

Actually, it should note that the q_c, q_{it} and E could be affected by some factors, such as curing time, binder type, water content, sample size and the experimental method used. In addition, the amount of measured data is significant since more data might give better statistical validation for different factors. Nonetheless, the proposed Equations (5-3), (5-4) and (5-5) for the OPC-CSA composite binder treated sediments in this investigation, were established with little data. Thus, more experimental data is required to confirm these equations in the future.

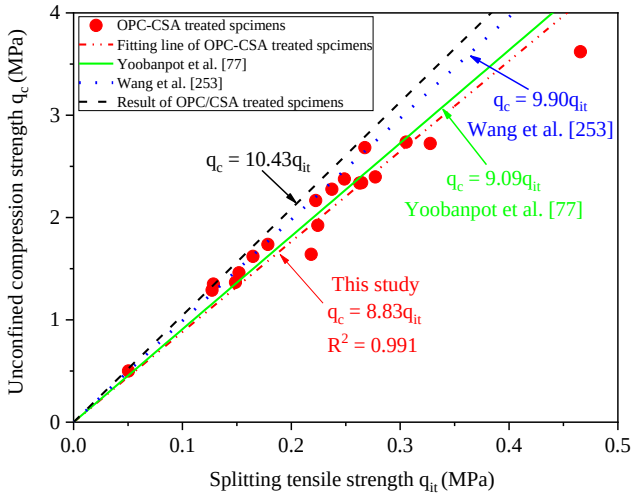

(a)

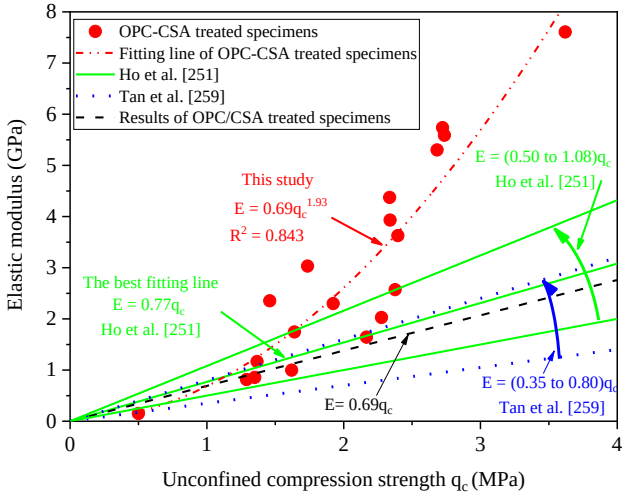

(b)

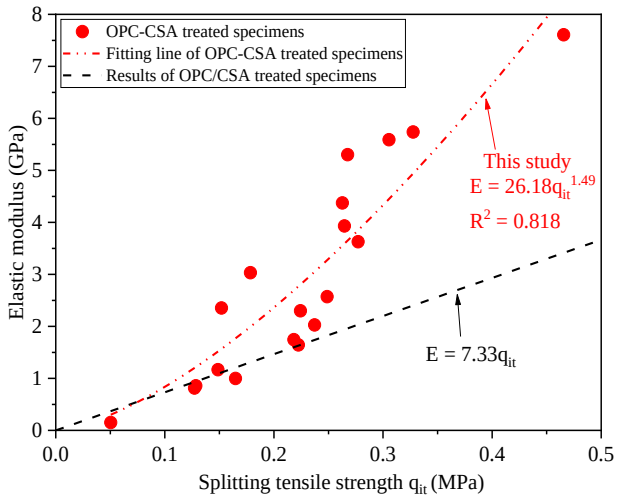

(c)

Figure 5-10 Relationship of (a) q_c versus q_{it}; (b) q_c versus E and (c) q_{it} versus E for the OPC-CSA composite binder treated sediments.

5.3.7 Evaluation of solidified sediments as road materials

In order to estimate the suitability of the OPC-CSA composite binder treated dredged marine sediments to be reused as road material, the mechanical characteristics of the solidified dredged marine sediments at 180 d are reported on the specific classifying diagram (Figure 5-11), according to the GTS road guide [281]. It should be noted that the direct tensile strength (q_t) is calculated from the indirect tensile strength (q_{it}) according to Equation (5-6) [261]. The different classification zones of road materials are also shown in Figure 5-11, based on the GTS road guide [281].

$$q_t = 0.8q_{it} \tag{5-6}$$

Figure 5-11 shows the classification of OPC-CSA composite binder solidified dredged sediments as road materials based on mechanical characteristics. It could be easily found that only SD, SD6C and SD2P2C samples are below Zone 5, whereas the SD6P2C sample falls within class 3 (Zone 3). Meanwhile, SD6P with the remaining OPC-CSA treated samples (SD4P2C, SD2P4C, SD2P6C and SD4P4C) belong to class 5 (Zone 5). This indicated that treating sediments with the OPC-CSA composite binder could improve the material classification than using the OPC/CSA single binder. It should be noted that the standard prescribes that class 5 is the minimum necessary for prospective use as subgrade material. Hence, these OPC-CSA composite binder-treated materials (SD4P2C, SD2P4C, SD2P6C, SD4P4C and SD6P2C) meet the thresholds of subgrade material in this study.

According to the compressive strength threshold at 7 d (Table 4-3) from Chinses standard CJJ 169-2011 [262], the SD6P2C sample could be used in the sub-base layer with special heavy traffic, or base layer with light traffic. The SD2P6C and SD4P4C samples could be used in the sub-base layer with heavy traffic. The SD4P2C sample could be used in the sub-base layer with light traffic.

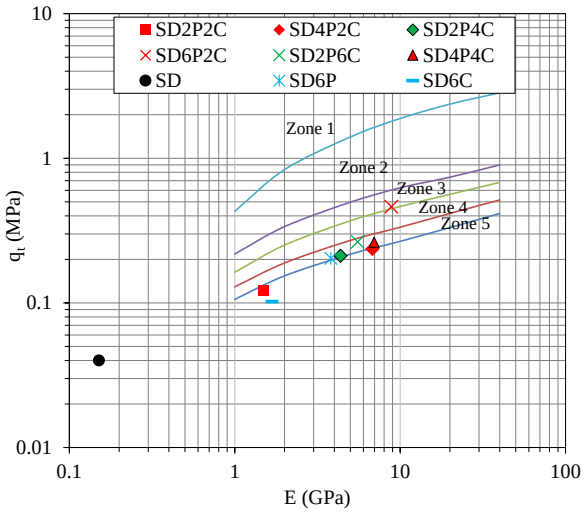

Figure 5-11 Classification of the OPC-CSA composite binder treated sediments.

5.3.8 X-ray diffraction analysis

XRD analysis is used to identify the hydrates of the OPC-CSA binder. Two different ratios of OPC/CSA paste specimens were prepared with 28 d curing, the OPC/CSA ratios are 1:3 (2P6C) and 3:1 (6P2C), the water-to-binder ratio is 0.5.

Figure 5-12 shows the XRD results for the two specimens. The differences in hydration products are visible for the OPC-CSA composite binders with the different OPC/CSA ratios. For low OPC/CSA ratio specimen 2P6C, ettringite is the main hydration product, portlandite and CSH is the minor hydration products. Besides, AFm phases could be found, such as monosulfate (Ms), hemicarbonate (Hc) and strätlingite (C_2ASH_8). For high OPC/CSA ratio specimen 6P2C, the portlandite peak is more significant than ettringite in the XRD patterns. There is no strätlingite observed for the 6P2C specimen.

When the OPC/CSA ratio is less than one, the CSA (ye'elimite) hydration is fast as reaction (1-10) first. The OPC hydration mainly occurs after several days [282]. However, in the aluminum-rich environment, the OPC hydration reaction is different from OPC alone [142]. Tricalcium aluminate (C_3A) from OPC could hydrate to form ettringite as shown in reaction (5-7). Alite (C_3S) from OPC main occur reaction (5-8), hydration produces strätlingite (C_2ASH_8) and portlandite (CH). A part of Alite still produces CSH gel associated with portlandite, as reaction (5-9). Belite (C_2S) can hydrate to form strätlingite (C_2ASH_8) (reaction (1-12)). When the portlandite is present, reaction (1-10) can be transformed into reaction (5-10) [134] [142].

When the OPC/CSA ratio is more than one, the addition of CSA does not affect the

hydration mechanism of alite and belite from OPC [283]. Alite and belite form CSH gel and portlandite. After the portlandite is present, CSA (ye'elimite) hydration is transformed into reaction (5-10) [134]. The presence of anhydrite from CSA causes the delay in the Tricalcium aluminate (C_3A) hydration, C_3A could hydrate with anhydrite, form ettringite rapidly as the reaction (5-7), increasing the amount of ettringite [283].

$$C_3A + 3C\bar{S} + 32H \rightarrow 3C_6A\bar{S}_3H_{32} \quad (5\text{-}7)$$

$$C_3S + AH_3 + 6H \rightarrow C_2ASH_8 + CH \quad (5\text{-}8)$$

$$C_3S + 3.7H \rightarrow CSH_{1.7} + 2CH \quad (5\text{-}9)$$

$$C_4A_3\bar{S} + 8C\bar{S} + 6CH + 90H \rightarrow 3C_6A\bar{S}_3H_{32} \quad (5\text{-}10)$$

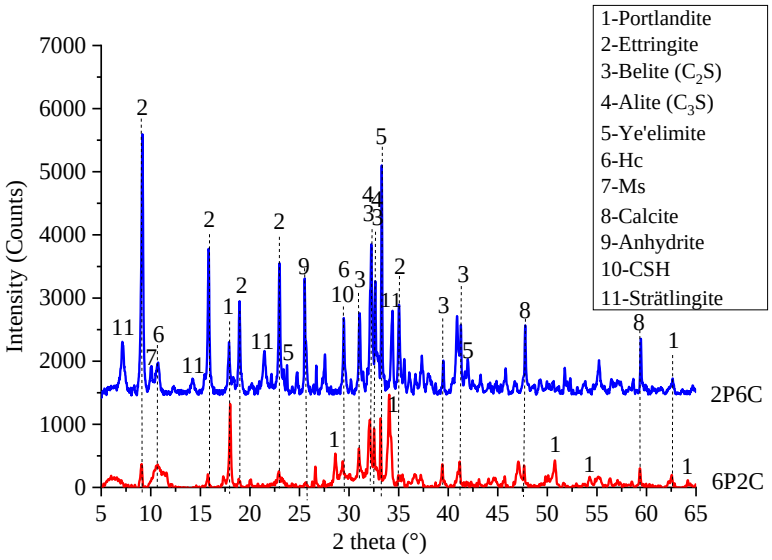

Figure 5-12 XRD traces of OPC-CSA composite paste (Cu Kα).

5.3.9 Scanning electron microscopy analysis

Scanning electron microscopy (SEM) was carried out on the selected 28d-specimens to observe the surface morphology changes. Figure 5-13(a) shows the obtained SEM image of the treated sediments specimen SD6P2C, with a high OPC/CSA ratio. The local marked magnified area image, Figure 5-13 (b), clearly shows that like fine fibrillar C-S-H gels, hexagonal plate-shaped portlandite (CH) and needle-like ettringite (AFt). It should be noted that the morphology of AFt is different from the short rod-like AFt of the CSA-treated sediments (Figure 4-15). This finding agrees well with the previous literature [134] [263]. The addition of OPC can influence the

hydration of ye'elimite and the morphology of ettringite. Reactive (5-10) can form finer needle-like ettringite [268]. Meanwhile, these hydration products filled the interparticle spaces and adhered to particles of sediments, forming larger volume aggregates, which strengthened the interaction among sediments particles, thus treated sediments specimens present a dense and strong microstructure.

Figure 5-13(c) shows the typical SEM image of the SD2P6C specimen, with a low OPC/CSA ratio. In the local marked magnified area in Figure 5-13(d), it can be observed that a large number of needle-like AFt and less hexagonal plate-shaped CH covering sediments particle formed larger volume aggregates and the whole structure, there are fewer pores in the structure.

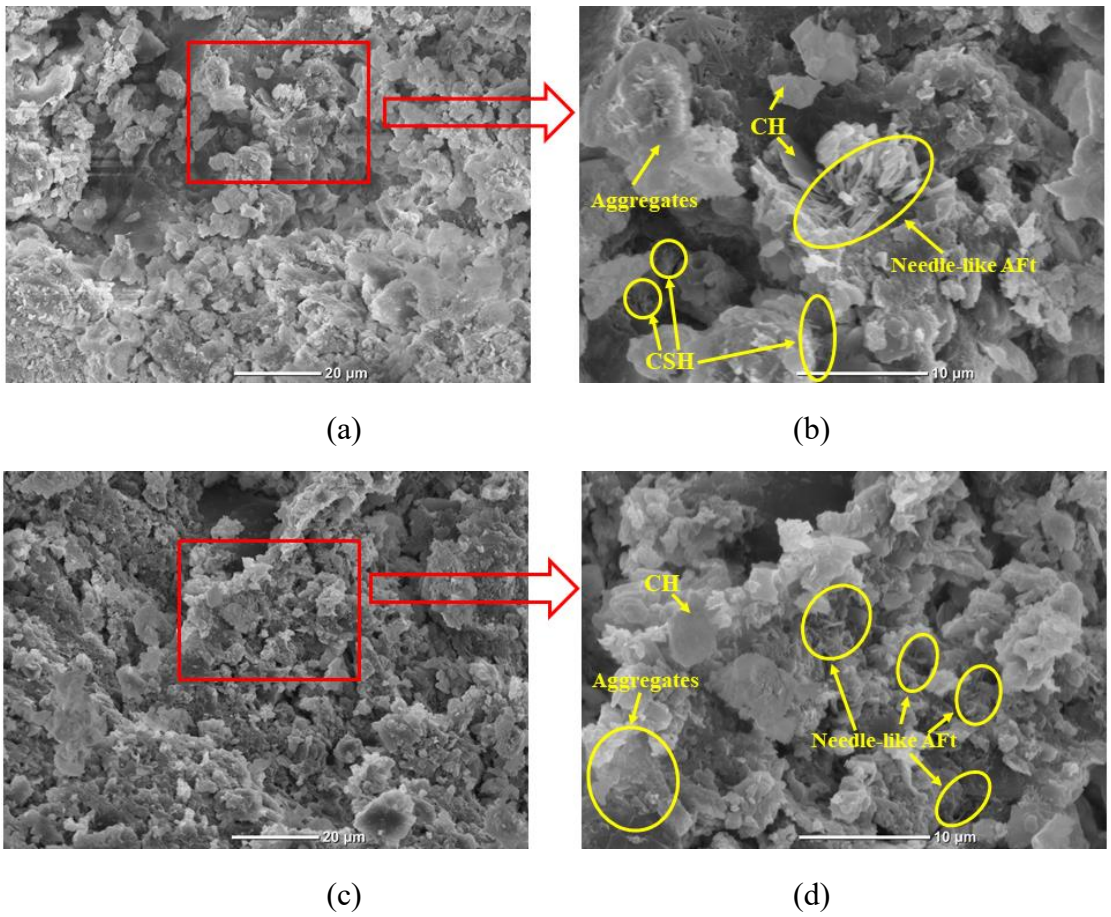

Figure 5-13 SEM images of typical specimens. (a) SD6P2C (×1000); (b) local marked magnified area of (c) (×3000); (c) SD2P6C (×1000); (d) local marked magnified area of (e) (×3000).

5.3.10 Micropore structure analysis

The micropore structure of the typical untreated and OPC-CSA composite binder treated sediments specimens was investigated, and the results are shown in Figure 5-14. The same as the OPC/CSA single binder treated specimens' results, all the pore size distribution curves are bimodal and distributed in the ranges of 0.01-1.00 μm and 1.00-40.00 μm.

The untreated specimen has higher larger pores (1.00-40.00 μm and > 40.00 μm) percentages and fewer smaller pores (< 0.01 μm and 0.01-0.10 μm) percentages. The treatment of sediments makes the larger pores transform into smaller pores. Besides, Table 5-2 shows the pore volume percentage of the OPC-CSA composite binder treated sediments, in different pore size ranges. For the SD6P2C specimens, the pores volume percentage of large pores in the ranges of 0.10-1.00 μm is less than SD2P6C specimens. While the pores volume percentage of the smaller pores in the range of < 0.01 μm and 0.01-0.10 μm are more than SD2P6C specimens. This indicated that compared to SD2P6C specimens, more large pores transform into small pores (< 0.01 μm and 0.01-0.10 μm) for SD6P2C specimens. This induces the pores to become finer and denser for the OPC-CSA composite binder treated sediments. This result agrees well with the finding of mechanical analysis. The denser structure of SD6P2C specimens may cause higher mechanical properties than SD2P6C specimens.

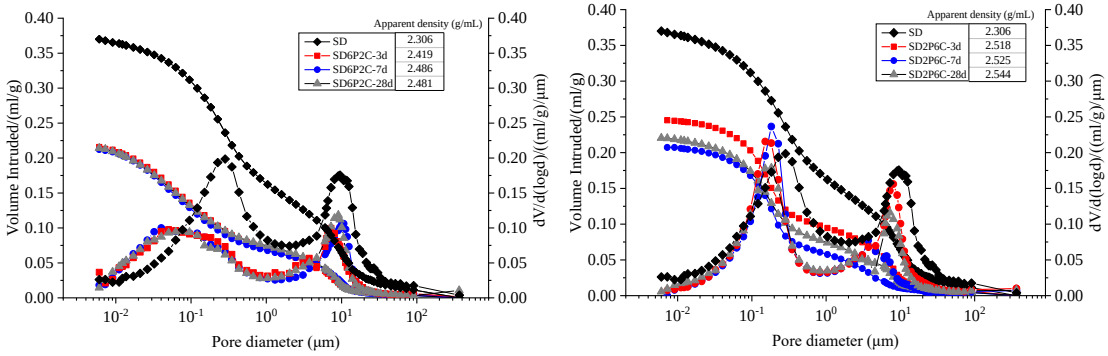

(5) (b)

Figure 5-14 Micropore structure analysis of (a) SD6P2C and (b) SD2P6C.

Table 5-2 Pore size distribution of the OPC-CSA binder treated sediments.

Pore size (μm)	Pore size distribution (%)						
	SD	SD6P2C -3d	SD6P2C -7d	SD6P2C -28d	SD2P6C -3d	SD2P6C -7d	SD2P6C -28d
>40.00	5.01	2.85	2.34	2.50	3.45	2.75	3.01
1.00-40.00	38.84	29.84	29.42	32.18	35.12	25.01	30.58
0.10-1.00	40.44	30.36	29.01	27.18	38.26	47.32	45.41
0.01-0.10	14.03	33.49	36.10	34.39	22.27	23.97	19.59
<0.01	1.68	3.45	3.13	3.74	0.89	0.95	1.42
Total	100.00	100.00	100.00	100.00	100.00	100.00	100.00

5.3.11 Environmental assessment

The environmental characterization of the typically OPC-CSA composite binder treated sediments was evaluated, by standard leaching tests, based on the standard NF EN 12457-2 [242]. The results are listed in Table 5-3.

As seen in Table 5-3, all the pH values of the OPC-CSA treated sediments are higher than that of untreated sediments (7.42). This indicated the leaching solution of the OPC-CSA composite binder treated sediments have strong alkalinity. Meanwhile, the pH values of the high OPC/CSA ratio specimen SD6P2C are higher than that of the low OPC/CSA ratio specimen SD2P6C. This is because CSA is a kind of low alkaline binder compared to OPC [284].

In terms of the OPC-CSA composite binder treated sediments specimens, based on the European directive 2003/33/CE [201], the measured leaching values for these elements (As, Ba, Cd, Cr, Ni, Pb, Se, Sb and Zn) are in the thresholds of Class III (inert waste). At the same time, all the leaching values of Mo, chlorides, sulfates and soluble fraction, parts of the values of Cu and fluorides are above the thresholds of Class III (inert waste) and correspond to the level fixed for Class II (non-hazardous waste). Thus, all these OPC-CSA treated sediments specimens could be considered as non-hazardous waste.

Besides, the pollution level of the OPC-CSA composite binder treated sediments materials is less than the thresholds of the French SETRA guide for road engineering [202], which is allowed to be reused in road engineering. In conclusion, OPC-CSA treated sediments meet the environmental requirements of the regulations.

It's worth noting that both SD6P2C and SD2P6C specimens have lower sulfate

leaching values than raw sediments. This is significantly different from the CSA treated sediments. Sulfate leaching levels did not increase for the OPC-CSA composite binder treated sediment. This could be because the pH values of the OPC-CSA composite binder treated specimens were higher than those of the CSA treated specimens. The pH values in the lower pH specimen SD2P6C are about 10.7. (10.53-10.94). We believe that the sulfate ion could form ettringite when it reacts with the OPC-CSA composite binder. In a highly alkaline environment, OPC-CSA composite binder treated specimens' ettringite remains stable. As a result, it's possible that, sulfates leaching levels in OPC-CSA treated sediments can decrease.

In addition, the changes in other elements' leaching values are similar to OPC/CSA single binder treated sediments. The explanation was given in chapter 4.

Table 5-3 Leaching results of the OPC-CSA treated sediments.

Elements	Values (mg/kg)						European directive 2003/33/CE [201]			SETRA road guide [202]
	SD6P2C -3d	SD6P2C -7d	SD6P2C -28d	SD2P6C -3d	SD2P6C -7d	SD2P6C -28d	Class III	Class II	Class I	Limit values
pH	11.86	11.69	11.65	10.60	10.53	10.94	/	/	/	/
As	< 0.1	< 0.1	< 0.1	< 0.1	< 0.1	< 0.1	0.5	2	25	2
Ba	0.15	0.14	0.13	0.06	0.07	0.06	20	100	300	100
Cd	< 0.009	< 0.009	< 0.009	< 0.009	< 0.009	< 0.009	0.04	1	5	1
Cr	0.51	0.76	0.63	0.32	0.33	0.41	0.5	10	70	10
Cu	2.56	2.19	2.51	0.77	0.77	0.96	2	50	100	50
Hg	< 0.06	< 0.06	< 0.06	< 0.06	< 0.06	< 0.06	0.01	0.02	0.03	0.2
Mo	0.65	0.64	0.65	0.61	0.60	0.61	0.5	10	30	10
Ni	0.33	0.26	0.28	< 0.05	< 0.05	0.06	0.4	10	40	10
Pb	< 0.06	< 0.06	< 0.06	< 0.06	< 0.06	< 0.06	0.5	10	50	10
Sb	< 0.06	< 0.06	< 0.06	< 0.06	< 0.06	< 0.06	0.06	0.7	5	0.7
Se	< 0.08	< 0.08	< 0.08	< 0.08	< 0.08	0.09	0.1	0.5	7	0.5
Zn	< 0.05	< 0.05	< 0.05	< 0.05	< 0.05	< 0.05	4	50	200	50
Chlorides	2270	2310	2345	2275	2215	2345	800	15 000	25000	15000
Fluorides	23.50	18.00	19.00	9.00	8.00	10.00	10	150	500	150
Sulfates	5594	5816	6390	6669	7047	5616	1 000	20 000	50000	20000
Soluble fraction	18318	17238	17272	18679	19148	18368	4000	60000	100000	60000

(Note: Class I is hazardous waste, Class II is non-hazardous waste, Class III is inert waste.)

5.4 Simplified carbon footprint analysis

The OPC-CSA composite binder has a significant environmental benefit, when compared with the conventional OPC binder. There is some qualitative evidence indicating that CO_2 emissions are lower, due to the combination of lower temperatures and less limestone required during the CSA binder manufacturing process. In this part, based on the previous study [129], we used a simplified theoretical (thermodynamic) approach for estimating the level of reductions in CO_2 emissions during the production of the OPC-CSA composite binder compared with the OPC binder.

The actual CO_2 emissions of a binder manufacturing process include three parts: (a) fuel energy derived; (b) raw materials derived and (c) indirect energy/emissions (e.g., clinker grinding and transportation). For simplicity, indirect energy/emission is not considered in the following analysis, it is assumed to be the same as for OPC. Table 5-4 shows the manufacturing enthalpy and raw material CO_2 emissions values calculated for clinker phases; detailed calculations can be found in the previous study [129]. Normally, gypsum and anhydrite are mined from naturally sourced or are recovered from flue gas desulfurization waste. We consider adding it to the binder, without energy consumption and CO_2 emissions. Using these values in Table 2-24, it is easy to calculate the manufacturing enthalpy and raw materials CO_2 emissions for any binder, by simply adding the contributions weighted by the mass fraction in the binder.

Table 5-4 Manufacturing enthalpy and raw material CO_2 of various clinker phases [129].

Clinker phase	Symbol	Manufacturing enthalpy (GJ/t)	Raw material CO_2 emissions (kg/t)
Alite	C_3S	1.82	579
Ferrite	C_4AF	1.36	362
Aluminate	C_3A	2.01	489
Belite	C_2S	1.30	512
Ye'elimite [from $CaSO_4$]	$C_4A_3\bar{S}$	0.77	216

Table 5-5 shows the CO_2 emission value of the OPC and CSA binder in this study. Specifically, the composition of the OPC binder in this study is 63.74% C_3S, 18.04% C_2S, 7.25% C_3A, 9.82% C_4AF and 1.14% gypsum. Thus, the theoretical manufacturing enthalpy of the OPC binder in this study is 1.674 GJ/t. However, it

should be noted that the total heat required in the kiln is the sum of the theoretical enthalpy plus a heat loss, which is closer to 3 GJ/t [129]. For carbon-rich fuel burned to produce one GJ, ~90 kg of CO_2 emissions can be considered for calculation [129, 285]. This means that if we use the theoretical enthalpy value, the total CO_2 emission of fuel energy derived is 150.66 kg/t OPC. Based on the OPC composition in this study, the CO_2 emission value from raw material is 532.42 kg/t. Thus, the total CO_2 emission value of the OPC binder is 683.08 kg/t in this study. In fact, this value for OPC is typically more than 800 kg/t, which is due to the indirect energy/emissions are not considered in this study. For the studied CSA binder, similarly, the total CO_2 emission value is 305.21 kg/t, assuming the source of sulfur for the Ye'elimite ($C_4A_3\bar{S}$) is from calcium sulfate.

Table 5-5 CO_2 emission value of the used OPC and CSA binder in this study.

	OPC	CSA
Manufacturing enthalpy (GJ/t)	1.674	0.722
Fuel energy CO_2 emissions (kg/t)	150.66	65.00
Raw material CO_2 emissions (kg/t)	532.42	240.21
Total CO_2 emissions (kg/t)	683.08	305.21

However, these calculations are meant for the single OPC/CSA binder. For the used binder in this study (Figure 5-15), the total CO_2 emission for the OPC/CSA ratio of 1:1 binder would be 494.14 kg/t, so it's possible to estimate roughly 28% of CO_2 emissions are avoided compared with the OPC binder. This value is further reduced to 399.67 kg/t of the OPC-CSA composite binder with an OPC/CSA ratio of 1:3, which may reduce 41% CO_2 emission. Even the OPC-CSA composite binder with the OPC/CSA ratio of 3:1, could reduce 14% CO_2 emission (588.60 kg/t). Thus, the above analysis indicated that, this study's OPC-CSA composite binder used for the treatment of sediments, offers potential with 14–41% CO_2 emissions savings, compared to the conventional OPC binder. It is to note that this calculation for CO_2 emissions savings in this study is based on the same binder content. Taking into account the higher mechanical characteristics for the OPC-CSA composite binder treated specimens, it would reduce the required amount of OPC-CSA binder for the treatment of sediments, if a similar level of expected mechanical parameters of treated sediments was assumed. This would make the CO_2 emissions savings more impressive.

In this study, these OPC-CSA composite binder-treated materials (SD4P2C, SD2P4C, SD2P6C, SD4P4C and SD6P2C) met the mechanical requirements of subgrade material (Figure 5-11). In terms of CO_2 emissions, SD2P4C (OPC: CSA=1:2) and SD2P6C (OPC: CSA=1:3) appear to be the optimum formulations for 6% and 8% OPC-CSA composite binder-treated materials. Because the two formulations have the greatest promise for reducing CO_2 emissions while meeting the mechanical requirements of subgrade material.

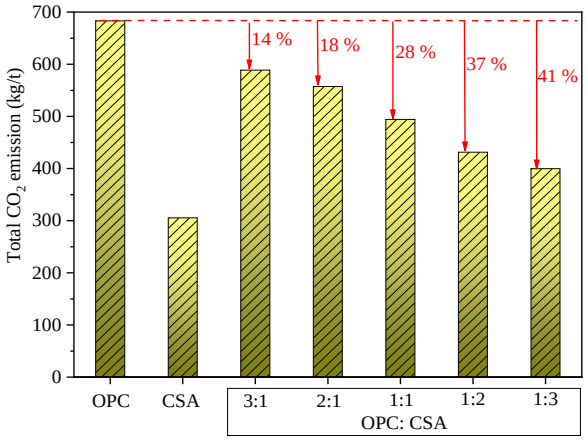

Figure 5-15 Total CO_2 emission of different binders in this study.

5.5 Conclusion

This study investigates the effectiveness of the treatment for dredged marine sediments with low carbon and sustainable OPC-CSA composite binder. First, the physical, mechanical, chemical and environmental aspects of the treated dredged sediments are assessed. In the end, the reduction potential of the carbon-dioxide emission of the OPC-CSA composite binder used in this study is assessed. The main conclusions are summarized as follows.

(1) The OPC-CSA composite binder could effectively improve the bearing capacity characteristics of the treated marine sediments. It's better than the OPC/CSA single binder.

(2) The OPC-CSA composite binder treatment allows a significant increase in the mechanical characteristics of the dredged sediments, such as unconfined compressive strength, splitting tensile strength and elastic modulus. These characteristics are influenced by the OPC-CSA dosage, OPC/CSA ratio and curing age. The OPC-CSA composite binder is better than the OPC/CSA single binder, used to treat dredged sediments.

(3) These OPC-CSA composite binder-treated materials (SD4P2C, SD2P4C, SD2P6C, SD4P4C and SD6P2C) in this study, met the mechanical requirements of subgrade material.

(4) Simple models were proposed to correlate the relationships between the compressive strength, splitting tensile strength and elastic modulus of the OPC-CSA composite binder treated sediments. It is worth noticing that these simple models were established with limited data in this investigation, more experimental data is required to confirm these models in the future.

(5) The XRD results indicated that the chemical reactions are different for the OPC-CSA composite binder with different OPC/CSA ratios. The SEM results showed that the morphology of needle-like ettringite in the OPC-CSA treated sediments is different from the short rod-like ettringite in the CSA-treated sediments. The denser structure of high OPC/CSA ratio binder treated specimens may cause higher mechanical properties than the low OPC/CSA ratio binder treated specimens.

(6) The laboratory tests have revealed the environmental behaviors of the OPC-CSA treated dredged sediments that meet the regulations and road guide requirements, which means that the treated materials could be reused as road materials.

(7) The simplified carbon footprint analysis indicated that the OPC-CSA composite binder offers potential with 14–41% CO_2 emissions savings in this study, compared to the conventional OPC binder. In terms of CO_2 emissions, SD2P4C (OPC: CSA=1:2) and SD2P6C (OPC: CSA=1:3) appear to be the optimum formulations for 6% and 8% OPC-CSA composite binder-treated materials. Because the two formulations have the greatest promise for reducing CO_2 emissions, while meeting the mechanical requirements of subgrade material.

Chapter 6 Modeling of the compaction parameters of treated dredged fine sediments

6.1 Introduction

For valorization of dredged sediments in road construction, the compaction parameters such as Maximum Dry Density (MDD) and Optimum Moisture Content (OMC), are very important geotechnical parameters. The MDD and OMC must be obtained from the Proctor compaction test in the laboratory. However, the Proctor compaction laboratory test is time- and labor-consuming. Therefore, to determine the compaction parameters of treated dredged sediments more efficiently, it is paramount to model the compaction parameters of treated dredged fine sediments.

In this chapter, to model the compaction parameters of the treated dredged fine sediments, the first step is to collect the data from the literature and build a database about the compaction properties of the treated dredged sediments. The second step is to analyze the database with a statistical approach. The third step is to develop models to predict the compaction properties (MDD and OMC) of the treated dredged sediments, with the basic physical parameters of raw sediments and treatment binder types and quantities. Furthermore, the fourth step is to analyze the variance and residual of the proposed models. The proposed models were validated with new data and compared with previous models from the literature.

6.2 Data collection and method

6.2.1 Data collection

The data were collected from several published papers [6, 53, 74, 180, 236, 252, 286-296] to build the database. Within the overall database, there were 94 observations (i.e., rows) for 17 variables (i.e., columns). Table 6-1 represents the ranges in all the input and output parameters in the database. As shown in Table 6-1, a total of 17 different dredged sediments are included in the database. Besides, it can be seen from Table 6-1 that the 15 input parameters were: (1) particle size composition of raw sediments: the percentage of sand (Sand), silt (Silt) and clay (Clay); (2)

Atterberg limits of raw sediments: Liquid Limit (LL), Plastic Limit (PL) and Plasticity Index (PI); (3) Organic Matter (OM) content of raw sediments; (4) Methylene Blue Value of raw sediments (MBV); (5) six different binder types used for the treatment of sediments: Portland cement (P), Lime (L), Fly Ash (FA), Silica Fume (SF), Sand (Sa) and Calcium sulfoaluminate cement (C); (6) compaction Energy (E). The two output parameters were: Optimal Moisture Content (OMC) and Maximum Dry Density (MDD).

Table 6-1 Ranges of all the data from the literature.

No	Sand	Silt	Clay	LL	PL	PI	O.M.	MBV	P	L	FA	SF	Sa	C	E	OMC	MDD	Reference
	(%)	(%)	(%)	(%)	(%)	(%)	(%)	(g/100g)	(%)	(%)	(%)	(%)	(%)	(%)	(MJ/m^3)	(%)	(KN/m^3)	
1	10.00	56.00	34.00	55.00	34.00	21.00	1.50	2.40	-	-	-	-	-	-	0.60-2.70	23.50-27.00	14.86-16.33	[286]
2	10.80	74.70	14.50	76.10	35.30	40.80	6.27	3.10	0-9	0-9	0-6	-	-	-	2.70	20.40-23.90	15.20-16.50	[287] [236]
3	10.80	74.70	14.50	51.40	25.60	25.80	4.40	2.20	0-9	0-9	-	-	-	-	2.70	17.40-23.40	15.80-17.40	[74]
4	60.10	34.00	5.90	82.00	38.00	44.00	11.10	3.20	0-6	0-2	-	-	-	-	2.70	18.90-22.40	15.70-15.90	[288]
5	11.60	77.40	11.00	47.00	25.20	21.80	4.24	4.32	0-2	0-3	-	0-1	0-15	-	0.60-2.70	17.30-24.00	14.60-19.40	[289]
6	0.20	90.90	8.90	112.60	49.30	64.30	10.02	4.08	0-6	0-6	-	-	-	-	2.70	20.00-29.00	14.00-15.80	[180]
7	49.73	43.33	6.94	85.00	42.00	43.00	7.00	2.90	-	-	-	-	-	-	2.70	18.00	16.40	[290]
8	29.00	61-69	2.00-10.00	36.80-41.50	22.90-26.40	13.90-15.10	3.90-4.30	2.55-4.00	0-15	-	-	-	-	-	0.60	12.00-16.02	14.60-19.60	[291]
9	61.10	28.90	9.80	58.00	25.00	33.00	7.17	5.40	0-7	0-4	-	-	0-30	-	0.60	16.00-20.00	13.50-16.40	[292]
10	78.00	20.00	2.00	20.00	10.00	10.00	4.00	0.75	-	-	-	-	-	-	2.70	13.00	17.50	[293]
11	35.00	55.00	10.00	45.00	29.00	16.00	9.40	3.76	-	-	-	-	-	-	2.70	19.80	16.00	[53]
12	11.90-71.00	24.00-73.10	4.00-20.20	36.00-130.00	21.00-60.0	15.00-70.00	4.80-14.10	1.20-3.30	-	-	-	-	-	-	0.60	19.00-30.00	12.00-16.00	[294]
13	24.02-34.77	50.03-54.74	15.20-19.38	29.00-62.00	17.00-50.00	11.00-14.00	5.67-15.00	0.93-1.49	-	-	-	-	-	-	0.60-2.70	17.80-24.90	13.89-17.00	[6]
14	49.00	31.40	19.60	57.00	37.00	20.00	5.40	1.40	6-15	3	-	-	-	-	0.60	23.00-23.10	15.10-16.41	[295]
15	53.55	39.48	6.97	39.50	28.00	11.50	7.67	0.79	0-6	-	-	-	-	0-6	2.70	20.20-23.50	15.58-16.41	[252]
16	53.55	39.48	6.97	39.50	28.00	11.50	7.67	0.79	2-6	-	-	-	-	2-6	2.70	19.03-22.40	15.70-16.66	[296]

6.2.2 Data analysis

The database size for each output is the same with 94 samples for the OMC and the MDD. The implementation of the predicting work for each output was performed separately. Table 6-2 lists all the statistical descriptions of inputs and outputs. Figure 6-1 displays the histogram of the OMC and MDD data. The distributions of both OMC and MDD are approximately normally distributed. This indicated that both OMC and MDD could be the response variable with the multiple linear regression (MLR) approach.

Table 6-2 Descriptive statistics for the properties of the collected sediments.

Parameters	Units	Mean	Median	Standard Deviation	Range	Min	Max	Sum
Sand	(%)	29.16	29.00	20.03	77.85	0.15	78.00	2741.46
Silt	(%)	59.52	61.00	18.32	70.24	20.00	90.24	5594.85
Clay	(%)	11.24	10.00	5.77	32.00	2.00	34.00	1056.24
LL	(%)	56.44	48.00	22.12	110.00	20.00	130.00	5305.15
PL	(%)	31.04	28.00	8.81	50.00	10.00	60.00	2917.95
PI	(%)	25.45	21.40	15.55	60.00	10.00	70.00	2392.20
OM	(%)	6.57	6.27	2.77	13.50	1.50	15.00	617.31
MBV	(g/100g)	2.72	2.73	1.36	4.65	0.75	5.40	256.04
P	(%)	2.84	2.00	3.86	15.00	0	15.00	267.00
L	(%)	1.06	0	2.00	9.00	0	9.00	100.00
FA	(%)	0.26	0	1.05	6.00	0	6.00	24.00
SF	(%)	0.04	0	0.20	1.00	0	1.00	4.00
Sa	(%)	1.28	0	5.02	30.00	0	30.00	120.00
C	(%)	0.34	0	1.16	6.00	0	6.00	32.00
E	(MJ/m^3)	1.72	2.70	1.05	2.10	0.60	2.70	161.40
OMC	(%)	19.90	20.50	3.84	18.00	12.00	30.00	1870.18
MDD	(KN/m^3)	15.95	15.81	1.29	7.60	12.00	19.60	1499.20

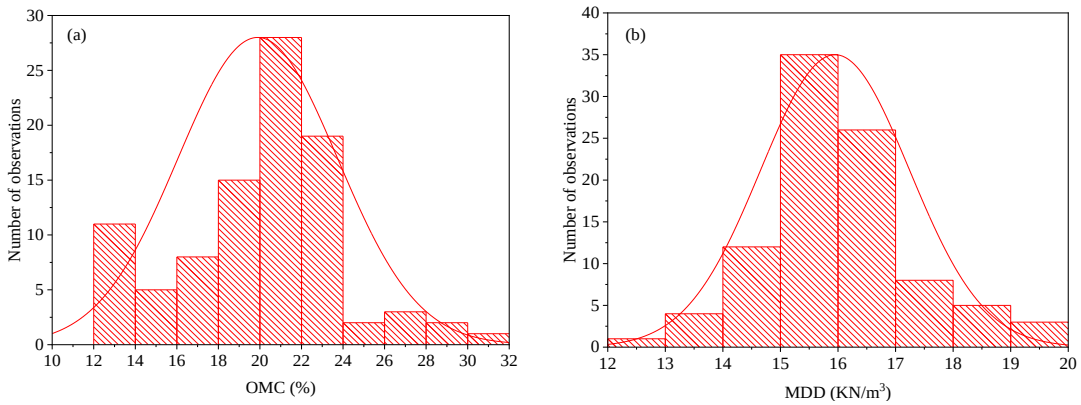

Figure 6-1 Histograms of (a) OMC and (b) MDD.

6.2.3 Multiple linear regression and error analysis

Multiple Linear Regression (MLR) is a statistical approach that aims to simulate the linear relationship between explanatory and response variables [297]. The general form used by MLR to estimate the response variable y as a function of n explanatory is shown in Equation (6-1) [298].

$$y = \beta_0 + \beta_1 x_1 + \beta_2 x_2 + \cdots + \beta_n x_n + \varepsilon \quad (6\text{-}1)$$

where, y is response (dependent) variables; x_1, x_2, $\cdots$, x_n are explanatory (independent) variables; β_0, β_1, β_2, $\cdots$, β_n are the slop coefficients for each explanatory (independent) variable; ε is the residuals of the model.

The correlation coefficient (R) and Root Mean Squared Error (RMSE) are two key parameters that are routinely used to quantitatively measure the performance of any model and quantify its performance. The expressions of R and RMSE are shown in Equations (6-2) and (6-3).

$$R = \frac{\sum(y_k - \overline{y_k})(y'_k - \overline{y'_k})}{\sqrt{\sum(y_k - \overline{y_k})^2 \sum(y'_k - \overline{y'_k})^2}} \quad (6\text{-}2)$$

$$RMSE = \sqrt{\frac{\sum_{k=1}^{n}(y'_k - y_k)^2}{n}} \quad (6\text{-}3)$$

where, y_k is the experimental value indexed with k; y'_k is the predicted value indexed with k; $\overline{y_k}$ is the mean of y_k; $\overline{y'_k}$ is the mean of y'_k; n is the number of samples.

The correlation coefficient R value belongs to interval $[-1, +1]$, the accepted guidelines for evaluating R are as follows [299]:

$|R|$ > 0.7 means strong correlation.

0.7 > $|R|$ > 0.3 means correlation exists.

$|R|$ < 0.3 means weak correlation.

6.3 Results and discussion

6.3.1 Parameter correlation analysis

As illustrated in Table 6-3, the correlation matrix describes the pairwise relationship between different parameters. When two parameters are correlated, only one should be kept and used for MLR. Moreover, based on this correlation analysis, it could easily find that some input parameters have high correlations (R > 0.7), as follows:

Sand and Silt; LL and PL; LL and PI; PL and OM.

This observed result is agreed well with the previous study [147]. Only one of Sand and Silt is chosen as an independent variable for the following modeling work. Because the PI equals LL–PL and has no correlation with any other parameter, it is selected as the representative factor for sediment plasticity. Thus, PL and LL are eliminated. In this way, OM also could be kept and used for modeling.

Table 6-3 Matrix of correlation for different parameters.

		Sand	Silt	Clay	LL	PL	PI	OM	MBV	P	L	FA	SF	Sa	C	E	OMC	MDD
		(%)	(%)	(%)	(%)	(%)	(%)	(%)	(g/100g)	(%)	(%)	(%)	(%)	(%)	(%)	(MJ/m^3)	(%)	(KN/m^3)
Sand	(%)	1.00																
Silt	(%)	**-0.96**	1.00															
Clay	(%)	-0.42	0.14	1.00														
LL	(%)	-0.22	0.21	0.06	1.00													
PL	(%)	-0.08	0.04	0.15	**0.84**	1.00												
PI	(%)	-0.27	0.29	0.00	**0.95**	0.64	1.00											
OM	(%)	0.33	-0.33	-0.11	0.46	**0.70**	0.27	1.00										
MBV	(g/100g)	-0.28	0.34	-0.09	0.34	0.03	0.48	-0.21	1.00									
P	(%)	0.09	-0.02	-0.24	-0.18	-0.22	-0.14	-0.29	0.15	1.00								
L	(%)	-0.33	0.31	0.14	0.25	0.07	0.32	-0.11	0.28	-0.17	1.00							
FA	(%)	-0.23	0.20	0.14	0.22	0.12	0.24	-0.03	0.07	-0.06	0.10	1.00						
SF	(%)	-0.18	0.21	-0.01	-0.09	-0.14	-0.05	-0.18	0.25	-0.05	0.21	-0.05	1.00					
Sa	(%)	0.09	-0.09	-0.04	-0.05	-0.17	0.03	-0.08	0.40	0.11	0.12	-0.06	0.26	1.00				
C	(%)	0.36	-0.32	-0.22	-0.23	-0.10	-0.27	0.12	-0.42	-0.07	-0.16	-0.07	-0.06	-0.08	1.00			
E	(MJ/m^3)	-0.10	0.08	0.09	0.25	0.21	0.24	0.25	-0.36	-0.26	0.09	0.23	-0.22	-0.27	0.28	1.00		
OMC	(%)	-0.16	0.04	0.42	0.51	0.61	0.38	0.50	-0.16	-0.36	0.31	0.07	-0.03	-0.18	0.10	0.43	1.00	
MDD	(KN/m^3)	-0.12	0.21	-0.21	-0.41	-0.55	-0.27	-0.54	-0.02	-0.02	-0.07	-0.08	0.17	0.25	0.03	-0.07	-0.65	1.00

6.3.2 Modeling with the whole database

Based on the above analyses and considering the whole database, the developed four different models (as shown in Table 6-4) to predict OMC and MDD were evaluated, respectively.

Table 6-4 Inputs and output parameters for each investigation model using the whole database.

Model No.	Input	Output
1	Sand (%), Clay (%), PI (%), OM (%), MBV (g/100g), P (%), L (%), FA (%), SF (%), Sa (%), C (%), E (MJ/m^3)	OMC (%)
2	Silt (%), Clay (%), PI (%), OM (%), MBV (g/100g), P (%), L (%), FA (%), SF (%), Sa (%), C (%), E (MJ/m^3)	OMC (%)
3	Sand (%), Clay (%), PI (%), OM (%), MBV (g/100g), P (%), L (%), FA (%), SF (%), Sa (%), C (%), E (MJ/m^3)	MDD (KN/m^3)
4	Silt (%), Clay (%), PI (%), OM (%), MBV (g/100g), P (%), L (%), FA (%), SF (%), Sa (%), C (%), E (MJ/m^3)	MDD (KN/m^3)

6.3.2.1 Prediction of the OMC using the whole database

Models 1 and 2 were developed to predict the OMC of the treated sediments by the MLR approach, with 94 observations and 12 input parameters. In reality, three input parameters describe the particle size composition of the material (% of clay, % of sand and % of OM). Two input parameters describe the material's physical properties (PI and MBV). One input parameter represents the energy of compaction (E). The six other input parameters are related to the type and dosage of binders used for S/S of the sediments (P, L, FA, SF, Sa and C). The equations of Models 1 and 2 for OMC prediction are single linear expressions, as shown in Equations (6-4) and (6-5). The OMC values predicted by Models 1 and 2 versus the experimental values in whole datasets are shown in Figure 6-2 and Figure 6-3, respectively. The comparative analysis indicates that Models 1 and 2 could successfully build the relationship between the input parameters and output OMC. Both Models 1 and 2 have a high correlation coefficient R, especially Model 1 has a higher R-value (0.850) than Model 2 (0.832). However, both Models 1 and 2 exhibit relatively high RMSE values, although Model 1 has a lower RMSE value (2.015) than Model 2 (2.120). The models' performance could be improved in the next step, to get a higher R-value and lower

RMSE value.

$$OMC = 8.532 + 0.039 \times Sand + 0.332 \times Clay + 0.076 \times PI + 0.617 \times OM - 0.211 \times MBV + 0.058 \times P + 0.487 \times L - 0.309 \times FA + 0.995 \times SF - 0.105 \times Sa + 0.473 \times C + 0.227 \times E \quad (6\text{-}4)$$

$$OMC = 8.983 + 0.010 \times Silt + 0.315 \times Clay + 0.062 \times PI + 0.660 \times OM - 0.190 \times MBV + 0.030 \times P + 0.486 \times L - 0.300 \times FA + 1.688 \times SF - 0.093 \times Sa + 0.662 \times C + 0.397 \times E \quad (6\text{-}5)$$

Where, OMC is the Optimum Moisture Content (%), Sand is the percentage of sand (%), Silt is the percentage of silt (%), Clay is the percentage of clay (%), PI is the Plasticity Index (%), OM is the Organic Matter content (%), MBV is the Methylene Blue Value (g/100g), P is the percentage of Portland cement (%), L is the percentage of Lime (%), FA is the percentage of Fly Ash (%), SF is the percentage of Silica Fume (%), Sa is the percentage of Sand (%), C is the percentage of Calcium sulfoaluminate cement (%) and E is the compaction energy (MJ/m^3).

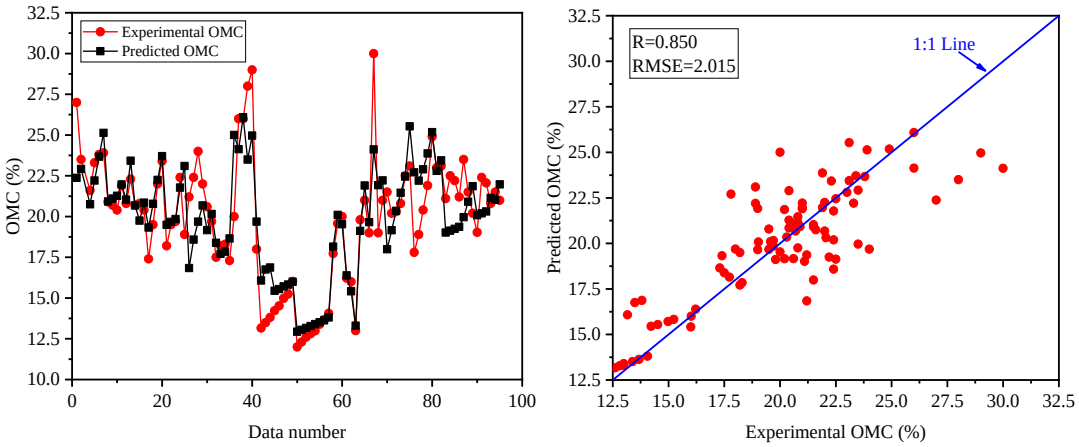

(a) (b)

Figure 6-2 Comparison of experimental and predicted OMC by Model 1 using the whole database.

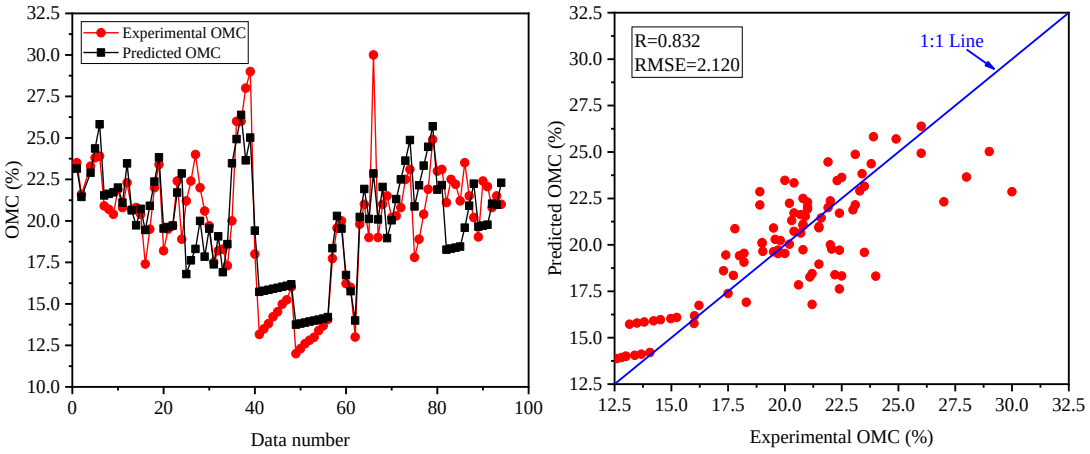

(a) (b)

Figure 6-3 Comparison of experimental and predicted OMC by Model 2 using the whole database.

6.3.2.2 Prediction of the MDD using the whole database

The same as Models 1 and 2, using the MLR technique, predict MDD of the treated sediments with 94 data and 12 input parameters. The expressions of Models 3 and 4 are given by Equations (6-6) and (6-7). The comparison of experimental and predicted MDD for the treated sediments are shown in Figure 6-4 and Figure 6-5, respectively, for the proposed Models 3 and 4. As demonstrated, the R-values are less than 0.8 for both models: R=0.772 for Model 3 and R=0.788 for Model 4. The RMSE values of Model 3 and Model 4 were 0.816 and 0.791, respectively. These results indicate that these proposed Model 3 and Model 4 cannot provide satisfying prediction accuracy, they have low correlation and comparatively high error values.

$$\begin{aligned}\mathrm{MDD} = {} & 20.100 - 0.004 \times Sand - 0.091 \times Clay - 0.002 \times PI - 0.342 \times OM \\ & - 0.260 \times MBV - 0.113 \times P - 0.100 \times L - 0.061 \times FA \\ & + 0.411 \times SF - 0.091 \times Sa - 0.157 \times C + 0.200 \times E\end{aligned} \tag{6-6}$$

$$\begin{aligned}\mathrm{MDD} = {} & 19.172 + 0.015 \times Silt - 0.091 \times Clay - 0.003 \times PI - 0.310 \times OM \\ & - 0.306 \times MBV - 0.109 \times P - 0.114 \times L - 0.080 \times FA \\ & + 0.091 \times SF + 0.102 \times Sa - 0.124 \times C + 0.125 \times E\end{aligned} \tag{6-7}$$

Where, MDD is the Maximum Dry Density (KN/m^3), Sand is the percentage of sand (%), Silt is the percentage of silt (%), Clay is the percentage of clay (%), PI is the Plasticity Index (%), OM is the Organic Matter content (%), MBV is the Methylene

Blue Value (g/100g), P is the percentage of Portland cement (%), L is the percentage of Lime (%), FA is the percentage of Fly Ash (%), SF is the percentage of Silica Fume (%), Sa is the percentage of Sand (%), C is the percentage of Calcium sulfoaluminate cement (%) and E is the compaction energy (MJ/m^3).

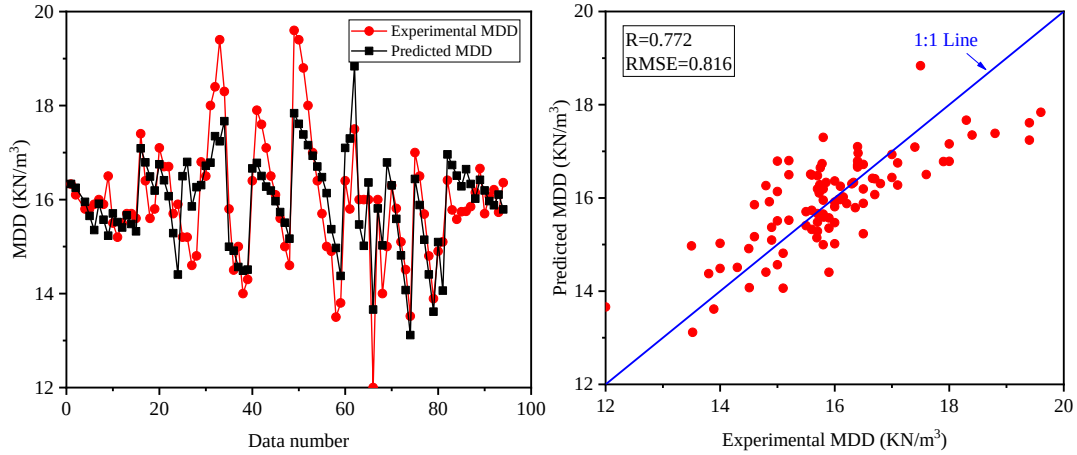

(a) (b)

Figure 6-4 Comparison of experimental and predicted MDD by Model 3 using the whole database.

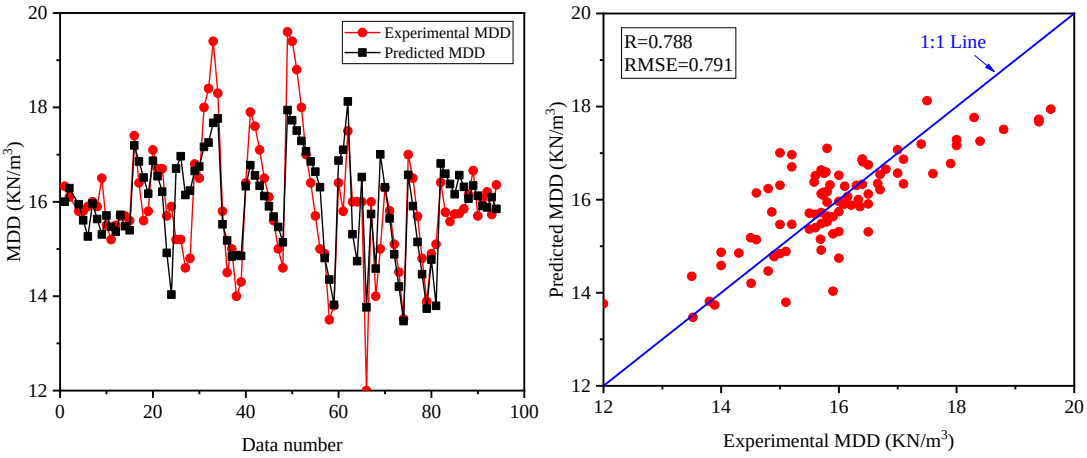

(a) (b)

Figure 6-5 Comparison of experimental and predicted MDD by Model 4 using the whole database.

In this first investigation, the model prediction is developed based on the whole database. It is known that a wide range of different materials is included in the database. It is also known that some input parameters' effects on the compaction parameters could depend on the type of materials, such as sandy materials and silty sediments. Thus, it was decided to follow such a strategy, to investigate the performance of developing predictive models by using only a subset of the database, which belongs to the same family of material in terms of grains sizes distribution.

The sandy or silty sub-databases are generated by choosing the corresponding data from the whole database. This selective sorting is performed according to the following rules. Firstly, for a certain one observation from 94 observations (i.e., rows) in the whole database, compare the three values of grains sizes distribution: sand (%), silt (%) and clay (%). If the maximum value is sand (%), this observation will be included in the sandy sub database. If the maximum value is silt (%), this observation will be included in the silty sub database. Otherwise, this observation will be kept in the whole database. Repeat this procedure 94 times, until all 94 observations rows have been checked. In the end, the sandy sub database has 28 observations, the silty sub database has 66 observations.

Table 6-5 and Table 6-6 show the correlation between OMC/MDD and other parameters for the total database, sandy sub-database and silty sub-database. It's evident that many absolute values of correlation coefficients for the sub-databases are higher than the total database. Therefore, there is reason to believe that the developing models would get better performance, by using only a sub-database (sandy or silty sediments) next stage.

Table 6-5 Correlation of parameters for total database, sandy and silty sub-database (I).

Database	Parameters	Sand (%)	Silt (%)	Clay (%)	LL (%)	PL (%)	PI (%)	O.M. (%)	MBV (g/100g)
Total	OMC (%)	-0.16	0.04	0.42	0.51	0.61	0.38	0.50	-0.16
	MDD (KN/m^3)	-0.12	0.21	-0.21	-0.41	-0.55	-0.27	-0.54	-0.02
Sandy	OMC (%)	**-0.53**	**0.42**	0.27	0.06	0.46	-0.19	**0.54**	**-0.36**
	MDD (KN/m^3)	-0.03	**0.26**	**-0.35**	-0.36	-0.45	-0.26	-0.49	**-0.38**
Silty	OMC (%)	**-0.62**	**0.28**	**0.54**	**0.69**	**0.69**	**0.59**	0.48	-0.03
	MDD (KN/m^3)	**0.13**	0.05	**-0.29**	**-0.44**	**-0.60**	**-0.30**	-0.52	**0.10**

Table 6-6 Correlation of parameters for total database, sandy and silty sub-database (II).

Database	Parameters	P	L	FA	SF	Sa	C	E
		(%)	(%)	(%)	(%)	(%)	(%)	(MJ/m^3)
Total	OMC (%)	-0.36	0.31	0.07	-0.03	-0.18	0.10	0.43
	MDD	-0.02	-0.07	-0.08	0.17	0.25	0.03	-0.07
Sandy	OMC (%)	0.01	-0.04	/	/	**-0.42**	0.10	0.01
	MDD	-0.02	**-0.37**	/	/	0.14	**0.29**	**0.59**
Silty	OMC (%)	**-0.46**	**0.43**	**0.11**	0.03	-0.05	/	**0.51**
	MDD	**-0.03**	-0.06	**-0.13**	0.17	**0.47**	/	**-0.27**

6.3.3 Modeling with the sandy sub database

In this part, as shown in Table 6-7, Models 5-8 were used to predict OMC and MDD of the treated sandy sediments. As can be noticed, due to the lack of data sets that include sandy sediments treatments with the FA and/or SF, these two input parameters are discarded in the following study.

Table 6-7 Inputs and output parameters for each investigation model using the sandy sub database.

Model No.	Input	Output
5	Sand (%), Clay (%), PI (%), OM (%), MBV (g/100g), P (%), L (%), Sa (%), C (%), E (MJ/m^3)	OMC (%)
6	Silt (%), Clay (%), PI (%), OM (%), MBV (g/100g), P (%), L (%), Sa (%), C (%), E (MJ/m^3)	OMC (%)
7	Sand (%), Clay (%), PI (%), OM (%), MBV (g/100g), P (%), L (%), Sa (%), C (%), E (MJ/m^3)	MDD (KN/m^3)
8	Silt (%), Clay (%), PI (%), OM (%), MBV (g/100g), P (%), L (%), Sa (%), C (%), E (MJ/m^3)	MDD (KN/m^3)

6.3.3.1 Prediction of the OMC using the sandy sub database

With 28 observations and ten input parameters, Models 5 and 6 were developed to predict the OMC of the treated sandy sediments using the MLR technique. Equations

(6-8) and (6-9) present the expression of Models 5 and 6 for OMC prediction. Figure 6-6 and Figure 6-7 show the comparison of experimental and predicted OMC by Models 5 and 6, respectively. In comparison to Models 1 and 2, both Models 5 and 6 have significant improvements in R and RMSE values. The correlation coefficient R is 0.938 and 0.937 for Models 5 and 6, respectively (it was respectively 0.850 and 0.832 for Models 1 and 2). The RMSE values of Models 5 and 6 are 1.036 and 1.040 (it was respectively 2.015 and 2.120 for Models 1 and 2). Therefore, Model 5 is better than Model 6 to predict the OMC of the treated sandy sediments.

$$OMC = 18.048 - 0.084 \times Sand + 0.245 \times Clay - 0.083 \times PI + 1.235 \times OM - 0.413 \times MBV + 0.002 \times P + 0.062 \times L - 0.091 \times Sa - 0.100 \times C - 0.697 \times E \quad (6\text{-}8)$$

$$OMC = 9.735 + 0.079 \times Silt + 0.333 \times Clay - 0.082 \times PI + 1.238 \times OM - 0.415 \times MBV + 0.001 \times P + 0.054 \times L - 0.091 \times Sa - 0.097 \times C - 0.685 \times E \quad (6\text{-}9)$$

Where, OMC is the Optimum Moisture Content (%), Sand is the percentage of sand (%), Silt is the percentage of silt (%), Clay is the percentage of clay (%), PI is the Plasticity Index (%), OM is the Organic Matter content (%), MBV is the Methylene Blue Value (g/100g), P is the percentage of Portland cement (%), L is the percentage of Lime (%), Sa is the percentage of Sand (%), C is the percentage of Calcium sulfoaluminate cement (%) and E is the compaction energy (MJ/m^3).

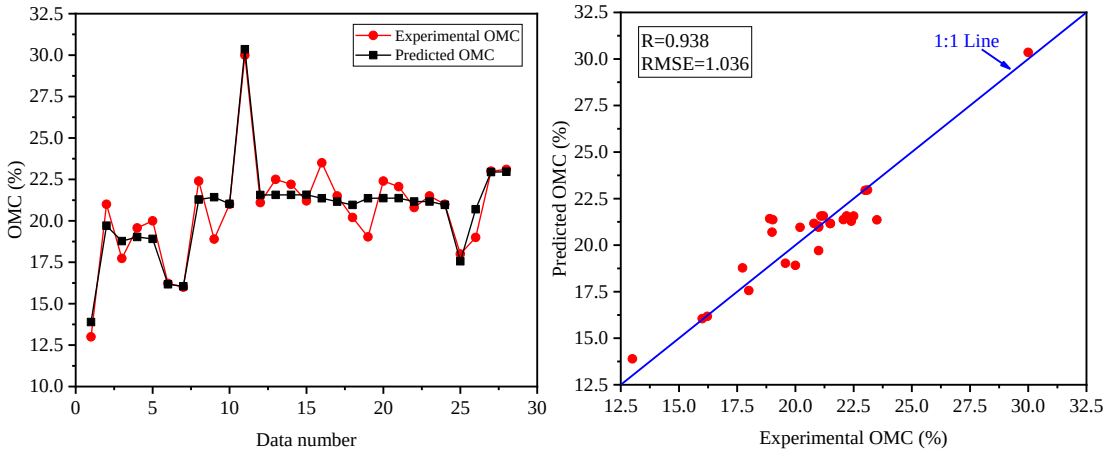

(a) (b)

Figure 6-6 Comparison of experimental and predicted OMC by Model 5 using the sandy sub database.

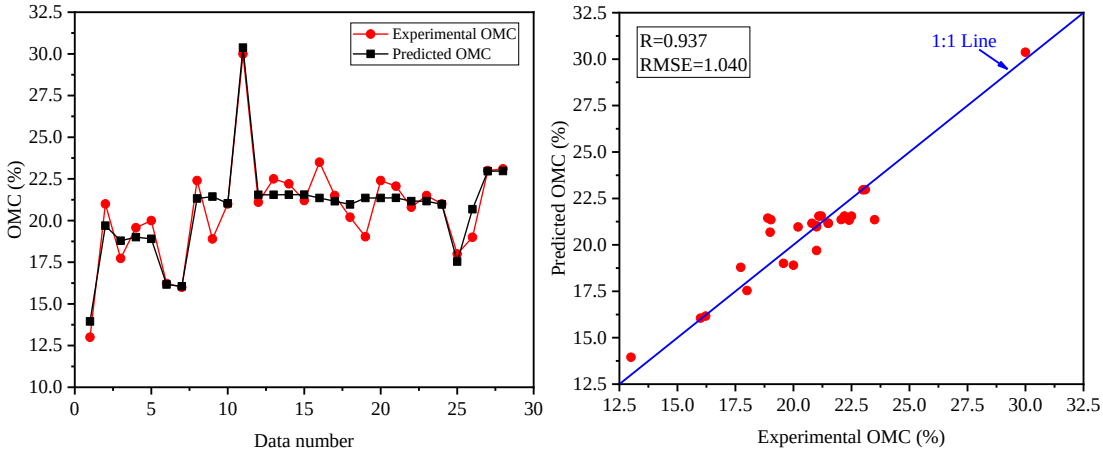

(a) (b)

Figure 6-7 Comparison of experimental and predicted OMC by Model 6 using the sandy sub database.

6.3.3.2 Prediction of the MDD using the sandy sub database

The regression analyses were carried out with 28 observations and ten independent variables, in order to obtain Models 7 and 8 to predict the MDD of the treated sandy sediments. The expressions of Models 7 and 8 are given by Equations (6-10) and (6-11). The comparison between the experimental and predicted MDD of Model 7 and 8 is presented in Figure 6-8 and Figure 6-9, respectively. It was easily found that the error is significantly reduced by Models 7 and 8, compared to Models 3 and 4. Meanwhile, it can be observed that the higher R value and lower RMSE value were obtained for Model 8 (R=0.916, RMSE=0.436), compared to Model 7 (R=0.915 RMSE=0.438). Consequently, Model 8 could be better to predict MDD of the treated sandy sediments.

$$\begin{aligned}\mathrm{MDD} = {} & 17.114 - 0.011 \times Sand - 0.006 \times Clay - 0.043 \times PI - 0.367 \times OM \\ & - 0.221 \times MBV - 0.005 \times P - 0.142 \times L + 0.061 \times Sa \\ & + 0.022 \times C + 0.737 \times E\end{aligned} \tag{6-10}$$

$$\begin{aligned}\mathrm{MDD} = {} & 16.038 + 0.013 \times Silt + 0.001 \times Clay + 0.043 \times PI - 0.369 \times OM \\ & - 0.223 \times MBV - 0.005 \times P - 0.135 \times L + 0.061 \times Sa \\ & + 0.021 \times C + 0.721 \times E\end{aligned} \tag{6-11}$$

Where, MDD is the Maximum Dry Density (KN/m^3), Sand is the percentage of sand (%), Silt is the percentage of silt (%), Clay is the percentage of clay (%), PI is the

Plasticity Index (%), OM is the Organic Matter content (%), MBV is the Methylene Blue Value (g/100g), P is the percentage of Portland cement (%), L is the percentage of Lime (%), Sa is the percentage of Sand (%), C is the percentage of Calcium sulfoaluminate cement (%) and E is the compaction energy (MJ/m^3).

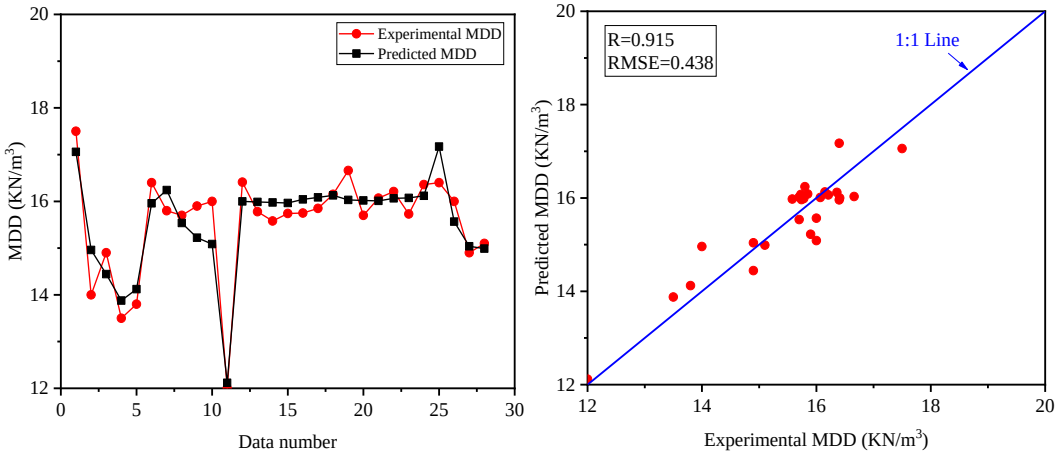

(a) (b)

Figure 6-8 Comparison of experimental and predicted MDD by Model 7 using the sandy sub database.

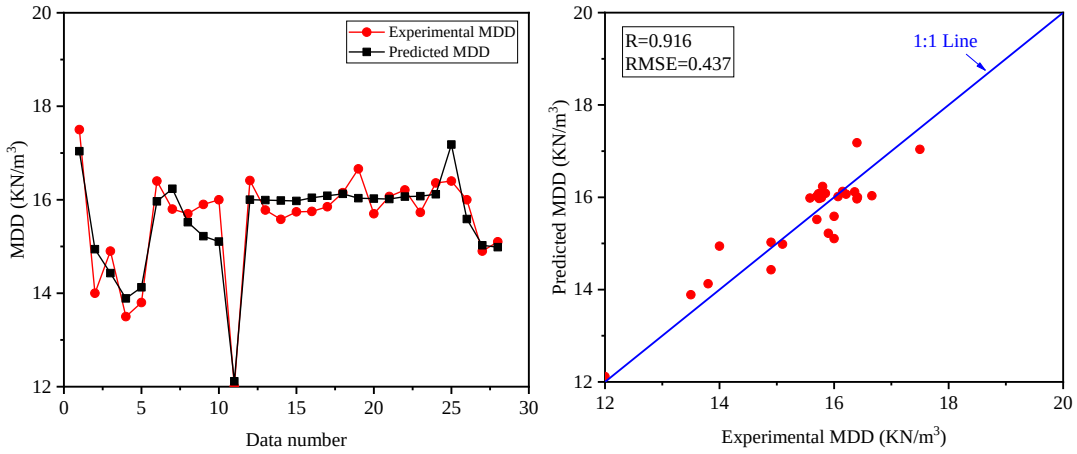

(a) (b)

Figure 6-9 Comparison of experimental and predicted MDD by Model 8 using the sandy sub database.

6.3.4 Modeling with the silty sub database

As shown in Table 6-6, Models 9-12 were used to predict OMC and MDD of the treated silty sediments in this part. As the above analysis, the generated silty sub database has 66 observations. Due to the lack of data that includes silty sediments treatments with the C, this input parameter is discarded in the following study.

Table 6-8 Inputs and output parameters for each investigation model using the silty sub database.

Model No.	Input	Output
9	Sand (%), Clay (%), PI (%), OM (%), MBV (g/100g), P (%), L (%), FA (%), SF (%), Sa (%), E (MJ/m^3)	OMC (%)
10	Silt (%), Clay (%), PI (%), OM (%), MBV (g/100g), P (%), L (%), FA (%), SF (%), Sa (%), E (MJ/m^3)	OMC (%)
11	Sand (%), Clay (%), PI (%), OM (%), MBV (g/100g), P (%), L (%), FA (%), SF (%), Sa (%), E (MJ/m^3)	MDD (KN/m^3)
12	Silt (%), Clay (%), PI (%), OM (%), MBV (g/100g), P (%), L (%), FA (%), SF (%), Sa (%), E (MJ/m^3)	MDD (KN/m^3)

6.3.4.1 Prediction of the OMC using the silty sub database

With 66 observations and 11 input parameters, Models 9 and 10 were developed to predict the OMC of the treated silty sediments using the MLR technique. The expressions of Models 9 and 10 are shown in Equations (6-12) and (6-13). The comparison of experimental and predicted OMC of the treated silty sediments using Models 9 and 10 are plotted in Figure 6-10 and Figure 6-11, respectively. As demonstrated, R values in Model 9 and Model 10 are 0.947 and 0.946, respectively. While the RMSE values of Model 9 and Model 10 are 1.311 and 1.319, respectively. Therefore, it is noticeable that both Model 9 and Model 10 can provide higher prediction accuracy than Model 1 and Model 2 (for Models 1 and 2, R values were 0.850 and 0.832, RMSE values were respectively 2.015 and 2.120). Model 9 has the best prediction performances of OMC for the treated silty sediments.

$$OMC = 15.650 - 0.339 \times Sand + 0.301 \times Clay - 0.107 \times PI + 1.051 \times OM + 0.897 \times MBV + 0.107 \times P + 0.444 \times L - 0.105 \times FA - 0.572 \times SF - 0.331 \times Sa - 0.323 \times E \quad (6\text{-}12)$$

$$OMC = -18.080 + 0.337 \times Silt + 0.636 \times Clay - 0.097 \times PI + 1.052 \times OM + 0.860 \times MBV + 0.104 \times P + 0.436 \times L - 0.131 \times FA - 0.585 \times SF - 0.332 \times Sa - 0.369 \times E \quad (6\text{-}13)$$

Where, OMC is the Optimum Moisture Content (%), Sand is the percentage of sand

(%), Silt is the percentage of silt (%), Clay is the percentage of clay (%), PI is the Plasticity Index (%), OM is the Organic Matter content (%), MBV is Methylene Blue Value (g/100g), P is the percentage of Portland cement (%), L is the percentage of Lime (%), FA is the percentage of Fly Ash (%), SF is the percentage of Silica Fume (%), Sa is the percentage of Sand (%) and E is the compaction energy (MJ/m^3).

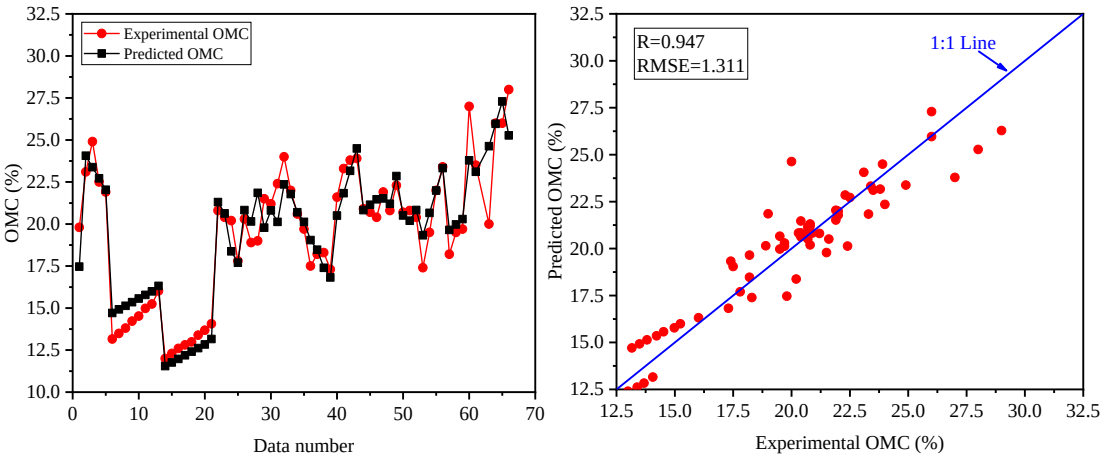

(a) (b)

Figure 6-10 Comparison of experimental and predicted OMC by Model 9 using the silty sub database.

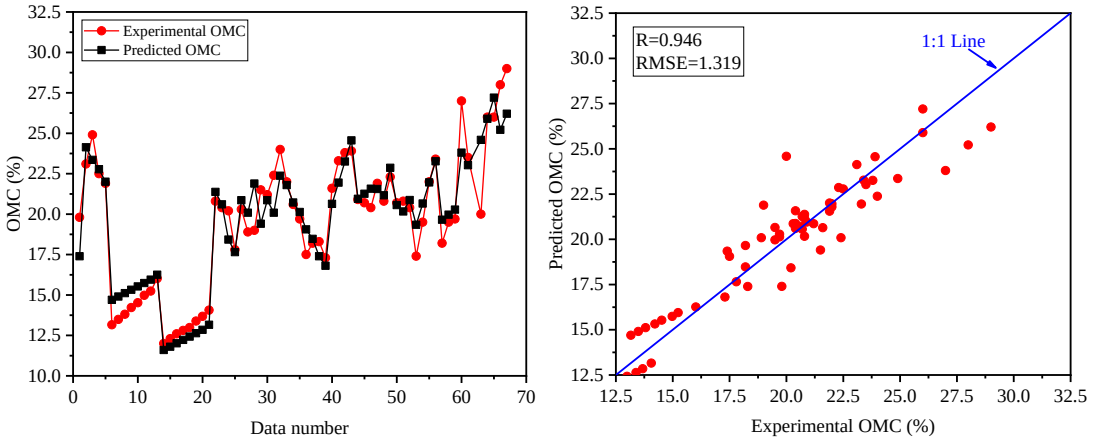

(a) (b)

Figure 6-11 Comparison of experimental and predicted OMC by Model 10 using the silty sub database.

6.3.4.2 Prediction of the MDD using the silty sub database

Models 11 and 12 were used in regression analyses with 66 observations and 11 input parameters to predict the MDD of the treated silty sediments. The results of Models 11 and 12 are given by Equations (6-14) and (6-15). Figure 6-12 and Figure 6-13 represent the comparison between the experimental and predicted MDD values of the

treated silty sediments. The results indicate that both Model 11 (R=0.917, RMSE=0.530) and Model 12 (R=0.914, RMSE=0.538) have higher correlation coefficient R and lower RMSE values, as compared to Model 3 (R=0.772, RMSE=0.816) and Model 4 (R=0.788, RMSE=0.791). Therefore, Model 11 has the best MDD prediction performance of MDD for the treated silty sediments.

$$\begin{aligned}\mathrm{MDD} = {} & 17.791 + 0.121 \times Sand - 0.098 \times Clay + 0.073 \times PI - 0.501 \times OM \\ & - 0.526 \times MBV - 0.190 \times P - 0.159 \times L - 0.152 \times FA \\ & + 0.018 \times SF + 0.306 \times Sa + 0.357 \times E\end{aligned} \tag{6-14}$$

$$\begin{aligned}\mathrm{MDD} = {} & 29.663 - 0.118 \times Silt - 0.216 \times Clay + 0.068 \times PI - 0.498 \times OM \\ & - 0.509 \times MBV - 0.188 \times P - 0.156 \times L - 0.142 \times FA \\ & - 0.011 \times SF + 0.305 \times Sa + 0.373 \times E\end{aligned} \tag{6-15}$$

Where, MDD is the Maximum Dry Density (KN/m^3), Sand is the percentage of sand (%), Silt is the percentage of silt (%), Clay is the percentage of clay (%), PI is the Plasticity Index (%), OM is the Organic Matter content (%), MBV is the Methylene Blue Value (g/100g), P is the percentage of Portland cement (%), L is the percentage of Lime (%), FA is the percentage of Fly Ash (%), SF is the percentage of Silica Fume (%), Sa is the percentage of Sand (%) and E is the compaction energy (MJ/m^3).

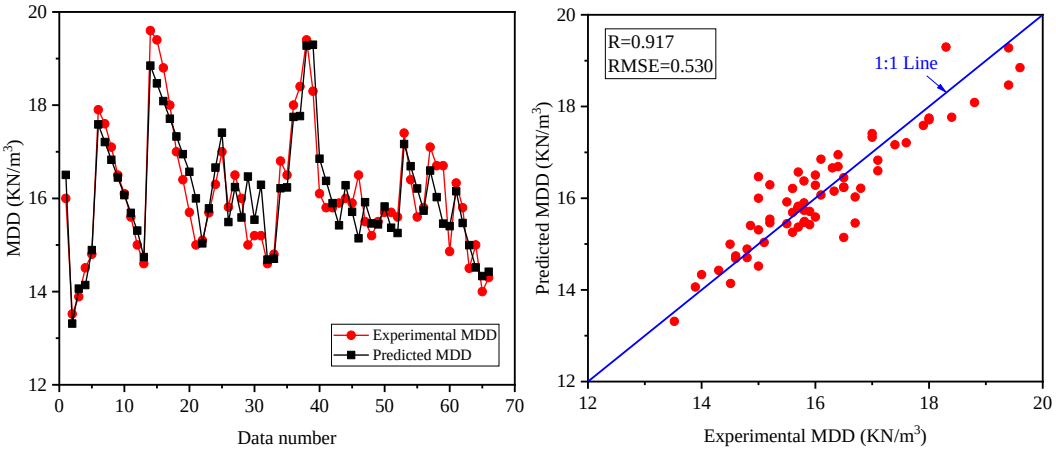

(a) (b)

Figure 6-12 Comparison of experimental and predicted MDD by Model 11 using the silty sub database.

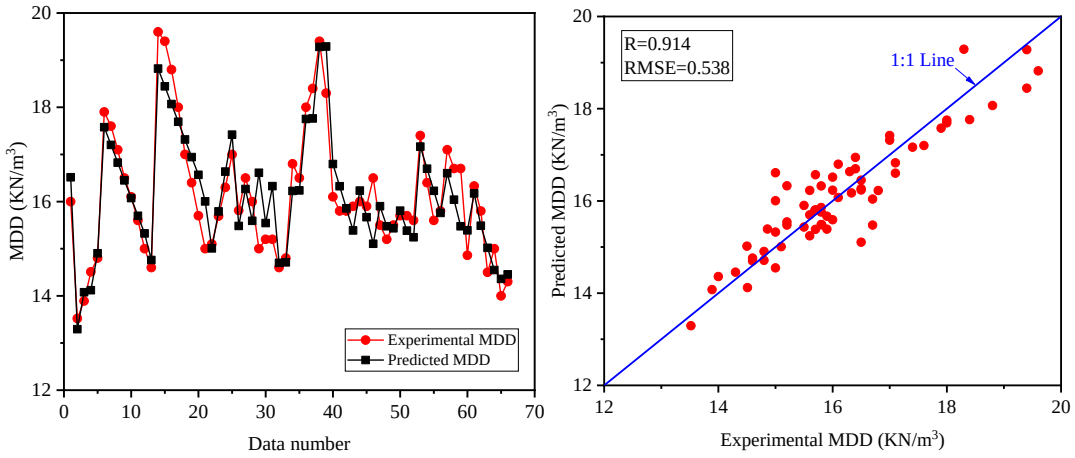

(a) (b)

Figure 6-13 Comparison of experimental and predicted MDD by Model 12 using the silty sub database.

6.3.5 ANOVA test

Based on the above analyses, Models 5, 8, 9 and 11 were chosen as the best models to predict the compaction parameters of the treated dredged sediments. To assess the adequacy of the chosen four models, the analysis of variance (ANOVA test) on the chosen four models is a necessary step. This analysis was conducted with the null hypothesis that the response variable is unrelated to the explanatory variables, whereas the alternate hypothesis is that the response variable is related to the explanatory variables. The results of the ANOVA test of the Models 5, 8, 9 and 11 are shown in Table 6-9. It could be easily found that all four P-value is significantly less than 0.05, indicating the null hypothesis is rejected. This indicates that the explanatory and response variables have a good relationship. To put it another way, all these chosen models (Models 5, 8, 9 and 11) meet the statistical requirements.

Table 6-9 ANOVA test results of the chosen models.

Models		df	SS	MS	F	P-value
Model 5	Regression	10.00	218.84	21.88	12.39	5.9E-06
	Residual	17.00	30.03	1.77		
	Total	27.00	248.87			
Model 8	Regression	10.00	27.79	2.78	8.83	5.93E-05
	Residual	17.00	5.35	0.32		
	Total	27.00	33.14			
Model 9	Regression	11.00	929.58	84.51	26.92	3.04E-18
	Residual	55.00	172.65	3.14		
	Total	66.00	1102.23			
Model 11	Regression	11.00	89.52	8.14	12.61	1.91E-11
	Residual	55.00	35.50	0.65		
	Total	66.00	125.03			

(df: degree of freedom, SS: sum of squares, MS: mean square, F: F-statistic, P-value: significance of F.)

6.3.6 Residual analysis

To further ensure that the chosen four models meet the statistical requirements, residual analysis was conducted. The residual analysis results of the Models 5, 8, 9 and 11 are displayed in Figure 6-14, Figure 6-15, Figure 6-16 and Figure 6-17, respectively. The most common graphic made during a residual analysis is a "residuals versus predict values figure." It is a scatter figure that with its residuals on the y-axis and forecasts values on the x-axis. Non-linearity, uneven error variances and outliers are all detected using this figure [300]. As shown in Figure 6-14(a), Figure 6-15(a), Figure 6-16(a) and Figure 6-17(a), all the residual analysis results of the four models indicated that the residuals exit around the 0-line at random. As a result, the assumption of a linear relationship appears to be fair.

Besides, Figure 6-14(b), Figure 6-15(b), Figure 6-16(b) and Figure 6-17(b) indicated that the residuals values were uniformly or symmetrically distributed around the neutral line representing the zero residuals. This further showed that the chosen four models meet the statistical requirements. The compaction parameters of the treated dredged sediments could be predicted using these models.

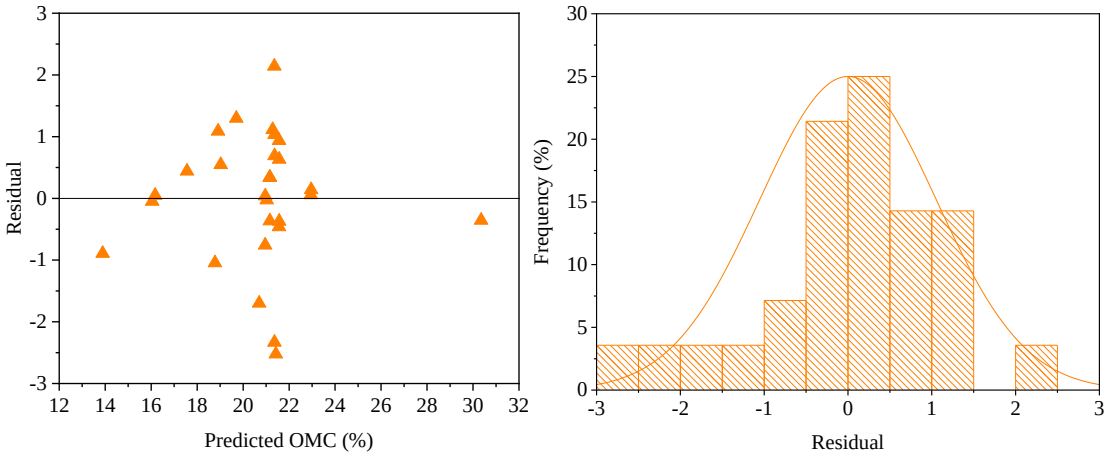

(a) (b)

Figure 6-14 Residual analysis of Model 5.

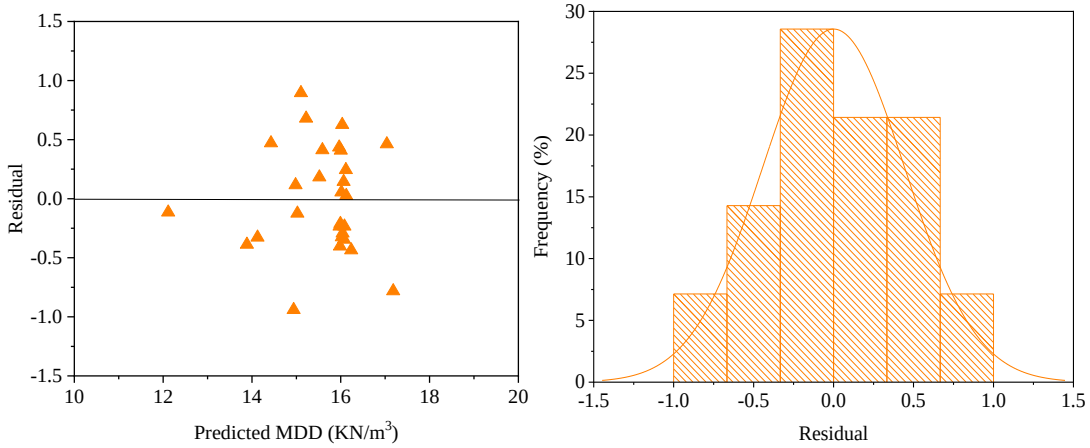

(a) (b)

Figure 6-15 Residual analysis of Model 8.

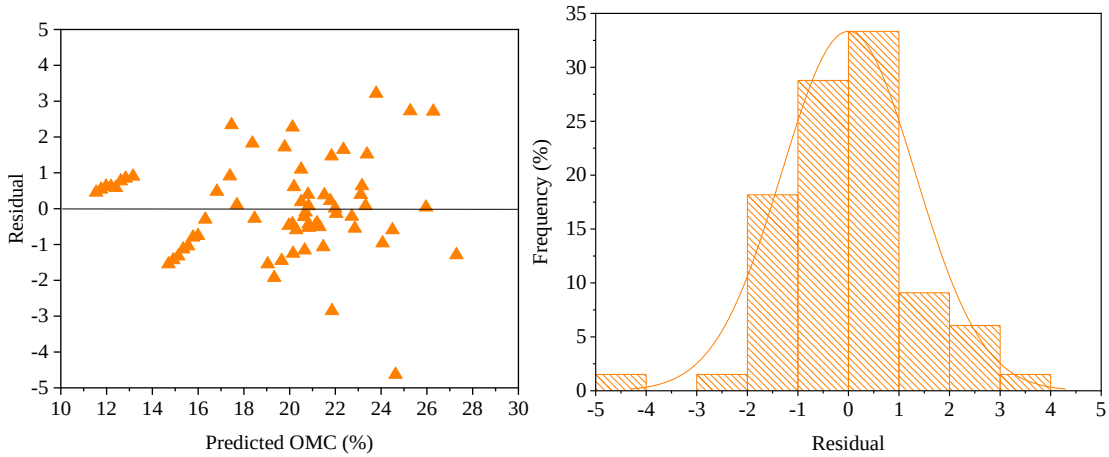

(a) (b)

Figure 6-16 Residual analysis of Model 9.

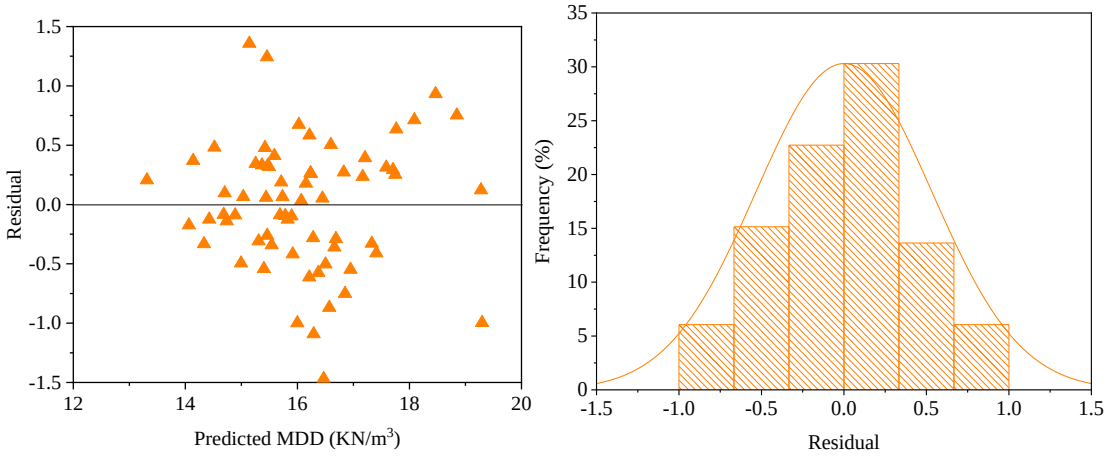

(a) (b)

Figure 6-17 Residual analysis of Model 11.

6.3.7 Variable importance assessment

Figure 6-18 shows each variable's standardized regression coefficient for Models 5, 8, 9 and 11. These values represent the relative importance of each explanatory variable to the response variable. Regarding the relative importance of the explanatory variable, the basic physical parameters of raw sediments (Sand, Clay, PI, OM and MBV) are more important than treatment binder types and quantities (except Sa). Especially, the organic matter (OM) content of raw sediments is one of the most important parameters for predicting the compaction parameter of the treated dredged sediments.

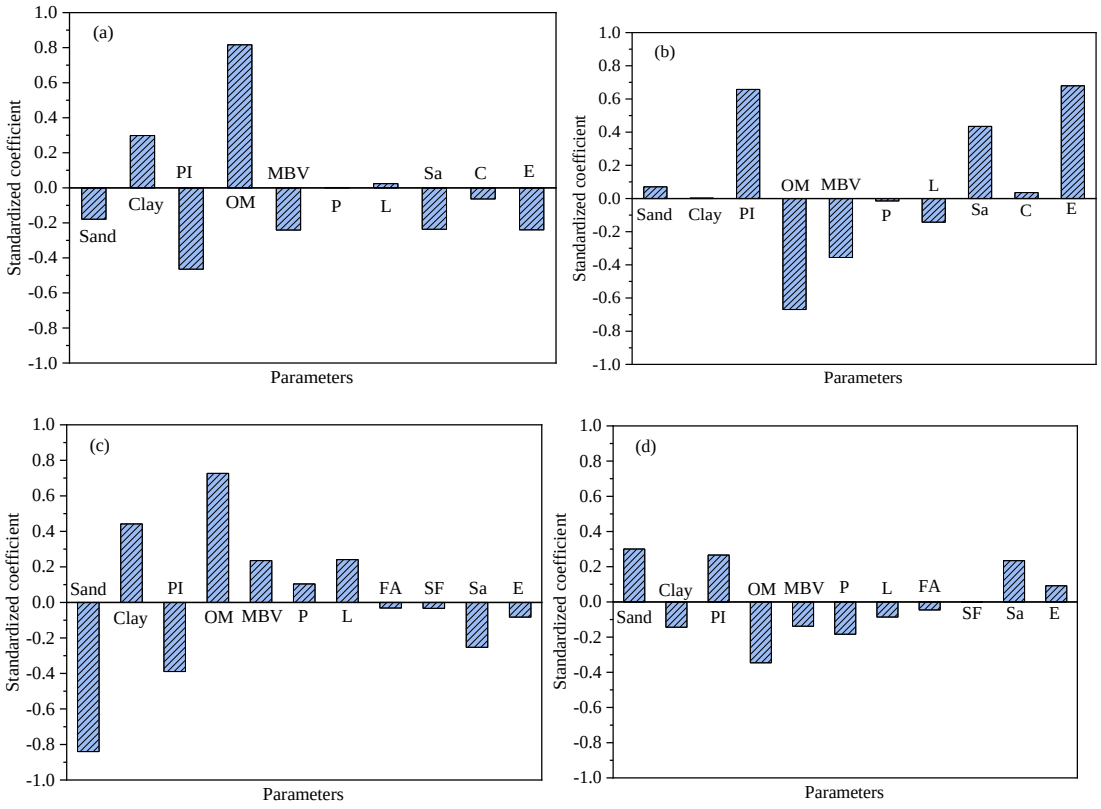

Figure 6-18 Standardized coefficient of (a) model 5, (b) model 8, (c) model 9 and (d) model 11 (with 95% interval of confidence).

6.3.8 Model validation

New experimental data from our group and other authors [287-290] are used to further validate the proposed four models. These new data were not included in the database of Table 6-1. Figure 6-19 compares the experimental and predicted values. Each percentage error (PE) is calculated with Equation (6-16), the results are also shown in Figure 6-19. It should note that $Value_{pre}$ is the predicted value with the model, $Value_{exp}$ is the experimental value. These results indicated that the proposed four models could be used to predict the compaction parameters of the treated dredged sediments with acceptable accuracy.

$$\mathrm{PE} = (Value_{pre} - Value_{exp})/Value_{exp} \times 100\% \quad (6\text{-}17)$$

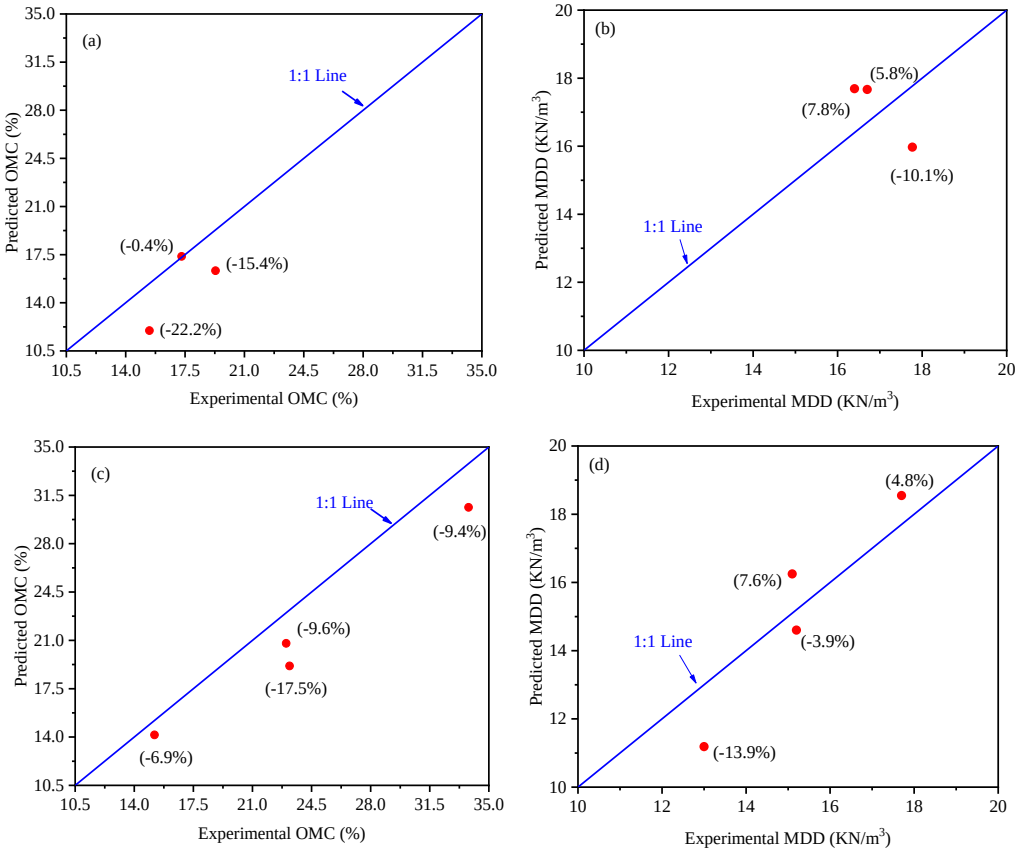

Figure 6-19 Validation of (a) model 5, (b) model 8, (c) model 9 and (d) model 11.

In addition, the proposed models in this study are compared to several previous models for soil's compaction parameters from the literature. Table 6-10 lists these models from the literature for predicting the OMC and MDD. These previous models could be used for both sandy and silty materials. The mean absolute percentage error (MAPE) values are calculated as in Equation (6-18), used to compare the prediction accuracy. The data are chosen from the database and validation dataset.

$$\text{MAPE} = \frac{1}{n}\sum_{i=1}^{n}\left|\frac{Value_{pre} - Value_{mea}}{Value_{mea}}\right| \times 100\% \qquad (6\text{-}18)$$

Table 6-10 Prediction models for OMC and MDD in the literature.

No.	Models		Reference
	OMC	MDD	
A	OMC=(12.39−12.21×logLL) ×(3+logE)+0.67×LL+9.21	MDD=(2.27×logLL-0.94) ×(3+logE)-0.16×LL+17.02	[157]
B	OMC=0.92×PL	MDD=0.23×(93.3−PL)	[158]
C	OMC=0.35×LL+0.163×PL+6.26	MDD=21.07-0.119×LL+0.02×PL	[159]
D	OMC=0.76×PL	MDD=20.82−0.17×PL	[160]
E	OMC=0.133×LL+0.02×PI −5.99×(3+logE)+28.60	MDD=−0.055×LL+0.014×PI+2.21 ×(3+logE)+12.84	[161]

Note: these models have been modified to keep the same symbols and units. Where OMC is optimum moisture content (%), MDD is maximum dry density (KN/m^3), LL is liquid limit (%), PL is plastic limit (%), PI is plasticity index (%) and E is compaction energy (MJ/m^3).

Figure 6-20 compares the prediction accuracy between the present and previous models for sandy materials. It can be found from Figure 6-20 that the present model shows the highest prediction accuracy for the prediction of OMC and MDD of sandy materials, with the lowest MAPE values. Models D and E exhibit comparable and low MAPE values, they could be used to predict the OMC and MDD of sandy materials. The rest of Models A, B and C have high MAPE values for predicting OMC of sandy materials, but have low MAPE values for predicting MDD of sandy materials.

Figure 6-21 compares the prediction accuracy between the present and previous models for silty materials. The present model and Model E could be considered the best two models. The present model has the lowest MAPE value for OMC prediction and the second-lowest MAPE value for the prediction of MDD. Model E has the second-lowest MAPE value for OMC prediction and the lowest MAPE value for the prediction of MDD. However, Models A, B, C and D have high MAPE values for predicting OMC of silty materials, but low MAPE values for predicting MDD of silty materials.

Therefore, the proposed models in this study seem to have higher prediction accuracy than previous models from the literature.

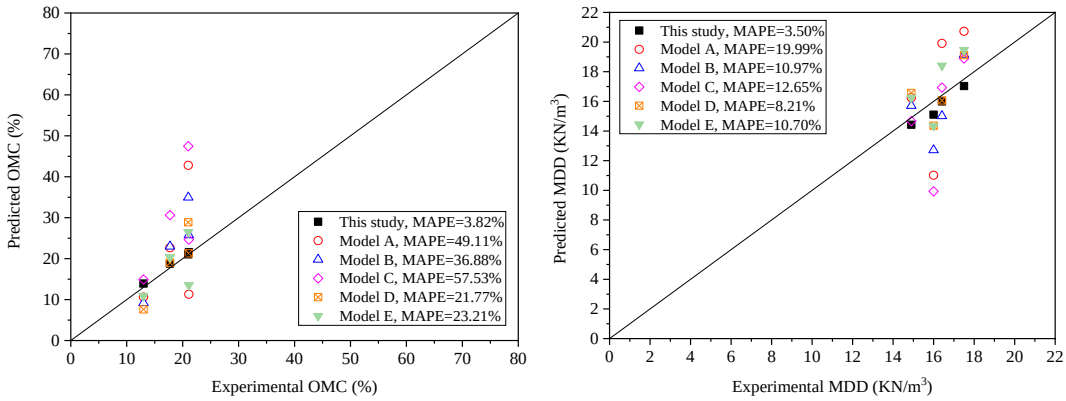

(a) (b)

Figure 6-20 Comparison of the prediction accuracy between the present and previous models, for (a) OMC and (b) MDD of sandy materials.

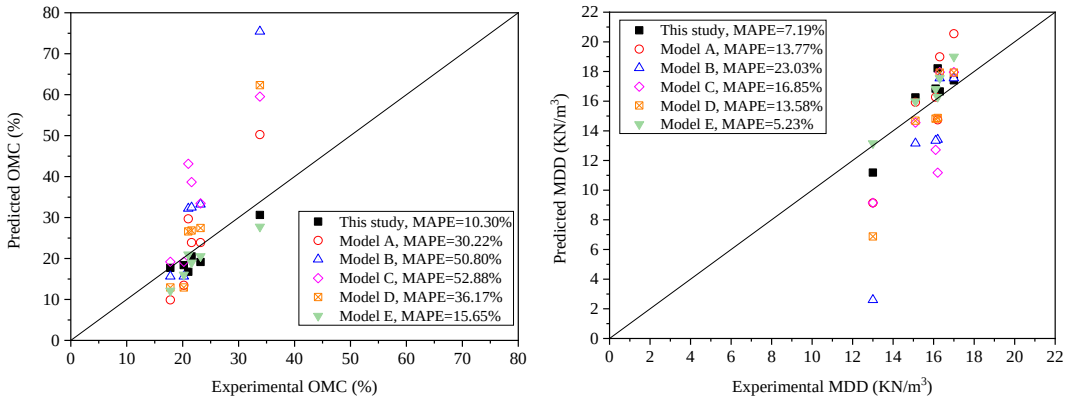

(a) (b)

Figure 6-21 Comparison of the prediction accuracy between the present and previous models, for (a) OMC and (b) MDD of silty materials.

6.4 Conclusion

This study developed simple statistical models to predict the treated dredged sediments' compaction parameters (MDD and OMC). A database of 94 measurements was established from different research papers to develop the models. Influencing factors considered in this database include the particle size composition (% of sand, % of silt and % of clay); Atterberg limits (LL, PL and PI); organic matter content (OM); Methylene Blue Value (MBV); different binder types and quantities (P, L, FA, SF, Sa and C) used for the treatment of sediments; compaction energy (E). The main conclusion is as follows:

(1) The analysis of the correlation matrix for different parameters indicated that several parameters have high correlations: OM and LL of raw sediments seem to be

correlated with PL of raw sediments, LL of raw sediments seems to be correlated with PI of raw sediments, sand content seems to be correlated with silt content. Thus, only one influencing factor between sand and silt is chosen for the modeling work, the OM and PI factors are also kept, PL and LL factors are eliminated.

(2) The developed models based on the whole database, for predicting the OMC and MDD of the treated sediments, cannot provide satisfying prediction accuracy and have low correlation and comparatively high error values.

(3) The statistical performance of models to predict OMC and MDD of the treated sediments could be improved, by using sub databases relative to sandy and silty materials.

(4) The variance and residual analysis proved that all four chosen models meet the statistical requirements. The comparison of the predicted values with experimental values suggested that the developed models reasonably predicted the MDD and OMC of the treated dredged sediments in the database.

(5) The proposed four models were further validated using new experimental data, indicating that the proposed four models could be used to predict the compaction parameters of the treated dredged sediments with acceptable accuracy. The proposed models seem to have higher prediction accuracy than previous models from the literature.

To summarize, the four models created in this study, are robust and are a feasible tool for predicting the MDD and OMC of the treated dredged sediments.

Conclusions and perspectives

With the rapid growth of urbanization and industrialization, many construction and maintenance activities for riverways and ports are carried out each year, which produce a huge volume of dredged sediments. Under the circular economy concept, the reuse of the treated dredged sediments with low carbon binder as road material, is a promising green solution. This study was focused on three original objectives:

(a) The first objective is to study the rheological behavior of the dredged fine-grained sediment, to improve the understanding of sediment, particularly the pipeline transport of the dredged sediments.

(b) The second objective is to solidify the dredged marine sediments with the selected low carbon and sustainable binder for road construction. The investigation of the engineering properties, microscopic mechanisms and environmental properties of the treated sediments is carried out, to verify the effectiveness of using the selected novel binder to treat the dredged sediments in road construction. The low carbon and sustainable binder is selected by SWOT analysis.

(c) The third objective is to develop simple statistical models to enhance and optimize the valorization of the dredged sediments. This model will allow determining an approach to predict the compaction parameters of the treated dredged sediments, using the properties of raw sediments and the type and dosages of binders.

I. Conclusion

Objective (a):

In the steady flow curve measurements, the different rheological parameters values could be observed for artificial and natural sediments. But no matter the artificial or natural samples, the fine-grained sediments are non-Newtonian viscous fluids. The presence of yield stress in fine-grained sediments is evident, the W/S ratios influence it.

The results obtained for artificial fine-grained sediments demonstrated the efficiency of the proposed method, for determining measured yield stress. It can be considered as a method of determining the yield stress, which is more direct and accurate. The Casson model was the best to predict the yield stress of artificial fine-grained sediments, because of its high R^2 and the lowest MAPE, which is close to the measured yield stress value. However, all the models (Bingham, modified Bingham,

Herschel-Bulkley and Casson models) have very high MAPE values for the natural fine-grained sediments. This means none of them can be claimed to be a superior model to predict the yield stress for natural fine-grained sediments. It's worth finding and comparing other more advanced models to predict the yield stress of the natural sediments.

In the dynamic state measurement condition, the loss modulus (G'') is markedly smaller than the elastic modulus (G'), indicating that artificial fine-grained sediment is predominantly elastic (in the range of amplitude and frequencies explored). The complex viscosity (η^*) sharply decreases with the frequency increase, but the G' and G'' frequency dependence is weak. The G', G'', η^* and loss factor ($\tan \delta$) significantly reduced with the increase of the W/S ratio. In the end, the dynamic rheological properties of artificial fine-grained sediments can be expressed as appropriate functions of the W/S ratios.

The study of the rheological parameters for sediment is complex and highly site-specific. The different values of rheological parameters for natural and artificial sediment in this study, highlight the necessity of direct rheological tests on natural sediment to obtain accurate rheological parameters. The difference in rheological parameters between the artificial and natural fine-grained sediments may be attributed to the differences in particle size (d_{50} is 5.72 μm for kaolinite and 10.78 μm for sediments). The strong flocculation between fine particles for kaolinite, enhanced yield stress and apparent viscosity. It should also be noted that extracting proper rheological parameters of natural sediments is somehow challenging.

Objective (b):

The basic physical properties of raw sediments showed it could be classified as weakly organic and low plastic silt, according to the GTR guide. Therefore, raw sediments could be used in embankment (without treatment) and subgrade (with the treatment of hydraulic binder).

The SWOT analysis showed that the low carbon and sustainable binder-Calcium Sulfo-Aluminate cement (CSA) was the best for sediment treatment. Ordinary Portland cement (OPC) was chosen as a standard binder for comparisons. The CSA cement has many advantages: a lower calcination temperature (1250°C), fewer CO_2 emissions, lower limestone demand (35-40%), energy-saving, easy-to-grind property, high early and final strength. However, the price of CSA is higher than OPC, which is

because of the excessive need for aluminum in raw materials to manufacture CSA clinker. Considering the huge environmental benefit of CSA, it's still interesting to try to use the low carbon and sustainable CSA binder to treat dredged sediments. It should also be noted that only a few studies used CSA binder to treat soil and sediments.

For the OPC/CSA single binder treated sediments, the increase in the bearing capacity is almost linear with the increase of the binder content. The addition of the OPC/CSA binder improves the mechanical behavior of the treated dredged sediments, including compressive strength, splitting tensile strength and elastic modulus. The XRD and SEM tests proved the main hydration products observed in OPC are portlandite, calcium silicate hydrate and ettringite. Meanwhile, ettringite is the only hydration product observed for CSA in this study. The microstructure induced by OPC treatment and CSA treatment seems comparable. The bimodal pore size distributions could be observed for both OPC and CSA treated sediments. The leaching values of the OPC/CSA treated sediments are below the limit of non-hazardous waste and the SETRA road guide. Therefore, the OPC/CSA treated sediments could be reused as alternative materials in road construction.

The evaluation of the effectiveness of treatment with OPC/CSA binder has revealed that, only SD4OPC and SD6OPC could be used as subgrade material, the treated materials with 2-6% CSA didn't meet the thresholds of subgrade material based on the GTS guide. To improve the classification of CSA-treated material, the amount of binder could be increased and/or the combined effect of OPC and CSA (OPC-CSA composite binder) might be investigated in the next stage.

The experiment showed that the OPC-CSA composite binder outperformed the OPC/CSA single binder in terms of bearing capacity and mechanical properties (unconfined compressive strength, splitting tensile strength and elastic modulus) of the treated marine sediments. These OPC-CSA composite binder-treated materials (SD4P2C, SD2P4C, SD2P6C, SD4P4C and SD6P2C) met the mechanical requirements of subgrade material.

The XRD results indicated that the chemical reactions are different for OPC-CSA composite binder with different OPC/CSA ratios. The SEM results show that the morphology of needle-like ettringite in the OPC-CSA treated sediments is different from the short rod-like ettringite in the CSA treated sediments. The denser structure of high OPC/CSA ratio treated specimens may cause higher mechanical properties than

low OPC/CSA ratio treated specimens. The laboratory tests have revealed the environmental behaviors of OPC-CSA composite binder treated dredged sediments that meet the regulations and road guide requirements, which means that the treated materials could be reused as road materials.

The simplified carbon footprint analysis indicated that the OPC-CSA composite binder offers potential with 14–41% CO_2 emissions savings in this study, compared to the conventional OPC binder. In terms of CO_2 emissions, SD2P4C (OPC: CSA=1:2) and SD2P6C (OPC: CSA=1:3) appear to be the optimum formulations for 6% and 8% OPC-CSA composite binder-treated materials. Because the two formulations have the greatest promise for reducing CO_2 emissions while meeting the mechanical requirements of subgrade material.

In a word, the treatment of dredged sediments with low carbon and sustainable CSA or OPC-CSA binder, could be a promising green method to reuse sediments waste as road materials.

Objective (c):

Firstly, a database in terms of the treated sediments of 94 measurements was established from different literature. Influencing factors considered in this database include the particle size composition (% of sand, % of silt and % of clay); Atterberg limits (LL, PL and PI); organic matter content (OM); Methylene Blue Value (MBV); different binder types and quantities (P, L, FA, SF, Sa and C) used for the treatment of sediments; compaction energy (E).

Then, the observed compacted behavior of the treated dredged sediments was modeled using the statistical approach. The developed models based on the whole database, used for predicting the OMC and MDD of the treated sediments, cannot provide satisfying prediction accuracy, have low correlation and comparatively high error values. The statistical performance of models to predict OMC and MDD of the treated sediments could be improved, by using sandy and silty sub database. The four models based on sub datasets were chosen as the optimum model to predict the MDD and OMC of the treated dredged sediments.

The variance analysis (ANOVA test) and residual analysis proved that all four chosen models meet the statistical requirements. The proposed four models were further validated using new experimental data, indicating that the proposed four models could

be used to predict the compaction parameters of the treated dredged sediments with acceptable accuracy. The proposed models seem to have higher prediction accuracy than previous models from the literature.

To summarize, the four models created in this study, are robust and are a feasible tool for predicting the MDD and OMC of the treated dredged sediments.

II. Perspectives

In the end, there are still some considerable perspectives for this research.

(i) It would be interesting to investigate the durability of the CSA or OPC-CSA treated dredged marine sediments. Such as immersion in water and freeze-thaw cycle tests. This would further help to clarify the impact of the local weather on the mechanical properties of the CSA-based binder treated sediments in road construction.

(ii) To reuse treated sediments as road materials and meet the high traffic intensity requirement, the effective way may be to combine the treated sediments with coarser materials (such as dredged sand) to improve the mechanical properties and capacity. Although this procedure has been employed for OPC and/or lime treated sediment in several studies. It appears still interesting to extend this method to current CSA or OPC-CSA treated sediment.

(iii) It has proved the effectiveness for the treatment of sediments with OPC and by-products in the past. It would be interesting to investigate CSA cement and by-products, such as ground granulated blast-furnace slag and high-calcium fly ash. It may help reduce the cost of binder and achieve the co-valorization of dredged sediments with by-products.

(iv) The reduction of CO_2 emissions was calculated using a simplified theoretical (thermodynamic) approach. However, it's worth performing a life cycle analysis (LCA) by considering all the treatment materials and processes and calculating the corresponding environmental emissions.

(v) It would be worth enhancing the number of the treated dredged sediments database data, by collecting more data from the articles of different countries. It could also add other basic parameters, such as the solid density and mineral composition (especially clay minerals and carbonate content) of raw sediments. This would help improve the accuracy of the developed statistical models to predict compaction parameters.

(vi) The model for predicting compaction parameters in this research is developed using a statistical approach. It is worth using an artificial intelligence approach, such as genetic expression programming and artificial neural network, to predict compaction parameters of the treated sediments. This may improve the model accuracy in the future.

(vii) Trying to have an experimental pilot in situ, which will make it possible to validate the developed novel low carbon road material: CSA or OPC-CSA treated dredged sediments.

References

[1] Schneider M., M. Romer, M. Tschudin, and H. Bolio. Sustainable cement production-present and future. Cement and Concrete Research. 2011, 41(7): 642-650.

[2] INEC. Major Circular Economy Networks in Europe. France: Institut National de l'Economie Circulaire; 2020 April.

[3] Commission E. 2000/532/EC: Commission Decision of 3 May 2000 replacing Decision 94/3/EC establishing a list of wastes pursuant to Article 1(a) of Council Directive 75/442/EEC on waste and Council Decision 94/904/EC establishing a list of hazardous waste pursuant to Article 1(4) of Council Directive 91/689/EEC on hazardous waste. 2000. p. 3-24.

[4] SOA. Bulletin of Marine Ecology and Environment Status of China. China: Ministry of ecology and environment of china; 2017.

[5] Faure A., C. Coudray, B. Anger, I. Moulin, H. Colin, L. Izoret, et al. Beneficial reuse of dam fine sediments as clinker raw material. Construction and Building Materials. 2019, 218: 365-384.

[6] Hamouche F., and R. Zentar. Effects of organic matter on mechanical properties of dredged sediments for beneficial use in road construction. Environmental Technology. 2020, 41(3): 296-308.

[7] Business A. China aggregates demand stays on a high. Cited 2021 December 3. Available from: https://www.aggbusiness.com/feature/china-aggregates-demand-stays-high.

[8] Dimoudi A., and C. Tompa. Energy and environmental indicators related to construction of office buildings. Resources Conservation and Recycling. 2008, 53(1-2): 86-95.

[9] Chen H., W. L. Lee, and X. L. Wang. Energy assessment of office buildings in China using China building energy codes and LEED 2.2. Energy and Buildings. 2015, 86: 514-524.

[10] Zhang Y., D. Yan, S. Hu, and S. Y. Guo. Modelling of energy consumption and carbon emission from the building construction sector in China, a process-based LCA approach. Energy Policy. 2019, 134.

[11] Chaunsali P., and P. Mondal. Influence of Calcium Sulfoaluminate (CSA) Cement Content on Expansion and Hydration Behavior of Various Ordinary Portland Cement-CSA Blends. Journal of the American Ceramic Society. 2015, 98(8): 2617-2624.

[12] Dung N. T., and C. Unluer. Carbonated MgO concrete with improved performance: The influence of temperature and hydration agent on hydration,

carbonation and strength gain. Cement & Concrete Composites. 2017, 82: 152-164.

[13] Scrivener K. L., V. M. John, E. M. Gartner, and U. Environment. Eco-efficient cements: Potential economically viable solutions for a low-CO2 cement-based materials industry. Cement and Concrete Research. 2018, 114: 2-26.

[14] Renella G. Recycling and Reuse of Sediments in Agriculture: Where Is the Problem? Sustainability. 2021, 13(4): 1648.

[15] Schneider A. R., H. M. Stapleton, J. Cornwell, and J. E. Baker. Recent declines in PAH, PCB, and toxaphene levels in the northern Great Lakes as determined from high resolution sediment cores. Environmental science & technology. 2001, 35(19): 3809-3815.

[16] McLaren P. An interpretation of trends in grain size measures. Journal of Sedimentary Research. 1981, 51(2): 611-624.

[17] Uddin M. K. A review on the adsorption of heavy metals by clay minerals, with special focus on the past decade. Chemical Engineering Journal. 2017, 308: 438-462.

[18] Yeh C. K. J., and C. C. Young. Effects of soil fines and surfactant sorption on contaminant reduction of coarse fractions during soil washing. Journal of Environmental Science and Health Part a-Toxic/Hazardous Substances & Environmental Engineering. 2003, 38(11): 2697-2709.

[19] Drira A. Inversion géoacoustique: amélioration et extension de la méthode des sources images [Doctoral dissertation]. Brest, France: Université de Bretagne occidentale-Brest; 2015.

[20] Abriak N. E., G. Junqua, V. Dubois, P. Gregoire, F. Mac Farlane, and D. Damidot. Methodology of management of dredging operations I. Conceptual developments. Environmental Technology. 2006, 27(4): 411-429.

[21] Infrastructure T. M. a. Dredging. Dubai, UAE. Cited 2021 December 3. Available from: https://www.trelleborg.com/en/marine-and-infrastructure/markets-and-applications/infrastructure/dredging.

[22] EPA U. Introduction to Contaminated Sediments. EPA 823-F-99-006. Washington DC: Office of Science and Technology; 1999.

[23] Yu K. C., L. J. Tsai, S. H. Chen, and S. T. Ho. Correlation analyses on binding behavior of heavy metals with sediment matrices. Water Research. 2001, 35(10): 2417-2428.

[24] Hamouche F., and R. Zentar. Effects of Organic Matter on Physical Properties of Dredged Marine Sediments. Waste and Biomass Valorization. 2020, 11(1): 389-401.

[25] Hamouche F. Influences des matières organiques sur les propriétés physiques et le comportement mécanique des sédiments de dragage en vue d'une valorisation dans

les travaux publics [Doctoral dissertation]. Lille, France: Ecole nationale supérieure Mines-Télécom Lille Douai; 2018.

[26] Karam R. Valorisation de sédiments marins non calcinés dans un liant alcali-activé à base de Laitier de Haut-Fourneau [Doctoral dissertation]. Nantes, France: École centrale de Nantes; 2019.

[27] EPA U. Batch type procedures for estimating soil adsorption of chemicals, EPA/530/SW-87/006-F. Washington DC: Office of solid waste and emergency response; 1991.

[28] Arndt S., B. B. Jorgensen, D. E. LaRowe, J. J. Middelburg, R. D. Pancost, and P. Regnier. Quantifying the degradation of organic matter in marine sediments: A review and synthesis. Earth-Science Reviews. 2013, 123: 53-86.

[29] Burdige D. J. Preservation of organic matter in marine sediments: controls, mechanisms, and an imbalance in sediment organic carbon budgets? Chemical Reviews. 2007, 107(2): 467-485.

[30] Song B., G. M. Zeng, J. L. Gong, J. Liang, P. Xu, Z. F. Liu, et al. Evaluation methods for assessing effectiveness of in situ remediation of soil and sediment contaminated with organic pollutants and heavy metals. Environment International. 2017, 105: 43-55.

[31] Zhu D. W., S. Z. Wu, J. C. Han, L. J. Wang, and M. Y. Qi. Evaluation of nutrients and heavy metals in the sediments of the Heer River, Shenzhen, China. Environmental Monitoring and Assessment. 2018, 190(7).

[32] Long E. R., D. D. MacDonald, C. G. Severn, and C. B. Hong. Classifying probabilities of acute toxicity in marine sediments with empirically derived sediment quality guidelines. Environmental Toxicology and Chemistry. 2000, 19(10): 2598-2601.

[33] Ali H., E. Khan, and I. Ilahi. Environmental Chemistry and Ecotoxicology of Hazardous Heavy Metals: Environmental Persistence, Toxicity, and Bioaccumulation. Journal of Chemistry. 2019, 2019: 6730305.

[34] Ciszewski D., and T. M. Grygar. A Review of Flood-Related Storage and Remobilization of Heavy Metal Pollutants in River Systems. Water Air and Soil Pollution. 2016, 227(7): 1-19.

[35] Ansari T., I. Marr, and N. Tariq. Heavy metals in marine pollution perspective-a mini review. Journal of Applied Sciences. 2004, 4(1): 1-20.

[36] Brown D., and E. Flagg. Empirical prediction of organic pollutant sorption in natural sediments. Journal of Environmental Quality. 1981, 10(3): 382-386.

[37] Van Cauwenberghe L., A. Vanreusel, J. Mees, and C. R. Janssen. Microplastic pollution in deep-sea sediments. Environmental Pollution. 2013, 182: 495-499.

[38] Yang X. E., X. Wu, H. L. Hao, and Z. L. He. Mechanisms and assessment of water eutrophication. Journal of Zhejiang University-Science B. 2008, 9(3): 197-209.

[39] Wang D. Solidification et valorisation de sédiments du port de Dunkerque en travaux routiers : Lille 1; 2011.

[40] Manap N., and N. Voulvoulis. Environmental management for dredging sediments - The requirement of developing nations. Journal of Environmental Management. 2015, 147: 338-348.

[41] Qian Y., and S. Kawashima. Distinguishing dynamic and static yield stress of fresh cement mortars through thixotropy. Cement & Concrete Composites. 2018, 86: 288-296.

[42] Yuan Q., D. J. Zhou, K. H. Khayat, D. Feys, and C. J. Shi. On the measurement of evolution of structural build-up of cement paste with time by static yield stress test vs. small amplitude oscillatory shear test. Cement and Concrete Research. 2017, 99: 183-189.

[43] Qian Y., and S. Kawashima. Use of creep recovery protocol to measure static yield stress and structural rebuilding of fresh cement pastes. Cement and Concrete Research. 2016, 90: 73-79.

[44] Van Kessel T., and C. Blom. Rheology of cohesive sediments: comparison between a natural and an artificial mud. Journal of Hydraulic Research. 1998, 36(4): 591-612.

[45] Faas R. W., and S. I. Wartel. Rheological properties of sediment suspensions from Eckernforde and Kieler Forde bays, western Baltic Sea. International Journal of Sediment Research. 2006, 21(1): 24-41.

[46] Soltanpour M., and F. Samsami. A comparative study on the rheology and wave dissipation of kaolinite and natural Hendijan Coast mud, the Persian Gulf. Ocean Dynamics. 2011, 61(2-3): 295-309.

[47] Yang W. Y., S. K. Tan, H. K. Wang, and G. L. Yu. Rheological Properties of Bed Sediments Subjected to Shear and Vibration Loads. Journal of Waterway Port Coastal and Ocean Engineering. 2014, 140(1): 109-113.

[48] Yang W. Y., G. L. Yu, S. K. Tan, and H. K. Wang. Rheological properties of dense natural cohesive sediments subject to shear loadings. International Journal of Sediment Research. 2014, 29(4): 454-470.

[49] Xu J. Y., and A. Huhe. Rheological study of mudflows at Lianyungang in China. International Journal of Sediment Research. 2016, 31(1): 71-78.

[50] Shakeel A., A. Kirichek, and C. Chassagne. Rheological analysis of mud from Port of Hamburg, Germany. Journal of Soils and Sediments. 2020, 20(6): 2553-2562.

[51] Fonseca D. L., P. C. Marroig, J. C. Carneiro, M. N. Gallo, and S. B. Vinzon.

Assessing rheological properties of fluid mud samples through tuning fork data. Ocean Dynamics. 2019, 69(1): 51-57.

[52] Messaoudi A., M. Bouzit, and N. Boualla. Physical and rheological properties of the Chorfa dam mud: dependency on solids concentration. Applied Water Science. 2018, 8(6): 1-9.

[53] Achour R., N. E. Abriak, R. Zentar, P. Rivard, and P. Gregoire. Valorization of unauthorized sea disposal dredged sediments as a road foundation material. Environmental Technology. 2014, 35(16): 1997-2007.

[54] Benzerzour M., M. Amar, and N. E. Abriak. New experimental approach of the reuse of dredged sediments in a cement matrix by physical and heat treatment. Construction and Building Materials. 2017, 140: 432-444.

[55] Amar M., M. Benzerzour, and N. E. Abriak. Towards the establishment of formulation laws for sediment-based mortars. Journal of Building Engineering. 2018, 16: 106-117.

[56] Safhi A. E., M. Benzerzour, P. Rivard, N. E. Abriak, and I. Ennahal. Development of self-compacting mortars based on treated marine sediments. Journal of Building Engineering. 2019, 22: 252-261.

[57] Safhi A. E., M. Benzerzour, P. Rivard, and N. E. Abriak. Feasibility of using marine sediments in SCC pastes as supplementary cementitious materials. Powder Technology. 2019, 344: 730-740.

[58] Zhao Z. F., M. Benzerzour, N. E. Abriak, D. Damidot, L. Courard, and D. X. Wang. Use of uncontaminated marine sediments in mortar and concrete by partial substitution of cement. Cement & Concrete Composites. 2018, 93: 155-162.

[59] Junakova N., and J. Junak. Sustainable Use of Reservoir Sediment through Partial Application in Building Material. Sustainability. 2017, 9(5): 852.

[60] Said I., A. Missaoui, and Z. Lafhaj. Reuse of Tunisian marine sediments in paving blocks: factory scale experiment. Journal of Cleaner Production. 2015, 102: 66-77.

[61] Samara M., Z. Lafhaj, and C. Chapiseau. Valorization of stabilized river sediments in fired clay bricks: Factory scale experiment. Journal of Hazardous materials. 2009, 163(2-3): 701-710.

[62] Tuan B. L. A., M. G. Tesfamariam, Y. Y. Chen, C. L. Hwang, K. L. Lin, and M. P. Young. Production of Lightweight Aggregate from Sewage Sludge and Reservoir Sediment for High-Flowing Concrete. Journal of Construction Engineering and Management. 2014, 140(5): 04014005.

[63] Snellings R., O. Cizer, L. Horckmans, P. T. Durdzinski, P. Dierckx, P. Nielsen, et al. Properties and pozzolanic reactivity of flash calcined dredging sediments. Applied

Clay Science. 2016, 129: 35-39.

[64] Sadok R. H., N. Belas, M. Tahlaiti, and R. Mazouzi. Reusing calcined sediments from Chorfa II dam as partial replacement of cement for sustainable mortar production. Journal of Building Engineering. 2021, 40: 102273.

[65] Aoual-Benslafa F. K., D. Kerdal, M. Ameur, B. Mekerta, and A. Semcha. Durability of mortars made with dredged sediments. 2011 International Conference on Green Buildings and Sustainable Cities. 2015, 118: 240-250.

[66] Fytili D., and A. Zabaniotou. Utilization of sewage sludge in EU application of old and new methods - A review. Renewable & Sustainable Energy Reviews. 2008, 12(1): 116-140.

[67] Amar M., M. Benzerzour, J. Kleib, and N.-E. Abriak. From dredged sediment to supplementary cementitious material: characterization, treatment, and reuse. International Journal of Sediment Research. 2020, 36(1): 92-109.

[68] Mezencevova A., N. N. Yeboah, S. E. Burns, L. F. Kahn, and K. E. Kurtis. Utilization of Savannah Harbor river sediment as the primary raw material in production of fired brick. Journal of Environmental Management. 2012, 113: 128-136.

[69] Slimanou H., D. Eliche-Quesada, S. Kherbache, N. Bouzidi, and A. K. Tahakourt. Harbor Dredged Sediment as raw material in fired clay brick production: Characterization and properties. Journal of Building Engineering. 2020, 28: 101085.

[70] Liu R., and R. Coffman. Lightweight Aggregate Made from Dredged Material in Green Roof Construction for Stormwater Management. Materials. 2016, 9(8): 611.

[71] Chen H. J., M. D. Yang, C. W. Tang, and S. Y. Wang. Producing synthetic lightweight aggregates from reservoir sediments. Construction and Building Materials. 2012, 28(1): 387-394.

[72] Dalton J. L., K. H. Gardner, T. P. Seager, M. L. Weimer, J. C. M. Spear, and B. J. Magee. Properties of Portland cement made from contaminated sediments. Resources Conservation and Recycling. 2004, 41(3): 227-241.

[73] Snellings R., L. Horckmans, C. Van Bunderen, L. Vandewalle, and O. Cizer. Flash-calcined dredging sediment blended cements: effect on cement hydration and properties. Materials and Structures. 2017, 50(6).

[74] Wang D. X., N. E. Abriak, R. Zentar, and W. Y. Xu. Solidification/stabilization of dredged marine sediments for road construction. Environmental Technology. 2012, 33(1): 95-101.

[75] Sahu V., A. Srivastava, A. K. Misra, and A. K. Sharma. Stabilization of fly ash and lime sludge composites: Assessment of its performance as base course material. Archives of Civil and Mechanical Engineering. 2017, 17(3): 475-485.

[76] Zentar R., V. Dubois, and N. E. Abriak. Mechanical behaviour and environmental impacts of a test road built with marine dredged sediments. Resources, Conservation and Recycling. 2008, 52(6): 947-954.

[77] Yoobanpot N., P. Jamsawang, H. Poorahong, P. Jongpradist, and S. Likitlersuang. Multiscale laboratory investigation of the mechanical and microstructural properties of dredged sediments stabilized with cement and fly ash. Engineering Geology. 2020, 267: 105491.

[78] Li J. S., Y. F. Zhou, Q. M. Wang, Q. Xue, and C. S. Poon. Development of a Novel Binder Using Lime and Incinerated Sewage Sludge Ash to Stabilize and Solidify Contaminated Marine Sediments with High Water Content as a Fill Material. Journal of Materials in Civil Engineering. 2019, 31(10): 04019245.

[79] Huang Y. H., C. Dong, C. L. Zhang, and K. Xu. A dredged material solidification treatment for fill soils in East China: A case history. Marine Georesources & Geotechnology. 2017, 35(6): 865-872.

[80] Wang D. X., R. Zentar, and N. E. Abriak. Durability and Swelling of Solidified/Stabilized Dredged Marine Soils with Class-F Fly Ash, Cement, and Lime. Journal of Materials in Civil Engineering. 2018, 30(3): 04018013.

[81] Huang Y. H., W. Zhu, X. D. Qian, N. Zhang, and X. Z. Zhou. Change of mechanical behavior between solidified and remolded solidified dredged materials. Engineering Geology. 2011, 119(3-4): 112-119.

[82] Kang G., T. Tsuchida, and A. M. R. G. Athapaththu. Engineering behavior of cement-treated marine dredged clay during early and later stages of curing. Engineering Geology. 2016, 209: 163-174.

[83] Chiu C. F., W. Zhu, and C. L. Zhang. Yielding and shear behaviour of cement-treated dredged materials. Engineering Geology. 2009, 103(1-2): 1-12.

[84] Higgins D. GGBS and sustainability. Proceedings of the Institution of Civil Engineers - Construction Materials. 2007, 160(3): 99-101.

[85] Provis J. L. Green concrete or red herring? - future of alkali-activated materials. Advances in Applied Ceramics. 2014, 113(8): 472-477.

[86] Dowling A., J. O'Dwyer, and C. C. Adley. Lime in the limelight. Journal of Cleaner Production. 2015, 92: 13-22.

[87] Oates J. A. Lime and limestone: chemistry and technology, production and uses: John Wiley & Sons; 2008.

[88] Gutierrez A. S., J. Van Caneghem, J. B. C. Martinez, and C. Vandecasteele. Evaluation of the environmental performance of lime production in Cuba. Journal of Cleaner Production. 2012, 31: 126-136.

[89] Oti J. E., and J. M. Kinuthia. Stabilised unfired clay bricks for environmental and

sustainable use. Applied Clay Science. 2012, 58: 52-59.

[90] Ventola L., M. Vendrell, P. Giraldez, and L. Merino. Traditional organic additives improve lime mortars: New old materials for restoration and building natural stone fabrics. Construction and Building Materials. 2011, 25(8): 3313-3318.

[91] Wang D. X., N. E. Abriak, R. Zentar, and W. Z. Chen. Effect of lime treatment on geotechnical properties of Dunkirk sediments in France. Road Materials and Pavement Design. 2013, 14(3): 485-503.

[92] Todaro F., S. De Gisi, and M. Notarnicola. Contaminated marine sediment stabilization/solidification treatment with cement/lime: leaching behaviour investigation. Environmental Science and Pollution Research. 2020, 27(17): 21407-21415.

[93] Federico A., C. Vitone, and A. Murianni. On the mechanical behaviour of dredged submarine clayey sediments stabilized with lime or cement. Canadian Geotechnical Journal. 2015, 52(12): 2030-2040.

[94] Wang Z., X. Si-fa, and W. Guo-cai. Study of early strength and shrinkage properties of cement or lime solidified soil. Energy Procedia. 2012, 16: 302-306.

[95] Wang D. X., H. W. Wang, and Y. Z. Jiang. Water Immersion-Induced Strength Performance of Solidified Soils with Reactive MgO-A Green and Low Carbon Binder. Journal of Testing and Evaluation. 2019, 47(2): 1569-1585.

[96] Wang D. X., H. W. Wang, and S. J. Di. Mechanical properties and microstructure of magnesia-fly ash pastes. Road Materials and Pavement Design. 2019, 20(5): 1243-1254.

[97] Wang D. X., H. W. Wang, and X. Q. Wang. Compressibility and strength behavior of marine soils solidified with MgO-A green and low carbon binder. Marine Georesources & Geotechnology. 2017, 35(6): 878-886.

[98] Al-Tabbaa A. Reactive magnesia cement. In Eco-efficient concrete. Sawston, Cambridge, UK: Woodhead Publishing; 2013. 523-543.

[99] Ruan S., and C. Unluer. Comparative life cycle assessment of reactive MgO and Portland cement production. Journal of Cleaner Production. 2016, 137: 258-273.

[100] Yi Y. L., X. Zheng, S. Y. Liu, and A. Al-Tabbaa. Comparison of reactive magnesia- and carbide slag-activated ground granulated blastfurnace slag and Portland cement for stabilisation of a natural soil. Applied Clay Science. 2015, 111: 21-26.

[101] Al-Tabbaa A., F. Jin, Y. Bai, J. Qian, and L. Mo. Magnesia-bearing materials for challenging infrastructure and environment. International Workshop on Innovation in Low-carbon Cement & Concrete Technology; 2016.

[102] Xing Z. B., L. M. Bai, Y. X. Ma, D. Wang, and M. Li. Mechanism of

Magnesium Oxide Hydration Based on the Multi-Rate Model. Materials. 2018, 11(10): 1835.

[103] Wang L., L. Chen, D. W. Cho, D. C. W. Tsang, J. Yang, D. Hou, et al. Novel synergy of Si-rich minerals and reactive MgO for stabilisation/solidification of contaminated sediment. Journal of Hazardous materials. 2019, 365: 695-706.

[104] Wang L., T. L. K. Yeung, A. Y. T. Lau, D. C. W. Tsang, and C.-S. Poon. Recycling contaminated sediment into eco-friendly paving blocks by a combination of binary cement and carbon dioxide curing. Journal of Cleaner Production. 2017, 164: 1279-1288.

[105] Juenger M. C. G., F. Winnefeld, J. L. Provis, and J. H. Ideker. Advances in alternative cementitious binders. Cement and Concrete Research. 2011, 41(12): 1232-1243.

[106] Davidovits J. Geopolymers - Inorganic Polymeric New Materials. Journal of Thermal Analysis. 1991, 37(8): 1633-1656.

[107] Salas D. A., A. D. Ramirez, N. Ulloa, H. Baykara, and A. J. Boero. Life cycle assessment of geopolymer concrete. Construction and Building Materials. 2018, 190: 170-177.

[108] Nematollahi B., J. Sanjayan, J. S. Qiu, and E. H. Yang. Micromechanics-based investigation of a sustainable ambient temperature cured one-part strain hardening geopolymer composite. Construction and Building Materials. 2017, 131: 552-563.

[109] Huseien G. F., M. Ismail, N. H. A. Khalid, M. W. Hussin, and J. Mirza. Compressive strength and microstructure of assorted wastes incorporated geopolymer mortars: Effect of solution molarity. Alexandria engineering journal. 2018, 57(4): 3375-3386.

[110] McLellan B. C., R. P. Williams, J. Lay, A. van Riessen, and G. D. Corder. Costs and carbon emissions for geopolymer pastes in comparison to ordinary portland cement. Journal of Cleaner Production. 2011, 19(9-10): 1080-1090.

[111] Komnitsas K. A. Potential of geopolymer technology towards green buildings and sustainable cities. 2011 International Conference on Green Buildings and Sustainable Cities. 2011, 21: 1023-1032.

[112] Tempest B., O. Sanusi, J. Gergely, V. Ogunro, and D. Weggel. Compressive strength and embodied energy optimization of fly ash based geopolymer concrete. World of coal ash (WOCA) conference; 2009.

[113] Duxson P., J. L. Provis, G. C. Lukey, and J. S. J. Van Deventer. The role of inorganic polymer technology in the development of 'green concrete'. Cement and Concrete Research. 2007, 37(12): 1590-1597.

[114] Pangdaeng S., T. Phoo-ngernkham, V. Sata, and P. Chindaprasirt. Influence of

curing conditions on properties of high calcium fly ash geopolymer containing Portland cement as additive. Materials & Design. 2014, 53: 269-274.

[115] Jaditager M., and N. Sivakugan. Influence of Fly Ash-Based Geopolymer Binder on the Sedimentation Behavior of Dredged Mud. Journal of Waterway Port Coastal and Ocean Engineering. 2017, 143(5): 04017012.

[116] Jaditager M., and N. Sivakugan. Consolidation Behavior of Fly Ash-Based Geopolymer-Stabilized Dredged Mud. Journal of Waterway Port Coastal and Ocean Engineering. 2018, 144(4): 06018003.

[117] Shi C. J., A. F. Jimenez, and A. Palomo. New cements for the 21st century: The pursuit of an alternative to Portland cement. Cement and Concrete Research. 2011, 41(7): 750-763.

[118] Gao X. Alkali activated slag-fly ash binders: design, modeling and application [Doctoral dissertation]. Eindhoven, Netherlands: Eindhoven University of Technology; 2017.

[119] Shi C., D. Roy, and P. Krivenko. Alkali-activated cements and concretes. London, UK: CRC press; 2003.

[120] Shi C., F. He, and P. Angel. Classification and characteristics of alkali-activated cements. Journal of The Chinese Ceramic Society. 2012, 40(1): 69-75.

[121] Fernández-Jiménez A., A. Palomo, T. Vazquez, R. Vallepu, T. Terai, and K. Ikeda. Alkaline activation of blends of metakaolin and calcium aluminate. Journal of the American Ceramic Society. 2008, 91(4): 1231-1236.

[122] Fort J., E. Vejmelkova, D. Konakova, N. Alblova, M. Cachova, M. Keppert, et al. Application of waste brick powder in alkali activated aluminosilicates: Functional and environmental aspects. Journal of Cleaner Production. 2018, 194: 714-725.

[123] Thapa V. B., D. Waldmann, J. F. Wagner, and A. Lecomte. Assessment of the suitability of gravel wash mud as raw material for the synthesis of an alkali-activated binder. Applied Clay Science. 2018, 161: 110-118.

[124] Gu Z., S. Hua, W. Zhao, S. Li, Z. Gao, and H. Shan. Using alkali-activated cementitious materials to solidify high organic matter content dredged sludge as roadbed material. Advances in Civil Engineering. 2018, 2018: 1-10.

[125] Cho H. N., J. H. Shim, and J. Y. Park. Performance evaluation of solidification/stabilization of dredged sediment using alkali-activated slag. Desalination and Water Treatment. 2016, 57(22): 10159-10168.

[126] Obana M., D. Levacher, and P. Dhervilly. Durability properties of marine sediments stabilised by pozzolan and alkali-activated binders. European Journal of Environmental and Civil Engineering. 2012, 16(8): 919-926.

[127] Zhang L., and F. Glasser. New concretes based on calcium sulfoaluminate

cement. In Modern Concrete Materials: Binders, Additions and Admixtures: Thomas Telford Publishing; 1999. 261-274.

[128] Sui T., and Y. Yao. Recent progress in special cements in China. Proceeding of the 11th International Congress on Chemistry of Cement (ICCC), South Africa, Durban; 2003.

[129] Gartner E., and T. B. Sui. Alternative cement clinkers. Cement and Concrete Research. 2018, 114: 27-39.

[130] Marroccoli M., F. Montagnaro, A. Telesca, and G. L. Valenti. Environmental implications of the manufacture of calcium sulfoaluminate-based cements. Second International Conference on Sustainable Construction Materials and Technologies; 2010; Ancona, Italy.

[131] Coppola L., D. Coffetti, E. Crotti, G. Gazzaniga, and T. Pastore. An Empathetic Added Sustainability Index (EASI) for cementitious based construction materials. Journal of Cleaner Production. 2019, 220: 475-482.

[132] Ioannou S., K. Paine, L. Reig, and K. Quillin. Performance characteristics of concrete based on a ternary calcium sulfoaluminate-anhydrite-fly ash cement. Cement & Concrete Composites. 2015, 55: 196-204.

[133] Kaprálik I., and F. Hanic. Phase relations in the subsystem C4A3S-CSH2-CH-H2O of the system CaO-Al2O3-CS-H2O referred to hydration of sulphoaluminate cement. Cement and Concrete Research. 1989, 19(1): 89-102.

[134] Zhang J. J., G. X. Li, W. T. Ye, Y. Z. Chang, Q. F. Liu, and Z. P. Song. Effects of ordinary Portland cement on the early properties and hydration of calcium sulfoaluminate cement. Construction and Building Materials. 2018, 186: 1144-1153.

[135] Li G. X., J. J. Zhang, Z. P. Song, C. Shi, and A. Zhang. Improvement of workability and early strength of calcium sulphoaluminate cement at various temperature by chemical admixtures. Construction and Building Materials. 2018, 160: 427-439.

[136] Glasser F. P., and L. Zhang. High-performance cement matrices based on calcium sulfoaluminate-belite compositions. Cement and Concrete Research. 2001, 31(12): 1881-1886.

[137] Cabrera J. G., and A. S. Al-Hasan. Performance properties of concrete repair materials. Construction and Building Materials. 1997, 11(5-6): 283-290.

[138] Ge Z., H. Q. Yuan, R. J. Sun, H. Z. Zhang, W. L. Wang, and H. Qi. Use of green calcium sulphoaluminate cement to prepare foamed concrete for road embankment: A feasibility study. Construction and Building Materials. 2020, 237: 117791.

[139] Coumes C. C. D., S. Courtois, S. Peysson, J. Ambroise, and J. Pera. Calcium sulfoaluminate cement blended with OPC: A potential binder to encapsulate low-level

radioactive slurries of complex chemistry. Cement and Concrete Research. 2009, 39(9): 740-747.

[140] Luz C. A., J. Pera, M. Cheriaf, and J. C. Rocha. Behaviour of calcium sulfoaluminate cement in presence of high concentrations of chromium salts. Cement and Concrete Research. 2007, 37(4): 624-629.

[141] Ivanov R. C., C. A. da Luz, H. E. Zorel, and J. I. Pereira. Behavior of calcium aluminate cement (CAC) in the presence of hexavalent chromium. Cement & Concrete Composites. 2016, 73: 114-122.

[142] Trauchessec R., J. M. Mechling, A. Lecomte, A. Roux, and B. Le Rolland. Hydration of ordinary Portland cement and calcium sulfoaluminate cement blends. Cement & Concrete Composites. 2015, 56: 106-114.

[143] Pera J., and J. Ambroise. New applications of calcium sulfoaluminate cement. Cement and Concrete Research. 2004, 34(4): 671-676.

[144] Subramanian S., Q. Khan, and T. Ku. Strength development and prediction of calcium sulfoaluminate treated sand with optimized gypsum for replacing OPC in ground improvement. Construction and Building Materials. 2019, 202: 308-318.

[145] Subramanian S., S. W. Moon, J. Moon, and T. Ku. CSA-Treated Sand for Geotechnical Application: Microstructure Analysis and Rapid Strength Development. Journal of Materials in Civil Engineering. 2018, 30(12): 04018313.

[146] Moon S. W., G. Vinoth, S. Subramanian, J. Kim, and T. Ku. Effect of fine particles on strength and stiffness of cement treated sand. Granular Matter. 2020, 22(1): 1-13.

[147] Moghrabi I., H. Ranaivomanana, F. Bendahmane, O. Amiri, and D. Levacher. Modelling the mechanical strength development of treated fine sediments: a statistical approach. Environmental Technology. 2019, 40(14): 1890-1909.

[148] Harrington J., J. Murphy, M. Coleman, D. Jordan, and G. Szacsuri. Financial modelling and analysis of the management of dredged marine sediments–development of a decision support tool. Journal of Shipping and Trade. 2016, 1(1): 1-10.

[149] Shah S. A. R., Z. Mahmood, A. Nisar, M. Aamir, A. Farid, and M. Waseem. Compaction performance analysis of alum sludge waste modified soil. Construction and Building Materials. 2020, 230: 116953.

[150] Ozgan E., S. Serin, and I. Vural. Multi-faceted investigation and modeling of compaction parameters for road construction. Journal of Terramechanics. 2015, 60: 33-42.

[151] Huat B. B., A. Prasad, S. Kazemian, and V. Anggraini. Ground improvement techniques. Leiden: CRC Press; 2019.

[152] Miraoui M., R. Zentar, and N.-E. Abriak. Road material basis in dredged sediment and basic oxygen furnace steel slag. Construction and Building Materials. 2012, 30: 309-319.

[153] Basheer I. Empirical modeling of the compaction curve of cohesive soils. Canadian Geotechnical Journal. 2001, 38(1): 29-45.

[154] Sivrikaya O. Models of compacted fine-grained soils used as mineral liner for solid waste. Environmental Geology. 2008, 53(7): 1585.

[155] Omar M., A. Shanableh, O. Mughieda, M. Arab, W. Zeiada, and R. Al-Ruzouq. Advanced mathematical models and their comparison to predict compaction properties of fine-grained soils from various physical properties. Soils and Foundations. 2018, 58(6): 1383-1399.

[156] Gunaydin O. Estimation of soil compaction parameters by using statistical analyses and artificial neural networks. Environmental Geology. 2009, 57(1): 203-215.

[157] Blotz L. R., C. H. Benson, and G. P. Boutwell. Estimating optimum water content and maximum dry unit weight for compacted clays. Journal of Geotechnical and Geoenvironmental Engineering. 1998, 124(9): 907-912.

[158] Sridharan A., and H. Nagaraj. Plastic limit and compaction characteristics of finegrained soils. Proceedings of the institution of civil engineers-ground improvement. 2005, 9(1): 17-22.

[159] Saikia A., D. Baruah, K. Das, H. J. Rabha, A. Dutta, and A. Saharia. Predicting compaction characteristics of fine-grained soils in terms of Atterberg limits. International Journal of Geosynthetics and Ground Engineering. 2017, 3(2): 18.

[160] Nagaraj H. B., B. Reesha, M. V. Sravan, and M. R. Suresh. Correlation of compaction characteristics of natural soils with modified plastic limit. Transportation Geotechnics. 2015, 2: 65-77.

[161] Farooq K., U. Khalid, and H. Mujtaba. Prediction of Compaction Characteristics of Fine-Grained Soils Using Consistency Limits. Arabian Journal for Science and Engineering. 2016, 41(4): 1319-1328.

[162] Siddiqui F. I., and S. B. A. B. Osman. Simple and multiple regression models for relationship between electrical resistivity and various soil properties for soil characterization. Environmental Earth Sciences. 2013, 70(1): 259-267.

[163] Obianyo I. I., E. N. Anosike-Francis, G. O. Ihekweme, Y. Geng, R. Y. Jin, A. P. Onwualu, et al. Multivariate regression models for predicting the compressive strength of bone ash stabilized lateritic soil for sustainable building. Construction and Building Materials. 2020, 263: 120677.

[164] Khaboushan E. A., H. Emami, M. R. Mosaddeghi, and A. R. Astaraei.

Estimation of unsaturated shear strength parameters using easily-available soil properties. Soil & Tillage Research. 2018, 184: 118-127.

[165] Akan R., S. N. Keskin, and S. Uzundurukan. Multiple regression model for the prediction of unconfined compressive strength of jet grout columns. World Multidisciplinary Earth Sciences Symposium, Wmess 2015. 2015, 15: 299-303.

[166] CEN. Geotechnical investigation and testing - Laboratory testingof soil - Part 1 : determination of water content. NF EN ISO 17892-1, 2014. Brussels, Belgium.

[167] SETRA-LCPC. Réalisation des remblais et des couches de forme. 1992.

[168] CEN. Particle size analysis - Laser diffraction methods. ISO 13320, 2020. Brussels, Belgium.

[169] CEN. Geotechnical investigation and testing - Laboratory testing of soil - Part 12: determination of liquid and plastic limits. EN ISO 17892-12, 2018. Brussels, Belgium.

[170] CEN. Geotechnical investigation and testing - Laboratory testing of soil - Part 3: determination of particle density. NF EN ISO 17892-3, 2015. Brussels, Belgium.

[171] AFNOR. Soils: Investigation and testing - Measuring of the methylene blue adsorption capacity of a rocky soil - Determination of the methylene blue of a soil by means of the stain test. NF P94-068, 1998. Paris, France.

[172] AFNOR. Soils: investigation and testing - Determination of the organic matter content - Ignition method. XP P 94-047, 1998. Paris, France.

[173] CEN. Soil, waste, treated biowaste and sludge - Determination ofloss on ignition. NF EN 15935, 2021. Brussels, Belgium.

[174] CEN. Unbound and hydraulically bound mixtures. Part 2: Test methods for the determination of the laboratory reference density and water content. Proctor compaction. NF EN 13286-2, 2010. Brussels, Belgium.

[175] CEN. Unbound and hydraulically bound mixtures. Part 47: Test method for the determination of California bearing ratio, immediate bearing index and linear swelling. NF EN 13286-47, 2012. Brussels, Belgium.

[176] CEN. Sludge, treated biowaste and soil - Determination of pH. NF EN 15933, 2012. Brussels, Belgium.

[177] CEN. Sludge, treated biowaste and soil - Determination of specific electrical conductivity. CEN/TS 15937, 2013. Brussels, Belgium.

[178] AFNOR. Cement testing methods - Determination of density. NF P 15-435, 2021. Paris, France.

[179] CEN. Methods of testing cement - Part 2: Chemical analysis of cement. NF EN 196-2, 2013. Brussels, Belgium.

[180] Miraoui M. Prétraitement et traitement des sédiments de dragage en vue d'une valorisation dans le génie civil [Doctoral dissertation]. Lille, France: University of Lille 1; 2010.

[181] Dia M. Traitement et valorisation de sédiments de dragage phosphatés en technique routière [Doctoral dissertation]. Arras, France: University of Artois; 2013.

[182] Belles A., C. Alary, Y. Mamindy-Pajany, and N. E. Abriak. Relationship between the water-exchangeable fraction of PAH and the organic matter composition of sediments. Environmental Pollution. 2016, 219: 512-518.

[183] Capel E. L., J. M. D. R. Arranz, F. J. Gonzalez-Vila, J. A. Gonzalez-Perez, and D. A. C. Manning. Elucidation of different forms of organic carbon in marine sediments from the Atlantic coast of Spain using thermal analysis coupled to isotope ratio and quadrupole mass spectrometry. Organic Geochemistry. 2006, 37(12): 1983-1994.

[184] USDA-NRCS. Soil Quality Indicator Sheets-Soil Electrical Conductivity. December 2011.

[185] Mamindy-Pajany Y., F. Geret, C. Hurel, and N. Marmier. Batch and column studies of the stabilization of toxic heavy metals in dredged marine sediments by hematite after bioremediation. Environmental Science and Pollution Research. 2013, 20(8): 5212-5219.

[186] Couvidat J., V. Chatain, H. Bouzahzah, and M. Benzaazoua. Characterization of how contaminants arise in a dredged marine sediment and analysis of the effect of natural weathering. Science of the Total Environment. 2018, 624: 323-332.

[187] Couvidat J., C. M. Neculita, M. Benzaazoua, T. Genty, and V. Chatain. Evaluation of biogeochemical reactivity of fresh and weathered contaminated dredged sediments. Journal of Soils and Sediments. 2017, 17(2): 543-556.

[188] Li J. Y., R. K. Xu, and H. Zhang. Iron oxides serve as natural anti-acidification agents in highly weathered soils. Journal of Soils and Sediments. 2012, 12(6): 876-887.

[189] Taylor-Lange S. C., E. L. Lamon, K. A. Riding, and M. C. G. Juenger. Calcined kaolinite-bentonite clay blends as supplementary cementitious materials. Applied Clay Science. 2015, 108: 84-93.

[190] Sadok R. H., W. Maherzi, M. Benzerzour, R. Lord, K. Torrance, A. Zambon, et al. Mechanical properties and microstructure of low carbon binders manufactured from calcined canal sediments and ground granulated blast furnace slag (GGBS). Sustainability. 2021, 13(16): 9057.

[191] He C., E. Makovicky, and B. Osbaeck. Thermal stability and pozzolanic activity of calcined kaolin. Applied Clay Science. 1994, 9(3): 165-187.

[192] Mohammed S. Processing, effect and reactivity assessment of artificial pozzolans obtained from clays and clay wastes: A review. Construction and Building Materials. 2017, 140: 10-19.

[193] Jia F. F., J. Su, and S. X. Song. Can Natural Muscovite be Expanded? Colloids and Surfaces a-Physicochemical and Engineering Aspects. 2015, 471: 19-25.

[194] Alastair M., H. Andrew, P. Pascaline, E. Mark, and W. Pete. Alkali activation behaviour of un-calcined montmorillonite and illite clay minerals. Applied Clay Science. 2018, 166: 250-261.

[195] Bensharada M., R. Telford, B. Stern, and V. Gaffney. Loss on ignition vs. thermogravimetric analysis: a comparative study to determine organic matter and carbonate content in sediments. Journal of Paleolimnology. 2021, : .

[196] Konare H., R. S. Yost, M. Doumbia, G. W. McCarty, A. Jarju, and R. Kablan. Loss on ignition: Measuring soil organic carbon in soils of the Sahel, West Africa. African Journal of Agricultural Research. 2010, 5(22): 3088-3095.

[197] AFNOR. Soil quality - Determination of organic and total carbon after dry combustion (elementary analysis). NF ISO 10694, 1995. Paris, France.

[198] Rietveld H. M. A profile refinement method for nuclear and magnetic structures. Journal of Applied Crystallography. 1969, 2(2): 65-71.

[199] Trincal V., V. Thiery, Y. Mamindy-Pajany, and S. Hillier. Use of hydraulic binders for reducing sulphate leaching: application to gypsiferous soil sampled in Ile-de-France region (France). Environmental Science and Pollution Research. 2018, 25(23): 22977-22997.

[200] Trincal V., D. Charpentier, M. D. Buatier, B. Grobety, B. Lacroix, P. Labaume, et al. Quantification of mass transfers and mineralogical transformations in a thrust fault (Monte Perdido thrust unit, southern Pyrenees, Spain). Marine and Petroleum Geology. 2014, 55: 160-175.

[201] Union C. o. t. E. Council Decision establishing criteria and procedures for the acceptance of waste at landfills pursuant to Article 16 of and Annex II to Directive 1999/31/EC. 2003/33/EC, 2003.

[202] SETRA. Guide d'acceptabilité des matériaux alternatifs en technique routière – Evaluation environnementale. 2011.

[203] ASTM. Standard Practice for Classification of Soils for Engineering Purposes (Unified Soil Classification System). ASTM D2487-17, 2017. West Conshohocken, Pennsylvania.

[204] CEN. Geotechnical investigation and testing - Identification and classification of soil - Part 2 : principles for a classification. EN ISO 14688-2, 2017. Brussels, Belgium.

[205] ASTM. Standard Practice for Classification of Soils and Soil-Aggregate Mixtures for Highway Construction Purposes. ASTM D3282-15, 2015. West Conshohocken, Pennsylvania.

[206] JTG. Test methods of soils for highway engineering. JTG 3430-2020, 2020. Beijing, China.

[207] JTG. Specifications for Design of Highway Subgrades. JTG D30-2015, 2015. Beijing, China.

[208] Naqi A., and J. G. Jang. Recent Progress in Green Cement Technology Utilizing Low-Carbon Emission Fuels and Raw Materials: A Review. Sustainability. 2019, 11(2).

[209] Rougeau F. J.-P. Bétons bas carbone focus sur les nouveaux liants. Epernon, France: CERIB; 2020.

[210] Bouharoun S., N. Leklou, and P. Mounanga. Use of asbestos-free fiber-cement waste as a partial substitute of Portland cement in mortar. Materials and Structures. 2015, 48(6): 1679-1687.

[211] Bala M., R. Zentar, and P. Boustingorry. Comparative study of the yield stress determination of cement pastes by different methods. Materials and Structures. 2019, 52(5): 1-12.

[212] Zhang Q., R. Le Roy, M. Vandamme, and B. Zuber. Long-term creep properties of cementitious materials: Comparing microindentation testing with macroscopic uniaxial compressive testing. Cement and Concrete Research. 2014, 58: 89-98.

[213] CEN. Cement - Part 1: Composition, specifications and conformity criteria for common cements. NF EN 197-1, 2011. Brussels, Belgium.

[214] Stoian J., T. Oey, J. W. Bullard, J. Huang, A. Kumar, M. Balonis, et al. New insights into the prehydration of cement and its mitigation. Cement and Concrete Research. 2015, 70: 94-103.

[215] Mehrabani J. V., and M. Goharkhah. An Investigation on Tailing Slurry Transport in Kooshk lead-Zinc Mine in Iran Based on Non-Newtonian Fluid Rheology: an Experimental Study. Journal of Mining and Environment. 2021, 12(3): 877-893.

[216] Dikonda R. K., M. Mbonimpa, and T. Belem. Specific Mixing Energy of Cemented Paste Backfill, Part II: Influence on the Rheological and Mechanical Properties and Practical Applications. Minerals. 2021, 11(11): 1165.

[217] Otsubo K., and K. Muraoka. Critical shear stress of cohesive bottom sediments. Journal of Hydraulic Engineering. 1988, 114(10): 1241-1256.

[218] Sahdi F., C. Gaudin, and D. J. White. Strength properties of ultra-soft kaolin. Canadian Geotechnical Journal. 2014, 51(4): 420-431.

[219] Jeong S. W., S. Leroueil, and J. Locat. Applicability of power law for describing the rheology of soils of different origins and characteristics. Canadian Geotechnical Journal. 2009, 46(9): 1011-1023.

[220] Vance K., G. Sant, and N. Neithalath. The rheology of cementitious suspensions: A closer look at experimental parameters and property determination using common rheological models. Cement & Concrete Composites. 2015, 59: 38-48.

[221] Rahman M., J. Wiklund, R. Kotze, and U. Hakansson. Yield stress of cement grouts. Tunnelling and Underground Space Technology. 2017, 61: 50-60.

[222] Olmsted P. D. Perspectives on shear banding in complex fluids. Rheologica Acta. 2008, 47(3): 283-300.

[223] Schall P., and M. van Hecke. Shear Bands in Matter with Granularity. Annual Review of Fluid Mechanics. 2010, 42: 67-88.

[224] Gullu H. Comparison of rheological models for jet grout cement mixtures with various stabilizers. Construction and Building Materials. 2016, 127: 220-236.

[225] Peng J. W., D. H. Deng, Z. Q. Liu, Q. Yuan, and T. Ye. Rheological models for fresh cement asphalt paste. Construction and Building Materials. 2014, 71: 254-262.

[226] De Larrard F., C. F. Ferraris, and T. Sedran. Fresh concrete: A Herschel-Bulkley material. Materials and Structures. 1998, 31(211): 494-498.

[227] Mezger T. The rheology handbook: Vincentz Network; 2020.

[228] Jeong S. W., J. Locat, S. Leroueil, and J.-P. Malet. Rheological properties of fine-grained sediment: the roles of texture and mineralogy. Canadian Geotechnical Journal. 2010, 47(10): 1085-1100.

[229] Lin Y., L. K. J. Cheah, N. Phan-Thien, and B. C. Khoo. Effect of temperature on rheological behavior of kaolinite and bentonite suspensions. Colloids and Surfaces a-Physicochemical and Engineering Aspects. 2016, 506: 1-5.

[230] Parsons J. D., K. X. Whipple, and A. Simoni. Experimental study of the grain-flow, fluid-mud transition in debris flows. Journal of Geology. 2001, 109(4): 427-447.

[231] Torrance J. K. Physical, chemical and mineralogical influences on the rheology of remoulded low-activity sensitive marine clay. Applied Clay Science. 1999, 14(4): 199-223.

[232] Jeldres R. I., E. C. Piceros, W. H. Leiva, P. G. Toledo, and N. Herrera. Viscoelasticity and yielding properties of flocculated kaolinite sediments in saline water. Colloids and Surfaces a-Physicochemical and Engineering Aspects. 2017, 529: 1009-1015.

[233] Slatter P. Plant design for slurry handling. Journal of the Southern African

Institute of Mining and Metallurgy. 2006, 106(10): 687-691.

[234] Sellgren A., G. R. Addie, and L. Whitlock. The feasibility of transporting contaminated sediments as a slurry using centrifugal pumps. International Conference on Remediation of Contaminated Sediments; 2005: Battelle Press.

[235] Darby R., R. Mun, and D. Boger. Predict friction loss in slurry pipes. Chemical engineering. 1992, 99(9): 116-119.

[236] Zentar R., D. X. Wang, N. E. Abriak, M. Benzerzour, and W. Z. Chen. Utilization of siliceous-aluminous fly ash and cement for solidification of marine sediments. Construction and Building Materials. 2012, 35: 856-863.

[237] Wang D. X., N. E. Abriak, and R. Zentar. Strength and deformation properties of Dunkirk marine sediments solidified with cement, lime and fly ash. Engineering Geology. 2013, 166: 90-99.

[238] CEN. Unbound and hydraulically bound mixtures - Part 45 : Test method for the determination of the workability period of hydraulically bound mixtures. 2004. Brussels, Belgium.

[239] CEN. Unbound and hydraulically bound mixtures. Part 53: Methods for the manufacture of test specimens of hydraulically bound mixtures using axial compression. NF EN 13286-53, 2005. Brussels, Belgium.

[240] CEN. Unbound and hydraulically bound mixtures. Part 41: Test method for the determination of the compressive strength of hydraulically bound mixtures. NF EN 13286-41, 2003. Brussels, Belgium.

[241] CEN. Unbound and hydraulically bound mixtures. Part 42: Test method for the determination of the indirect tensile strength of hydraulically bound mixtures. NF EN 13286-42, 2003. Brussels, Belgium.

[242] CEN. Characterisation of waste - Leaching - Compliance test forleaching of granular waste materials and sludges - Part 2: Onestage batch test at a liquid to solid ratio of 10 l/kg for materialswith particle size below 4 mm (without or with size reduction). NF EN 12457-2, 2002. Brussels, Belgium.

[243] Pourakbar S., A. Asadi, B. B. Huat, and M. H. Fasihnikoutalab. Stabilization of clayey soil using ultrafine palm oil fuel ash (POFA) and cement. Transportation Geotechnics. 2015, 3: 24-35.

[244] Amini O., and M. Ghasemi. Laboratory study of the effects of using magnesium slag on the geotechnical properties of cement stabilized soil. Construction and Building Materials. 2019, 223: 409-420.

[245] Ghavami S., H. Naseri, H. Jahanbakhsh, and F. M. Nejad. The impacts of nano-SiO2 and silica fume on cement kiln dust treated soil as a sustainable cement-free stabilizer. Construction and Building Materials. 2021, 285: 122918.

[246] Kalkan E., and S. Akbulut. The positive effects of silica fume on the permeability, swelling pressure and compressive strength of natural clay liners. Engineering Geology. 2004, 73(1-2): 145-156.

[247] SETRA-LCPC. Assises de chaussées: guide d'application des normes pour le réseau routier national. 1998.

[248] CEN. Methods of testing cement - Part 1: Determination of strength. NF EN 196-1, 2016. Brussels, Belgium.

[249] CASABIEL L. B. a. L. La gamme. Colloque Le Pont; 2015; Labège, France.

[250] Scholey G. K., J. D. Frost, C. F. Lopresti, and M. Jamiolkowski. A review of instrumentation for measuring small strains during triaxial testing of soil specimens. Geotechnical Testing Journal. 1995, 18(2): 137-156.

[251] Ho T.-O., W.-B. Chen, J.-H. Yin, P.-C. Wu, and D. C. W. Tsang. Stress-Strain behaviour of Cement-Stabilized Hong Kong marine deposits. Construction and Building Materials. 2021, 274: 122103.

[252] Zentar R., H. Wang, and D. Wang. Comparative study of stabilization/solidification of dredged sediments with ordinary Portland cement and calcium sulfo-aluminate cement in the framework of valorization in road construction material. Construction and Building Materials. 2021, 279: 122447.

[253] Wang D. X., R. Zentar, N. E. Abriak, and S. J. Di. Long-term mechanical performance of marine sediments solidified with cement, lime, and fly ash. Marine Georesources & Geotechnology. 2018, 36(1): 123-130.

[254] Cai G. H., and S. Y. Liu. Compaction and mechanical characteristics and stabilization mechanism of carbonated reactive MgO-stabilized silt. Ksce Journal of Civil Engineering. 2017, 21(7): 2641-2654.

[255] Wang D. X., J. Xiao, and X. Y. Gao. Strength gain and microstructure of carbonated reactive MgO-fly ash solidified sludge from East Lake, China. Engineering Geology. 2019, 251: 37-47.

[256] CEN. Unbound and hydraulically bound mixtures. Part 43: Test method for the determination of the modulus of elasticity of hydraulically bound mixtures. NF EN 13286-43, 2005. Brussels, Belgium.

[257] AFNOR. Soils : investigation and testing — Lime and/or hydraulic binder treated materials — Test for determining the treatment ability of a soil. NF P 94-100, 1999. Paris, France.

[258] Tran K. Q., T. Satomi, and H. Takahashi. Tensile behaviors of natural fiber and cement reinforced soil subjected to direct tensile test. Journal of Building Engineering. 2019, 24: 100748.

[259] Baldovino J. A., E. B. Moreira, R. L. D. Izzo, and J. L. Rose. Empirical

Relationships with Unconfined Compressive Strength and Split Tensile Strength for the Long Term of a Lime-Treated Silty Soil. Journal of Materials in Civil Engineering. 2018, 30(8): 06018008.

[260] Tan T. S., T. L. Goh, and K. Y. Yong. Properties of Singapore marine clays improved by cement mixing. Geotechnical Testing Journal. 2002, 25(4): 422-433.

[261] LCPC-SETRA. Traitement des sols à la chaux et/ou aux liants hydrauliques. 2000. Paris, France.

[262] MOHURD. Code for pavement design of urban road. CJJ 169-2011, 2011. Beijing.

[263] Li P., X. Gao, K. Wang, V. W. Tam, and W. Li. Hydration mechanism and early frost resistance of calcium sulfoaluminate cement concrete. Construction and Building Materials. 2020, 239: 117862.

[264] Paul G., E. Boccaleri, L. Buzzi, F. Canonico, and D. Gastaldi. Friedel's salt formation in sulfoaluminate cements: A combined XRD and Al-27 MAS NMR study. Cement and Concrete Research. 2015, 67: 93-102.

[265] Wang D. X., H. W. Wang, S. Larsson, M. Benzerzour, W. Maherzi, and M. Amar. Effect of basalt fiber inclusion on the mechanical properties and microstructure of cement-solidified kaolinite. Construction and Building Materials. 2020, 241: 118085.

[266] Selim F. A., F. S. Hashem, and M. S. Amin. Mechanical, microstructural and acid resistance aspects of improved hardened Portland cement pastes incorporating marble dust and fine kaolinite sand. Construction and Building Materials. 2020, 251.

[267] Valls S., and E. Vazquez. Leaching properties of stabilised/solidified cement-admixtures-sewage sludges systems. Waste Management. 2002, 22(1): 37-45.

[268] Bertola F., D. Gastaldi, S. Irico, G. Paul, and F. Canonico. Behavior of blends of CSA and Portland cements in high chloride environment. Construction and Building Materials. 2020, 262: 120852.

[269] De Weerdt K., D. Orsakova, and M. R. Geiker. The impact of sulphate and magnesium on chloride binding in Portland cement paste. Cement and Concrete Research. 2014, 65: 30-40.

[270] Xu J. X., C. K. Zhang, L. H. Jiang, L. Tang, G. F. Gao, and Y. P. Xu. Releases of bound chlorides from chloride-admixed plain and blended cement pastes subjected to sulfate attacks. Construction and Building Materials. 2013, 45: 53-59.

[271] Karamalidis A. K., and E. A. Vouldrias. Release of Zn, Ni, Cu, SO42- and CrO42- as a function of pH from cement-based stabilized/solidified refinery oily sludge and ash from incineration of oily sludge. Journal of Hazardous materials. 2007, 141(3): 591-606.

[272] Li G. X., A. Zhang, Z. P. Song, S. J. Liu, and J. B. Zhang. Ground granulated

blast furnace slag effect on the durability of ternary cementitious system exposed to combined attack of chloride and sulfate. Construction and Building Materials. 2018, 158: 640-648.

[273] Gabrisova A., J. Havlica, and S. Sahu. Stability of calcium sulphoaluminate hydrates in water solutions with various pH values. Cement and Concrete Research. 1991, 21(6): 1023-1027.

[274] Malviya R., and R. Chaudhary. Leaching behavior and immobilization of heavy metals in solidified/stabilized products. Journal of Hazardous materials. 2006, 137(1): 207-217.

[275] Piekkari K., K. Ohenoja, V. Isteri, P. Tanskanen, and M. Illikainen. Immobilization of heavy metals, selenate, and sulfate from a hazardous industrial side stream by using calcium sulfoaluminate-belite cement. Journal of Cleaner Production. 2020, 258.

[276] Miller G. A., and S. Azad. Influence of soil type on stabilization with cement kiln dust. Construction and Building Materials. 2000, 14(2): 89-97.

[277] Hargis C. W., A. P. Kirchheim, P. J. M. Monteiro, and E. M. Gartner. Early age hydration of calcium sulfoaluminate (synthetic ye'elimite, C4A3S) in the presence of gypsum and varying amounts of calcium hydroxide. Cement and Concrete Research. 2013, 48: 105-115.

[278] Hargis C. W., A. Telesca, and P. J. M. Monteiro. Calcium sulfoaluminate (Ye'elimite) hydration in the presence of gypsum, calcite, and vaterite. Cement and Concrete Research. 2014, 65: 15-20.

[279] Hu C. L., D. S. Hou, and Z. J. Li. Micro-mechanical properties of calcium sulfoaluminate cement and the correlation with microstructures. Cement & Concrete Composites. 2017, 80: 10-16.

[280] Jardine R., D. Potts, A. Fourie, and J. Burland. Studies of the influence of non-linear stress–strain characteristics in soil–structure interaction. Geotechnique. 1986, 36(3): 377-396.

[281] CEN. Hydraulical bound mixtures. Part 15: Hydraulically stabilized soils. NF EN 14227-15, 2016. Brussels, Belgium.

[282] Pelletier L., F. Winnefeld, and B. Lothenbach. The ternary system Portland cement-calcium sulphoaluminate clinker-anhydrite: Hydration mechanism and mortar properties. Cement & Concrete Composites. 2010, 32(7): 497-507.

[283] Le Saout G., B. Lothenbach, A. Hori, T. Higuchi, and F. Winnefeld. Hydration of Portland cement with additions of calcium sulfoaluminates. Cement and Concrete Research. 2013, 43: 81-94.

[284] Coumes C. C. D., S. Courtois, D. Nectoux, S. Leclercq, and X. Bourbon.

Formulating a low-alkalinity, high-resistance and low-heat concrete for radioactive waste repositories. Cement and Concrete Research. 2006, 36(12): 2152-2163.

[285] Barcelo L., J. Kline, G. Walenta, and E. Gartner. Cement and carbon emissions. Materials and Structures. 2014, 47(6): 1055-1065.

[286] Serbah B., N. Abou-Bekr, S. Bouchemella, J. Eid, and S. Taibi. Dredged sediments valorisation in compressed earth blocks: Suction and water content effect on their mechanical properties. Construction and Building Materials. 2018, 158: 503-515.

[287] Wang D. X., N. E. Abriak, and R. Zentar. Co-valorisation of Dunkirk dredged sediments and siliceous-aluminous fly ash using lime. Road Materials and Pavement Design. 2013, 14(2): 415-431.

[288] Dia M., J. Ramaroson, A. Nzihou, R. Zentar, N. E. Abriak, G. Depelsenaire, et al. Effect of chemical and thermal treatment on the geotechnical properties of dredged sediment. Symphos 2013 - 2nd International Symposium on Innovation and Technology in the Phosphate Industry. 2014, 83: 159-169.

[289] Silitonga E. Valorisation des sédiments marins contaminés par solidification/stabilisation à base de liants hydrauliques et de fumée de silice [Doctoral dissertation]. Caen, France: University of Caen; 2010.

[290] Kasmi A., N. E. Abriak, M. Benzerzour, and H. Azrar. Effect of dewatering by the addition of flocculation aid on treated river sediments for valorization in road construction. Waste and Biomass Valorization. 2017, 8(3): 585-597.

[291] Banoune B., B. Melbouci, F. Rosquoet, and T. Langlet. Treatment of river sediments by hydraulic binders for valorization in road construction. Bulletin of Engineering Geology and the Environment. 2016, 75(4): 1505-1517.

[292] Benaissa A., Z. Aloui, M. S. Ghembaza, D. Levacher, and Y. Sebaibi. Behavior of sediment from the dam FERGOUG in road construction. Advances in Concrete Construction. 2016, 4(1): 15-26.

[293] Kasmi A., N. E. Abriak, M. Benzerzour, and H. Azrar. Environmental impact and mechanical behavior study of experimental road made with river sediments: recycling of river sediments in road construction. Journal of Material Cycles and Waste Management. 2017, 19(4): 1405-1414.

[294] Maherzi W., and F. B. Abdelghani. Dredged marine sediments geotechnical characterisation for their reuse in road construction. Engineering Journal. 2014, 18(4): 27-37.

[295] Maherzi W., M. Benzerzour, Y. Mamindy-Pajany, E. van Veen, M. Boutouil, and N. E. Abriak. Beneficial reuse of Brest-Harbor (France)-dredged sediment as alternative material in road building: laboratory investigations. Environmental Technology. 2018, 39(5): 566-580.

[296] Wang H., R. Zentar, D. Wang, and F. Ouendi. New Applications of Ordinary Portland and Calcium Sulfoaluminate Composite Binder for Recycling Dredged Marine Sediments as Road Materials. International Journal of Geomechanics. 2022, 22(6): 04022068.

[297] Olive D. J. Multiple linear regression. In Linear regression. Cham: Springer; 2017. 17-83.

[298] Jobson J. Multiple linear regression. In Applied multivariate data analysis. New York: Springer; 1991. 219-398.

[299] Ratner B. The correlation coefficient: Its values range between+ 1/− 1, or do they? Journal of targeting, measurement and analysis for marketing. 2009, 17(2): 139-142.

[300] Loske D. The impact of COVID-19 on transport volume and freight capacity dynamics: An empirical analysis in German food retail logistics. Transportation Research Interdisciplinary Perspectives. 2020, 6: 100165.

Résumé : Le réchauffement de la planète et le changement climatique sont devenus les défis les plus pressants à l'échelle mondiale. Ainsi, l'Union européenne a fixé l'objectif de passer à une économie circulaire et d'atteindre la neutralité climatique d'ici 2050. Dans le cadre de l'économie circulaire et du concept de neutralité climatique, la réutilisation des sédiments de dragage solidifiés avec un liant à faible teneur en carbone comme matériau routier, est une solution verte prometteuse. Parce que la fabrication du CSA consomme moins d'énergie et produit moins d'émissions de CO_2 que celle du ciment Portland ordinaire (OPC). Cette étude s'est concentrée sur trois objectifs originaux. Le premier objectif est d'étudier le comportement rhéologique des sédiments fins dragués, afin d'améliorer la compréhension des sédiments, en particulier le transport par tuyaux des sédiments dragués. Le deuxième objectif est d'étudier les propriétés techniques, les mécanismes microscopiques et les propriétés environnementales des sédiments traités avec les liants CSA et OPC-CSA. Ces résultats sont comparés aux traitements utilisant l'OPC. Afin de vérifier l'efficacité des liants CSA et OPC-CSA pour traiter les sédiments de dragage dans la construction routière. Le troisième objectif est de développer des modèles statistiques simples pour améliorer et optimiser la valorisation des sédiments de dragage. Cela permettra de prédire le paramètre compacté des sédiments de dragage traités, en utilisant les propriétés des sédiments bruts et le type et les dosages des liants.

Abstract: Global warming and climate change have become the most pressing challenges worldwide. Thus, the European Union established the target of transitioning to a circular economy and achieving climate neutrality by 2050. Under the circular economy and climate-neutral concept, the reuse of the treated dredged sediments with low carbon binder as road material, is a promising green solution. Calcium sulfoaluminate (CSA) cement can be a novel, eco-friendly and sustainable binder. Because the manufacturing of CSA consumes less energy and produces less CO_2 emissions than Ordinary Portland Cement (OPC). This study was focused on three original objectives. The first objective is to study the rheological behavior of the dredged fine-grained sediment, to improve the understanding of sediment, particularly the pipeline transport of the dredged sediments. The second objective is to investigate the engineering properties, microscopic mechanisms and environmental properties of the treated sediments with the CSA and OPC-CSA binders. These results are compared with the treatments using OPC. In order to verify the effectiveness of using the CSA and OPC-CSA binders to treat the dredged sediments for road materials. The third objective is to develop simple statistical models to enhance and optimize the valorization of dredged sediments. This will allow predicting the compacted parameter of the treated dredged sediments, using the properties of raw sediments and the type and dosages of binders.